NASA Contractor Report 172328

NASA-CR-172328
19840014466

THE DESIGN AND OPERATIONAL DEVELOPMENT OF SELF-STREAMLINING TWO-DIMENSIONAL FLEXIBLE WALLED TEST SECTIONS

Stephen W. D. Wolf

UNIVERSITY OF SOUTHAMPTON
Department of Aeronautics and Astronautics
Southampton, England

Grant NSG-7172
March 1984

National Aeronautics and
Space Administration

Langley Research Center
Hampton, Virginia 23665

CONTENTS

APPENDICES

UNIVERSITY OF SOUTHAMPTON

ABSTRACT

FACULTY OF ENGINEERING AND APPLIED SCIENCE
AERONAUTICS AND ASTRONAUTICS

Doctor of Philosophy

THE DESIGN AND OPERATIONAL DEVELOPMENT OF SELF-STREAMLINING TWO-DIMENSIONAL FLEXIBLE WALLED TEST SECTIONS

by Stephen W.D. Wolf

Self-streamlining two-dimensional flexible walled test sections eliminate the uncertainties found in data from conventional test sections particularly at transonic speeds. The test section sidewalls are rigid, while the floor and ceiling are flexible and are positioned to streamline shapes by a system of jacks, without reference to the model. The walls are therefore self-streamlining. Data is taken from the model when the walls are good streamlines such that the inevitable residual wall induced interferences are acceptably small and correctable. Successful two-dimensional validation testing at low speeds has led to the development of a new transonic flexible walled test section. Tunnel setting times have been minimised by the development of a rapid wall setting strategy coupled with on-line computer control of wall shapes using motorised jacks. Two-dimensional validation testing using symmetric and cambered aerofoils in the Mach number range up to about 0.85 where the walls are just supercritical, shows good agreement with reference data using small height-chord ratios between 1.5 and unity. The concept of a practical flexible walled test section has been shown by operational experience to be dependent on the use of a computer for data manipulation and wall control. Design analyses have confirmed the near optimum layout of the transonic test section and provide a basis for new test section design. This work has demonstrated the feasibility of almost eliminating wall induced interferences in two-dimensional transonic testing allowing advantage to be taken of the improved flow quality and reduced power requirements or increase Reynolds number inherent with a shallow unventilated test section.

ACKNOWLEDGEMENTS

The author is most grateful to his supervisor, Dr. Mike Goodyer, for his continual advice and guidance throughout the six and a half years of this work.

The building of the transonic test section was a major and sometimes daunting task, my sincere thanks go to Mr. Tim Judd, Mr. Mike Bartlett and all involved in the Aeronautics/ISVR workshop at the University of Southampton. An equally important task was the development of the test section wall control hardware, my thanks go to Mr. Tony Edgeley, Mr. John Berry and Mr. John Mason and all others involved from the Electronics workshop at the University of Southampton.

For the willing help of technicians like Mr. Dennis Odgers, Mr. Maurice Grinter and others too numerous to mention, I am most grateful. Without their assistance progress would have been at times impossible.

This work was funded by NASA under Grant NSG-7172 monitored through Langley Research Center and by the British Science and Engineering Research Council. I am most grateful for this financial backing, in particular the support given by Dr. Bob Kilgore and Mr. Charles Ladson.

In conclusion, my thanks go to all those involved with my project, many who I have not mentioned by name, for making my time at Southampton so enjoyable and allowing me to complete this work as originally intended.

1. INTRODUCTION

The wind tunnel exists as a design tool of the aeronautical engineer, helping to predict from scaled models the full scale performance of a lifting or non-lifting body travelling through air. Ideally, for complete simulation of free air flow conditions about a scaled model within the confines of a wind tunnel test section, the values of test Reynolds number, Mach number, turbulence level and the flowfield shape must all be properly matched to full scale.

Unfortunately it is normal practice to test at the correct Mach number with the other three parameters seldom well matched. This mismatch of test parameters continues to sometimes produce significant disparities between wind tunnel and flight data which in the past has resulted in the development and operation of inefficient and expensive aircraft. The continuing need to improve aircraft efficiencies and reduce wind tunnel testing costs spurs the quest for improved test environments and testing techniques in wind tunnels, especially at transonic speeds.

Recent developments in the wind tunnel technology have allowed the achievement of full scale test Reynolds number using cryogenic testing techniques. Partly as a result, more expenditure is planned for wind tunnel construction than ever before with the current building of major transonic facilities like NTF (National Transonic Facility) and eventually ETW (European Transonic Wind Tunnel) along with parallel developments in low speed aerodynamic and propulsion test facilities.

However, Reynolds number matching will still leave in error the important test parameters of turbulence and the shape of the test flowfield. These parameters must also approach full scale closely enough for the effects of any discrepancies to be small in terms of the indicated model performance. This thesis describes research activities dedicated to the minimisation of discrepancies in flowfield shape using a testing technique which may also lead to a lower turbulence level.

In current wind tunnels it is normal practice to correct the raw wind tunnel data. The corrections arise because the test section is only of finite size and therefore the test flowfield is constrained unnaturally in comparison with the free flowfield. The flow round the model experiences boundary interferences and it is somewhat unfortunate that the necessary corrections are uncertain, particularly for tests at transonic speeds.

However, the corrections become smaller with increasing test section size relative to the model and with the use of test section wall ventilation at transonic speeds. Therefore, it is deemed desirable to use one or both of these methods to reduce the uncertainty of the corrections. Consequently, these considerations have led to the development of large wind tunnels, expensive in terms of capital outlay and operating costs.

Conventional ventilated transonic wind tunnels have allowed valuable high speed aerodynamic research to be performed for over thirty years. However, the desire to raise Reynolds number by testing rather large models has meant that tunnel boundary interference is still significant. Despite a vast research effort devoted to the development of correction techniques for ventilated test sections, no method currently exists to satisfactorily compute the general boundary interferences. The uncertainty in the corrections arises from the inability of theoretical flowfield modelling to correctly represent the complex and uncontrolled porous test section boundaries. Also wall perforations produce high levels of flow turbulence and noise in the test section generating largely unknown interferences at the model. Furthermore, a ventilated test section requires around 50% more drive power in transonic testing than would be required by a smooth, solid walled test section. The development of new transonic testing techniques has arisen from the desire to remove imperfections and inefficiencies in current testing and the need to eliminate the requirement of a plenum chamber surrounding the test section to allow the efficient use of magnetic suspension of wind tunnel models in order to eliminate support interference effects.

Since the ventilated test section reduces boundary interference by generating streamline patterns near the wall boundaries approximating to an infinite flowfield, it would seem reasonable to expect further reductions and perhaps elimination of wall interferences if the flowfield adjacent to the walls could be better matched to that region of the free flowfield. Several embodiments of this notion have appeared in recent years and are identified by collective terms such as "adaptive" and "smart" test sections. In operation, most of these test sections are 'self streamlining' in that the process of matching the shape of the test flowfield to the free flowfield (a process referred to as streamlining the test section) is made by reference to the test section alone, independent of any knowledge of the model or the flow around it. This streamlining may be necessarily iterative, involving successive approximations of the test flowfield shape to that of the free flowfield. Each iteration involves numerous tunnel measurements and calculations to determine adjustments to the test section shape. The use of a computer for test section streamlining is therefore desirable to minimise wall setting times in a practical wind tunnel.

Two distinctly different adaptive wall testing techniques have arisen. One is a development of the existing ventilated wall technique, employing the new feature of controlled ventilation along the test section walls. The streamlines near the walls are made to conform to infinite flowfield streamlines by a controlled distribution of out-flow and in-flow of air between the test section and a finite number of surrounding plenum chambers. The other technique utilises solid impervious flexible walls which control the test flowfield by wall contouring. This method removes the need for test section ventilation and therefore offers the possibility of reduced noise and turbulence together with reduced drive power. It is this adaptive flexible wall technique which is the subject of this thesis.

The claim for the realisation of interference free flow requires some qualification. Ideally the test section should provide three dimensional control of the test flowfield. Using flexible walls, the test section could constitute some form of deformable elastic streamtube perhaps fixed in the plane of the model with free ends. Even with this

near ideal design, the test section still has a finite length and therefore truncation interferences will still be present. The control of a three dimensional flexible walled test section is perhaps impractical due to mechanical complexity and therefore initial research into the flexible wall technique has concentrated on walls having only single curvature. The test section design then simplifies to one with rigid sidewalls supporting a flexible floor and ceiling which extend upstream and downstream of the model. This layout is well suited to two dimensional testing with an aerofoil model supported between the rigid sidewalls.

The shape of the floor and ceiling of the test section can in principle eliminate wall interference in two dimensional testing. However, there will be residual interferences present due to normal experimental errors unrelated to the presence of the floor and ceiling and due to imperfections in the basis of associated wall shaping theories. As will be seen later, these errors are generally small and correctable. Furthermore, in two dimensional testing there may also be sidewall interference effects, and as with all wind tunnel tests, there will be an interference induced by the finite length of the test section which is also correctable.

Three dimensional testing may be possible with the same test section layout as for two dimensional work. While it cannot be claimed that test section wall interferences will be eliminated, the magnitudes of the interferences will probably be reduced. In principle the sources of the residual interferences will be known which may allow confident corrections to be applied to the model data, even at transonic speeds.

1.1 Objectives

1.1.1 Research into Flexible Wall Testing Techniques

At an early stage in the development of flexible walled test sections, it was considered that several advantages over conventional ventilated test sections may be offered:

1) Elimination of top and bottom wall boundary interferences in two dimensional testing.

2) Removal of uncorrectable wall boundary interferences in three dimensional testing.

3) Higher Reynolds number from a given test section size (cross sectional area) as a result of the increased model size permissible with boundary interferences eliminated or correctable.

4) Lower turbulence levels with impervious walls.

5) Reduction of tunnel drive power by elimination of test section ventilation, which is particularly significant at transonic speeds.

6) Ability of one test section to simulate test environments other than infinite flow, for example allowing the investigation of ground effect or pitch rate derivatives.

It was also appreciated there would be the following disadvantages:

1) Increased test section complexity.

2) Increased tunnel setting times between test points.

The recent developments in flexible wall testing techniques are aimed at proving the existance, or otherwise, of these advantages and minimising the disadvantages. By performing validation tests with models of known performance, it was intended to find acceptable levels of precision in wall positioning, and in the prediction of wall adjustments, and to gain valuable operational experience. The ultimate goal is to devise a scheme for a practical transonic flexible walled test section which will provide better testing environments than currently available, perhaps more economically.

1.1.2 Author's Research

It was recognised that for the concept of flexible walled test sections to be accepted, interference free performance of two dimensional models would have to be demonstrated. In addition, it would have to be shown that operation of the tunnel was acceptably easy and quick. Hence this project was initiated to achieve the following objectives:

a) Elimination of wall boundary interferences in two dimensional testing.

b) Minimisation of wall setting times to allow more efficient use of wind tunnel run time.

c) Generation of design data and operational experience for flexible walled test sections to assist future projects.

d) Determination of limits to the test conditions for a given size of flexible walled test section.

In addition, it was intended that the advantages of flexible wall testing techniques should be demonstrated in terms of increased Reynolds number and the ability to simulate numerous test environments.

The work of the author has therefore included the extension of previous validation testing at low speeds to include testing at transonic speeds, confined to steady aerodynamics. This gathering of validation data was made possible by improvements in the tunnel operating procedure which have minimised tunnel setting times. These improvements have included the development of a new wall setting strategy coupled with an on-line computer control system for actually setting the test section walls.

Validation testing at transonic speeds necessitated the design and construction of a suitable flexible walled test section. Design analyses have confirmed some otherwise intuitive features chosen for the

test section layout. In addition, the operating technique for flexible walled test sections has been further developed to overcome certain limits to test Mach number.

1.2 History

The walls of a large test section approximate to a free-air streamtube around a small model. However for models to be a practical size the test section walls or the flow near to the walls need to curve to simulate a free flowfield. The idea of eliminating test section boundary interferences by contouring the test section walls to streamline shapes is known to have originated before 1940. The first documented flexible walled wind tunnel was constructed by the National Physical Laboratory (NPL) during the early 1940s [1]. The tunnel was used for two dimensional testing employing a test section with rigid sidewalls and a flexible floor and ceiling. The walls are positioned by a system of jacks, and pressure tappings at these jacks provided wall data for streamlining. The strategy for test section streamlining involved determining experimentally the wall contours for constant pressure (constant Mach number) along each wall. For streamlining, the walls were then positioned to shapes roughly half way between straight wall and constant pressure contours. This approximate strategy was based on conclusions from a series of calculations of inviscid incompressible flows round simple models, but produced inconclusive evidence that the boundary interferences were eliminated, despite the use of a small model in a relatively large test section. It is unfortunate that the unavailability of high speed computers at that time prevented further improvement of the flexible wall testing technique, both in terms of the analytical prediction of streamlined wall contours and in terms of automation and therefore the minimisation of wall setting times. This observation perhaps explains the delay in development of flexible walled test sections until more recent times.

The work at NPL resulted from the need to relieve test section blockage which occurred at transonic speeds, a severe type of wall interference. Meanwhile parallel research efforts with a ventilated test section design produced encouraging results in terms of

interference reduction and proved more practical in operation by eliminating setting times. Hence the ventilated test section became widely adopted and has now been used in transonic testing for over thirty years.

However, the occasionally severe discrepancies between wind tunnel and flight data and the inadequacy of wind tunnel correction techniques to account for these discrepancies, has led to a renewal of efforts to improve testing environments which include the use of adaptive testing techniques. The general terms 'adaptive' or 'smart' have been applied to test sections which attempt to eliminate boundary interference by adapting the flow near their boundaries to match that of a free flowfield in the same area. When applied to flexible walled test sections the process is referred to as "streamlining the walls".

Wall streamlining strategies have become more complex since 1940 and now require, in addition to the sampling of tunnel velocities close to the boundaries, the comparison of these velocities with flow velocities calculated using a theoretical model of an infinite flowfield imagined surrounding the test section. The velocity imbalance is then used to determine adjustments to the test section boundaries. An important feature is that no reference is made to the model when streamlining the walls. The new strategies have emerged, and continue to develop, following the introduction and the continual improvements in readily available computing power.

The notion of self-streamlining or self-adapting test sections occurred to numerous researchers during the early 1970s. In particular Sears [2], Ferri, Rubert, Goodyer* and Chevalier are known to have put forward proposals for new 'interference-free' test sections.

The early work on the ventilated version of self-adaptive test sections began at Calspan USA [3,4,5,6.] using a high speed test section and has led to more detailed studies at AEDC.[7] The test sections are

* A proposal was placed on record and witnessed in the invention declarations 'Transonic Test-Section Design' and 'Self Adapted Flexible Test Section Walls' by M.J. Goodyer in July 1972 retained for reference at NASA Langley Research Center, Hampton, Virginia, U.S.A.

surrounded by a number of plenum chambers, each held at a controlled air pressure to control the quantity of inflow to or outflow from the test section. Work followed at NASA Ames [8] which has employed non-intrusive flow measurement techniques, using laser technology, to assess the quality of the control over the boundary, since intrusive flow measurements can introduce inaccuracies. Currently their tests have been confined to low speeds. The published work shows a sparsity of aerodynamic data with the test section adapted for interference free flow. There are indications that streamlining is a slow process due to inadequacies in the streamlining strategy and methods of measurement. Also the crude control of air in-flow and out-flow may require the test section to be large relative to the model.

Parallel development work with flexible wall testing techniques was initiated during 1973 in England by Goodyer [9,10] and in France by Chevalier [11]. By 1974 when the author became involved in this work, low speed flexible walled test sections had been constructed at Southampton University (see Figure 1.1) and ONERA/Chalais, France.

The low speed wind tunnel at Southampton, called the Self-Streamlining Wind Tunnel (SSWT) had by this time been used to simulate two dimensional infinite flow around a cylinder and an aerofoil model, but only one set of model data had been obtained with the walls streamlined around the aerofoil when lifting. At this time published data from the low speed ONERA facility was similarly sparse.

The simulation of infinite flow is only one of numerous simulations which can be performed with an adaptive test section (see Chapter 2). Other flow simulations were carried out using SSWT during 1974/6 for cascade, ground effect, open jet and steady pitching, using cylinder and aerofoil models. In addition, during 1975, a special tunnel with flexible walls was built by the author to investigate the simulation of two dimensional cascade flow around a single turbine blade[12] (see Figure 1.1). While the results of this work were encouraging, the findings were inconclusive due to the absence of reference data.

It was appreciated early that there were important advantages to be gained from developing a transonic flexible walled test section.

Work was started in October 1975 to build such a facility at Southampton, now called the Transonic Self-Streamlining Wind Tunnel (TSWT) (see Figure 1.2). This facility was commissioned in May 1978 but extensive two dimensional testing with wall streamlining was not practical, due to long wall setting times, until the Summer of 1979 when a semi-manual operating system linked to a mini-computer became operational [13]. Subsequently the operating system has been developed so that TSWT can be operated under closed loop computer control to minimise wall setting times.

During the period when TSWT was under design and construction. the operating procedure of SSWT was improved to allow a substantial body of low speed streamlined-wall data to be gathered on an NACA 0012-64 section [14,15,16]. This operating procedure was then adapted for high speed testing to allow the rapid generation of TSWT validation data with the walls streamlined for two dimensional flow also using an NACA 0012-64 section and the cambered NPL 9510 and CAST 7 sections.

Similar work on transonic flexible walled test sections carried out in France and Germany was not reported until 1979. The French for their part had developed a flexible walled test section insert for the CERT T2 blowdown wind tunnel at Modane. France [17] (see Figure 1.2). Limited validation testing with NACA 0012 and CAST 7 sections has been reported [18,19]. Operation of the test section at Cryogenic temperatures is anticipated soon.

Meanwhile in West Berlin, Ganzer has generated some streamlined wall data at transonic speeds using a flexible walled test section at the Aero Space Institute of Berlin Technical University [20,21] (see Figure 1.2). Their reported data from tests using an NACA 0012 and a CAST 7 aerofoil provide more validation of the concept.

The high speed data from all two dimensional tests in flexible walled test sections so far published in the literature can be summarised thus: The French claim in the T.2 tunnel to have generated streamlined wall data on an NACA 0012 section at Mach numbers up to 0.825 at zero α and a CAST 7 model at Mach numbers up to 0.7 at $\alpha = 4^{o}$.

For all the reported tests the flow at the walls was subcritical. The streamlining process was not completely automated and is known to be slow. Ganzer has reported streamlined wall data on an NACA 0012 model ($\alpha = 6^{o}$) up to Mach 0.55 and a lifting CAST 7 model up to Mach 0.82. His wall setting times are short and comparable with TSWT, since an on-line computer control system is used.

Published results from Southampton include validation data from TSWT on an NACA 0012-64 section at high speeds up to Mach .85 at $\alpha = 4^{o}$, where the walls were supercritical [22,23]. Further, the current wall setting strategy has been explored at Mach numbers up to 0.89 with the same model at $\alpha = 4^{o}$, with partial success. In addition, work has now been performed in TSWT with an NPL 9510 aerofoil at Mach numbers up to 0.87 with $\alpha = 2^{o}$, giving data on lift and drag [24]. This work was carried out to investigate streamlining around an aerofoil which was cambered, and also larger than the particular example of NACA 0012-04 which was available. In addition, validation data on a NACA 0012-64 section was gathered over a range of angle of attack through stall at low speeds in Southampton's SSWT. It is believed that the published data from SSWT and TSWT constitutes the most comprehensive set of streamlined wall data available.

It is interesting to observe how the relative height of flexible walled test sections have reduced with time. This is a desirable trend if the full advantages of this test section design are to be realised (see Chapter 3). In the NPL test reports the ratio of test section height to model chord was 4:1. It was therefore of conventional proportions by todays transonic testing standards. SSWT reduced the height to model chord ratio to 1.1:1 and TSWT has operated at ratios of 1:1 and 1.5:1. Ganzer has reported work with a height to chord ratio of 1.5:1, and the French T2 has been used with a ratio of 2.66:1.

The encouraging results from the work with TSWT have led to the design of a new two dimensional flexible walled test section insert for the NASA Langley 0.3 meter Transonic Cryogenic Wind Tunnel. This new facility will hopefully allow full scale Reynolds number matching to be linked with an improved testing environment provided by a flexible

walled test section. This test section should be commissioned soon. Experience with this facility could lead to the introduction of flexible walls into other existing major wind tunnel facilities.

2. MINIMISATION OF TEST SECTION BOUNDARY INTERFERENCES BY WALL CONTOURING

2.1 Principle of Wall Streamlining

Consider a model in free flight: an infinite number of streamtubes exist around it. If the walls of a test section could be curved to follow any one of these streamtubes the wall boundary interference on the model would be eliminated. In practice the streamtube shape varies with model shape, model attitude and test Mach number, so the test section walls would need to be flexible and controlled by a system of jacks. This is the basic principle of flexible wall streamlining.

This technique for eliminating wall interference applies equally to the two dimensional case, where the streamtube can simply be regarded as bounded by a pair of streamlines. Therefore, only two of the four test section walls need to be curved, and then only in single curvature. To illustrate the principle, consider the case of any two dimensional. aerofoil in an infinite flowfield. Two arbitrary streamlines are chosen to be followed by the flexible walls as shown on Figure 2.1. The flowfield is then broken into three parts:

i) A real portion within the test section - R

ii) An imaginary portion extending to infinity above the test section - I1

iii) An imaginary portion extending to infinity below the test section - I2.

When the walls are 'streamlined', there will be no pressure imbalance across the two boundaries between the real and imaginary flowfields.

The quality of streamlining is determined from the wall loadings given by the difference between the static pressures measured at the flexible walls inside the test section. and imaginary pressures at the

wall computed for free flowfields extending outwards from the walls, over the outside of the effective aerodynamic wall. These effective aerodynamic contours allow for the displacement thickness of the wall boundary layers. Ideally the wall loading should be zero for the walls to be "streamlined". In practice, the wall loading will be finite but reduced below some level determined by accuracy requirements (see Chapter 4).

A streamlining criterion was thus defined for the 'free air' case. In practice, there is a variety of other contours to which the flexible walls can be adjusted, depending on the type of flow simulation required as discussed later. At an early stage of development the fundamentally important criteria for wall streamlining were defined[9] as described in Section 2.3. A general feature was that each criterion was independent of any requirement for knowledge of the flowfield around the model. It is argued that if there was such a dependence, surely the ability to compute the flowfield would indicate a state of development in computational fluid dynamics such that wind tunnel tests would be unnecessary.

The flexible wall technique gives a wind tunnel a unique versatility. With a single two dimensional aerofoil mounted in the test section, it is possible to simulate six different two dimensional flowfields. Wall contouring can satisfy different streamlining criteria to simulate:

1) Conventional closed test section flow.

2) Conventional open test section flow.

3) Infinite flowfield.

4) Ground effect.

5) Cascade flow.

6) Steady pitching flow.

It had already been demonstrated that it is relatively easy to use these operating modes at low speeds. This thesis is devoted to work involved with infinite flowfield simulation up to transonic speeds.

2.2 Principles of Test Section Operation

The flexible walled test section itself, influenced by the flow disturbances generated by a model, provides all the information necessary for wall streamlining, hence the use of the descriptive phrase "self-streamlining". The only information used in streamlining in two dimensional testing is the tunnel reference flow conditions and the "wall data". This wall data consists of the wall geometry and the flexible wall longitudinal static pressure distributions, both of which are inherently easy to obtain.

The wall streamlining criterion is satisfied (within limits) by means of wall adjustments in iterative steps* which, for the infinite flow simulation, are made in accordance with the wall setting strategy described in Chapter 8. Nothing is assumed about the shape or position of the model during streamlining. Indeed the walls can be streamlined with no model present; this merely gives the "aerodynamically straight" contours for constant Mach number along the test section (as described in Chapter 6).

The general operating procedure of a self-streamlining wind tunnel is shown in the flow diagrams on Figure 2.2. In this example, it is assumed that the walls are to be re-streamlined after a small change in the test conditions of model attitude and of Mach number. The streamlining cycle starts with a scanning of the tunnel pressures. From the wall data a new pair of contours are computed, together with their imaginary external velocity distributions. Residual interferences due to wall loading are assessed as an indication of the current quality of wall streamlining. If the walls are not satisfactorily streamlined, then they are driven to new contours and the process is repeated until

* One iteration comprises setting the walls to known shapes, measuring wall pressures, assessing the quality of wall streamlining and computing new wall contours.

the residual interferences are small. When the walls are streamlined, the streamlining cycle is complete and the model pressures are scanned, and reduced.

The streamlining cycle[+] is necessarily iterative, involving repeated tunnel measurements and wall re-adjustments coupled to wall setting and data reduction calculations. The procedure requires a continual exchange of information between wind tunnel and computer which makes the self-streamlining wind tunnel ideally suited to on-line computer control. In fact, the use of a computer is mandatory if tunnel run times are to be acceptably short. As previously noted, the impracticality of implementing the streamlining process without using a high speed computer perhaps explains the delay in flexible wall research until recent years.

2.3 Alternative Modes of Wall Streamlining in Two Dimensional Testing

2.3.1 Closed tunnel mode

This is the mode of operation of low speed and supersonic wind tunnels of unventilated design. The tunnel walls are effectively 'nearly straight' and generate approximately the flowfield of an infinite array of images. Therefore the streamlining criterion is that the flexible wall aerodynamic contours follow the straight dividing streamlines between these images and the model, as shown in Figure 2.3a. Note that vertical movement of the model only affects the image pattern, and not the streamline shapes matched by the flexible wall contours which simply remain straight.

In this mode a model behaves as one of a group, an elementary form of a cascade. The meaning of 'straight' flexible wall contours requires some further explanation. In common with most unventilated test sections, the walls diverge to allow for wall boundary layer growth. This is to maintain, when empty, a constant velocity distribution along the walls. The flexible walls are adjusted to

---

[+] A streamlining cycle consists of a series of iterations bringing the walls to satisfactory streamlines.

'straight' walls experimentally by setting up a condition of constant static pressure along the walls with the test section empty. Adjustments for changes in the wall displacement thickness due to the presence of the model are made during streamlining, one small difference between the conventional closed test section and the flexible walled test section when operated in this mode.

2.3.2 Open jet mode

Some aerodynamic testing is still carried out in open jets. In this mode, the boundary of the jet is subject to ambient pressure. So for this simulation the streamlining criterion is satisfied when the flexible walls are contoured for a constant static pressure everywhere along their length equal to ambient pressure as shown in Figure 2.3b.

2.3.3 Infinite flowfield mode

This mode of operation is the most widely used in wind tunnel testing. Most wind tunnels attempt to simulate 'clean' or 'free' flow round the model. As described in the previous section, the streamlining criterion is simply that the flexible walls are shaped to eliminate inequalities between real wall static pressures measured inside the test section, and imaginary wall pressures computed for the imaginary flowfields over the effective aerodynamic wall shapes. The effective aerodynamic contours are the geometric contours corrected for variations of the displacement thicknesses of the wall boundary layers, brought about by the effect of the presence of the model.

For the imaginary flowfield to be easily computed, the pair of streamlines chosen to divide real and imaginary flowfields must not penetrate the wake or boundary layer of the model. Hence, the imaginary flowfield is completely irrotational and an inviscid solution of the flowfield is exact. This situation is a rare occurrence in the practical world of fluid dynamics.

For lifting or non-symmetric models, the two flexible walls are necessarily streamlined to different contours as shown in Figure 2.3c.

2.3.4 Ground effect mode

The flow to be simulated is a portion of the uniform flowfield about a pair of models, one the mirror image of the other. The flexible walls follow a pair of streamlines which bound the model as shown in Figure 2.3d. One streamline is straight and divides the model and image flows and the other is arbitrarily adjacent to the other surfaces of the model, but clear of the model's wake.

In this mode, the streamlining criterion is satisfied when one wall is set 'straight' (ground) as for the closed tunnel mode, while the other wall is contoured to satisfy the infinite flowfield criterion. In the few tests which have been carried out in this mode, the "ground" wall was in fact curved slightly to absorb its own variations in boundary layer displacement thickness.

2.3.5 Cascade mode

Conventional cascade testing still provides useful information on turbomachinery performance using specialised wind tunnels. In a flexible walled wind tunnel, it is possible to generate a part of the flow about an infinite cascade of cambered aerofoils. The test section bounds a single aerofoil with the walls contoured to streamlines between the aerofoils, as shown in Figure 2.3e.

Since the flowfield between each aerofoil is identical, it is possible to pick out identical streamlines above and below a single aerofoil in the cascade. The streamlines are necessarily spaced one aerofoil pitch apart in the plane of the cascade. The streamlining criterion is satisfied when the static pressures measured along each wall are matched in the plane of the cascade, that is at A and A', B and B', C and C' etc.

Turbine and compressor cascades (accelerating or decelerating flow) may be simulated around one model by simply restreamlining the walls for different cascade planes or matching angles. However in turbine work the flow may require large turning angles which necessitates the use of a specialised test section.

2.3.6 Steady pitching mode

Aerodynamic tests are often made using an oscillating model to determine dynamic stability derivatives. It has been demonstrated in a flexible walled wind tunnel that it is possible to simulate different steady pitching rates with a stationary model, to assess the associated changes in model force and pitching moment coefficients.

The procedure for adjusting the walls for steady pitching[25] first involved the streamlining of the test section for an infinite flowfield. Then some curvature of the tunnel centreline was introduced. The walls were adjusted in accordance with the local changes of the centreline position from straight to curved as shown in Figure 2.3f. The walls were then assumed streamlined for steady pitching. Different pitching rates were simulated by varying the magnitude of centreline curvature. In these tests the reference airspeed was held nominally constant throughout. This procedure, while not perfect, appears to be the best currently devised.

3. CHARACTERISTICS OF FLEXIBLE WALLED TEST SECTIONS

3.1 Advantages in Two-Dimensional Testing

3.1.1 Reynolds number

With test section wall boundary interference eliminated, the wind tunnel designer is free to reduce the test section height within the aerodynamic and structural limitations to be discussed later. Conversely, the model size can be increased. Both actions effectively reduce the test section height to model chord ratio (h/c), which can lead to improved Reynolds number capability.

For a given test section size and Mach number, enlarging the model gives a direct increase in Reynolds number. A value of h/c = 4 represents a typical conventional ventilated test section, while h/c = 1 represents the proportions so far explored with a flexible walled test section. This reduction of h/c doubles Reynolds number with model aspect ratio and test section cross sectional area held constant.

3.1.2 Power requirements

A reduction of tunnel drive power is an important alternative to increased Reynolds number capability. The reduction of test section size and the elimination of test section ventilation can lead to significantly reduced tunnel power requirements.

Transonic wind tunnels require high levels of drive power, a large proportion of which is associated with the test section plenum suction. For example, calibration of the 7ft x 10ft (2.13m x 3.05m) high speed tunnel at the NASA Langley Research Center revealed that at a freestream Mach number of .8, the overall tunnel drive power was 11.5 megawatts with a slotted test section and only 8.1 megawatts (a 30% reduction) with a closed test section. While blockage was relieved in the slotted test section, this was not possible in the closed test section. Wall streamlining may provide further reduction in power consumption by reducing tunnel blockage and the associated pressure losses.

The reduction in test section size made possible by the use of flexible walls also means a given Mach number can be achieved with reduced tunnel mass flow and therefore possibly with less drive power. It may be assumed that drive power varies approximately with air flow rate in comparing the power requirements of tunnels having the proportions of test section introduced above. Power would then vary as h/c. If this effect is combined with the power reduction brought about by the use of a closed section, the overall power reduction might exceed 80%.

3.1.3 Flow quality

The flow quality in wind tunnels is becoming increasingly recognized as an important characteristic, particularly for the investigation of unsteady aerodynamics and transonic aerodynamics. Unfortunately, existing transonic facilities employ ventilated test sections and the associated wall perforations or slots are known to produce high levels of turbulence and noise in the test section, generating largely unknown interference effects.

In a flexible walled test section the need for ventilation is removed. The test section walls are smooth and non-porous. Aerodynamically the flexible walled test section is less complex, and improved flow quality results.

The flow quality in a wind tunnel is also dependent on secondary flows. In two dimensional testing the magnitude of secondary flow effects can be considered a function of test section height and model aspect ratio. Flexible walls allow the use of shallower test sections and/or larger models since boundary interference is eliminated. Consider the reduction in test section height. The cross sectional shape of the test section then approaches a square, implying that the area above and below the model is rectangular and shallow. It may be argued that any secondary flow effects due to sidewall boundary layer interaction with the model and the floor or ceiling will tend to be limited to the tips of the model, and the two dimensionality of the flow will be maintained on the model centreline. With a conventional test section height this may not be the case.

3.1.4 Versatility

The principle of self-streamlining can be applied in a variety of flow simulations as described in Section 2.3, and each simulation may make its own unique demands in terms of test section hardware.

However, flexible walled test sections are inherently versatile and sometimes require only changes in the control software to perform different flow simulations. For example the pressure data from the wind tunnel can be analysed differently to generate different wall contours when streamlining for different modes.

Careful design of the test section hardware could allow all six modes of operation to be used. This can be achieved by anticipation of the maximum values of wall movement. It is desirable that sufficient movement be included to accommodate unanticipated requirements, as discussed in Chapter 4.

Change of operating modes requires software versatility. This is achieved by modular architecture of the control software. Modifications to the control program can consist of replacing or removing program segments (i.e. subroutines, functions, etc) which in most cases is quick and easy to implement.

The versatility of SSWT has been demonstrated by performing all six flow simulations[9]. While operating one tunnel in all modes is possible, the simulation of cascade flow around a cylinder performed in SSWT was a simple case only for evaluation purposes. A lifting model in cascade flow simulation calls for more demanding wall curvatures to generate the necessary flow angles, perhaps requiring a special test section.

3.1.5 Interference Correction

The 'wall data' used in test section streamlining also provides information which may be used to assess the levels of wall boundary interference at any stage throughout a streamlining cycle.

The simple boundaries of a two dimensional flexible walled test section allow this interference to be easily quantified (see Chapter 7). The option is therefore available to terminate the streamlining cycle before the walls have been set to good streamlines, and then to apply conventional corrections to the model data. This operation has the effect of reducing the time for wall setting by reducing the number of iterations. However, operational experience has shown that only small conventional corrections can be confidently applied in transonic testing, since large interferences induce errors in the positions of model shocks.

Alternatively, the walls can be driven towards streamline shapes until the model corrections are reduced to negligibly small values (see Chapter 7).

3.2 Disadvantages

3.2.1 Operational aspects

The operation of an adaptive walled wind tunnel differs from conventional operating procedures in one major respect. Before usable test data can be taken, the correct test section boundary conditions have to be generated. Tunnel run time used for wall setting will, in one sense, be non-productive and must be minimised.

Until a one-step wall setting algorithm is developed the streamlining process of a flexible walled test section will remain an iterative process involving successive approximations to the streamlined wall shapes. The number of iterations required to achieve good streamlined walls is a function of

1. The rate of convergence of the wall adjustment strategy which predicts the required wall movements.

2. The magnitude of the change in test conditions (i.e. Mach number and/or model angle of attack) between streamlining cycles.

Considerable progress has been made on 1., while suggestions are included for minimising the impact of 2.

While it is extremely important to reduce the number of wall adjustments during a test programme, minimisation of wall setting times necessitates automatic control of the wall shape to ensure efficient and economical use of wind tunnel run time. The increase in test section complexity is offset by the associated advantages of any computer application to a wind tunnel facility. These are:

1) Increased wind tunnel productivity due to more efficient use of tunnel run time. On-line computer control allows the display of real time data which can be used immediately to update the test programme. Also, test conditions can be established more rapidly after bringing the tunnel air on. Furthermore, it is possible to move more rapidly from one test condition to the next.

2) Test programmes can be made more extensive and therefore more comprehensive due to increased tunnel efficiency and software versatility. Of course, the quantity of data generated is greatly increased necessitating careful pre-planning of the test programme, with perhaps special attention being paid to data presentation.

3) Improved data quality comes from maintaining a consistent operating procedure and by minimising any deviations in test conditions.

3.2.2 Shockwave/flexible wall interaction

For the full advantages of the flexible wall technique to be realised, the walls are positioned close to the model. This implies that at high transonic speeds, the model shocks will probably extend to the walls and beyond into the imaginary flowfield surrounding the test section. Four problems can then arise

1) Shock reflections from the flexible walls.

2) Shock/wall boundary layer interactions.

3) Imaginary flowfield contains mixed flows.

4) The test section becomes choked.

Experience with TSWT has shown that aerofoil shock reflections from the walls are not evident, since shocks so far observed during NACA 0012-64 and NPL 9510 tests are locally normal to the wall. However, for supersonic testing there will be a need to cancel the bow shock reflections, perhaps by wall shaping.

The shock/wall boundary layer interaction has been observed as a significant thickening of the wall boundary layer by up to 70% of the wall boundary layer thickness just upstream of the shock. This interaction has an effect on the aerofoil in terms of errors in shock position and local pressure coefficient. However, preliminary work has shown that a localised hollow around the foot of the shock makes some allowance for the interaction. This is discussed in more detail in Chapter 10.

The imaginary flowfield computations are an integral part of the wall setting strategy. The numerical solution of mixed flowfields is complex and consequently demands more computer run time. So, depending upon the available computer, the inclusion in the wall setting strategy of numerical techniques to solve mixed flows may cause a significant wall setting time penalty. However, experience with TSWT and the models described later has shown that simple linearised compressible flow theory can be used successfully up to freestream Mach numbers of about 0.85. Ultimately the adequacy of any such relatively simple theory depends on the extent of the supercritical flow bubble present in the imaginary flowfield.

Once supercritical flow extends to both flexible walls, the test section becomes choked and the freestream Mach number becomes insensitive to changes of the wind tunnel drive power and also insensitive to the shapes of the walls downstream of choked zone. Experience with TSWT has shown that it is necessary to adjust the drive power to give freestream Mach number at the downstream end of the test section to ensure that the model shocks are not misplaced.

While some exploratory work has been done at higher Mach numbers, the situation is unsatisfactory because of the inability of the current wall setting strategy (described in Chapter 8) to cope with the complexities of the flow at these higher Mach numbers.

4. FLEXIBLE WALLED TEST SECTION DESIGN

4.1 Design Concept

For the realisation of an efficient self-streamlining facility, good test section design must satisfy three general requirements - data quality, versatility of operation and control system compatibility.

The design of a two dimensional flexible walled test section is unconventional in respect of one important dimension, namely, its height. For full benefits to be reaped from the flexible wall techniques, it is desirable to position the flexible walls as close to the model as possible. Aerodynamic considerations present the following limitations to closeness:

1) Merging of wall and model boundary layers.

2) Boundary layer separation on the top or bottom walls.

3) Onset of other secondary flow and boundary layer interference effects.

Additionally practical considerations may demand that supercritical flow must not extend through the flexible walls. Acceptance of this limitation eliminates the need for more sophisticated imaginary flowfield theories and associated numerical techniques, and may also avoid any shock/boundary layer interactions within the test section.

Any merging of wall and model boundary layers within the test section invalidates the current wall setting strategy. This is because the imaginary flowfields are assumed everywhere to be potential, and unknown interference effects may result in the real flowfield from the mixing of the model wake and wall boundary layer(s). This limitation would exist if a more complex imaginary flowfield theory could be developed to account for viscous effects in the imaginary flowfield.

Boundary layer separation on the flexible walls caused by wall curvature, model induced pressure gradients or model shocks is very undesirable. Uncorrectable interference effects would result from the separated flows, since aerodynamic wall contours would be of unknown shape.

Other interference effects may result from reductions in test section height. The aerodynamic coupling between flexible walls, due to a one dimensional continuity effect, may become too strong for practical streamlining. While shockwave reflections from the flexible walls have not been observed, there are significant interference effects at the model generated by shock/wall boundary layer interactions. These effects may be correctable (see Chapter 10). However the effects of shock/boundary layer interactions are likely to increase with decreasing test section height due to increased shock strength at the wall. Ultimately, more complex interferences could result from the shock's laminar or turbulent delta impinging on a wall.

The general design concept of a flexible walled test section is shown on Figure 4.1. Here, the aerofoil model is in a flowfield contained within a streamlined glove. The height of the glove is sufficient to contain the portion of the infinite flowfield influenced by the viscous reaction to the model. The length of the glove is determined by the acceptable streamlined wall slopes at the upstream and downstream ends of the flexible walls, as discussed later in this chapter.

The result is a long shallow test section with a flexible contraction and flexible diffuser (collectively referred to as the adaptor portions of the test section) at the upstream and downstream ends respectively. The adaptor portions are necessary because the remainder of the tunnel circuit is rigid.

The walls are contoured by a series of jacks which are linked to some form of self-streamlining control system. The model may need to translate vertically to reduce wall curvature for streamlining with varying up and down-wash and also to maintain the model between the pair of streamlines dictated by the fixed contraction.

The design concept is simple but the detailed design is complicated by the interaction of electronic, mechanical, aerodynamic and cost constraints. However a practical flexible walled test section needs on-line computer control of wall shape and therefore must incur a penalty of increased test section complexity (discussed in Chapter 3).

The design considerations particularly related to a flexible walled test section are basically concerned with the elimination of top and bottom wall-induced errors at the model. The following sections in this chapter will attempt to identify the questions that arise during the design phase of a new flexible walled test section and provide some guideline answers.

4.2 Performance Requirements

The performance requirements of a new test section are based on physical constraints and the expected use of the facility. The design philosophy for an insert into a completely new wind tunnel will be different from that associated with an insert into an existing facility. For example, the new facility may need to be energy efficient in operation, while the new test section insert in an old facility will probably be designed for performance enhancement.

The use of the flexible wall technique generates the need for additional information on the anticipated use of the test section. From this data the physical size of the test section can be decided within rigid tunnel constraints, if these exist. In addition, the operational modes and control system can be specified.

In general, the new test section must have the capability to cover a specified test envelope of Mach number and Reynolds number, and while it may be necessary to provide features such as pressurisation and/or cryogenic operation to generate these test conditions, this chapter only discusses those design considerations specifically linked to use of a flexible wall testing technique.

Normally the designer has to compromise Reynolds number because of a constraint on drive power. The higher test Mach number can only be

achieved by minimising the test section cross-sectional area which implies that small models must be used. However, as previously described, the flexible wall testing technique allows the model size to be increased for a given test section height with a corresponding increase in Reynolds number for a given test Mach number. Alternatively this advantage of flexible walls can be utilised as a power saving as described in Section 3.1.2.

The tunnel specifications for a required test envelope should include the test section dimensions, the maximum wall curvature and movement, the desired data accuracy, and the capacity of the control system hardware and software.

The anticipated variation of the model lift with Mach number and angle of attack will allow some theoretical estimate to be made of wall slopes and movement. The maximum permissible model lift could be determined by such wall limitations, or by model strength, test section length, or the tendency for the lower wall to rise towards the model under the influence of strong circulation.

The anticipated testing will specify the modes of operation of the tunnel and therefore the control software complexity. The mode likely to produce the severest wall curvature and deflection should then be used as a test section design target. The models to be tested will also specify the test data required from the model itself and the tunnel walls. This leads to some instrumentation requirement with a resolution matched to the overall tunnel error arising from the finite size of the test section. These tolerances in turn specify the accuracy of wall settings controlled by the jack spacing and jack setting accuracy. For efficiency reasons, this level of accuracy should be matched by the control software, as discussed in the next section.

A practical facility must employ on-line computer control of the wall shape which increases the complexity of the control hardware. Additional control requirements demand some form of rapid data acquisition from the tunnel and model. An accurate Mach number control system is desirable, particularly when the test section becomes choked.

A review of current productive wind tunnel facilities[26] quotes the following accuracy of measurements.

Mach number	± 0.002
Angle of attack	± 0.05 degrees
Lift coefficient	± 0.008
Drag coefficient	± 0.005
Pitching moment coefficient	+ 0.006

A new facility must match or better these measurement tolerances if it is to meet future demands on simulation accuracy. Mach number and angle of attack repeatability and accuracy are enhanced by computerised automation, while the accuracy with which model forces and moments are measured is dependent on the aerodynamic qualities of the tunnel as well as instrumentation precision and repeatability. In a practical sense the performance requirements of a new facility are only likely to be achieved by the integration of modern testing techniques with on-line computer control systems.

4.3 Identification of Error Sources in Flexible Walled Test Sections

The major sources of errors may be grouped as follows:-

1) Physical constraints such as finite length of the test section and finite number of wall jacks.

2) Measuring tolerances.

3) Theoretical basis of the wall setting strategy.

4) Numerical analysis and computation.

The theoretical and computational errors can easily be reduced to a less critical level than the other three, but this would be at the

expense of increased software sophistication and computer run times, a trend which is highly undesirable for on-line computer control of tunnel shape. Therefore it is more efficient to develop a simple program with a numerical process generating errors compatible with error levels from the other sources.

It is important to have some knowledge of the magnitude of these system errors to ensure total consistency. Consideration is given in the remainder of this chapter to some of the error sources in order to obtain test section design parameters. Since the ultimate measure of error acceptability is the level of aerodynamic interference at the model, it is logical to express the errors in these terms. It is important to note that economic penalties will be incurred if too close a tolerance is demanded during any stage of the design.

The sources of experimental error that have been so far identified are:-

a) test section length truncation.

b) boundary layers on the four test section walls.

c) differences between the structural shape of the flexible walls and the desired streamline contours.

d) wall deformation due to pressure load.

e) wall foreshortening due to curvature.

f) tunnel centreline curvature.

g) wall position measurement resolution.

h) pressure measurement resolution.

i) imaginary flowfield calculations leading to errors in wall position.

Test section interferences on the model due to the wall position errors between jacks, sidewall boundary layers and tunnel centreline curvature are un-correctable, since their interferences cannot be accurately quantified. The same comment can be extended to interferences due to the measurement resolution. However some maximum interference for a given resolution will presumably be known.

It is desirable to minimise all interferences by careful test section design using the interdependence of the interferences to advantage as shown in the following section. The uncorrectable interferences cannot be ignored as illustrated during curved centreline tests with SSWT[25], and shown by experiments with sidewall boundary layer treatment. The interference induced by sidewall boundary layers remains a problem for all two dimensional testing and is still not well understood. Centreline curvature may be eliminated by accurate determination of "aerodynamically straight" wall contours (see Chapter 6). Wall position errors between jacks can be reduced to the jack setting tolerance by sensible jack spacing as shown later.

4.4 General Factors Affecting Choice of Test Section Geometry

4.4.1 Length

The streamlined portion of the test section is necessarily finite. It can be assumed that the truncation of the test section length leads to:-

1) interferences due to the streamlines not being correctly represented by the flexible walls,

2) possible ambiguities in the reference line for model attitude measurement.

The simple potential-flow analysis of a two-dimensional lifting body indicates that there are still significant streamline angularities present, relative to the tunnel centreline, at distances of 5 to 10 model chords upstream and downstream of the model, even at moderate

C_L [9]. While the designer is free to increase the test section length until the flow angularities at the test section ends are arbitrarily reduced to an amount equal to the mechanical resolution of the wall settings, the maximum permissible model C_{Lmax}, will decrease, or else the test section height must be increased. These observations are confirmed by analysis of the potential flow around an isolated vortex in an infinite flow. Data was obtained for a C_{Lmax} case where the stagnation streamline passed through the normal position of one of the fixed ends of the flexible walls. The theoretical C_{Lmax} for various test section lengths and depths is summarised on Figure 4.2. Consider the case where the test section is five effective model chords in length (one chord is equivalent to the test section depth), the C_{Lmax} is 2.75 based on an effective model chord. If the length is increased to 10 model chords then C_{Lmax} reduces to 2.1. To maintain C_{Lmax} at 2.75, the test section height would have to be increased to about 1.35 chords with the larger test section. Therefore the acceptable test section length is a compromise between C_{Lmax} and the magnitude of the interference effects due to test section truncation.

Judd has shown[27,28] that the interferences due to the fixed geometry termination of the adaptable test section can be minimised by placing the model's centre of lift symmetrically between the test section ends. This arrangement eliminates the angle of attack error for all values of the ratio of test section height to test section length. However, lift interference will still be present, as in the case of a conventional solid walled test section. This interference can be integrated as an equivalent camber due to induced streamline curvature. If the separation between the downstream walls cannot be increased by an amount equal to the model wake displacement thickness, a wake blockage will also occur. In normal operation the flexible walls induce no wake blockage.

Analysis by Judd has led to the following results for the case where the test section height h is small compared with tunnel semi-length L:

Lift error due to induced camber: $\frac{\Delta C_L}{C_L} \simeq \frac{A1}{2\pi} \cdot \frac{1}{16} \left(\frac{c}{L}\right)^2$

Drag error due to wake blockage: $\frac{\Delta C_D}{C_D} \simeq - \frac{C_D}{4\pi} \left(\frac{c}{L}\right)$

where A1 is the lift curve slope and c is the model chord. Note the corrections for small h are independent of test section height. A lift interference of less than 1% is predicted for a test section semi-length of 5 chords.

The effects of compressibility can be assessed by use of the Prandtl-Glauert compressibility factor β

$$\left(\frac{\Delta C_L}{C_L}\right)_C = \frac{1}{\beta} \left(\frac{\Delta C_L}{C_L}\right)_I$$

where subscript I is for incompressible flow and c is for compressible flow. Alternatively for the same lift coefficient ratio and the same model chord, the tunnel semi-length/height ratio would have to be increased in the form

$$\left(\frac{L}{h}\right)_C = \frac{1}{\beta^2} \left(\frac{L}{h}\right)_I$$

Hence at Mach 0.8, a 30% longer tunnel would give the same interference level or conversely the same tunnel would generate 66% more lift interference. Unfortunately, this argument is not valid above about Mach 0.8, because the similarity rule breaks down in the transonic regime, and a new interference assessment technique will be required for use at higher Mach numbers, should this become necessary.

Ambiguities in the level of interference arise because of different interpretations of the tunnel semi-length. The termination of the streamlined portion of the test section is not clearly defined. There seem to be three options open for dealing with interferences due to test section length truncation, either:-

1) accept that the interference is present, but keep it small by suitable proportioning of the test section and make no corrections,

2) apply a correction assuming some test section length,

3) apply some form of aerodynamic correction during streamlining deliberately to cancel the interference at the model.

The first option has been used here, although the magnitude of the interference becomes uncertain at high transonic speeds. Further work is required in this area.

4.4.2 Ratio of Test Section Depth to Model Chord

Flexible wall testing techniques allow a significant reduction to be made in the test section depth to model chord ratio. While it is extremely desirable to bring the flexible walls as close as possible to the model, there are various aerodynamic and practical limitations which have already been discussed within the design concept.

In addition, the model must be positioned within the streamtube picked out by the upstream fixed ends of the flexible walls, over the desired range of angle of attack. Even then, the wall curvature necessary to reproduce the streamtube must not exceed structural limits. The sensitivity of the model performance to wall movement is expected to increase with reduction of test section depth. Also, demanded wall movements will lead to severe wall curvature. These considerations indicate the need of a more complex jack systems with improved setting tolerances. Also wall streamlining times may increase due to larger wall adjustments being demanded between successive streamlining cycles.

Analysis of the potential flow around an isolated vortex (described in the previous section) has provided some guidelines on the choice of the test section depth. This analysis shows that for a test section 10 chords in length the C_{Lmax} increases from 1.05 to 3.05 if the test section depth is increased from 1/2 chord to 3/2 chord (see Figure 4.2). So it is possible for the test section height to limit significantly the maximum model lift. Provision for simultaneous translation of the model in the vertical direction with change of angle of attack can avoid this problem.

The analysis was extended to investigate the curvature of the flexible walls in reproducing streamlines around the vortex. A summary of the findings is shown on Figure 4.3 as a plot of minimum radius of wall curvature found near the model against test section length for different test section depths with the model C_L equal to 1.0. The structural limit to radius of curvature for those portions of TSWT walls close to the model is 15.24cm (6 inches). Even with a moderate value of C_L, this structural limit is exceeded with a test section length of 10 chords and a depth of one chord. However, this flowfield is a very severe case, which will probably never be encountered experimentally due to the reduced model thickness and the viscous action of the model in the real flow. The model wake will tend to fill out the downstream end of the test section relieving wall curvature near the model. Nevertheless, this severe test case allows some important conclusions to be drawn from the analysis about choosing test section depth.

Firstly, the wall adjacent to the high pressure surface of the model always experiences more severe curvature. But there is an almost linear reduction in the wall curvature with translation of the model away from the wall adjacent to its high pressure surface. Secondly, there is a rapid decrease in wall curvature with increasing test section depth and/or decreasing test section length. For example, with a test section length of 10 chords, the maximum demanded wall curvature is reduced by 70% by increasing the test section depth from 1.25 chords to 1.5 chords. Hence this analysis suggests that for a given test section depth to length ratio wall curvature is the limiting factor on maximum model C_L.

The most important factors in choosing the test section depth would seem to be to minimise or avoid interference effects due to wall boundary layers, model wake, shock waves or streamlining imperfections. Experience has shown that a test section depth of only one chord is practical in two dimensional testing. However, other factors such as anticipated maximum model lift and wall jack complexity may be equally important at the design stage.

4.4.3 Width

The flexible wall testing technique has no observed significant effect on the designers choice of test section width. There remain other factors affecting the width common to all two-dimensional test sections:

i) Minimisation of secondary flows.

ii) Minimisation of other sidewall boundary layer effects.

iii) Existing wind tunnel dimensions.

The widths of TSWT and SSWT test sections were chosen to be compatible with existing wind tunnel circuits.

4.5 Assessment of System Accuracy

4.5.1 Instrumentation accuracy

The wall streamlining relies on wall static pressure measurements and jack position information both of which can only be resolved to some instrument tolerance. The overall accuracy of the wall settings and therefore the quality of the model data is dependent on the instrumentation accuracy.

Adjustments to the flexible walls are made with reference to the wall static pressures and the measures of streamlining quality rely on the wall information. With TSWT, the measures of streamlining quality which have been adopted are:-

1) E, the average of the modulus of the imbalance between real and imaginary wall pressure coefficients.

2) Residual interferences at the position of the model, due to some loading of the flexible walls. These are quantified as a wall induced angle of attack, wall induced camber and an induced streamwise velocity error at the model.

Experience with streamlining procedures has led to the belief that the walls are well enough streamlined when E is less than 0.01 and ΔC_L arising from each component of residual interference is less than 0.008. These arbitrary levels of acceptability are the result of observation of overall system resolution, and are roughly compatible with the figures in the table in Section 4.2.

Naturally the pressure measurement resolution must be as good as the overall system resolution. In SSWT, wall pressure coefficients could be resolved to about +0.006 with the manometers and speed used in these tests. In TSWT, wall pressures are resolved to $\pm$0.127mm ($\pm$.005 inch) Hg which is double the resolution of a conventional mercury manometer bank. This tolerance has been assessed to give a resolvable model C_L of about $\pm$0.005. This level of resolution is adequate and is also compatible with levels of accuracy normally required.

It is recognised that regardless of the accuracy of the wall setting strategy, the flexible walls can never follow the computed contours. The flexible wall is controlled by a finite number of jacks and it will lie within some positioning tolerance band, set by the accuracy of jack position measurement. However, care must be taken to ensure that the uncontrolled portions of the wall, between jacks, also lie within an acceptable tolerance band, as discussed in the next section.

The qualification of an acceptable tolerance level for wall setting must be the magnitude of the uncorrectable interference induced at the model by any wall position error. An analytical method has been devised to estimate the interference of such errors. In general, a test section will have a system of jacks along each wall, and wall position errors are likely to occur randomly, both in location and magnitude. In SSWT and TSWT, a wall setting accuracy of better than $\pm$0.127mm ($\pm$0.005 inch) has been maintained. This tolerance was originally dictated by the available position measuring equipment. In TSWT there was an economic penalty for increasing unduly the jack position sensor resolution.

In the analysis of wall setting errors, the same wall setting tolerance was adopted. The wall setting errors are modelled as bumps in an otherwise flat walled two dimensional test section. Each bump is represented in the potential flow model as an equal source/sink pair lying on the wall line, combined with a system of images. The source/sink separation is chosen to be equal to multiples of the jack spacing as described in more detail in Appendix A. While this analytical representation of the wall position errors is less than perfect, it does give an indication of the interference levels.

The need to cope in the analysis with the random nature of the error has been eliminated by recognising that a single bump will probably produce the worst error at the model in terms of flow disturbance. So the analysis has concentrated on estimating the maximum interference of a single bump, since there is a small but real chance of a single bump occuring in the test section. For a maximum disturbance the single bump is necessarily close to the model, and therefore only a few jacks are likely to cause such a disturbance. The analysis has shown that an increment in model C_L of about 0.002 can be expected from a single wall position error equal to the tolerance level, with a jack spacing of 1/4 model chord and a test section depth to model chord ratio of unity.

Since the bump is small, interference effects are expected to decrease linearly with a reduced wall tolerance and an increase in test section height. The effects of compressibility on the interference levels due to wall position errors have only been assessed in terms of the one-dimensional continuity effect on the tunnel freestream velocity. At Mach .9, the error induced in the freestream Mach number is only of the order .005 (1/2%), rapidly diminishing with reducing Mach number.

The wall setting tolerance of SSWT and TSWT, $\pm$0.127mm ($\pm$0.005 inch), has been shown to be adequate over the low subsonic speed range. Future high speed testing may indicate that finer tolerances on jack positioning are necessary. While the jack setting tolerance can be reduced, there is a limit to overall wall setting precision by virtue of the uncontrolled portions of the wall between jacks. However, significant reductions in interference levels should be achieved at minimum cost by reducing the tolerance only on jacks close to the model.

4.5.2 Flexible wall position errors

While the designer is free to choose the wall setting tolerance at the wall jacking points, there are in general other factors to consider in assessing the overall wall position errors. These factors are:-

1) The shape of the uncontrolled portions of the flexible walls between jacks.

2) The deformation of the flexible walls due to pressure load.

3) The deformation of the jack-to-wall attachments (flexures in our case) induced by wall slope and by wall foreshortening due to curvature.

4) Friction between the rigid sidewalls of the test section and the flexible top and bottom walls.

There is no independent control over the flexible wall shape between the wall jacks. The wall will deform to some contour dictated by its elastic properties, which will not necessarily match the streamline contour even if the jacks are exactly positioned. The magnitude of this source of wall position error is controlled by the number and spacing of the wall jacks. Obviously if there were an infinite number of exactly positioned jacks the wall would be perfectly contoured. To assess the effects of jack spacing on such wall position errors a theoretical analysis has been developed.

The basis of the analysis is that a portion of the flexible wall passes through a series of jacking points corresponding to discrete points on a theoretical streamline. It is then assumed that the maximum deviation between the wall and streamline contour will occur mid-way between jacks. This analysis is described in more detail in Appendix B.

When the analysis was applied to theoretical streamlines around a NACA 0012-64 section at $\alpha = 8^{o}$, the worst wall position errors occured if

there was no jack attachment on the wall over the quarter chord point or under the leading edge, at positive angle of attack. However, the maximum errors from this source can be reduced to acceptable levels (.0127mm/.005 inch) or similar by reducing the jack spacing to 1/3 model chord in the vicinity of the model, even with a test section depth of only one model chord.

The worst wall position error E_{wm} was calculated for both walls over a range of test section depths where h/c = 0.5, 1.0 and 2.0. The results are shown on Figure 4.4 for jack spacings up to 1.8 chords. As expected, the more shallow the test section the more rapid is the rise in E_{wm} with increasing jack spacing. Also it can be seen that one wall needs tighter control than the other. The wall adjacent to the high pressure surface of a lifting model has to reproduce a more complex streamline pattern than the other wall. This is due to the combined effect of upwash and the thickness of the model which causes an imprint to appear in the wall demanding three inflexions of the wall.

This analysis has shown that the close jack spacing adjacent to the model's high pressure surface employed in SSWT and TSWT of 2.54cm (1 inch) is more than adequate to hold the wall position error from this source to $\pm$0.127mm ($\pm$ 0.005 inch). The close jack spacing need only extend along each wall for about 1/2 chord upstream and downstream of the model. This approach allows the total number of jacks to be reduced without introducing unacceptable errors in wall shape.

Wall deformation due to pressure loading can be minimised in two ways; 1) by reducing the wall pressure loading by controlling the pressure in the air volume containing the jacking mechanisms on the outside of each flexible wall, 2) by strengthening the flexible wall to resist bending. However, these recommendation lead to a conflict in wall design requirements. The conflict is that wall flexibility is required for streamlining while the wall remains stiff enough to resist pressure bending. The solution to this was to compromise and to vary the flexible wall thickness depending on jack spacing. The wall is thin in the region of close jack spacing where the wall stresses tend to be high due to curvature. The wall is thick at the upstream and downstream

ends where the jack spacing is greatest and the curvature small. In TSWT, the flexible walls are 5.08mm (0.2 inch) thick over the end regions and 2.54m (0.1 inch) thick over the centre regions. This distribution of wall thicknesses was chosen to help ensure that the flexible walls can be positioned within the wall setting tolerance everywhere along their length.

Other factors affecting the jack position accuracy are the deformations of thin metal wall-to-jack flexures. These are used to allow for the local wall slope and the phenomena of wall 'pull-up'. Wall contouring produces a streamwise movement or 'pull-up' of the wall, since the walls are anchored at their upstream ends. Distortion of the flexures will generate a wall position error when position is measured at the ends of the flexures remote from the wall, as is the case in TSWT. However with TSWT the estimated maximum foreshortening of a flexure due to the wall being curved is only 0.068mm (0.0027 inch) at the downstream end of the wall. This error combined with the measured accuracy of the jack position sensing device (0.038mm (.0015 inches)) gives a jack position accuracy of 0.106mm (0.0042 inch). This tolerance is within the chosen target value of wall setting tolerance of 0.127mm (0.005 inch). Nevertheless, the option still remains to estimate the magnitude of the flexure distortions to allow the wall position to be estimated to a higher level of precision. Note that the stiffness of the flexures should be less than the wall stiffness so as not to modify the local wall shape.

The final factor which might cause wall position errors is the friction between rigid sidewall and flexible wall. This friction could cause wall deformation streamwise and spanwise as well as overloading the wall jacks. To remove this friction in SSWT and TSWT a physical clearance between flexible wall and sidewall was introduced with a light rubber seal to prevent flow. However vibration levels in transonic wind tunnels will assist in overcoming this friction.

So in the two flexible walled test sections designed at Southampton University, the magnitudes of the differences between wall and streamline contours have been reduced below the chosen wall setting tolerance everywhere along the wall. The wall position errors have been minimised by:-

1) grouping the wall jacks closely together, with the closest spacing where the greatest wall curvature occurs, i.e. adjacent to the model.

2) arranging for the pressure inside and outside of the flexible walls to be nominally equal, and making the flexible wall sufficiently rigid to withstand the residual pressure loads.

3) employing jack to wall flexures with stiffness very much less than that of the wall.

4) using feather-edge rubber seals between the flexible walls and sidewalls.

4.5.3 Accuracy of the imaginary flowfield calculations

The wall setting strategy described in Chapter 8 is fundamentally important to the satisfactory performance of the flexible walled test section. Basically the strategy must give rapid convergence of the walls to streamline shapes, and must require only simple software so that the strategy is quick and easy to use. The need for simple software implies that the wall setting algorithm is likely to have an approximate theoretical base.

With the current version of the wall setting strategy the flexible wall is represented by a vortex sheet which is assumed flat for the purpose of assessing both the required wall movements and the external imaginary velocities for the new wall shapes. Usually the flexible walls are curved. Hence the calculations contain a small error due to this assumption about the wall shape.

Since the majority of wall streamlining is achieved in the first iteration away from straight walls, the first iteration case was used by Judd [27,28] as a basis for estimating the error due to this approximation in the strategy. He shows that a conservative estimate of the velocity error Δu at the model due to the approximation is given by

$$\frac{\Delta u}{u_\infty} = -\ 1/2\ (\text{Maximum wall slope})^2$$

Even with a high lift coefficient of 5 and a shallow test section with a depth to model chord ratio of unity (h/c = 1), this leads to an estimated error in C_L of less than 2%. Hence, the assumption that the walls are flat is thought to be acceptable for most testing.

The two-dimensional streamtube to which the model responds is in fact bounded by the wall displacement thickness contours. There is a change in wall boundary layer displacement thickness from aerodynamically straight walls/empty test section to streamlined walls/model installed, which the strategy assumes is small. Analysis of wall pressures from SSWT and TSWT tests has shown that the change in displacement thickness can be of the order 0.5mm (0.02 inch). However at high transonic speeds, where shock/boundary layer interactions occur at the walls the change in wall displacement thickness can be of the order .254mm (0.1 inch) as discussed in Chapter 10.

While the accuracy of the wall setting strategy seems adequate at moderate Mach numbers, the option remains to monitor the maximum slope of the wall displacement thickness contours and apply corrections to the freestream velocity. For TSWT testing, the wall setting strategy has been assumed to have levels of accuracy comparable with that of the overall experimental procedure and no corrections have been applied.

5. DESCRIPTION OF THE LOW SPEED TUNNEL

The low speed facility called the Self-Streamlining Wind Tunnel (SSWT), was commissioned during 1973. SSWT was conceived as a simple research tool to investigate the feasibility of flexible wall techniques in two dimensional wind tunnel testing.

An existing atmospheric open return low speed fan driven wind tunnel was utilised with a new flexible walled test section insert[9,28]. Briefly, in its developed version, the test section consisted of a streamlined portion 69.67cm (27.43 inches) in length, with a flexible floor and ceiling controlled by a system of 18 thumb screw jacks. In its final form the nominal test section height was 15.24cm (6 inches) and its width was 30.48cm (12 inches). A schematic diagram of the test section is shown in Figure 5.1. There was no sidewall boundary layer treatment.

The SSWT design was based largely on engineering judgment using as a guide some estimates of streamline curvature using a severe case of the potential flow around a high blockage cylinder. The flexible wall material was acrylic plastic with a thickness of 1.59mm (0.0625 inch), chosen for its flexibility. A low stiffness wall of this type requires the pressure loading to be small and this was achieved by venting the volumes between flexible walls and the test section structure to the downstream end of the test section. Since wall pressure loading and streamline curvature were expected to peak near the model, wall jacks were pitched closer together in this region than elsewhere. So at the upstream and downstream ends of each wall, the jack spacing was 7.62cm (3 inches) reducing to 2.54cm (1 inch) in the middle portion of each wall. This choice of jack layout was substantiated later by theoretical analysis and is now regarded as near optimum.

The flexible walls are anchored at the fixed contraction. The free ends of the flexible walls formed an open jet at the downstream end of the test section. Minor modifications to the test section were prompted from time to time by aerodynamic considerations during its six

years of operation. Development changes have included the introduction of more symmetry into the test section geometry by the addition of two extra jacks and a length of straight wall to the downstream end of the test section. This was necessary to minimise the aerodynamic effects of length truncation. After beginning tests with an aerofoil it was found necessary to improve the control of wall shape near the model and a wall jack was added on each wall roughly in line with the leading edge.

The SSWT streamlining operation was manual with data reduction on a remote computer. Wing and model pressures were measured from a manometer bank. Wall adjustments were made with the thumb screw jacks, with wall position measured by a dial gauge depth micrometer. Initially, data reduction was performed on a WANG minicomputer with the associated BASIC software stored in six parts on punched tape. Analysis of the "wall data" could take up to two hours. Later the software was manipulated into a single FORTRAN program running on a DEC PDP 11/45 computer, with an execution time of about 18 seconds. Despite this speed-up the procedure of wall streamlining with SSWT remained impractically long, the wall setting time still being several hours. However, the quality of the data from this simple flexible walled test section has led to the development of the more complex transonic test section (TSWT).

6. DESCRIPTION OF THE TRANSONIC FACILITY

6.1 Wind Tunnel Aerodynamic Lines

The new flexible walled test section was designed to insert into an existing induced flow closed circuit atmospheric wind tunnel[29] with stagnation conditions of ambient pressure and temperature. Mach number in the tunnel is continuously variable from low subsonic to low supersonic by adjustment of inducing air pressure and test section wall contours.

The wind tunnel run time varies from near infinity at low speeds to a maximum of approximately three minutes at high speeds, using existing dried air compressor plant to drive the tunnel. Inducing air pressure control is handled by a pneumatic Fisher control valve system which allows the rapid setting up of test Mach number and provides good stabilisation of test Mach number despite the falling compressed air reservoir pressure experienced, particularly during a high speed run.

The nominal test section dimensions for which the wind tunnel was originally designed are width 15.24cm (6 inches), depth 22.86cm (9 inches) and length 2.03 metres (80 inches). There is a series of screens mounted in the settling chamber upstream of the contraction for flow smoothing while the injectors and the associated inducing air jets are downstream of the test section (see Figure 6.1). The tunnel cross-section at the screens is 91.44cm (36 inches) square. There is an air vent in the return circuit of the tunnel to maintain ambient conditions.

6.2 Flexible Walled Test Section

6.2.1 Layout

The layout of this new test section was chosen from experience with SSWT, and the results of the analysis of (i) interferences due to the finite dimensions of the test section and (ii) interferences due to

the imperfections of the wall contouring, (discussed in Chapter 4). In addition there was a desire to use existing sidewalls to minimise the construction time of the new test section.

The design philosophy was based on the aerodynamic requirements of testing a well known two dimensional validation aerofoil of 10.16cm (4 inches) chord over a range of Mach numbers and angles of attack and attempt to obtain interference-free pressure distributions. The testing of three dimensional models was also anticipated at the design stage by incorporating more pressure tappings than were needed purely for two-dimensional testing.

A schematic layout of the test section is shown on Figure 6.1 which represents what is currently regarded as a 'classical' (near optimum) design of a flexible walled test section.

The test section is 15.24cm (6 inches) wide and is shown at a nominal depth of 15.24cm (6 inches). Provision is made for varying the depth to a minimum of 7.62cm (3 inches) to allow investigation of changes to this dimension if necessary. Each flexible wall, 1.12 metres (44 inches) in length is anchored to the fixed contraction and is positioned by a system of 20 jacks. The 20th and last downstream jack controls the free end of the flexible wall in a sliding joint coupled to a variable diffuser. Hence, the streamlined section of the test section effectively extends from jack 1 to jack 19 on each wall. With the test section at its 15.24 cm (6 inch) depth, the contraction ratio is 36:1.

The flexible walls are made from woven man-made fibre (Terylene) laminate and deform between jacks to contours dictated by structural properties, rather than following streamlines. Substantiated by the analysis described in Section 4.5.2. there are eight closely grouped jacks per wall near the model with a spacing of 2.54cm (1 inch), while upstream and downstream of the model the jack spacing increases to 1.62cm (3 inches) as shown on Figure 6.1.

The jacks are housed in the test section 'backbones' which are large castings to support the heavy sidewall plates. The volumes formed

between backbones and walls are vented to the test section at the variable diffuser, as a means to minimise wall pressure loading. The walls are 5mm (.2 inch) thick at their ends, with a central portion delaminated to a thickness of 2.5mm (.1 inch) coinciding with the closely grouped jacks.

There is a clearance of approximately .8mm (0.03 inch) between the flexible walls and the rigid sidewalls to allow free movement. The gap is closed with a rubber seal bonded to the flexible wall (a feathered edge on the seal touching the sidewall) to prevent inflow and outflow of air around the walls.

The two dimensional aerofoil model is mounted horizontally on windows integral with the rigid sidewalls as shown by the picture on Figure 6.2. There is no provision for sidewall boundary layer control. The quarter chord point of the model translates vertically with change in angle of attack to minimise wall curvature and to help centralise the model between the wall in the presence of increasing up and downwash (see Section 4.4.2).

The tunnel freestream Mach number is determined from the static reference pressure measured on the sidewall in the plane of the flexible wall anchor points, as shown on Figure 6.1, and the total reference pressure is measured just downstream of the screens in the settling chamber.

A pitot rake has been positioned on each flexible wall between jacks 19 and 20 (see Figure 6.1) to search for a potential flow core between the wall boundary layer and the model wake. Experience at low speed has indicated that under certain conditions near model stall, the wall boundary layer and model wake mix invalidating the underlying assumptions which are essential to wall streamlining (see Chapter 4).

6.2.2 Wall jacks

From the outset, the test section was designed for closed loop on-line computer control. As a result the complexity of each jack has

increased compared with the earlier manually adjusted test section because of the drive motor and gears and also because each jack is now required to communicate with the computer to facilitate

1. Transmission of position information.
2. Transmission of wall static pressure information.
3. Change of wall position.

These demands are in addition to mechanical features required to prevent spanwise wall curvature. The layout of a single wall jack is shown on Figure 6.3. The design was constrained by the requirements of jack spacing and ease of construction and maintenance.

Consideration of theoretical streamline shapes around a symmetrical aerofoil in transonic infinite flow led to the choice of a minimum of 2.54cm (1 inch) jack travel. The movement limit happens only to be fixed by the position sensing device, and the jack travel can be set anywhere within 5.08cm (2 inches) of available mechanical travel. In TSWT, the jacks numbered 16 to 20 on each wall are biased to move away from the centreline, so that wall streamlining can be achieved round thick model wakes.

A wall setting accuracy of 0.127mm (.005 inch) was chosen from experience with SSWT and by analysis of wall setting errors (see Chapter 4). A linear potentiometer (Sakae 20 LP 30) provides simple analogue information on the wall position and since the device is connected directly to the connecting bar which is directly coupled to the wall (as shown on Figure 6.3) there is an added advantage of removing the need for anti-backlash mechanisms in the jack design.

The jacks 1 to 19 are attached to the wall by thin metal flexures and ribs. The ribs are bonded and screwed to the wall and each supports three surface static pressure tappings which are connected to the data acquisition system. One tap is on the tunnel centreline and one 5.04cm (2 inches) on either side of the centreline, although only the centreline tap is used for two dimensional testing. The metal flexures accommodate varying local wall slopes and allow wall 'pull-up' due to

wall curvature. The flexures have a short free length (6.35mm (.25 inch)) to prevent buckling under compressive loading.

Each jack is driven through a worm reduction gear by a stepper motor (SLO-SYN M051-DW601) allowing easy digital control by a computer. Simple electronic control logic with latches loaded with direction information, allows the computer to send a 'go' pulse to the wind tunnel to increment the motor a predetermined number of steps, or indefinitely, until a 'stop' pulse is sent. Each step corresponds to 15^{o} of motor shaft rotation. Hence there are twenty-four steps per motor shaft revolution which corresponds to a wall movement of .035mm (.0014 inch).

Since forty jacks were required for TSWT, a prototype jack rig was built to evaluate the chosen wall jack hardware, layout and ease of operation. The prototype is shown on Figure 6.4. Maximum motor power was achieved at a step rate of 200 Hz giving a wall movement of .304mm (.012 inch) per second. Calibration of the linear potentiometer has demonstrated a linearity of .038mm (.0015 inch) which is 0.13% of its full 30mm (1.18 inches) stroke. The prototype rig simulated a wall jack in situ with adjacent fixed jacks. The rig demonstrated that a single jack has sufficient power available to contour the flexible wall but insufficient to damage either the jack flexures or the wall itself (see Figure 6.5).

The compactness of the new test section imposed severe constraints on the wall jack layout,particularly in the region of close jack spacing. Both stepper motors and linear potentiometers had to be mounted clear of the jacking mechanism. In addition, the stepper motors for adjacent jacks were mounted on alternate sides of the test section (see Figure 6.5).

6.2.3 Data acquisition system

Data acquisition involves computer sampling of tunnel and model pressures from a semi-continuous wind tunnel. For this application a Scanivalve system is the most efficient method of converting pressures to analogue signals for computer sampling.

TSWT is fitted with a Scanivalve module system consisting of a solenoid drive coupled to four 48 port scanner modules and an encoder. Hence four pressure transducers can rapidly sample 192 inputs. The minimum number of inputs for two-dimensional testing is eighty-six: 38 wall pressures plus top and bottom wall/backbone volume pressures. tunnel reference static and stagnation pressure plus a model dependent number of pressures (i.e. 44 for the 0012-64 section). In practice. more inputs were required for the pitot rake (8 pressures) and the NPL 9510 model (50 pressures in total). The Scanivalve may be stepped manually or by a computer.

One transducer is rated at 103.4kN/m^2 (15 PSI) maximum differential pressure. while the other three are rated at 17.2kN/m^2 (2.5 PSI). The 15 PSI type transducer. referenced to atmosphere. monitors the reference static pressure every sixth port during the 48 port scan. and handles large suction pressures on the aerofoil model. in addition to the reference total pressure and pitot rake pressures. All 2.5 PSI type transducers are referenced to the tunnel reference pressure. and handle all other tunnel wall and model pressures.

Signal levels from the four transducers are low. of the order 14 milli-volts at maximum pressure. The analogue to digital converter used has a ±5 volt range. so some signal conditioning was required to achieve a pressure resolution better than 0.25mm (.01 inch) Hg. Simple operational amplifiers giving a gain of about 290 on the 15 PSI transducer output and about 180 on all 2.5 PSI transducer outputs were used. No short term drift in the outputs of the transducer bridge circuits and amplifiers was observed. Zero readings were taken from each transducer before each tunnel run to minimise the effects of long term drift.

The rise time of the transducers was at worst 20 milli-seconds. nevertheless a dwell of at least 50 milli-seconds at each port has been used. Each recorded transducer signal was an average of fifteen samples taken at a kilo-hertz to minimise noise interference. A manually controlled 48 port scan took approximately 20 seconds. Automatic control has reduced this time to about 6 seconds.

A mercury manometer bank was used to monitor nine tunnel and model pressures during each run. Computed values of these nine pressures make calibration checks available with each run.

Before each test session, the stagnation temperature in TSWT (measured by a thermocouple device) was read by the computer via an analogue to digital converter. Ambient pressure and test conditions were fed to the computer by the operator.

6.3 Test Section Control System

The operating procedure outlined in Section 2.2 has been applied to TSWT operation. The main functions of the online computer control system for TSWT are:

a) to streamline the flexible walls

b) to acquire test data from the model.

The basis of the control system is shown in Figure 6.6. The indicated interaction between wind tunnel, operator and computer generates the required test data. Note that Mach number control is manual and that test parameters such as angle of attack and ambient pressure are manually fed into the computer.

The basic operation of the self streamlining wind tunnel relies on a continual exchange of information between tunnel walls and computer. Briefly there are two control loops, one for Scanivalve control and one for wall shape control. Each loop relies on a complex interaction of tunnel and computer hardware with the computer software.

6.3.1 Hardware

The anticipated hardware layout of the TSWT control system is shown on Figure 6.7 . The system is complete except for the system monitor. The heart of the complete system is a dedicated DEC PDP 11/34

computer which communicates with the wind tunnel through its peripheral devices using digital and analogue signals. The system hardware is designed for four functions:-

i) Wall movement.
ii) Wall and model pressure sensing.
iii) Wall position sensing.
iv) System monitoring functions.

The wall movement function involves the loading of 4 bits of direction data onto each of forty motor latch boards. Each motor then 'knows' whether to stop, forward-go or reverse-go when the power is switched on. This data is check read after loading using a 'write before read' command. Finally a 'go' pulse is sent to the single pulse sequence generator board. Up to forty stepper motors then move through a pre-determined number of steps. The wall has then moved one increment, set by a variable and programmable time limit, giving between .05mm (.002 inch) and .12mm (.048 inch) of movement. On completion of the move a 'finished' pulse is sent to the computer from the pulse sequence generator. The control sequence repeats until the two walls are correctly contoured.

The wall and model pressure measurement function is a sequence which involves the driving of the Scanivalve by a series of 'step' pulses. The Scanivalve begins its scan from a known starting point, and dwells on each port to allow for stabilisation of pressures and then averaged transducer signals are recorded by the computer. The Scanivalve encoder indicates to the computer that steps have occurred relative to the start position. Provision is made for a 'Scanivalve home' command which will ensure the Scanivalve is set on port 48, the normal starting point, when the system is initialised.

The wall position sensing function is simply the computer sampling of the output from each of forty linear potentiometers after suitable signal conditioning. All of these analogue signals are, in

theory, continually available for sampling during a run. However care must be taken to minimise electrical interference between these channels and the motor control system, if the wall position is to be sampled while the wall moves. For this tunnel the potentiometer outputs are not isolated and cannot be usefully sampled while the walls are moving.

The system monitoring function was intended for pure 'housekeeping'. The monitor would provide information on system faults and may allow rapid error diagnosis as well as provide additional protection against accidents. On request from the host computer, the system monitor could give a status check on all power supplies (there are eight in all) plus selected system hardware, with up to 16 bits of information. This has not yet been incorporated due to the reasonable reliability of the current system.

The computer system integrated with TSWT is shown on Figure 6.8. Both digital and analogue hardware have been designed to interface with a DEC system, but generalisations can be made. Analogue input is relatively straightforward while digital input/output is more hardware dependant. However the digital system increases system versatility and reduces system complexity by eliminating the need for a large number of wire connections between wind tunnel and computer.

The 45 analogue inputs to the computer are conditioned to the requirements of resolution set by the DEC AD-11K module and the AM-11K expansion multiplexer which constitute a 64-channel 12 bit analogue to digital converter system which gives a resolution of 1 part in 4096 over a range of ±5 volts. A settling delay of 30 micro-seconds has to be provided by the software for each analogue to digital conversion. This conversion can be initiated under program control, or by overflow of the real time programmable clock.

Digital input/output is controlled by the DEC DR-11K module which provides 16 bits of input and output plus control bit input/output. Each 16 bit signal is coded in BCD at standard high and low levels of 0 and 5 volts. Digital outputs to the control system consist of 6 bits of address, 3 bits of control data and 4 bits of information. Digital

input is simply up to 16 bits of hardware-generated information (see Appendix C). The transmission of digital signals is performed with computer/wind tunnel handshaking under software control and address decoder control.

The address decoder is the 'telephone exchange' of the digital control system. Digital data bits are transmitted to all fifty-two hardware devices but only one device, that selected by the address decoder, can read the data. Similarly for digital inputs, the address decoder selects under software control what information the computer reads. Having 6 address bits, the address decoder has the capability of addressing 64 different devices.

The hardware layout of the control system shown in Figure 6.6 has been simplified. In practice there are more control lines between the system devices and the computer for synchronisation purposes. These links are vital to any digital system to prevent 'race' problems.

The operation of the control system can be monitored from a command VDU console. The tunnel operator is able to display test data in real time, with the facility of hard copy on a DECwriter and/or a Tektronix 4662 XY plotter. Stagnation temperature in the tunnel is fed direct to the computer via a thermocouple device. Stagnation pressure and model angle of attack have to be fed to the computer by the tunnel operator.

There is growth potential in the system with 19 spare analogue channels and 12 digital device addresses unused. Automatic control of a wake traverse is presently performed by addressing the traverse as a wall jack as described in Section 6.4. In the future on-line control of test parameters such as Mach number and model angle of attack may be incorporated. The facility will only then have the full advantages of a conventional computer/tunnel combination in terms of repeatability and efficiency of operation.

The option still remains to move the test section walls with a manual control system used in early TSWT development. This system allows

each wall jack to be individually selected and moved to a known position. This system now provides means of checking the jack hardware independently of the computer, (see Figure 6.8).

6.3.2 Software

Computer software has been developed for the on-line control system using a versatile modular architecture. Hence the main program has been reduced to a collection of manageable subprograms which can be combined to control the wind tunnel and output real time results, or provide more detailed re-analysis of previously acquired data.

An overview of the control software package is shown below.

File type	File Name	Function
Main Program (TSWT)	OFLEX	i) Control and sequence subroutine calls. ii) Read test parameters from the operator.
Subroutine 1 (DATA)	OAD	Acquire pressure data from the wind tunnel.
Subroutine 2 (REDUCE)	ODR	Read tunnel data from disc storage and reduce raw pressure data from the wind tunnel.
Subroutine 3 (WAS)	OJUDD	Perform wall setting calculations.
Subroutine 4 (STAR)	ODST	Calculate local boundary layer displacement thickness and Mach number along each wall.
Subroutine 5 (SUME)	OERR	Assess wall induced interferences at the model.

Subroutine 6 (FORCE)	OWING ONPL	Calculation of model forces for NACA 0012-64 and NPL 9510 sections respectively.
Subroutine 7 (SET)	OUT	i) Store run data on disc. ii) Output data to the terminal and/or the plotter.
Subroutine 8 (WALL)	OADJ	Move the walls to new contours.

This breakdown of the software into modules has been extremely useful. particularly for storage, editing and debugging purposes.

The software. written in FORTRAN IV language, is run on a DEC PDP 11/34 with a DEC RT-11 V4 operating system. The software is linked to a system library and a FORTRAN library to access functions and system subroutines and a Real Time System Library (RTSL) to access peripheral control subroutines. The complete compiled and linked program requires over 100 blocks (25.6k words) of memory.

Current 16-bit computer processors are only capable of addressing 32k words (64k bytes) of real memory space. But of this. only 22k words of storage is available in the PDP 11/34 memory for a user's program. This storage capacity is dependent on the size of the operating system. Therefore. to run the TSWT control software on the PDP 11/34 a technique of overlaying has to be used. so that only part of the software is stored in the real memory at any instant during execution.

Each subroutine is a self contained program communicating with the main program via common data blocks, so in theory only one subroutine is required in the real memory at any one time for execution. In practice. the subroutines have been grouped together to minimise the number of overlays thereby reducing the time required for overlaying itself. The overlaying structure of the control software is shown below

TABLE

	Segment 1	Segment 2	
Overlay Region	Subroutine 1 Subroutine 2 Subroutine 3 7762 words	Subroutine 5 Subroutine 6 Subroutine 7 Subroutine 8 6558 words	7762 words
Root Segment	Main Program + System Library FORTRAN Library RTSL Library		9470 words

This program structure is implemented at 'Link' time during the program cycle as below.

```
R LINK.
*OFLEX = OFLEX,FORLIB,RTSL/C
*OAD,ODR,OJUDD/O:1/C
*OERR,ONPL,O UT,OADJ/D:1
*ONPL,OUT,OADJ/O:1
```

These commands generated a runable program called OFLEX. The program memory requirement drops from 27k words to 17.3k words.

At 'Run time'. the program OFLEX requires that four data files exist on the computer storage device. Data file ADC.DAT receives the raw analogue-to-digital counts of the 'wall' and 'model' data for each streamlining iteration. PAD.DAT provides and receives sets of wall contours and the associated external imaginary wall velocity distributions; NPL.DAT or WING.DAT receives pressure coefficients from the NPL 9510 and NACA 0012-64 models respectively for each streamlining iteration. TSWT.DAT holds all fixed tunnel data. i.e. jack positions. potentiometer calibrations. scaling and coupling factors. matrix coefficients for camber interference assessment. and boundary layer information. RUN.DAT holds run data i.e. ambient temperature and

pressure, run number, iteration record number, and the number of model tappings. The data files ADC.DAT, PAD.DAT and NPL.DAT/WING.DAT each hold 50 records: Records 1 to 3 in PAD.DAT hold data on the three aerodynamically straight contours described in Chapter 6. Records 4 to 50 are available to store data from each streamlining iteration. Hence iteration record numbers range from 4 to 50. When the record iteration number equals 50, ADC.DAT, PAD.DAT and NPL.DAT/WING.DAT must be copied since the original data is then overwritten by subsequent iterations. The upper limit on the iteration record number has been set to keep the size of the data files in manageable proportions (i.e. 25.6k words maximum). The total storage requirement for data files is 61.7k words.

A complete listing of the control software is described in Appendix C. Where possible, standard FORTRAN has been used but peripheral control commands are peculiar to the DEC system used. These subroutine calls can be grouped into Analogue to Digital sampling commands (ADC and RTS) and programmable clock commands (SETR and LWAIT). In addition there are calls to the system library routines (IPEEK and IPOKE) for digital input and output.

An example of the brief print-out from the control software is described in Appendix C. This print-out can be extended if necessary, to encompass more test information.

The versatility of the software has allowed simple generation of programs for particular tasks such as straight wall streamlining (see Chapter 6) and tunnel data re-analysis. Using the existing subroutines as building blocks, each program has been made up of a series of these subroutines linked to a new main program. For example, data re-analysis is achieved by running the program ORLEX (see Appendix C). The main program OREF is a modification of OFLEX with different subroutine calls and an extended print out trigger set. The program structure is very similar to that for the control software and is implemented with the following link command with a memory requirement of 17.1k words.

```
R LINK
*ORLEX = OREF,FORLIB,RTSL/C
```

```
*OAD,ODR,OJUDD/O:1/C
*OERR,ODST/O:1/C
*ONPL,OUT/O:1.
```

An example of the print-out is described in Appendix C.

Should any new analysis technique become available. then a new subroutine could replace or supplement the existing subroutines, as appropriate in program ORLEX and OFLEX.

During TSWT development numerous programs have been used to check sections of the control software. A number of these remain in use to assist with TSWT operation as follows:

i) Set both walls to known contours together or individually.

ii) Allow operator modification of known wall contours for research purposes.

iii) Display current position of both walls.

iv) Display and/or load contents of any specified data record.

In addition programs have been written to command the Tektronix 4662 plotter to display model pressure distributions. flexible wall Mach number distributions and wall shapes.

6.3.3 Safety features

The control system is complex and numerous safety features are included in both the hardware and software to guard against the many possible system failures. These features will hopefully prevent physical damage to the test section and ensure that valid data is received by the computer.

The hardware has the following safety features:

1) Wall adjustment is made as a series of safe increments of movement which allows continual checking of jack/potentiometer performance.

2) Pressure data scan includes a sample of the tunnel static reference pressure every sixth port during each scan.

3) Flexible walls and flexures are strong enough to withstand the full stall force of a single jack.

4) An electronic guard against accidental jack power-on at system switch-on.

In addition. there are the following software system checks.

1) Jack movement direction information is checked after loading.

2) Jack position information is sampled after each increment of movement.

For a production system. a useful feature would be a need for a hardware time switch on the motor power supplies independent of the computer. The jacks would then only be able to move during a specified time interval. safeguarding against computer failure. Also. feedback of the Scanivalve port position would positively confirm the authenticity of the pressure data read by the computer.

In addition. the incorporation of a system monitor would allow regular software safety checks throughout the tunnel run. Hence the failure of certain important items of system hardware could be detected earlier and remedial action taken sooner in the tunnel operating sequence.

6.3.4 Operation

The speed of operating TSWT has always been paced by the state of the control system. The TSWT control system has passed through four distinct development stages:

Stage	Description	Computer Support
1)	Manual mode as for SSWT	Remote WANG, then Remote PDP 11/45
2)	Semi-manual mode with on-line data acquisition of tunnel pressures.	Dedicated PDP 11/34
3)	Semi-manual mode with on-line computer control of wall shape	
4)	Automatic mode for on-line computer controlled wall streamlining.	

Operating in the manual mode. TSWT offered a considerable advance over SSWT with the use of a manual jack control system as shown on Figure 6.8[16]. This device allows each of the jack motor and linear potentiometer pairs to be individually selected for wall adjustment. and is still available for use with TSWT. Then a manually stepped Scanivalve data acquisition system was introduced. which provided a direct data link between wind tunnel and computer. TSWT operation then became semi-manual and allowed aerodynamic testing to proceed with unaccustomed haste. since wall setting times were reduced to less than an hour.

When on-line computer control of the wall shape was introduced (see Figure 6.8). the final stage in automation was taken. After extensive use of the computer for controlling wall shape. sufficient confidence had been gained to devise an automatic system. In fact. this automatic system was also effected by aerodynamic considerations and hardware experience gained throughout TSWT development.

A typical streamlining cycle can now take less than two minutes. The actual time will depend on the severity of changes in test conditions between subsequent cycles which dictates the magnitude of the demanded wall movement as discussed in Chapter 10. A cycle now consists of the following stages:

1) The model is set to a required angle of attack if a change is necessary or may even be replaced with a different model.

2) The test section walls are set to known contours from previous tests, which may or may not require actual wall movement.

3) The control software is actuated and the test conditions are manually entered into the computer memory by the tunnel operator.

4) The tunnel air is turned on and the test Mach number is stabilised by adjustments of the inducing air pressure, or at high speeds by adjusting a downstream throat (see Chapter 10).

5) The tunnel pressures are scanned by the computer.

6) The computer analyses the tunnel pressures and generates a new set of wall contours.

7) The computer assesses the quality of the wall streamlining and displays its findings to the tunnel operator.

8) If the streamlining criteria have not been satisfied the walls are adjusted to new wall contours in incremental wall movement steps, with all jacks travelling at the same speed. Then stages 5 to 8 are repeated until the walls are streamlined.

9) Model test data and tunnel test information are available to be displayed on a VDU and line-printer.

For small wall adjustments at moderate speeds it is possible to have the tunnel running throughout the streamlining cycle. Otherwise the tunnel

air is turned on and off between each iteration to minimise air consumption while ensuring the correct test Mach number is stabilised for each scan of the tunnel pressures.

All sets of raw pressure data and wall contours during a streamlining cycle are loaded onto the computer's disc storage device. Therefore subsequent re-analysis or plotting of model or wall data is routine. using software mentioned in Section 6.3.2.

The development goal has been to achieve minimal wall setting times. Initially improvements with the wall setting strategy reduced the number of actual wall adjustments. More recently. the introduction of wall setting automation has reduced actual wall adjustment times. Future reductions in the wall setting time. if considered necessary. will only be possible with quicker jack movement and consistent wall streamlining in one iteration. Initial wall streamlining with SSWT took of the order of two working weeks! TSWT operation offers a dramatic reduction in time to a few minutes.

6.4 Wake Traverse System

6.4.1 Hardware

An existing rigid sidewall plate has been modified to carry a pitot-static probe with its jacking mechanism[30] (see Figure 6.9). The probe was a combination of a disc-static type with a conventional pitot type as shown on Figure 6.10. Since the probe would be traversed in a region of the test section flow influenced by model induced downwash. the probe design was chosen for its insensitivity to flow angle in one plane. for this particular application, this plane was vertical.

The probe was held in the test section by stainless steel tubes connected to a narrow plate. able to move vertically within a slot cut in the sidewall (see Figure 6.9). This plate was of sufficient length to ensure that the sidewall slot was not uncovered in the test section throughout the range of movement of the probe. The probe was able to move 7.62 cm (3 inches) above and 2.54 cm (1 inch) below the tunnel

centreline. these limits being set by mechanical considerations. However. the entire traverse hardware can be inverted to allow the probe to traverse to 7.62 cm (3 inches) below the tunnel centreline should it become necessary.

The movement band was considered adequate for traversing envisaged high speed wakes and would also allow investigations of the flexible wall boundary layers. Thick model wakes were not expected. since the angle of attack was limited by model loading and the availability of wall movement for streamlining.

The probe was positioned by a jacking mechanism (see Figure 6.9) which was similar to that of a TSWT wall jack. This design feature ensured the traverse was compatible with the wall control system developed for TSWT. The jack was powered by a 3-phase SLO - SYN type M051-DW601 stepper motor connected through a worm reduction gear to a lead screw. to which the probe was attached. The probe translated vertically at a rate of 0.43 mm (.017 inch) per second. This was considered sufficiently slow to allow continual sampling of probe pressures during a steady sweep of the probe.

The vertical position of the probe relative to the tunnel centreline datum was determined by a linear potentiometer with a 10.16 cm (4 inch) stroke capable of a measuring accuracy of ±.01016 cm (±.004 inch). The spanwise position of the probe was set on the tunnel centerline. although there is an option to position the probe off centerline should this prove necessary.

The probe pressures were fed directly to the computer from a transducer, together with tunnel reference pressures.

6.4.2 Software

The software had three functions:

1) Position the probe.
2) Acquire probe and reference pressures.
3) Analyse the pressures to determine the model drag coefficient C_D.

The movement function was achieved in the following manner:

a) The operator informs the computer where the probe is to move to relative to the tunnel centerline.

b) The direction of movement of the probe is determined from its current location. and the traverse jack control system is loaded with direction information.

c) The operator indicates that the traverse can commence by depressing the 'computer-return' key.

d) The probe moves and its position is continually scanned until the desired position is reached within a tolerance of ±0.127 mm (±.005 inch).

Traverse data acquisition was performed by sampling the pressure transducer channels. Each recorded pressure was in fact the average of fifteen samples taken at 1 milli-second intervals. to reduce the effect of signal noise. All pressure signals were referenced to channel 'zeros' taken before each traverse. to eliminate long term amplifier drift.

Each time that the probe position was sampled. it was recorded with the three tunnel and probe pressures as a data set. The reference stagnation pressure was assumed atmospheric. Unfortunately. due to effects of computer 'housekeeping' the data sets were not obtained at regular movement intervals in the traverse.

The reduction of the pressure data was performed off-line using a standard numerical technique[31] to determine the drag coefficient. From this reference

$$C_D = \int_{-\infty}^{+\infty} C_D' \, d(Y/c)$$

where the local drag component in the wake C_D' is given by

$$C_D' = 2\left|\frac{H_1}{H_0}\right|^{\frac{\gamma-1}{2\gamma}} \left|\frac{P_1}{P_0}\right|^{\frac{\gamma+1}{2\gamma}} \left|\frac{\lambda_1}{\lambda_0}\right|^{\frac{1}{2}} \{1 - (1 - \frac{\lambda_2}{\lambda_0})^{\frac{1}{2}}\}$$

where $$H = P + \tfrac{1}{2}\rho V^2 = P(1 + \tfrac{1}{2}\gamma M^2)$$

and $$\lambda_0 \simeq \frac{H_0 - P_0}{P_0} \; ; \quad \lambda_1 \simeq \frac{H_1 - P_1}{P_1} \; ; \quad \lambda_2 \simeq \frac{H_0 - H_1}{H_1}$$

Note suffix 'o' corresponds to local freestream values and suffix '1' to probe values.

The static pressures indicated by the probe were corrected for probe interferences using the calibration curve shown on Figure 6.10 and discussed in the following section. A small correction for the stream displacement effect of the finite size of the probe was also included in the calculation of C_D. No account was taken of the possible contribution to C_D from flow beyond the wake edges arising from small differences which exist between the local freestream and the reference freestream.

6.4.3 Operation and calibration

There are two optional methods for performing a wake traverse in a shallow flexible walled test section. The first option is to streamline the walls around the probe and the model during the wake traverse, giving different streamline contours for each vertical position of the probe. In the second option the walls could be set to streamlined contours found with only the model present in the test section. The walls would then remain fixed throughout each wake traverse. In view of the low blockage of the probe and its mounting tubes, and the fact that they did not form a two dimensional shape, the second method was considered more practical and was used to obtain all the wake data discussed here.

The probe was calibrated for static error in Mike Goodyer's home wind tunnel, then in TSWT with the flexible walls set 'aerodynamically straight' (see Section 6.5) over a range of test Mach numbers up to 0.856. The probe was positioned on the tunnel centerline and a C_p correction was determined, based on the tunnel reference static pressure and reference Mach number. The onset of compressibility is clearly visible in the probe calibration shown on Figure 6.10, at Mach numbers greater than about 0.6.

During each wake traverse the freestream Mach number was held nearly constant by manual adjustments of the inducer air pressure. For wakes thicknesses of the order 2.54 cm (1 inch), the probe traversing speed required the tunnel to be run for about six minutes.

6.5 Tunnel Calibration

6.5.1 Instrumentation

In a streamlining cycle, the tunnel is required to transmit pressure data and jack position data to the control computer. Both sets of data are conveniently transmitted in analogue form to the computers A-D converter. Calibration of the tunnel instrumentation was performed by subjecting the various tunnel transducers to known effects and monitoring the output of the computer 12-bit A-D converter. The resolution of the tunnel transducers was equal to 1 in 4096 A-D counts.

After signal amplification, the pressure transducers had a resolution of 0.33mm Hg on the 103.4kN/m^2 (15 P.S.I.) range device and 0.14mm Hg on the 17.2kN/m^2 (2.5 P.S.I.) range devices. The wall position transducers (linear potentiometers) were resolvable to 0.0003 inch .

The pressure transducers were calibrated to determine the ratio between pressure (cm Hg) and A-D counts. This ratio was found to be 0.03317:1 for the 15 PSI type transducer and an average of 0.014:1 for the 2.5 PSI type transducer. Linearity was found to be better than 0.84mm Hg for the 15 PSI type transducer and 0.25mm Hg for the 2.5 PSI

type transducer. The linear potentiometer was calibrated and gave an average ratio between A-D counts and movement (inches) of 3468:1. The linearity of the potentiometers was found to be better than 0.051mm (0.0025 inch).

The stability of the analogue signals derived from the pressure transducers was monitored during the development phase using the computer. With the wind off, the pressure signal channels showed an average of 4 A-D counts wander over a minute and a half. With wind on, this wander averaged about 6 A-D counts, suggesting a 2 count wander due to airflow instabilities. High frequency fluctuations in the static pressure measurements are dampened by the length of tubing from the static pressure tappings to the Scanivalve system.

6.5.2 Aerodynamically straight walls

The aerodynamic calibration of TSWT was performed with the test section empty.

Four sets of 'aerodynamic straight' wall contours were determined experimentally at freestream Mach numbers of 0.3, 0.5, 0.7 and 0.9.[23] For these contours, allowances have been made for boundary layer growth on the four test section walls, so that the velocity along the walls is nearly constant. For Mach numbers below 0.7 the walls were initially adjusted entirely in accordance with the demands of the wall setting strategy using numerous iterations. At Mach 0.9 the wall adjustment was unsatisfactory since the local wall Mach numbers were very sensitive to wall movement and the wall setting strategy was found to be inadequate. The Mach number distributions along each wall centreline are shown for the Mach 0.3 and 0.9 straight wall cases in Figure 6.11. This plot illustrates the difficulty in setting 'straight walls' at high Mach numbers.

The standard deviation σ of the average Mach numbers between both walls was as follows: Mach 0.5: .0022; Mach 0.7: .004; Mach 0.9: .0034. While these Mach number tolerances were considered satisfactory for testing to proceed, it was noticed that the model was not positioned

symmetrically between the straight walls. This asymmetry in the wall contours was observed in the aerofoil data discussed in Chapter 9 taken with the walls set straight.

This imperfection coupled with a desire to reduce the standard deviation of the wall Mach number distributions spurred a series of TSWT tests to determine a new set of aerodynamically straight wall contours[35]. It had been observed that the variation of "straight" wall contours was a weak function of Mach number. Hence it would appear adequate and would be very convenient to determine only a few such straight wall contours and to designate each as the aerodynamically straight contour for a band of freestream Mach numbers.

In this series of tests the walls were adjusted by use of an old streamlining method[9] due to the evident unsuitability of the current wall setting strategy for this particular task. The relationship between the wall movement δy and the desired change in Mach number δM, which worked satisfactorily with TSWT, was simply $\frac{\delta y}{\delta M}$ = 0.4 to 0.5 inch.

Aerodynamically straight contours (which are stored as a set of readings of the jack position transducers) were determined at reference Mach numbers of 0.7, 0.8 and 0.85, contours A, B and C respectively.[35] During the tests in which these contours were selected the wall adjustments were continued until the variations in the wall Mach numbers were small. The standard deviations of the Mach number at 18 measuring points on each wall from the reference Mach number were then computed, typically lying in the band 0.002 to 0.005. The A Contours are used as the aerodynamically straight contours for all reference Mach numbers M_∞ up to 0.725. Figure 6.12 shows the wall Mach number distributions and σ after streamlining at M_∞ = 0.7 and also for the same contours at M_∞ = 0.3, 0.5, 0.6 and 0.725. The B Contours cover the Mach band 0.725 to 0.825 (see Figure 6.13) and the C Contours the band 0.825 to 0.90 (see Figure 6.14).

On Figures 6.12, 6.13 and 6.14 there is an indication of where an airfoil model of typical chord size would be positioned relative to the test section. Of course no model was present during these tests. The standard deviations may tend to rise with Mach number.

The consequence of running one of the contours at a Mach number outside its designated band of validity does not appear to be serious. For example the B contours when run at Mach 0.85 showed a standard deviation of roughly 0.004.

The standard deviations shown on Figures 6.12, 6.13 and 6.14 are thought to be quite acceptable for immediate purposes, showing that the tunnel and its computer control have adequate precision. The contours are used when necessary as initial wall shapes for the streamlining process with a model present.

It is expected that the control of Mach number with an empty test section will become rapidly more difficult as Mach 1 is approached. Serious attempts have not yet been made to determine aerodynamically straight contours applicable to Mach numbers above 0.9.

The aerodynamic performance of the tunnel has not presented any major problems. There has been no attempt to measure actual flow direction in the test section and the aerodynamic angle of attack of the model is in doubt as discussed later. At low Mach numbers, the inducing air pressure regulated by a Fisher control valve can stabilise freestream Mach number to about 0.002 during a three minute run. At higher Mach numbers, care is required not to reduce the air reservoir pressure too rapidly otherwise the control valve is unable to maintain a constant inducing air pressure. However, with a secondary throat at Jacks 20 for high transonic testing, the flow in the test section can be stabilised aerodynamically as discussed in Chapter 10. In this case, the test section flow Mach number is insensitive to fluctuations in the inducing air pressure.

Turbulence levels present in the test section flow have not been quantified, but operational experience with TSWT indicates that flow steadiness is within acceptable limits for two-dimensional testing.

7. STREAMLINING PROCEDURES AND THE ASSESSMENT OF STREAMLINING QUALITY

7.1 Control Concept

The concept of the control system for a self-streamlining wind tunnel is simply based on the operating procedure outlined in Section 2.2. The streamlining of the flexible walls relies on a comparison of real measured wall pressures and imaginary calculated wall pressures. Both sets of pressures are dependent on the wall shapes only, for a given model attitude and Mach number.

In general, the control concept consists of a feedback loop between the position of the flexible walls and the pressure distributions along the flexible walls. The number of iterations or wall adjustments required for streamlining is a function of the severity of the change in test conditions between successive streamlining cycles, and, more importantly, the adequacy of the predictive wall setting algorithm employed.

Both SSWT and TSWT have been operated extensively in a manual mode. Whilst the control system is based around the wind tunnel and the computer, the link between these two section of the system was provided by the tunnel operator as shown in the flow diagram on Figure 7.1.

Manual operation of SSWT consisted of setting the model to a required attitude and manually adjusting the flexible walls to some start contours, using thumb screws. The tunnel was then run and wall (and optionally model) pressures were recorded from a manometer bank by hand, after which the tunnel was turned off.

The tunnel data was then entered into a computer for data reduction and analysis using two wall setting strategies, one of which was predictive. The computer output gave information on the quality of wall streamlining as described in the next section, and also gave a new set of wall co-ordinates. If the walls were poorly streamlined then another iteration would be required and the walls would be manually set

to the new wall contours and the process repeated until acceptable measures of streamlining were achieved. During each iteration, model data was taken in order to observe the effects of wall movements on its performance.

Manual operation of a flexible walled test section is very slow, and each iteration could for various reasons take up to one working day. Wall setting times for a complete streamlining cycle were strongly dependent on the rapid convergence of the walls to streamlines. The development of the predictive wall setting algorithm described in Chapter 8 dramatically reduced the number of iterations from about eight to, in some cases, only one. This advance, together with introduction of semi-manual adjustment of the flexible walls and semi-automatic data acquisition for TSWT, allowed massive reductions in wall setting times from up to two working weeks to typically one hour.

The nature of this control concept makes it ideally suited to closed loop computer control, and therefore the TSWT control system was devised, providing on-line data acquisition and control of wind tunnel shape. During closed loop operations the operating procedure for a run involves the sequence of events shown in the flow diagram on Figure 7.2.

The pattern of events is the same as for the manual mode of operation except that the wall setting times are so short that the wind tunnel can remain on throughout the entire streamlining cycle. Pressure measurements, which include both test section wall and model static pressures, are taken by a Scanivalve data acquisition system and the walls are set by motorised wall jacks.

The control system reduces to three feedback loops. There is the main control loop which governs wall streamlining and nested within it are the Scanivalve control loop and the jack control loop. With the operator links removed from the main control loop, a streamlining cycle can be completed rapidly.

7.2 Measures of Streamlining Quality

The practical interpretation of the phrase "walls streamlined" requires some explanation. The flexible walls can only be positioned within some tolerance band set by experimental and theoretical features of the system (see Chapter 4). Good streamlining is assumed when the various measures of errors in wall streamlining lie below acceptable limits. For TSWT the measures adopted are:

i) E for each flexible wall, which is the average for all jacks of the modulus of the imbalance in pressure coefficient between real and imaginary flows.

ii) Residual interference effects at the model due to the existence of the pressure imbalances across both flexible walls, in terms of induced angle of attack at the model leading edge, induced camber, and a streamwise velocity error at the 1/4 chord point expressed as an error in C_p.

Experience has shown that for good streamlines E should be less than 0.01 on both walls, and that none of the three components of the residual interference should induce an error in C_L greater than about 0.008. Typically this limit in C_L results in maximum wall induced errors of

$$\alpha : 0.015 \text{ degree}$$
$$\text{Camber} : 0.07 \text{ degree}$$
$$C_p : 0.007$$

These wall induced errors are necessarily based on linearised incompressible theory since the wall loading is presently assessed using linearised incompressible imaginary flowfield calculations. With wall induced errors larger than these values, at high transonic speeds, position errors have been noted in the model shock. Further, it is considered undesirable to apply anything but small corrections to model data in two dimensional transonic testing because of uncertainties in the magnitudes of corrections.

Since during a streamlining cycle the walls provide a sequence of estimates of the magnitudes of residual wall induced lift interferences, it is possible to halt the streamlining cycle at any time with a knowledge of this estimate of streamlining quality in terms of C_L. In assessing wall interference, the loading of a wall is represented by a distribution of vorticity along the wall boundary layer displacement thickness (δ^*) contour. The local magnitude of the vorticity is determined by the imbalance of the real and imaginary wall velocities at a station along the wall. The effects of the wall vorticity are then summed in the region of the model to assess wall induced interferences. Typical effects of streamlining on wall induced velocity perturbations along the centreline of the test section are shown on Figure 7.3 for the case of a NACA 0012-64 aerofoil at $M_\infty = 0.7$ and $\alpha = 4^o$. Gross interference is present with the walls set straight: the non-dimensional horizontal perturbation u/U_∞ shows the blockage effect of the model and its wake; the vertical perturbation v/U_∞ shows a lift interference centered about the 1/4 chord. Both velocity perturbations were reduced in this example to less than 1/4% by streamlining.

Typical variations of corrected and un-corrected model C_Ls are shown for two streamlining cycles on Figure 7.4: (1) $M_\infty = 0.7$; $\alpha = 4^o$ starting from $M_\infty = .7$ straight wall contours (described in Chapter 10). (2) $M_\infty = 0.5$; $\alpha = 4^o$ starting with streamlined walls for $\alpha = 2^o$. The corrections to C_L are for convenience the sums of the estimated effects on C_L of the wall induced effects on α, camber, and velocity or C_p.

It can be seen from the first iteration of cycle (1) that the existence of a small total C_L correction is not a reliable indication that the walls are streamlined. In fact for this iteration the walls were not good streamlines since other measures of streamlining quality were not small. The second iteration shows the corrected C_L value in good agreement with the finally accepted value. This confirms that as long as gross interference effects have been eliminated, small corrections may be applied with confidence.

The plot on Figure 7.4 for cycle (2) illustrates the relative ease of streamlining at low Mach numbers following a small increment in α

between streamlining cycles, and the good accuracy of the small corrections. This evidence suggests that, at least for determining lift during this test, no wall streamlining was necessary since corrections could have been applied.

7.3 Wall Information

The boundary of the flexible walled test section is solid and non-porous, and therefore the wall static pressures and wall positions contain useful information on the model in the test section.

In principle, this 'wall data' can provide information on 1) lift, 2) pitching moment, 3) model wake displacement thickness, 4) model aerodynamic shape, and 5) pressure distribution throughout the test section around the model. However, only lift and model wake displacement thickness have so far been satisfactorily estimated from wall data[32].

The model lift can be extracted from the corresponding forces on the flexible walls together with the vertical components of momentum in the test section flow at the test section ends. A variety of test cases have been analysed for both low speeds and high speeds with the walls streamlined and the walls straight. The average C_L error for all cases analysed (which covered the majority of TSWT testing configurations and Mach numbers) is 0.011.

The displacement thickness of the model wake is immediately available from the movement-apart of the flexible walls downstream of the model after wall streamlining. The flexible walls naturally adjust themselves in a manner returning the flow to the freestream Mach number at the downstream end of the test section. This is achieved by the walls moving apart to allow for the model wake blockage. The relative separation of the walls, compared with straight wall contours, is shown for various model attitudes and Mach numbers on Figure 7.5.

Downstream of the model, markedly different wake thicknesses are evident, produced by changes in lift and shock induced separations on

the model. Interestingly, the curves show the increase of model blockage with Mach number, particularly for the cases of $\alpha = 4^{o}$. This observation highlights the rapid changes of the flowfield characteristics as the supercritical flow region grows about the model with increasing test Mach number.

The 'wall data' can assist with estimates of model performance as well as provide essential information for wall streamlining and assessing induced wall residual interferences, as shown in the previous section. It can be argued that flexible walled test sections can provide much more reliable boundary information than conventional transonic designs, leading to a better knowledge of flow perturbations in the region of the model and perhaps a correctable interference wind tunnel[33].

8. DEVELOPMENT OF A PREDICTIVE WALL SETTING STRATEGY

The wall setting strategy is a fundamental component of the self-streamlining concept described in Section 2.1. A rapid convergence to streamlines depends on the adequacy of the adopted wall setting strategy.

The function of this strategy is twofold:

i) to predict the wall movements required for streamlining.

and ii) to compute a pair of imaginary wall pressure distributions (or velocity perturbations) over these wall contours

In general, for the testing covered by this thesis the viscous effects of the model and its shocks are contained within the test section boundaries and therefore the imaginary flowfields are irrotational. At low speeds the imaginary flowfield can be solved exactly* using potential flow theory.

While theoretical complexity increases as sonic velocity is approached, it can be argued that the imaginary flowfield will always be less complex than the flowfield round the model, partly because it may be treated as inviscid, but also because perturbations at the wall are relatively weak. Hence the accuracy of the imaginary flowfield computations over the wall shapes will be better than theoretical estimates of model performance, whatever the state of the art.

The current wall setting strategy, detailed below, is the product of several development stages involving innovation and continual theoretical and experimental checks. Initial work with SSWT used a non-predictive wall setting strategy,[28] which was soon replaced by a rapid

*This word is used in the mathematical sense. In practice the positions of the wall are only known at discrete points, and here only within a tolerance.

convergence method devised by Judd[28], this reduced the number of iterations per streamlining cycle.

The analytical prediction of the required wall movements is complex but computation time is acceptable. This complexity is partly because of the strong aerodynamic coupling between the two flexible walls which affects the rate of convergence of the wall streamlining process. The consistency of analytical predictions of wall shape is essential for test repeatability.

8.1 Strategy Theory

The basis of Judd's theory[27,28] applies to a single isolated flexible wall adjacent to any wind tunnel model, as shown on Figure 8.1. For the nth iteration the wall will be set to a shape Y_n. Iterations are necessary because the flowfield around the model will change with each wall adjustment. The theory is developed initially for incompressible flow.

The flexible wall is represented by a vortex sheet having a local vorticity $\gamma(\xi)$ derived from the local wall loading at streamwise position ξ, given by the difference between real and imaginary wall velocities. For the nth iteration $\gamma_n(\xi) = U_n(\xi) - V_n(\xi)$, where U_n is the real velocity measured inside a wall, V_n the velocity at the same position on a wall, on the imaginary flowfield side. Since the object of moving the walls is to eliminate this loading, the local normal velocity component induced by the distribution of vorticity has therefore to be replaced by a change in the component of the free stream. In the analysis the vortex sheet is always assumed flat, and velocity perturbations and changes in the wall boundary layer displacement thickness are assumed to be small. Hence the local normal velocity component induced by the vorticity simply becomes the local vertical velocity component. This component is replaced by suitable adjustment of the vertical velocity component of the free stream, achieved by locally modifying the wall slope by an amount

$$\frac{d\Delta Y_n(x)}{dx} = \frac{1}{2\pi U_\infty} \int_{-\infty}^{+\infty} \frac{\gamma_n(\xi)}{(\xi - x)} d\xi \qquad (1)$$

at jack location x for the nth iteration $\frac{d\Delta Y_n(x)}{dx}$ is assumed to be small and is obtained by the interpolation of wall velocities using a cubic spline fit to obtain vorticity strengths at regular points (ξ) between jacks. Numerical integration of the wall loading is then performed along the wall at each jacking point (x), thus avoiding the singularity at ξ = x.

The predicted position of one isolated wall for the next iteration is then

$$Y_{n+1}(x) = Y_n(x) + \Delta Y_n(x) \qquad (2)$$

by straightforward integration of equation (1).

The numerical solution relies on the calculation of the external imaginary wall velocities over the wall shape since the wall vorticity must be known.

The vortex sheet $\gamma_n(x)$ is perturbing the velocities either side of the wall shape $Y_n(x)$ by equal and opposite amounts. On streamlining according to the above procedure giving shape $Y_{n+1}(x)$ the vorticity is eliminated and the external imaginary wall velocity is changed to a value mid-way between those which created the vorticity.

Hence

$$V_{n+1}(x) \simeq \tfrac{1}{2}(U_n(x) + V_n(x)) \qquad (3)$$

If the wall shape $Y_{n+1}(x)$ has been found using this wall setting strategy, then the external velocity distribution over the wall shape is available from known velocity components determined during a previous run. However, to avoid all imaginary flowfield calculations for a starting case it is necessary to start the initial streamlining cycle with aerodynamically straight walls so that

$$V_0(x) = U_\infty = \text{Constant} \qquad (4)$$

In general, the flexible wall and hence the vortex sheet are not flat. Also the flexible wall has a finite length. These deviations from the ideal simplify the theory and account for the approximation of equation (3), and produce streamlining errors which are assessed in Section 4.5.3.

8.2 Modifications of the Strategy to Suppress Wall Coupling Effects

The theory considers only one wall in isolation. When the strategy is applied to both walls a divergent streamlining process can result.

The adaption of the above theory to SSWT operation was not straightforward. During the development period the basis of the theory remained unaltered but detailed changes were introduced to take account of the strong aerodynamic interactions between the flexible walls.

Initial SSWT streamlining cycles with the new wall setting strategy were terminated prematurely due to increasing wall divergence with each wall adjustment. This phenomenon arose largely from the effects of one dimensional flow continuity in the test section. A satisfactory solution was found by forming an analytical link between the wall movements. Convergence to streamlined wall shapes was achieved by feeding a proportion of the demanded movement of one wall to the other wall.

The wall coupling was implemented in the strategy by use of scaling factors a1 and a2 such that the local wall movements for the (n+1)th iteration $\Delta Y_{n+1}(x)_{TOP}$ and $\Delta Y_{n+1}(x)_{BOTTOM}$ for top and bottom walls respectively were given by the equations

$$\left.\begin{aligned} \Delta Y_{n+1}(x)_{TOP} &= \Delta Y'_{n+1}(x)_{TOP} + a2\ \Delta Y'_{n+1}(x)_{BOTTOM} \\ \Delta Y_{n+1}(x)_{BOTTOM} &= \Delta Y'_{n+1}(x)_{BOTTOM} + a1\ \Delta Y'_{n+1}(x)_{TOP} \end{aligned}\right\} \quad (5)$$

where $Y'_{n+1}(x)_{TOP}$ and $Y'_{n+1}(x)_{BOTTOM}$ are the original wall movement demands given by equation (2). Suitable values for a1 and a2 were determined by experiment. Satisfactory wall convergence was obtained with each set to 0.35. Since V_{n+1} is proportional to Y_{n+1} the external velocity distributions for these new wall shapes can be calculated thus

$$\left.\begin{aligned} V_{n+1}(x)_{TOP} &= V'_{n+1}(x)_{TOP} + a2\ V'_{n+1}(x)_{BOTTOM} \\ V_{n+1}(x)_{BOTTOM} &= V'_{n+1}(x)_{BOTTOM} + a1\ V'_{n+1}(x)_{TOP} \end{aligned}\right\} \quad (6)$$

where $V'_{n+1}(x)_{TOP}$ and $V'_{n+1}(x)_{BOTTOM}$ are the external velocities originally calculated for the next wall shape from equation (3). Streamlining cycles of four iterations from straight to streamlined walls and as little as one iteration from previous streamline contours to new streamline wall shapes have been demonstrated with this strategy.

However, it was noticed during the SSWT tests that there was usually an overshoot with the first wall adjustment in a streamlining cycle. To further improve the rate of wall convergence to streamlines, two more scaling factors were introduced to reduce the demanded wall movements (a3 and a4). The predicted wall movements $\Delta\bar{Y}_{n+1}(x)_{TOP}$ and $\Delta\bar{Y}_{n+1}(x)_{BOTTOM}$ were written

$$\begin{aligned} \Delta\bar{Y}_{n+1}(x)_{TOP} &= a3\ \Delta Y'_{n+1}(x)_{TOP} + a2\ (a4\ \Delta Y'_{n+1}(x)_{BOTTOM}) \\ \Delta\bar{Y}_{n+1}(x)_{BOTTOM} &= a4\ \Delta Y'_{n+1}(x)_{BOTTOM} + a1(a3\ \Delta Y'_{n+1}(x)_{TOP}) \end{aligned} \quad (7)$$

for top and bottom walls respectively, with corresponding changes in external wall velocities.

Values of a3 and a4 equal to 0.8 led to further reductions in the number of iterations with typically three iterations required for a streamlining cycle starting from straight walls at the low speeds used in SSWT.

The simplicity of the software required to implement the wall setting strategy was initially offset by computer memory limitations and program storage on paper tape. However, it was possible to analyse both walls at once and also to neglect any allowance for variations in wall boundary layer displacement thickness since these changes were now assumed small. The use of more powerful computers has allowed the full potential of the strategy to be realised. Analysis of both walls now takes about 5 seconds using a DEC PDP 11/34 mini-computer fitted with a Floating Point Processor.

8.3 Introduction of Compressibility Terms

The wall setting strategy with the modifications outlined in the previous section demonstrated rapid convergence of the walls to streamlines at low speeds. However, the need for testing at transonic speeds has led to further modifications of the predictive wall setting strategy to allow for compressibility effects, using linearised theory.

The theory of the wall setting strategy is based on incompressible flow. The compressibility factor β from linearised compressible flow theory, allows the scaling of compressible tunnel parameters and measurements to the incompressible form using

$$C_{p_I} = \beta . C_{p_C} \text{ for wall pressure coefficients}$$

$$\text{and } \Delta Y_{n+1_I}(x) = \frac{\Delta Y_{n+1_C}(x)}{\beta} \text{ for wall movements}$$

where suffix I = Incompressible and c = Compressible.

This scaling allows all the wall adjustment calculations to remain incompressible with only the input and output data associated with the strategy calculations modified for compressibility.

These simple changes to the original wall setting strategy have allowed wall streamlining to be rapidly achieved at Mach numbers up to 0.85. While two iterations normally are required for streamlining at the higher Mach numbers, one iteration streamlining cycles have been demonstrated. Tests have been conducted above Mach 0.85 where the presence of large regions of supercritical flow between the walls and model degraded the rapid convergence of the strategy and probably invalidated the assessment of the wall streamlining quality. This may be due to the reduced validity of linearised theory as Mach number approaches unity. The normally accepted Mach number limit for use of linearised compressible flow theory is 0.8. More important is the inability of linearised theory to represent the sudden pressure rise across a shock wave. These together have led to the apparent breakdown of the wall setting strategy when supercritical flow with strong shocks reaches the walls and extends 'through' into the imaginary flowfields.

The current Mach number limit for satisfactory convergence with a test section height to model chord ratio of 1.5 can only be increased by the development of suitable numerical techniques to solve for the mixed flows in the imaginary flowfields. While methods do exist, they demand more computer time and more computer capacity than is available for this project.

If a simple rapid numerical technique is found for coping with mixed imaginary flowfields, the strategy may be modified so that the wall loadings are determined from the differences between the real measured wall velocities and imaginary wall velocities calculated using the new numerical techniques. The imaginary flowfields could be calculated over the top and bottom wall displacement thickness contours, since the wall boundary layers will be complicated by shock/boundary layer interactions, if a shockwave extends from the model to the walls. The present method of predicting wall movement from the wall loadings is likely to remain, with suitable adjustments to the scaling factors. Whatever form the wall setting strategy takes, there will probably be an analysis time penalty associated with the increased complexity.

8.4 Analytical Validation of the Strategy

During low speed testing at high angles of attack it was found that wall movements and hence wall slopes were becoming large, and it was thought that the strategy theory was perhaps invalidated leading to errors in model performance. Therefore independent checks were made on the external imaginary wall velocities calculated by the wall setting strategy.

These checks were made by applying the original 'source and sink' method of calculating the imaginary wall velocities to the displacement thickness contours [28] of the streamlined walls. The method is applied to each wall separately and reproduces the wall contours as the envelope of appropriate source and sink distributions in a uniform flowfield. The software routines for this method had been extensively checked against exact two dimensional potential flow streamlines.

Raw low speed data from SSWT runs 13, 10 and 4 detailed in Table 2, which are streamlined cases for the representative incidences of 0^{o}, $6^{o}$and 12^{o} respectively, was re-analysed using the 'source-sink' method. As a measure of the wall loadings found using the 'source-sink' method, the average error in pressure coefficient ΔC_p (the difference between real and imaginary Cps) is presented for the twelve jack positions adjacent to the model - six on each wall. Wall-induced flow errors at the model are most strcngly affected by wall loading in these areas. The average errors found were

α	0^{o}	6^{o}	12^{o}
$\frac{\Sigma \lvert \Delta C_p \rvert}{12}$	.0078	.0178	.0182

At worst, the induced velocity error at the model and a corresponding error in pressure coefficient on the model would be equal to the pressure coefficient imbalance at the walls, if there was a uniform error along both walls assumed extended to infinity. In practice, the levels of wall pressure coefficient errors given above would normally generate smaller errors due to randomness in the distributions of the wall loadings, and due to their finite length.

The largest wall error is at $\alpha = 12^{o}$ where the model is stalled and there is a large separated wake downstream of the model, causing sizeable wall movements from straight contours. There were disparities between SSWT and reference model data at this incidence, therefore more wall adjustments were made in an effort to further reduce the wall loading. However no improvement could be made and no significant changes in the model pressure distribution were observed with minor wall adjustments.

These checks proved analytically that streamlining using the predictive wall setting strategy was satisfactory when applied to a low speed two dimensional testing environment. In practice, three dimensional flows can be present in the test section which may affect estimates of model performance made at the model's mid span, as discussed in Chapter 4.

At high subsonic Mach numbers the wall setting strategy imaginary flowfield calculations have been checked by a time marching technique developed by Spurr and Mason[34]. Mach number distributions over known streamlined top wall shapes were computed using the time-marching technique, an example of which is shown on Figure 8.2 for the NACA 0012-64 test case $M_{\infty} = .84$; $\alpha = 2^{o}$. The top wall was just critical, and reasonable agreement between real and imaginary Mach numbers can be observed. The results of this work gave further confidence in the use of the wall setting strategy.

9. VALIDATION OF THE FLEXIBLE WALL TESTING TECHNIQUE

A validation of the concept must ultimately rely on comparisons of data obtained in the new test section with trusted data for the same model derived elsewhere. The latter is called Reference Data. In this chapter such data is presented on several models, derived in order to demonstrate the ability of the flexible walled test section to produce data essentially free from top and bottom wall interference.

9.1 Model Aerodynamic Data from the Low Speed Tunnel

9.1.1 Description of the model

The low speed model was a two dimensioned aerofoil with a NACA 0012-64 section (see Table 1 for surface co-ordinates). This 12% thick symmetrical aerofoil had an aspect ratio of 2.2 with a chord of 13.71cm (5.4 inches) and a span of 30.48cm (12 inches). The model was constructed from stainless steel, by NASA at Langley Research Center.

There were nineteen pressure tappings on each surface positioned at 5% chord intervals, plus a leading edge tapping. All tappings were staggered about the model centerline to prevent local hole interferences. A narrow transition strip was located at about 7% chord, on both surfaces, for all tests.

For some tests in the 7 x 5 wind tunnel at Southampton University and all NASA tests the model was fitted with two wing tip extensions which increased the span to .91 metre (3 feet) and aspect ratio to 6.6. In addition end plates were fitted to suppress three dimensional effects in 7 x 5 tests.

During SSWT tests, leading edge and trailing edge fences were mounted onto the model. The leading edge fences were circular discs 5.84 cm (2.3 inches) in diameter positioned 1.27cm (.5 inch) inboard from the wing tips. The trailing edge fences extended 2.54cm (1 inch) from the model surface over the entire rear three quarters of the chord on both surfaces. The trailing edge fence was also attached to the model 1.27cm (.5 inch) inboard from the wing tips.

9.1.2 Reference data from the NASA Langley Research Center's Low Turbulence Pressure Tunnel (LTPT)

The low speed model was tested in a deep test section to obtain its free air behaviour. LTPT has a test section 213.4cm (84 inches) deep, equivalent to 15.55 chords. The model was fitted with 30.48cm (12 inch) wing tip extensions to span the 91.4cm (36 inch) wide test section.

The reference data was obtained over a Reynolds number range from 264,000 to 319,000. Angle of attack was varied between $+12.176^{o}$ and -8.111^{o}.

There were fifty-five test points which constitute three groups of angle of attack rakes at Reynolds numbers of approximately 317,000. 285.000 and 265,000. For each test point there is information on the model pressure distribution and tunnel pressures. Model forces were calculated from the integrated pressure distributions.

The reference data is tabulated. but is unpublished. All model pressure coefficients were listed. together with force coefficients and a pitching moment coefficient about the leading edge. The data is summarised by the plot of C_L-v-α on Figure 9.1. By fitting least square curves to all available sets of C_L data in the α range $+8^{o}$ to -8^{o}, the slopes are:

LTPT reference data	Slope per radian
Rc ≃ 265,000	4.916
≃ 285,000	4.847
≃ 315,000	4.625

Particularly noticeable is the lift reduction at $\alpha = \pm 6^{o}$ with increasing Reynolds number.

9.1.3 Data from the Low Speed Flexible Walled Tunnel compared with reference data

The series of SSWT tests using the low speed model covered a range of angles of attack from -6^{o} to $+12^{o}$, with the freestream Mach number at approximately 0.1 throughout. Test section height to model chord ratio was 1.1:1. The model tested was the same as used to obtain reference data in LTPT. A summary of the low speed SSWT streamlined runs appears in Table 2.

A complete set of the aerodynamic data has been published[14,16]. A selection of model pressure distributions for angles of attack -6^{o}, -4^{o}, 0^{o}, 8^{o} and 12^{o} are shown on Figure 9.2 compared with LTPT results. For clarity the latter are shown as continuous lines, although they were in fact point measurements. It is clearly seen from these plots that agreement between SSWT and LTPT data is good up to the stall at about 8^{o} angle of attack. However, beyond stall the suction peak in SSWT tests has contributed to the lift coefficients being significantly higher than during corresponding LTPT tests.

This observation is supported by the plot of normal force coefficient C_N and the chordwise coefficient C_c against angle of attack as shown on Figure 9.3 and Figure 9.4 respectively. C_N and C_c are defined on Figure 9.5. Both values are determined from the integrated model pressures.

On Figure 9.3(a), C_N results for LTPT, SSWT streamlined walls and straight walls are plotted below stall. Straight lines have been drawn through the three sets of data using the least squares method. In the range $-6^{o} < \alpha < 7^{o}$ the slopes of the lines and their zero C_N intercepts are

Tunnel	Slope per Radian	Zero C_N Intercept
LTPT	4.924	-.121
SSWT Streamlined Walls	4.797	+.228
SSWT Straight Walls	5.527	-.028

The ratio of streamlined-walls SSWT and LTPT C_N slopes is about 0.97, with an upward shift, in α by about 0.35 degree between LTPT and SSWT values. This shift in angle of attack may be due to sidewall effects. Work by Goodyer has determined the reduction in lift at the model tips and allowed some estimate of spanwise lift distribution to be made. The angle of attack correction due to the finite span of the wing was a few tenths of a degree at $\alpha = 6^{o}$.

At values of α above 8^{o}, differences between SSWT and LTPT data becomes significant. The LTPT curve has a relatively pronounced peak at $\alpha \simeq +9^{o}$ beyond which the slope becomes steeply negative. The SSWT data shows a more gradual rise to a slightly lower maximum C_N at about 11^{o}, followed by a gradual fall in C_N. However, with the SSWT flexible walls set straight, the C_N data indicates no apparent stall and also illustrates the gross interference effects on lift which is normally present in a shallow test section.

The plot of C_c on Figure 9.4 again shows good agreement between the two sets of data except for an apparent upward shift of SSWT angle of attack by about half a degree, roughly in agreement with an equivalent shift in the C_N-v-α data. The straight wall SSWT data diverges at high angles of attack as expected.

A trailing edge stall was expected for the aerofoil and it was thought that secondary flows were preventing complete flow separation on the suction surface. This possible explanation for the discrepancies between LTPT and SSWT results was investigated by use of flow visualisation and simple 'aerodynamic fixes'.

Firstly, leading edge fences described in Section 9.1.1 were fitted for Run 216 at $\alpha = 12^{o}$. The test results plotted on Figure 9.3(b) and 9.4 show that while the model normal force was reduced beyond stall, the original difference between SSWT and LTPT data was only halved. Further tests at $\alpha = +6^{o}$ and $+9^{o}$ yielded little change in C_N or C_c.

Two dimensionality of the flow around the aerofoil was checked by surface flow visualisation. Oil impregnated with fluourescent dye was

deposited in discrete spots on the wing surfaces. After a brief tunnel run, the oil entrained into the surface flow over the model was traced out by the dye. These dye tracks were photographed in ultra violet light and are reproduced on Figure 9.6. The model is set at $\alpha = 12^{o}$, and it will be noticed that the aerofoil in SSWT is set 12^{o} nosedown since the model is mounted upside down.

At $\alpha = 12^{o}$ the flow over the pressure surface appears to be uniform and two dimensional even near the wing fences. However the suction surface patterns are more confused and irregular, with leading edge separation and a large reverse flow region. Only a small leading edge separation bubble was shown by dye on one of the wing fences. Noticeable is the tendency for the dye traces to move towards one side of the wind tunnel, indicating the existence of some three dimensional effects. This problem was resolved by re-gritting the model transition strip, but no significant changes in the aerofoil pressure distribution were noted. Increasing the test section flow area downstream of the streamlined portion of the test section to perhaps allow for the thicker separated wake also produced no significant changes in model performance[14].

An alternative aerodynamic fix was the fitting to the model of trailing edge fences described in Section 9.1.1. After re-streamlining the walls at $\alpha = 12^{o}$, it was found that C_N had increased to worsen the comparison with LTPT values. Surface flow details are shown on Figure 9.7 and are similar to those patterns found with the leading edge fences fitted.

It is known that aerofoil stall is sensitive to freestream turbulence. Although no measure of turbulence levels have been made in SSWT, it is most probably higher than in LTPT causing the effective test Reynolds number to be higher in SSWT than LTPT. The LTPT tests have shown that at some angles of attack the pressures at certain stations on the aerofoil are extremely sensitive to Reynolds number.

To investigate the effect of changes in wind tunnel airspeed on the model, a series of four SSWT runs were performed over a range of R_c

from 170,000 to 370,000 with the flexible wall set to previously determined 'streamlined' shapes for run 180 with $\alpha = 12.1^{o}$ and R_c = 287,000. The walls were not re-streamlined for each change of Reynolds number because of the protracted time the operation was taking with the equipment then in use. The variations of C_N and C_c with Reynolds number are shown on Figure 9.8.

The SSWT data indicates a gradual increase of C_N with R_c and the converse for C_c, although the overall change in values is less than 10%. The LTPT data varied insignificantly over its narrow R_c range. A 25% reduction in C_N and a 30% increase in C_c would be the changes necessary in SSWT data for agreement with LTPT results.

Although the flexible walls were not set to good streamlines during any of these tests, the weak variation of the model force coefficients with Reynolds number indicate that small differences in Reynolds number probably do not account for the data discrepancies. The walls were re-streamlined for the case of R_c = 287,000 for run 228. There were only small changes in the model force coefficients from the unstreamlined run 224. This re-streamlining became necessary because of some changes in the test conditions. Both angle of attack and the transition strip had been re-set. There were still differences between the aerofoil pressure distribution for runs 180 and 228 both with walls streamlined as shown on Figure 9.9. Both tests were nominally at the same Reynolds number and angle of attack with the walls streamlined. These changes may be due to some form of stall hysteresis caused by wall streamlining from different start contours, in addition the changes may be due to differences in the test conditions.

It was thought possible that the flexible walls were impressing an incorrect flow pattern on the stalled model, even when the walls were judged streamlined by wall measurements alone. Large wall movements and associated wall slopes probably invalidate the imaginary flowfield calculations as discussed in Section 4.5.3. These calculations, as part of the wall setting strategy, rely on the model viscous action being contained within the effective aerodynamic contours of the test section walls. This may not have been the case with a stalled model.

A series of wake surveys were made on the low speed model in SSWT at $\alpha = +12^{o}$, $+6^{o}$, 0^{o} and -6^{o}, at a chord Reynolds number of about 287,000. It was intended that these surveys should give some insight into the effect of wall streamlining on model drag and also give information on the existence or otherwise of a potential flow core between model wake and flexible wall boundary layer.

In addition, wake surveys were made on the low speed model mounted in a deep 1.52m (5 feet) by 2.13m (7 feet) test section of the University of Southampton Low Speed (7 x 5) Wind Tunnel. Wing extensions were fitted to the low speed model to minimise three dimensional effects, making the span of the model 91.44cm (3 feet). These tests were intended to provide information on the model wake beyond stall in a flowfield which can be considered free of boundary interferences.

These wake traverses were made 1.25 model chords downstream of the trailing edge and 2.28cm (.9 inch) to the side of the model mid span, as shown on Figure 9.10. Either total or static pressures were measured in a run by the fitting of either a Kiel total probe or a static probe respectively, shown on Figure 9.11. Tunnel reference pressures were taken upstream of the model. Drag coefficient C_D was calculated by numerical integration of the wake's momentum defect.

The wake profile in SSWT for $\alpha = 12^{o}$ with the walls streamlined is shown on Figure 9.12. It is apparent that the wake practically fills the tunnel from floor to ceiling at the traversing plane. Such an extensive wake was not expected and its size may have been enhanced by sidewall separations. Interaction of wake and flexible wall boundary layers would nullify any attempts to streamline the walls downstream of the model. This discovery may account for discrepancies in the aerofoil data at high angles of attack.

For comparison purposes, the wake profile for $\alpha = 12^{o}$ found in the 7 x 5 tests is also shown on Figure 9.12. The 7 x 5 data shows some flow velocity anomalies due to inherent tunnel faults. Nevertheless, there is reasonable agreement with SSWT data in terms of wake depth.

The position of the wake in SSWT appears to have been slightly displaced vertically possibly due to wall induced curvature of the effective tunnel centreline. The drag coefficient found in the 7 x 5 tests is some 17% greater than the value found in SSWT. Meanwhile the lift coefficient found in the 7 x 5 tests is 2% higher than the value found in SSWT. The 7 x 5 data has not been corrected for any three dimensional effects. For the purposes of this comparison, the lift is matched adequately and differences in drag can probably be attributed to the badly defined edges of the wake. It would appear that the wake found in SSWT with streamlined walls is representative of the free air case.

Presumably, downstream of the traversing plane at this angle of attack, there was no region of potential flow in SSWT with 'streamlined' walls. The flowfield is very roughly as indicated in Figure 5(a) of reference 9 which illustrates a possible limit to reduction in test section height. At high angles of attack the streamlining procedure may be invalid and model separation is probably sensitive to wall position. Therefore the current 'wall streamlining' strategy could be inadequate for testing at high angles of attack. A limit to the technique has probably been found in these tests.

This experience suggested that flow at the downstream end of the test section should be monitored to check for the existence of two potential flow zones between the wake and wall boundary layers. This feature was incorporated in the transonic test section.

SSWT tests at smaller α show more acceptable wake profiles. For $\alpha = +6^{o}$, the wake occupied only 17% of the test section height at the traversing plane and the wake experienced a small vertical displacement with streamlining but no significant increase in size as shown on Figure 9.13. This wake displacement is probably the result of the wall movement apart to allow for wake blockage downstream of the model. Note that streamlining of SSWT removes the freestream velocity error due to wake blockage which is present with straight walls. Straight wall data for $\alpha = 0^{o}$ and $\pm 6^{o}$ shown on Figure 9.14 illustrates the extent and movement of the wake as affected by attitude. The profiles at $\alpha = \pm 6^{o}$

show reasonable symmetry about the tunnel centreline, but the wake at $\alpha = 0^{o}$ shows some vertical displacement from the tunnel centreline.

In most cases low speed two dimensional aerodynamic data can be confidently corrected for test section boundary interferences by standard methods. To examine this claim, straight-wall C_L data was corrected by the Goldstein method for tunnel interference and viscous effects. These corrections are made by use of small perturbation theory where the ratio of test section height to model chord is assumed to be large. In TSWT the ratio was small at 1.11, but useful corrections have been determined. In addition there was a blockage correction made for $\alpha > +9^{o}$, where the separated wake of the stalled aerofoil resembles the wake of a bluff body, as postulated by Maskell.

The complete range of available C_L data is plotted on Figure 9.15 showing that in the unstalled regime the corrected straight wall SSWT data compares favourably with corresponding LTPT values. No corrections are applied to LTPT data. The sets of C_L data are again conveniently summarised by fitting straight lines through the data over the angle of attack range $-6^{o} < \alpha < +8^{o}$, using the least squares method. The slopes and intercepts of these line fits are as follows.

Data Source	Lift Curve Slope per Radian	Zero α Intercept C_L
LTPT	4.853	.0095
Streamlined Wall SSWT	4.72	-0.0194
Straight Wall SSWT Corrected	5.042	-0.0077
Uncorrected	5.615	-0.0086

The lift curve slope ratios are

$$\frac{\text{Straight walls, uncorrected}}{\text{LTPT}} = 1.157$$

$$\frac{\text{Straight wall SSWT corrected}}{\text{LTPT}} = 1.039$$

and

$$\frac{\text{Streamlined wall SSWT}}{\text{LTPT}} = 0.973$$

This shows that, below stall, the lift curve slope obtained in SSWT is corrected from an error of 15.7% with straight walls to an error of 2.7% by wall streamlining alone. Similarly, standard wind tunnel corrections reduce the error to 3.9%. It is interesting to observe that LTPT data straddles both the streamlined wall data and the straight wall corrected data.

Beyond stall there are larger disparities in the C_L data. The standard wind tunnel corrections are insufficient, suggesting that the associated theory is inadequate when applied to models with separated flow suppressed by gross wall interference. Note that there is no stall indicated in the raw straight wall data. The disparity between LTPT data and streamlined walls SSWT data in the region of stall can be attributed to some form of error in wall streamlining due to the merging of model wake and wall boundary layers, as discussed earlier.

As an example of the effectiveness of streamlining compared with that of standard correcting techniques through stall, consider the C_L data for $\alpha = 12^o$. Assuming the LTPT data to be correct, the straight wall SSWT result is 128% in error. Standard corrections reduce the C_L error to 44% whereas wall streamlining alone gives only a 28% error in C_L. While significant differences still exist between LTPT and SSWT

results beyond stall the reasons have probably been identified during the attempts to improve SSWT data.

It would appear that wall streamlining of a shallow test section has a favourable effect on model lift before and after stall. The effectiveness of the flexible wall technique is comparable with standard correction techniques before stall, and is about as good as could be expected. However, validation of the flexible wall technique at low speeds has revealed some fundamental limitations to test conditions beyond the stall which must be monitored in high speed testing.

9.2 Model Aerodynamic Data from the Transonic Facility

9.2.1 Description of the high speed models

The original high speed model was a NACA 0012-64 aerofoil (see Table 1) of 10.16cm (4 inch) chord and 15.24cm (6 inch) span. The model was constructed from stainless steel. This validation model was chosen because of its predictable behaviour and also because its performance is reasonably well known.

Each surface has twenty-two static pressure tappings with five tappings grouped within the first 10% of the chord and the remainder spaced at approximately 5% chord intervals as shown on Table 1. The tappings on the upper surface are positioned along a chord line 5.71cm (2.25 inches) from one sidewall. The tappings on the lower surface are positicned along a chord line 9.52cm (3.75 inches) from the same sidewall. Hence, the sets of upper and lower tappings are displaced spanwise by 3.81cm (1.5 inches) symmetrically about the model mid-span.

A grit transition band was positioned around the leading edge to about 3% chord, for the high speed testing in TSWT. A short transition band was chosen in the hope that satisfactory shock free flow would be obtained around the leading edge. However, the concentration of grit did produce shock waves under some conditions. The shock waves affected the detailed shape of the pressure suction peak near the transition band.

The other high speed model was an NPL 9510 section. This is an 11% thick cambered model (see Table 3) having a chord of 15.24cm (6 inches) and a span of 20.32cm (8 inches), constructed of HP9-4-20 alloy steel. The section co-ordinates are shown on Table 3 and the section profile is plotted on Figure 9.16.

Surface pressure tappings were positioned over the mid-span portion of the model on both surfaces. The position of the taps concentrated on specific parts of the aerofoil profile, namely the 50% chord region on the upper surface and the trailing edge region on the lower surface, as shown in Table 4. Tests were performed with and without a transition strip positioned around the leading edge to about 3% chord.

9.2.2 Reference data

Since TSWT tests were conducted at a low chord Reynolds number (about 1.5 million) there was a paucity of reference data on the two high speed models. A search of literature did uncover data on NACA 0012-64 from very early tests at transonic speeds. Fortunately, the 0012-64 model used in TSWT had earlier been tested in the NASA Langley Research Center 19" x 6" blowdown transonic wind tunnel fitted with a slotted test section. This provided a source of reference data with a ratio of test section height to model chord of 4.75 which is substantially higher than the height:chord ratio of 1.5 in TSWT with this model.

NPL 9510 lift and drag data was obtained on the same model in the NASA Langley Research Center (LRC) 0.3 Meter Transonic Cryogenic Wind Tunnel. Its slotted two-dimensional test section gave a height/chord ratio just greater than two. The LRC tests were performed at a stagnation pressure above ambient and at a stagnation temperature somewhat below ambient and in nitrogen, which together resulted in chord Reynolds numbers being about 66% higher than in TSWT at the same Mach number.

Reference lift and drag data was also available from original NPL tests for comparison purposes. This data was obtained from a 25.4cm (10 inch) chord model in an NPL transonic tunnel fitted with a two-

dimensional slotted test section with a height equal to 3 chords. The tests were performed at ambient stagnation conditions giving chord Reynolds numbers also about 66% greater than for TSWT. A transition band was fitted to the lower surface of the model from 6-8% chord for all NPL and LRC tests and also for the majority of those tests from 4-6% chord on the upper surface.

When comparing TSWT data with that from LRC and NPL it should be noted that:

1) The reference data is not corrected for any boundary interference effects.* Where possible, when pressure distributions are compared, the model C_Ns are closely matched to remove uncertainty about angle of attack.

2) The chord Reynolds number of the reference data is higher than that for TSWT data. This difference could lead to misinterpretation of data comparisons since model shocks may be sensitive to the position of the transition point. For a clean wing the transition point is dependent on Reynolds number.

In view of this situation it must be concluded that the reference data can only be used as an indication of model performance.

For the NACA 0012-64 section, the NASA reference data+ covers a range of angle of attack from 0^o to 16^o for Mach numbers from 0.5 to 1.1. Most of the data is for a clean wing, but additional tests at 4^o, 8^o, 12^o and 16^o were carried out for each test Mach number with a transition strip fitted to the model.

The NASA tests+ on the NPL 9510 section covered a range of angle of attack from 0^o to 6^o over a Mach number band from 0.4 to 0.81.

---

*Following private communications with NASA Langley Research Center it was decided as a first step to validate the TSWT data with transonic data currently available from ventilated test sections.

+Unpublished work.

For both sets of reference data on the NPL section, lift was obtained from integrated pressure distributions. Drag was obtained from conventional wake traverses made 0.736 chord downstream of the trailing edge in the LRC tests and one chord downstream in the NPL tests. All reference drag data presented here was obtained from traverses down the tunnel centreline.

9.2.3 NACA 0012-64 results compared with reference data

Initial validation testing in TSWT has generated a body of straight wall and streamlined wall data over the Mach number range of 0.3 to 0.89, during the course of over two hundred and fifty runs. Model data included its surface pressure distribution and wake velocity profile. The test section height to model chord ratio was 1.5:1. The walls were streamlined around the model when set at various angles of attack between 0^{o} and 6^{o}. The maximum angle of attack for a given Mach number was limited by model lift, to protect the schlieren glass into which the model was mounted. Angle of attack was set geometrically and may not be closely related to aerodynamic angle of attack due to upwash present at the upstream end of the flexible walls. It is therefore more aerodynamically meaningful to study the effects of changes in α rather than absolute values. The Reynolds number of the tests, which varied with wind tunnel airspeed, was about 1.23 million at Mach 0.7, based on chord.

Currently, there have been twenty-four runs with the flexible walls streamlined around this aerofoil as summarised in Table 5. In addition, twenty-three runs have been made with the walls set aerodynamically straight as summarised in Table 6. (The setting of straight walls is discussed in Section 6.5.2).

It is only possible to run with the walls set straight at subsonic and low transonic speeds when this model is present, since at high transonic speeds, the model chokes the straight walled test section preventing any changes in Mach number upstream of the model. Nevertheless the straight wall test conditions provide an ideal starting point for an initial streamlining cycle, since the imaginary flowfield

is then uniform. The straight walls generate the gross interference which would be present in a conventional solid walled test section of this size. In particular the existence of initially strong wall interferences can prolong the streamlining cycle as discussed in Chapter 10.

The gross interference of straight walls is well illustrated on Figure 9.17 which shows plots of lift curve slope against Mach number with straight and streamlined walls. Straight wall slopes are much greater than corresponding streamlined wall slopes. Also plotted for comparison with each set of data is a prediction of the effects of compressibility on the lift curve slope relative to a low speed value, using linearised theory. The agreement between theory and experiment is good up to about Mach 0.7.

The conventional wind tunnel correction method by Allan and Vincenti has been applied to straight wall C_L and from drag coefficient values. This correction method is based on linearised compressible theory. The results of this analysis applied to straight wall C_L data are also plotted on Figure 9.17.

As a comparison, a second method of correction has been applied to the straight-wall model data. This correction method uses the wall loadings assessed according to the method of Section 7.3. The wall loadings induce flow disturbances at the model which are interpreted as wall-induced angle of attack error, wall-induced camber and wall-induced blockage. The measured straight-wall lift coefficients were corrected by the estimated effects of these disturbances, and this data is also shown on Figure 9.17.

The two sets of corrected data, together with streamlined-wall TSWT data are compared with the straight wall C_L and form drag coefficient data on Figure 9.18 and Figure 9.19 respectively for the Mach numbers 0.5 and 0.7.

The lift curve slopes determined by the fitting of least square straight lines to each set of data, are summarised as follows:

Data Description	Slope Per Radian		Zero α Intercept	
	Mach 0.5	Mach 0.7	Mach 0.5	Mach 0.7
Straight Wall Data	6.858	8.955	-.0752	-.0898
Straight Wall Data Corrected for Interferences Derived from Wall Loading	5.248	6.893	-.0672	-.0775
Straight Wall Data Corrected According to Allan & Vincenti Method	5.013	5.311	-.0552	-.0519
Streamlined Wall Data	5.529	6.749	-.0574	-.0753

At Mach 0.5, both sets of corrected straight wall TSWT data are in reasonable agreement with streamlined wall TSWT data but there is some divergence of the sets of corrected data at negative angles of attack. At Mach 0.7 the straight wall data corrected for interferences derived from wall loading is in fair agreement with streamlined wall results, despite the rapid divergence of the raw straight wall data. However, the compressible corrections appear to be consistently too strong.

The straight wall form drag data shown on Figure 9.19 suggests some asymmetry in the model position relative to initial 'straight' wall contours, particularly at Mach .5. The standard wind tunnel corrections appear insufficient to improve the data. However form drag determined from model pressures is only a small component of the total drag, making quantitative assessment of form drag meaningless.

It is apparent from the plots of C_L-v-α that the interferences derived from wall loading are probably the most accurate up to Mach 0.7. The standard correction technique is not as good particularly at Mach .7. It is well known that at high subsonic speeds, solid test section

walls generate gross interference effects. This gross interference usually causes the model shocks to be misplaced eventually leading to the tunnel choking at the model with increasing Mach number. Corrections in the conventional sense become meaningless and the tunnel must be capable of unchoking itself if the model shocks are to be correctly positioned and the desired test Mach number achieved. Both adaptive wall and ventilated test sections have this facility.

It has been successfully demonstrated that flexible wall techniques can be applied to cases where supercritical flow extends to the straight walls, and then to streamline at the same Mach number which will give sub-critical flow at the streamlined walls. A representative case is $M_\infty = 0.7$; $\alpha = 4^0$. Aerofoil pressure distributions for this case are given on Figure 9.20 with walls straight and streamlined. The corresponding NASA reference data is also shown. Gross interference is evident with the wall straight, with a high value of model lift generated by the upper surface shock lying too far aft at about 65% chord and extending to the top wall. After streamlining alone, the shock moved to about 22% chord and away from the wall giving a pressure distribution which is in good agreement with the reference data. The powerful effects of streamlining are illustrated in the corresponding spark schlieren pictures on Figure 9.21.

This schlieren serves to illustrate an important point which became apparent as the testing proceeded. The airfoil shocks are always normal to the flexible walls in their outer reaches, and therefore there were no shock reflections from the walls. Each wall supports the sudden pressure rise at the shock and prevents any change in the flow direction downstream of the shock which might otherwise occur with a ventilated test section.

Model data with streamlined walls for test Mach numbers up to Mach 0.7 was obtained routinely and has provided a useful extension of low speed SSWT results. Beyond Mach 0.7, the effects of compressibility on model performance become increasingly significant and supercritical flow can reach the flexible walls. Sets of data were taken at $M_\infty = 0.85$ where it was found that upper and lower shock locations and shapes were

sensitive to transition fixing. This finding is illustrated by the pressure distributions on Figure 9.22. With a clean aerofoil, the upper surface shock is aft and there is evidence of a laminar delta. With a transition strip fitted, the upper shock moved forward by about 14% chord while no movement of the lower shock was observed with no evidence of a laminar delta on either shock. Since the reference data shows characteristics of a turbulent boundary layer at the upper surface shock with and without transition fixing the comparisons of TSWT data with reference data are made with grit on at this Mach number and above. The pressure distributions are on Figure 9.23.

The TSWT and reference data at Mach 0.85 generally show excellent agreement in shape and in detail. The upper and lower shock positions agree to within about 2% and 3% of chord respectively. With pressure orifices at each 5% chord it is difficult to be more precise. It should be noted that these results were obtained despite the fact that the walls were not good streamlines and the upper shock extended to the top wall. (A maximum Mach number of 1.047 was recorded on the top wall).

At a higher Mach number of 0.89, the strengths of the shocks at the walls had risen significantly. The extent of the supercritical flow at the walls is shown on Figure 9.24 by Mach number distributions scaled to the corresponding spark schlieren picture. The model data was in fair agreement with the reference data. In TSWT the upper shock was correctly positioned but the lower shock appeared to be 6% too far aft and there were also deficiencies in the pressure coefficient over the aft sections of the suction surface of between 0.05 to 0.1.

The schlieren shows the existence of shock/boundary layer interactions, one of particular concern being on the top wall. There is a significant thickening of the wall boundary layer downstream of the shock, which causes an aerodynamic throat between model wake and wall boundary layer. This throat produces a weak unsteady shock downstream of the model as shown on Figure 9.24. Study of the series of schlieren pictures taken at intervals of a few seconds during the same test run suggests that the flowfield is not being influenced by tunnel noise, since pressure waves were not seen moving upstream to the model shocks where the test section was choked.

Based on the imaginary flowfield simulations described in Section 10.3, the high speed model was re-tested at Mach 0.89 with a localised hollow introduced into the top wall. The depth of the hollow and its extent downstream of the model was varied to investigate the effects of these changes at the model. Variation of hollow depth produced some differences in model pressure distribution. But continuation of the hollow downstream of the model resulted in the downstream Mach number being below freestream. If freestream Mach number was then restored at the downstream end of the test section, the model shocks moved aft.

Simple shock/boundary layer theory developed by the Royal Aircraft Establishment predicted a step increase of the wall displacement thickness just upstream of the shock. A localised hollow of this depth introduced into the top wall produced favourable effects on the aerofoil pressure distribution as shown on Figure 9.25. This aerofoil data is in excellent agreement with the reference data. However, the walls did not completely satisfy all the streamlining criteria for infinite flow due to the wall setting strategy limitations discussed in Chapter 8.

The accumulated NACA 0012-64 aerofoil data from TSWT is summarised in Figure 9.26 which shows the normal force coefficient slope as a function of M_∞. Streamlined wall TSWT data is compared with reference data. There is most encouraging agreement particularly in the reproduction of shock stall.

A NACA 0012-64 schlieren model of 10.16 cm (4 inch) chord was used for the preliminary wake traverse work. The ratio of test section height to model chord was 1.5. The wake traverses were performed 2¼ chords downstream of the trailing edge, and over sufficient vertical distance to locate both edges of the wake i.e. to locate where the local Mach number became near constant with probe movement.

Traverses were performed at reference Mach numbers of 0.3, 0.5, 0.6 and 0.7 for angles of attack of 0^o, 2^o and 4^o (see Table 7) with the walls streamlined. The drag data is summarised on Figure 9.27, a plot of C_D-v-M_∞ for different angles of attack. The onset of wave drag is

particularly evident above Mach 0.6. Also included on Figure 9.27 are reported C_D values at $M_\infty = .17$ which agree reasonably well with the lower Mach number (i.e. $M_\infty < .6$) TSWT results over the α range. The low Reynolds number of the TSWT tests ($R_c = 0.67 - 1.3 \times 10^6$) has limited the amount of available reference drag data.

To supplement the above data with walls streamlined, a series of traverses were performed with the walls 'aerodynamically straight' at M_∞ equal to 0.5 and 0.7 (see Table 7) to observe the effect of strong boundary interference. For all cases, the effect of straight walls was to displace the wake vertically.

The $M_\infty \simeq .7$; $\alpha = 4^0$ case shows the largest difference between streamlined and straight wall wake profiles as shown on Figure 9.28. These profiles relate favourably to the wakes shown in the spark schlieren on Figure 9.21 also taken at $M_\infty \simeq .7$ with the walls straight and streamlined. This case serves to illustrate the severe interference which can be generated by a straight walled test section at high subsonic Mach numbers. The act of wall streamlining correctly positioned the model shock and is shown here to produce a reasonable value for drag.

While wall streamlining appears to have favourable effects on drag, a lack of reference data for comparison purposes does not allow any positive conclusion to be made about the accuracy of the drag data. In contrast, the lift curve slopes are in good agreement with reference data from low speeds through shock stall. Comparisons between detailed pressure distributions are also good which further confirms the validity of the flexible wall testing technique at high subsonic speeds. It would also appear that wall streamlining is better than standard interference correction techniques particularly at high subsonic speeds.

9.2.4 NPL 9510 results compared with reference data

Further work to validate the flexible wall technique in two-dimensional testing has been carried out using an NPL 9510 section, larger, cambered and perhaps of more challenging design than the NACA 0012-64 section previously tested.

Data on lift and drag was obtained over a Mach number range up to 0.87 and at angles of attack from zero to 6^{o}. The results taken with the walls streamlined were then compared with two sources of reference data obtained in conventional slotted walled transonic test sections. The reference data cannot be considered interference free but is the best currently available at low Reynold's numbers, and has to provide a basis for assessing the quality of TSWT data.

9.2.4.1 Lift

A total of fifty-two sets of data were acquired with the walls 'Streamlined'. Twenty-one points were with no transition strip fitted to the model (as listed on Table 8) and thirty-one were with the transition strip fitted (as listed on Table 9) to observe its effect on model performance[24].

The TSWT lift data is summarised in the plots of the normal force coefficient C_N versus angle of attack for freestream Mach numbers of approximately 0.5, 0.6, 0.7, 0.75 and 0.8 shown on Figure 9.29. Both transition fixed and transition free data is shown together with the reference data for comparison. The NPL data was available and is therefore plotted conveniently as lift coefficient, which is little different from C_N at the moderate angles of attack discussed here.

For $M_\infty \simeq 0.5$, there is a small difference between the normal force curve slope ($dC_N/d\alpha$) for the TSWT data (transition fixed) and LRC data. However the TSWT data (transition free) shows better agreement at lower angles of attack. The ratios of the two TSWT curve slopes with the LRC slope have the values:

Transition Fixed : 1.10
Transition Unfixed: 1.04

over the angle of attack range $0^{o} < \alpha < +6^{o}$.

Reynolds number effects could account for some of this difference.

The NPL data shows a consistent shift in angle of attack relative to the other data sets but the slope compares favourably with the TSWT result.

For $M_\infty \simeq .6$, there is agreement between LRC and TSWT data (transition fixed). The NPL data is again displaced by an amount corresponding to an angle of attack of roughly half a degree.

For $M_\infty \simeq .7$, there is good agreement between LRC and TSWT data. The NPL data at low angles is again displaced, but has a slope roughly equal to that of the TSWT data. At the higher angles the slope is seen to increase and the data diverge from the other two sources.

For $M_\infty \simeq .75$, the TSWT data (transition fixed) shows the same trend as the reference data, an increasing lift curve slope with angle of attack. A disparity between TSWT and LRC data appears at the higher angles of attack, while the NPL data diverges more strongly.

For $M_\infty \simeq .8$, the values of C_N from the TSWT tests (transition fixed) compares favourably with LRC data above about 1^o angle of attack, see Figure 9.29(e). There is however, a discrepancy between LRC and TSWT data at $\alpha = 0^o$. At this Mach number, the shock positions are sensitive to the boundary layer condition and there is a correspondingly large difference in model performance for the TSWT tests with transition fixed and free, as clearly shown in the model pressure distributions for the test case $M_\infty \simeq .8$; $\alpha = 3^o$ shown on Figure 9.30. The upper surface shock is shown to travel from about 60% chord, transition free to about 45% chord, transition fixed. It is apparent that the TSWT data (transition free) is substantially different from the other data sources at high subsonic Mach numbers. The NPL data at $M_\infty \simeq .8$ shows a disparity with both TSWT and LRC equivalent to up to half a degree in angle of attack. There is also a pronounced reduction of the lift curve slope in the NPL data beyond about $\alpha = 2^o$, not evident in the TSWT data. This perhaps indicated an earlier stall due to a larger effective angle of attack of the NPL model.

TSWT data was obtained at higher Mach numbers over only a limited angle of attack range, partly to limit loads. The intention was to locate the important limit to test Mach number giving a breakdown in the wall setting strategy in the manner discussed in Chapter 10. The highest Mach number at which wall streamlining was achieved was 0.87 with $\alpha = 2^{o}$. It is interesting to observe the variation of C_N over the Mach number band 0.5 to 0.87 at this angle of attack shown on Figure 9.31. A shock stall is evident at about Mach 0.85. Again there is reasonable agreement with LRC data as far as it goes. Evidence of an angle of attack error is visible in the NPL data which is above the remainder up to the shock stall. The shift of the onset of shock stall from Mach 0.85 in TSWT to Mach 0.79 in the NPL tests is also indicative of a disparity in angle of attack.

Further detailed comparisons of TSWT results with reference data have been made. The model pressure distributions for the test case $M_\infty \simeq .7$; $\alpha = 4^{o}$ are shown on Figure 9.32 from TSWT data (transition fixed) and the LRC data sets. Normal force coefficients are not perfectly matched but the upper surface shock is roughly in the same position for both tests. However, the pressure recovery downstream of this shock is different for the two tests perhaps due to different thicknesses of the model's boundary layer during each test. The disparities in the pressure distributions on the lower surface could be similarly caused. The peak Mach number on the top walls was 0.82.

For the test case $M_\infty \simeq .75$; $\alpha = 2^{o}$ the upper surface shock may be slightly misplaced forwards by some 5% chord in the TSWT tests, as shown on Figure 9.33. The suction peak obtained in the LRC tests is slightly lower than the TSWT result, which may have been caused by different grit concentrations on the leading edge. A comparison between TSWT and NPL data for similar test cases, shown on Figure 9.34, illustrates similar orders of differences. The upper surface shock position is matched but there are discrepancies downstream of the shock and on the lower surface. Unfortunately, using the available data, lift coefficients were only roughly matched between the TSWT and NPL tests.

The peak top wall Mach number in this TSWT test was 0.837. At higher freestream Mach numbers the supercritical areas extended towards the walls such that for the cases: $M_\infty = .8$; $\alpha = 2^0$ and $M_\infty = .87$; $\alpha = 2^0$ the peak Mach numbers on the top wall were 0.964 and 1.087 respectively. The need for some shaping of the wall to absorb the thickening of its boundary layer under the shock boundary layer interaction has been demonstrated in previous NACA 0012-64 tests, but further work is required before this procedure can be followed on a regular basis (see Chapter 10).

The repeatability of results has been investigated. For the case $M_\infty \simeq .7$; $\alpha = 2^0$ (transition free) two values of C_L were obtained from different streamlining paths. One streamlining cycle was initiated with the walls set to the $M_\infty = .7$; $\alpha = 1^0$ streamlined contours, requiring only one iteration for streamlining and giving $C_L = .4589$. The other cycle was initiated with the walls set to the $M_\infty = .7$; $\alpha = 0^0$ streamlined contours. Here three iterations were required giving $C_L = .4478$. There is a difference of .0111 (2.5%) in C_L. The residual errors were greater than previously reported values[13] (α error $< 0.015^0$) which may adversely affect this comparison. For the test case of $M_\infty = .7$; $\alpha = 0^0$ (transition fixed) a repeat run was performed (Run 390) with the walls reset to the Run 380 streamline contours after some routine streamlining cycles over a range of angle of attack. The difference in C_L between the two tests reduced to 0.0123 (8%) with a correspondingly small change in the residual wall-induced α error from -0.011 to -.0079. The absolute values of the differences in coefficients is indicative of the repeatability of the tunnel system. This includes the effect of repeatability in setting angle of attack which is not claimed to be better than $\pm 0.1^0$. A setting error of this magnitude would itself introduce an error in C_N of about 0.013 with this model, the same order as the figures observed.

Wall streamlining has once again had a favourable effect on lift such that lift curve slopes compare favourably with LRC reference data over a Mach number range from 0.5 to 0.8. This is further evidence of the validity of the flexible wall testing technique up to high subsonic speeds.

9.2.4.2 Drag

Using the TSWT Wake Traverse technique (see Section 6.4), drag data was obtained on the NPL 9510 model for a limited number of test points, over the Mach number range 0.5 to 0.8.

The traversing plane was 1.083 chords downstream of the model trailing edge, on the tunnel centerline. A total of thirteen traverses were performed. The resulting drag coefficient data is plotted on Figure 9.35, compared with the LRC and NPL reference data, for approximate freestream Mach numbers of 0.5, 0.6, 0.7, 0.75 and 0.8.

At $M_\infty \simeq .5$, the TSWT data is in good agreement with the other sources only at $\alpha = 0^0$. From the C_D data shown on Figure 9.35(a), it is possible to identify the possibility of the existence of an angle of attack error in the TSWT data at $\alpha = 4^0$. Allowance for this would have the effect of shifting the drag data sets closer together. At $\alpha = 2^0$ there is also a significant difference in drag coefficients, part of which may be the effect of ill-defined edges of the wake observed in this test. Unfortunately, the freestream Mach number at the traversing plane is only known to be approximately that of the reference freestream. The NPL data is misplaced from the LRC results by a roughly equal amount in common with the lift data.

At $M_\infty \simeq .6$ there is reasonable agreement particularly with the NPL data and likewise at $M_\infty \simeq .7$ and $M_\infty \simeq .75$ albeit over a reduced angle of attack range. The LRC and NPL data at $M_\infty \simeq .8$ is scattered and TSWT drag data is shown to lie below the reference data.

The best that can be claimed is that these results show the drag data from the flexible walled test section to be plausible - in common with other TSWT drag data. However, there remains the problem of defining the edges of the wake. The choice of this value has been found to have a significant effect on the derived value of C_D. The lack of agreement between the sources of data shown on Figure 9.35 may just illustrate the discrepancies found between results from different wind tunnels.

10. OPERATIONAL EXPERIENCE

10.1 Streamlining Performance

10.1.1 Low speed testing

The low speed testing in SSWT was spread over six years. While its manual operation was initially rather impractical, sufficient improvements in the streamlining performance were achieved to allow extensive validation testing as described in Chapter 9.

The earliest streamlining cycles using SSWT required eight or more iterations which could take over two working weeks to complete. The incorporation of the more sophisticated predictive wall setting strategy described in Chapter 8 and the availability of a more powerful remote computer, allowed streamlining cycles to be performed in about two days. Nevertheless, all SSWT data was hard won.

The majority of SSWT tests with the NACA 0012-64 aerofoil were performed at Mach 0.1 and only the model attitude was varied between test points. With reference to Table 2, it can be seen that sixteen streamlining cycles were performed in SSWT with the overshoot scaling factors (a3 and a4) in the wall setting strategy set to 0.8 (see Chapter 8). This experience has shown that wall streamlining round a model can be achieved sometimes in one iteration if the increment in model angle of attack between successive streamlining cycles is small, say 2^{o}. If the streamlining cycle was initiated with the walls set to 'straight' contours, then three or possibly four iterations would be required for streamlining depending on the magnitude of the model lift.

The 'straight' wall contours were obtained experimentally for the test Mach number 0.1 by manual adjustment of the walls. The test section was, in effect, streamlined with no model present producing a uniform velocity distribution along each flexible wall. In fact the 'straight' walls diverge apart to allow for the boundary layer growth on the four test section walls, and are then said to be aerodynamically straight.

The straight wall contours provided a useful start condition for the first streamlining cycle. All subsequent streamlining cycles can be initiated with the walls curved as long as they are to known contours. This operating technique has the effect of reducing the number of iterations per streamlining cycle. Known contours are those for which the shapes and the imaginary side velocities are known.

10.1.2 Transonic testing

The basis of TSWT operation differs from the low speed SSWT operation in respect of:

1. The demands of the various effects of compressibility on testing techniques.

2. Wall setting strategy incorporating compressibility terms.

3. Provision for on-line computer control.

By the gradual introduction of the on-line control system described in Chapter 6, the wall setting times for a streamlining cycle in TSWT have been dramatically reduced from hours to minutes. The presence of compressible flow in TSWT tests has necessitated modifications to the wall setting strategy described in Chapter 8. In addition several limits to freestream Mach number have been encountered which have necessitated changes in the tunnel operating procedures to achieve high speed testing.

The first limit to test Mach number was found when the test section choked with the walls set aerodynamically straight. This choking was the result of the gross boundary interference generated by a shallow solid walled test section at transonic speeds. Since straight walls are only essentially starting contours for an initial streamlining cycle, as found during SSWT testing, the problem was overcome by the use of test sequences where Mach number or angle of attack were held constant between streamlining cycles. The sequence would start with the walls streamlined for moderate M_∞ or α (with no choking) then M_∞ or α would

be raised to the required value perhaps in steps. The walls would be streamlined for each test condition. This sequence could easily be incorporated in a test program, by starting the tests at moderate M_∞ or α and working to higher M_∞ and α in useful steps. This fact is demonstrated by a series of streamlining cycles performed in TSWT over the Mach number range 0.3 to 0.84 with model α held constant at 2^o. A graph of the behaviour of the uncorrected model C_L throughout the test sequence is shown on Figure 10.1. Notice the large changes in model C_L at high Mach numbers during wall streamlining due to wall induced movement of the model shocks.

At high subsonic Mach numbers, greater than 0.8, supercritical flow can extend to the flexible walls even when they are streamlined as shown on Figure 9.24. The tunnel is choked again and the model shock positions become sensitive to the inducing air pressure while M_∞ is insensitive. At these high speeds, the downstream Mach number was controlled by a secondary throat formed at Jacks 20, where there is a sudden change in test section cross sectional area due to the variable diffussor attachments on the flexible walls (see Figure 6.1). It was found that the best model results were obtained with the downstream Mach number roughly equal to the test Mach number measured upstream of the model. A situation which was routinely achieved with wall streamlining at lower speeds. Further increases in test Mach number with the model's supercritical flow region extending to both walls, were achieved by increasing the flow Mach number downstream of the model. This action caused the wall setting strategy to demand the walls move further away from the model unchoking the test section and allowing a higher reference Mach number to be achieved. This technique has only been used in the absence of a wall setting strategy capable of accepting mixed flows in the imaginary flowfield. Presently the streamlining criteria for the walls cannot be satisfied with strong model shocks reaching the walls. Nevertheless, high speed testing in TSWT has allowed investigation of the breakdown in the wall setting strategy and the study of current limits to TSWT operation. While the reflection of model shocks from the walls does not seem to be a problem, spark schlieren pictures have shown the existence of significant shockwave/wall boundary layer interaction (see Figure 9.24). The

effects of this interaction are discussed in Section 10.3 and may necessitate some modification to the tunnel operating procedure for high speed testing.

The transonic testing can be split into two sections, that work with the NACA 0012-64 section which used a semi-manual control system, and work with the NPL 9510 section using both the semi-manual and the automatic control system described in Chapter 6.

A) NACA 0012-64 testing

In total, twenty four TSWT runs have been performed with the flexible walls streamlined[22] round this section over the Mach number range from 0.3 to 0.89 as shown in Table 5. By limiting the increments in the test variables α and M_∞ between streamlining cycles it has been possible to demonstrate streamlining in just one iteration. The average number of iterations was two for this series of tests. Either Mach number, angle of attack, transition strip or combinations thereof were changed from one streamlining cycle to the next. These changes were, in magnitude, typical of those which would normally be made during aerodynamic tests.

The repeatability of results obtained using different streamlining 'paths' has been demonstrated at Mach numbers up to 0.7. A good example is for the test case $M_\infty = .7$; $\alpha = 4^o$ where for Run 72 C_L equals 0.3993 and for Run 63 C_L equals 0.4026, an error of 0.0033 or 0.8% despite the use of different streamlining 'paths'. Run 72 wall contours were obtained in four iterations from straight walls and Run 68 wall contours were found in only two iterations from the streamlined wall contours for $M_\infty = .7$; $\alpha = 3^o$.

For tests above Mach 0.85, the streamlining process became unstable due to the inadequacies of the wall setting strategy theory described in Chapter 8. The walls may not have reached a good streamline form since E was greater than 0.01 (see Section 7.2), but the residual interferences were still acceptably small. A tendency for the number of iterations per streamlining cycle to increase at high speeds

was eliminated by the reduction of the overshoot scaling factors to 0.5 from the value of 0.8 used for all other tests.

A comparison of the real and imaginary velocity perturbations from freestream along each flexible wall for the test case $M_\infty = 0.89$; $\alpha = 4^o$ reveals a disparity between real and imaginary velocities near the wall position where the model upper surface shock impinges on the top wall. The real velocity distribution shows one velocity peak while the imaginary distribution has two peaks roughly straddling the real velocity peak. On the bottom wall, the imaginary velocity distribution overestimates the real velocity peak at the same location on the wall. The resultant effect of these disparities is the cancellation of residual interferences at the model.

The instability of the wall setting process at high speeds is further aggravated by the increased sensitivity of model pressures to wall movement. The largest zone of near-sonic flow will occupy the test section with this model at $M_\infty \simeq 0.9$. At this Mach number the sensitivity of model pressures to wall movement will probably be a maximum. Observations at Mach .89 have shown that wall movements as small as 0.1mm (.004 inches) produce noticeable effects at the model in terms of shock movement. Model pressures are insensitive to such small wall movements at Mach numbers less than about .85.

B) NPL 9510 testing

Fifty-one streamlining cycles have been performed in TSWT with an NPL 9510 aerofoil over a Mach number range from .5 to .87 as shown on Table 8 and 9. Experience was gained on the effects of modifications of the wall setting strategy on the number of iterations registered in streamlining. The modifications were to the overshoot factors (a3 and a4) described in Chapter 8.

Only three streamlining cycles were initiated with straight walls for the test conditions of $M_\infty = .5$; $\alpha = 0^o$ and $M_\infty = .7$; $\alpha = 0^o$ each requiring an average of four iterations with the overshoot factors (a3 and a4) equal to 0.8. All other streamlining cycles were initiated with

the walls contoured to known shapes usually streamline contours from a previous cycle. No straight wall tests at significantly higher angles of attack or high speed were possible due to test section choking caused by the high blockage of the model. For example the test section choked at the condition $M_\infty = .7$; $\alpha = 0^0$.

For data sets at Mach 0.5, 0.7, 0.75 and 0.8 the test Mach number was held constant while the model angle of attack was increased in 1^0 steps from 0^0 to a maximum angle of attack determined by limits to wall movement. Test Mach number was then increased with the model set to zero angle of attack while the walls remained fixed.

At Mach 0.5, it was found that an average of one iteration was required per streamlining cycle with the overshoot factors set at 0.8, while an average of two iterations was required with the overshoot factors equal to 0.6. At Mach 0.7 the average number of iterations increased to two with the overshoot factors set to 0.8. Changing the factors to 0.6 produced an average of three iterations. At Mach 0.75, the average number of iterations reduced to two with the overshoot factors set to 0.6. At Mach 0.8, there was an average of three iterations for the overshoot factor set at 0.5 or 0.6. However, the tests with a3 and a4 equal to 0.5 may not have determined good wall streamlines since one measure of streamlining quality, E (see Section 7.2) could not be reduced to an acceptable level in these tests, although the residual interferences were acceptably small.

A series of tests were performed at $M_\infty = .6$, with the angle of attack decreased from 5^0 to 0^0 in 1^0 steps. The average number of iterations per streamlining cycle for the series was two with a minimum of one. These results were achieved with the overshoot factors equal to 0.6.

At Mach numbers greater than 0.8, no meaningful information is available on the number of iterations required per cycle. For the most critical test case of $M_\infty = .87$; $\alpha = 2^0$ the wall setting strategy began to break down as indicated by numerous iterations in the hunt for wall streamlines. The set of contours which were finally reached coincided

coincided with E reaching a minimum. However the residual interferences had still not reached the usual low levels due to the mismatch between real and imaginary wall velocities shown on Figure 10.2. At this particular test condition there was a supercritical patch of flow reaching the top wall having a peak wall Mach number of 1.087. This test condition compares, in terms of this peak wall Mach number, with the case encountered during the NACA 0012-64 tests where strategy breakdown was observed at $M_\infty = 0.89$; $\alpha = 4^o$.

Streamlining was a routine operation for all Mach numbers up to 0.8. To achieve higher speeds it was necessary to introduce changes in the tunnel operating procedure to generate the required test Mach number in a manner discussed for earlier NACA 0012-64 tests.

The NPL 9510 tests have provided further useful experience with the on-line control system. Streamlining cycles were performed rapidly under computer control with wall setting times of order minutes, one iteration typically taking thirty seconds. In fact, thirty streamlining cycles were completed in less than the time it took to perform the first ever streamlining cycle at Southampton in 1973 - two working weeks!

10.2 Examples of Wall Contours

A family of wall shapes has now been generated from SSWT and TSWT during validation testing. These wall shapes are all possible starting wall contours for future streamlining cycles, since the external imaginary velocity distributions are known over these wall shapes.

During SSWT tests with streamlined walls, angle of attack was varied from 0^o through 12^o. The model stalled at around 8^o in these low speed tests. Plots of the effective wall movements of the wall adjacent to the pressure surface of the model, relative to the 'straight wall' contours, for various α are shown on Figure 10.3. As model lift increases, the wall adjacent to the pressure surface moves towards the model and an imprint of the model appears in the wall shape. This is quite remarkable when one considers that the walls are adjusted with no reference to the model. The double curvature of the wall for high lift cases shows the need for close wall jack spacing in the vicinity of the model to maintain adequate wall setting accuracy everywhere along the

wall. Past the stall, there is a considerable increase in the wake thickness which explains the sudden change in the wall contours for α = 12^{o}. This fact is clearly shown on Figure 10.4 where the streamlined wall contours for $\alpha = 6^{o}$ and 12^{o} are compared.

In TSWT testing, both Mach number and angle of attack are test variables. A comparison of wall contours for different Mach numbers at constant angle of attack confirms the changing flowfield characteristics as shown on Figure 10.5. For the NACA 0012-64 aerofoil at $\alpha = 4^{o}$ over the Mach number range 0.5 to 0.89, the wall movements are shown on an exaggerated scale as a deflection up from straight wall contours. There are marked differences in the streamline contours for high and low Mach numbers. The effects of compressibility are seen to demand increased wall movement as expected. At high Mach numbers the walls are seen to move apart a distance equal to the section thickness. Also noticeable is the increase of the model wake with Mach number. This is due to shock induced separation of the model boundary layer as shown in the spark schlieren on Figure 9.24.

It is interesting to observe how the walls move during a streamlining cycle. The wall contours for each iteration of the test case for a NACA 0012-64 aerofoil $M_{\infty} = .89$; $\alpha = 4^{o}$ are plotted on Figure 10.6. They illustrate the reduction in wall streamlining convergence at high speeds when compared with a lower speed test case $M_{\infty} = .5$; $\alpha = 4^{o}$. The wall contours for this streamlining cycle at a more moderate Mach number are shown on Figure 10.7. At high speeds it is evident that small wall movements significantly affect measures of streamlining quality such as E. The wall movement demands during streamlining are best summarised by examination of the movement of one jack on each wall adjacent to the model. The movement demands for jack 9, close to the model $\frac{1}{4}$ chord, are shown on Figure 10.8 for streamlining cycles with the NACA 0012-64 aerofoil set at 4^{o} over the Mach number range from 0.5 to 0.89. As the Mach number increases so the jack movements for streamlining diminish.

In the NPL 9510 tests, the use of a larger model, as expected, caused greater wall movements to be demanded during wall streamlining

than in equivalent NACA 0012-64 tests. Similar changes in test conditions between streamlining cycles were made in both sets of tests. A family of wall contours covering a range of angles of attack for a freestream Mach number of approximately 0.7 are shown on Figure 10.9. These are streamlined wall contours, showing the strong effects of a large model and its attitude on test section shape. There is a reasonably linear increase in the movement of the walls apart with increasing angle of attack. The change of upwash with lift is apparent ahead of the model, with the opposite effect downstream. It should perhaps be re-emphasised that the walls take up these shapes quite automatically, in response to measurements made only at the walls.

The variation of streamline wall contours with Mach number is shown on Figure 10.10 over the Mach number range 0.5 to 0.87 for $\alpha = 2^{o}$. An effect of compressibility is visible in the walls moving apart in the region of the model, progressively more rapidly as Mach number is increased above 0.7. It is interesting to note that at Mach 0.87 the walls in the region of the model have moved apart by an amount roughly equal to the model thickness.

For the test case $M_{\infty} \simeq .8$; $\alpha = 3^{o}$ there was a significant difference between TSWT C_L data with transition fixed and unfixed (see Figure 9.30) although the walls were streamlined in both cases. The two sets of contours are shown on Figure 10.11, they are significantly different and are supporting evidence that the flow round the model was different in the two cases. The separation of the walls around the model and its wake have changed in the same sense as the model lift between the two runs.

For tests at Mach 0.8 and below, the only limitation on model angle of attack was the available wall movement. This limit is reached with the existing hardware at the following test conditions: $M_{\infty} = 0.5$, $\alpha = 6^{o}$; $M_{\infty} = 0.7$, $\alpha = 5^{o}$; $M_{\infty} = 0.75$, $\alpha = 4^{o}$. The severity of the wall movement required for streamlining is clearly shown on Figure 10.12 for the case $M_{\infty} = 0.87$, $\alpha = 2^{o}$. More wall movement than the current restrictions allow (limited by transducer stroke at present) is available should it be required.

The wall shapes corresponding to the aerodynamically straight contours A and C described in Section 6.5.2 have been investigated to determine the geometric wall divergence along the test section. A depth micrometer was used to measure the separation of the walls at jack stations along the test section. The results are plotted on Figure 10.13 as a change in wall separation from Jack 1. The non linear movement of the walls apart can probably be attributed to wall imperfections. At Jack 19, downstream of the model, the wall movement apart corresponds to .411 inch at M_∞ = .7 and .393 inch at M_∞ = .85. This movement is an allowance for boundary layer growth on the four test section walls at the Jack 19 station. An equation which represents the growth of a turbulent boundary layer on a flat plate is

$$\frac{\delta^*}{x} = \frac{0.0322}{R_x^{1/6}}$$

this gives Jack 19, $\delta^* \doteq .0891$ at M_∞ = .85 and δ^* = 0.0907 at M_∞ = .7. This represents the boundary layer growth on one wall from Jack 1. Hence the predicted separation of the aerodynamically straight contours is 0.356 inch at M_∞ = .85 and 0.363 at M_∞ = .7. These predictions compare favourably with the experimental values.

10.3 Preliminary Attempts at Alleviating Shock/Wall Boundary Layer Interaction

At higher Mach numbers the model shock-wall boundary layer interaction can be strong and it becomes necessary to account for the change in wall boundary layer displacement thickness. This is illustrated by NACA 0012-64 data from tests at M_∞ = 0.89 and $\alpha = 4^0$. The local Mach number on the top wall reached about 1.1 ahead of the shock and the boundary layer displacement thickness was estimated to increase by about 80% through the shock.*. With the walls streamlined, there is a noticeable effect on model pressures due to the introduction of a localised hollow in the top wall. Figure 9.25 shows the two airfoil

* This work formed part of Batchelors degree dissertation by B. Mason who received advice on shock displacement thickness effects from Dr. J. Green, R.A.E., Farnborough.

pressure distributions with and without the wall hollow, compared with reference data. It can be seen that introducing the hollow to accommodate a thickening of the wall boundary layer of approximately 0.76mm (0.03 inch) changed the pressure coefficient over the aft half of the upper suction surface by .05 to 0.1, and moved the airfoil lower shock forward by 5% chord to give good agreement with the reference data. The presence of boundary layer interactions at model and wall is well shown by the spark schlieren on Figure 9.24 for the case with no top wall hollow introduced. Reproduced to scale are the distributions of wall Mach number indicating the extent of the supercritical flow regions.

The introduction of a hollow extending the whole way downstream from the shock position on the wall introduced a Mach number deficiency at the downstream end of the test section adversely affecting the position of both top and bottom surface model shocks. This was not the case if only a localised hollow was introduced in the top wall. The walls will streamline satisfactorily around viscous action within the test section, provided the viscous action does not introduce step changes in flow direction at the wall which the wall cannot match.

There has been some effort to simulate in TSWT a portion of the imaginary flowfield immediately above the test section, to assist with the understanding of shockwave/boundary layer interactions and the development of imaginary flowfield computations for tests at high speeds. With an empty test section, the bottom wall effective aerodynamic contour was adjusted to match that of the top wall effective aerodynamic contour obtained from an earlier TSWT run with the model installed. The top wall was streamlined normally for each bottom wall shape. At M_∞ = 0.89, it was found that some further adjustment of the bottom wall was necessary to generate the required velocity distribution along the wall, apparently to allow for shock/boundary layer interactions. A localised hollow in the vicinity of the model has been introduced equal in depth to the hollow used in the model test described earlier. Run 208 generated the best velocity distribution along the bottom wall for freestream Mach numbers of approximately 0.89. Mach number distribution is compared with an equivalent distribution along

the top wall with a model present on Figure 10.14. There are velocity disparities upstream and downstream of the model which may account for the disparity in the matching of the peak Mach number. However the shock on the bottom wall in the imaginary flowfield simulation at Mach 0.89 is in good position agreement with the shock in the real flowfield over the airfoil.

It is interesting to observe that the hesitation in the wall Mach number downstream of the model shock is represented in the imaginary flowfield simulation. This is despite the non-existence of any visible flow expansion process downstream of the shock as shown by spark schlieren on Figure 10.15.

Other empty test section tests at freestream Mach numbers of 0.84 and 0.7 generated bottom wall Mach number distributions which compared favourably with top wall distributions for corresponding model tests. It was not necessary to introduce any hollows in the bottom wall because the peak Mach number on the wall was sonic or below for these tests.

These preliminary attempts at alleviating shock/wall boundary layer interaction have served to highlight the importance of using some form of special operating procedure with flexible walled test sections when the walls are supercritical. More investigation work is required to determine a practical procedure, which is beyond the scope of this work.

11. DISCUSSION OF FINDINGS

A large quantity of aerodynamic data has now been accumulated from both the low speed and high speed flexible walled test sections at Southampton University (SSWT and TSWT respectively). This data provides a basis for assessing the viability of using a flexible walled technique in wind tunnel testing, both in terms of model performance and test section operation.

All the models used in SSWT and TSWT had previously been tested in conventional high speed and low speed test sections, so that some reference data on each model was available. The notion was to determine the effectiveness of test section streamlining by comparing the model performance found using a flexible walled test section with results from conventional test sections.

At low speeds ($M_\infty \simeq .1$), a NACA 0012-64 section was tested in SSWT over a range of angle of attack, up to and beyond stall, as described in Section 9.1.3. Most encouraging agreement was found between SSWT and data and reference data on lift before the stall. However, after the stall there were significant differences between the two data sets. After extensive investigations, this disparity was attributed to the presence of a large separated model wake which extended from the floor to the ceiling of the shallow test section in SSWT, downstream of the model. The mixing of model wake and wall boundary layers had been recognised as a limit to testing in flexible walled test sections since the wall adjustment theories become invalid. The findings from the SSWT tests proved this point. The effects of wall streamlining on lift were significant as shown previously by comparing model data with the walls straight and walls streamlined for the same reference flow conditions. It was also found that conventional wind tunnel corrections could be used successfully with an unstreamlined flexible walled test section at low speeds and well below stall.

At higher speeds a NACA 0012-64 section and an NPL 9510 section were tested as described in Sections 9.2.3 and 9.2.4 respectively. The model data obtained from TSWT was extensive, covering a Mach number band

from 0.3 to 0.89 with both models unstalled. Unfortunately the reference data on these high speed models was not ideal for comparison, since test Reynolds numbers were not matched and test section interferences were known to be present but not accounted for in some of the reference data. Nevertheless, reasonable comparisons between TSWT data and reference data on lift were found, up to and including transonic speeds. These findings add confidence to the use of a flexible walled testing technique but still leave some doubt about the accuracy of TSWT data.

However, subsequent to the series of tests described earlier, a CAST 7 aerofoil was tested in TSWT[36], not by the author but using the same hard- and soft-ware[37]. TSWT model lift data agrees well with other sources (see Appendix D) over the test Mach number band from 0.6 to 0.82, which includes a shock stall. This finding confirms that the quality of the model data from TSWT is as good as data from other existing tunnels.

The effects of wall streamlining on the performance of the high speed models were significant due to compressibility effects. Gross interference was induced at the model by unstreamlined or straight walls resulting in the shockwaves on the model being significantly displaced from their free-air positions. Both lift and drag were shown to change favourably with wall streamlining as the shockwaves were re-positioned. Conventional correction techniques were found to be inadequate when gross boundary interference effects were present in the model data. However, small corrections can be applied to model data from an unstreamlined test section, with some degree of confidence. Therefore, there exists an option during a streamlining cycle to terminate wall adjustments before the walls are streamlined.

During the execution of these model tests, the actual test sections provided information on operational aspects of the flexible walled testing technique. The wall setting strategy had to be developed to provide rapid convergence of the wall shapes to streamlines as described in Chapter 8. Also it was found that there were limits on the test conditions at which wall streamlining could be achieved as described in Chapter 10.

This rapid convergence of the walls to streamlines has always been regarded as very important to the efficient use of flexible walled techniques. For tests at low speeds up to transonic speed, where the walls are just sonic in the vicinity of the model, experience has shown that the severity of the wall interference at the beginning of the streamlining cycle strongly influences the number of iterations in the cycle. This fact means that a test programme must be carefully planned if the number of iterations is to be minimised.

By limiting the increments in the variables α and M_∞ to values typical of conventional aerodynamic tests, between streamlining cycles, it is normal to streamline in just one iteration. This is a good illustration of the power of the predictive streamlining strategy, which is about as efficient as it is possible to be. Since the computing time is short, any further reduction in streamlining time now depends mainly on improvements in the speed of wall movement. Of course, no re-streamlining is required with change of M_∞ at low speeds. With supercritical walls the streamlining process becomes less stable due to the inadequacies of the strategy, and more iterations become necessary.

This breakdown of the wall setting strategy necessitates a limit to test Mach number that has yet to be overcome. Other limits that were encountered during TSWT operation (discussed in Chapter 10) have been removed by introducing changes in the test section operating procedures. Over the Mach number band so far explored, shockwave reflections from the walls appear not to be a problem, but may be at higher speeds when a bow shock is formed. However, shock/wall boundary layer interactions cannot be ignored if the test Mach number is to be raised above current limits. None of the current Mach number limits are regarded as fundamental and will probably be overcome at the expense of increased complexity of the test section control system.

The test sections themselves have performed remarkably well, with only minor mechanical problems and as previously mentioned, the layouts of SSWT and TSWT test sections have proved to be near optimum. Design analyses have substantiated engineering intuition in respect of the choices of test section geometries. Limits to model angle of attack

have been encountered, due to physical constraints on the wall movements set by design specifications. New flexible walled test sections may have more specific test requirements which should allow this problem to be designed out. However, there remains uncertainty about testing models beyond the stall.

Design analyses have also confirmed that the level of precision in wall positioning available in TSWT is adequate, since interferences at the model induced by wall position errors are thought to be acceptably small. Aerodynamically the test section has confirmed this finding since it was possible to generate empty test section constant Mach number distributions along each wall with good precision. In addition, wall induced interferences remaining after wall streamlining, were comparable with acceptable resolution in the model performance data.

The use of a computer-based on-line control system with TSWT has provided the massive reduction in wall setting times that are required for a practical flexible walled test section. It is considered that wall setting times of the order a few minutes are acceptable. However, further reductions in wall setting times could be achieved with faster jack movement, but this refinement will probably incur a financial penalty.

The situation has now been reached where a shallow flexible walled test section can be used successfully, in two dimensional testing, at low speeds and up to transonic speeds where the flexible walls are just supercritical. Over this speed range the flexible wall testing technique has been validated by the quality of the model data obtained from SSWT and TSWT. Operationally the TSWT control system has achieved all its goals. This work has demonstrated the feasibility of a flexible wall technique in transonic testing, which allows advantage to be taken of the improved flow quality and reduced power requirements or increased Reynolds number inherent with a shallow unventilated test section.

The success of TSWT has already led to the construction of a two-dimensional flexible walled test section for use in a transonic cryogenic wind tunnel. Research continues using TSWT to develop the

flexible wall testing technique for use in three dimensional testing utilising the existing TSWT two-dimensional test section. Future developments of flexible walled test sections will probably concentrate on three dimensional testing since even greater rewards await the development of a three dimensional correctable interference transonic test section.

12. PRINCIPAL CONCLUSIONS

1) Test section wall streamlining has been routinely performed around several two-dimensional aerofoils, with test section height to model chord ratios varying between 1.5 and unity, over a Mach number range up to where the walls are just supercritical.

2) The model data found with the walls streamlined indicates that top and bottom wall interferences have been eliminated.

3) Tunnel setting times as short as 1.5 minutes are achieved as a result of the adopted rapid wall setting strategy coupled with automation of the facility using a dedicated mini-computer.

4) Design analyses for flexible walled test sections have confirmed the near optimum layout of the SSWT and TSWT test sections. These analyses now provide a basis for design of new flexible walled test sections.

5) The upper test Mach number in TSWT is limited by a breakdown in the wall setting strategy, and by the magnitude of interferences due to shock/boundary layer interactions. Supercritical flow reaching the walls is not a major practical problem since the associated shocks so far observed are locally normal to the wall and do not reflect. A method is required to cope analytically with the attendant mixed imaginary flowfields.

6) Wall streamlining has a favourable effect on model lift and drag which becomes more significant with increasing Mach number.

7) Wall induced interferences at the model and some measurements of model performance are given by information routinely provided by the flexible walls. Experience has shown that with the walls not fully streamlined, model data can be corrected for small wall induced interferences using conventional techniques.

8) The application of a flexible wall technique to two dimensional testing has been shown to be feasible in terms of model performance and test section operation.

9) The concept of a practical self-streamlining wind tunnel requires the use of a computer for data manipulation and wall control.

13. LIST OF SYMBOLS

α	Angle of attack
A1	Lift curve slope
a1/a2	Wall coupling factors
a3/a4	Overshoot factors
AR	Aspect ratio
β	Prandtl-Glauert compressibility factor
c	Model chord
C_c	Chordwise force coefficient
C_D	Drag coefficient
C_L	Lift coefficient
$C_{L_{max}}$	Maximum permissible lift coefficient
C_N	Normal force coefficient
C_p	Pressure coefficient
δ^*	Boundary layer displacement thickness
ξ	Dummy variable
E	Average of the modulus of the pressure coefficient error between real and imaginary flows along a flexible wall
E_{AV}	Average value of E from top and bottom wall values
E_{WM}	Maximum wall position error (inches)
γ_n	Local wall vorticity strength for the nth iteration
h	Test section height
L	Tunnel semi-length
M	Local Mach number
M_∞	Freestream Mach number
R_c	Chord Reynolds number
U	Local wall velocity
u'	Local horizontal wall velocity perturbation
u	Model induced velocity component
U_n	Local real wall velocity from the nth iteration
U_{mo}	Model induced horizontal velocity perturbation
U_∞	Freestream velocity
v'	Local vertical wall velocity perturbation
V	Image induced velocity component
V_n	Local imaginary wall velocity from the nth iteration
X/X_c	Chordwise position relative to the leading edge

x	Longitudinal position along a wall relative to a datum point
Y	Vertical displacement from the leading edge
Y_c	Vertical position of the mid-wake point relative to the tunnel centreline
Y_n	Wall Jack position for the nth iteration
Y_T	Wake thickness

14. LIST OF REFERENCES

1. C.H.N. Lock and J.A. Beavan. 'Tunnel Interference at Compressible Speeds using Flexible Walls of a Rectangular High Speed Tunnel', ARC R&M 2005, 1944.

2. W.R. Sears. 'Self-Correcting Wind Tunnels', 16th Lanchester Lecture to the R.Aero.Society, May 1973.

3. R.J. Vidal, J.C. Erickson and P.A. Catlin. 'Experiments with a Self Correcting Wind Tunnel', AGARD Conference Proceedings, No.174 - Wind Tunnel Design and Testing Techniques, London, October 1975.

4. R.J. Vidal and J.C. Erickson. 'Research on Adaptive Wall Wind Tunnels', AEDC-TR-78-36, November 1978.

5. W.R. Sears, R.J. Vidal, J.C. Erickson and A. Ritter. 'Interference-Free Wind Tunnel Flows by Adaptive-Wall Technology', ICAS Paper No.76-02, October 1976.

6. W.R. Sears. 'Adaptive Wind Tunnels with Imperfect Control', AIAA Journal of Aircraft, Vol.16, May 1979, pp.344-348.

7. E.M. Kraft and R.L. Parker. 'Experiments for the Reduction of Wind Tunnel Interference by Adaptive Wall Technology', AEDC Report, AEDC-TR-79-51, October 1979.

8. S. Bodapati, E. Schairen and S. Davis. 'Adaptive-Wall Wind Tunnel Development for Transonic Testing', AIAA Paper 80-0441, 11th Aerodynamic Testing Conference, March 1980.

9. M.J. Goodyer. 'The Self Streamlining Wind Tunnel', NASA TMX-72699, August. 1975.

10. M.J. Goodyer. 'A Low Speed Self-Streamlining Wind Tunnel', AGARD CP-174 - Wind Tunnel Design and Testing Techniques, London, October 1975.

11. J.P. Chevallier. 'Self-Correcting Walls for a Transonic Wind Tunnel', NASA TT F-17,254, November 1976.

12. S.W.D. Wolf. 'Turbine Blade Cascade Testing in a Flexible Walled Wind Tunnel', B.Sc. Honours Project, University of Southampton, April 1975.

13. M.J. Goodyer and S.W.D. Wolf. 'The Development of a Self-Streamlining Flexible Walled Transonic Test Section', AIAA Paper No.80-0440, 11th Aerodynamic Testing Conference, March 1980.

14. S.W.D. Wolf and M.J. Goodyer. 'Self-Streamlining Wind Tunnel-Low Speed Testing and Transonic Test Section Design', NASA CR-145257, October 1977.

15. S.W.D. Wolf. 'Self-Streamlining Wind Tunnel Testing and Final Design Studies for the Transonic Facility', NASA CR-158900, June 1978.

16. S.W.D. Wolf and M.J. Goodyer. 'Studies of Self Streamlining Wind Tunnel Real and Imaginary Flows', NASA CR-158831, August 1979.

17. P. Poisson-Quinton. 'Some New Approaches for Wind Tunnel Testing Through the Use of Computers', ONERA TP-1979-24, March 1979.

18. J.M. Gely. 'Self-Streamlining and Wall Corrections in a Transonic Wind Tunnel', Ph.D. Thesis ENSAE, September 1979.

19. J.P. Archambaud, J.P. Chevallier. 'Use of Adaptive Walls in 2D Tests', Paper 14, AGARD Specialists' Meeting - Wall Interference in Wind Tunnels, May 1982.

20. U. Ganzer. 'Wind Tunnels with Adapted Walls for Reducing Wall Interference', Z. Flugwiss, Weltraumforsch, Vol.3, March-April 1979, pp.192-133.

21. U. Ganzer. 'On the Use of Adaptive Walls for Transonic Wind Tunnel Testing', Paper 13, AGARD Specialists' Meeting - Wall Interference in Wind Tunnels, May 1982.

22. S.W.D. Wolf. 'Selected Data from a Transonic Flexible Walled Test Section', NASA CR-159360, September 1980.

23. S.W.D. Wolf. 'Model and Boundary Aerodynamic Data from High Blockage Two-Dimensional Airfoil Tests in a Shallow Unstreamlined Transonic Flexible Walled Test Section', NASA CR-165685, April 1981.

24. S.W.D. Wolf. 'Aerodynamic Data from a Two-Dimensional Cambered Airfoil Section in a Shallow Transonic Flexible Walled Test Section', NASA CR-166005, October 1982.

25. M.J. Goodyer. 'Developments in Airfoil Testing at the University of Southampton', Paper No.26, NASA CP 2045, 1979.

26. B.W. Marschner and R.L. Young et al. 'Integrating Wind Tunnels and Computers', AFOSR-77-3289, August 1977.

27. M. Judd, S.W.D. Wolf and M.J. Goodyer. 'Analytical Work in Support of the Design and Operation of Two-Dimensional Self Streamlining Test Sections', NASA CR-145019, July 1976.

28. M. Judd, M.J. Goodyer and S.W.D. Wolf. 'Definition and Control of Wind Tunnel Shape for Minimum Boundary Interference', AGARD CP-210 - Numerical Methods and Wind Tunnel Testing, June 1976.

29. D.W. Holder and R.J. North. 'The 9" x 3" NPL Induced-Flow High Speed Wind Tunnel', ARC TP 285, June 1949.

30. S.W.D. Wolf. 'Wake Traverse Technique for Use in a Two-Dimensional Transonic Flexible Walled Test Section', NASA CR 165995, September 1982.

31. C.N.H. Lock, W.F. Hilton and S. Goldstein. 'Determination of Profile Drag at High Speeds by a Pitot Traverse Method', ARC R&M 1971, September 1940.

32. M.J. Goodyer. 'Extraction of Model Performance from Wall Data in a Two-Dimensional Transonic Flexible Walled Test Section', NASA CR 165994, September 1982.

33. W.B. Kemp. 'Towards the Correctible Interference Transonic Wind Tunnel', AIAA 9th Aerodynamic Testing Conference, June 1976.

34. B.I.F. Mason. 'Development of a Program for the Flexible Wall Tunnel at Transonic Speeds', B.Sc. Honours Project, University of Southampton, May 1980.

35. S.W.D. Wolf, M.J. Goodyer and I.D. Cook. 'Streamlining the Walls of an Empty Two-Dimensional Flexible Walled Test Section', NASA CR 165936, May 1982.

36. A. Rahman. 'Comparison of Theoretical and Experimental Data of a CAST 7 Aerofoil Section', M.Sc. Thesis, University of Southampton, 1983.

37. S.W.D. Wolf. 'Application of Data Acquisition Systems for On-Line Definition and Control of Wind Tunnel Shape', VKI Lecture Series - Data Acquisition Systems and Data Analysis in Fluid Dynamics = February 1979.

TABLE 1 NACA 0012-64 SECTION DETAILS

SECTION CO-ORDINATES	
$X_{c/C}$	$Y_{/C}$
0.0	0.0
0.005	0.0118
0.01	0.0163
0.015	0.0196
0.02	0.0223
0.025	0.0245
0.035	0.0283
0.05	0.0327
0.07	0.0372
0.085	0.04
0.1	0.0424
0.14	0.0475
0.17	0.0505
0.2	0.0529
0.25	0.0561
0.3	0.0583
0.35	0.0596
0.4	0.06
0.45	0.0596
0.5	0.0583
0.55	0.0561
0.6	0.0531
0.65	0.0494
0.7	0.0448
0.75	0.0394
0.8	0.0332
0.85	0.0263
0.9	0.0187
0.95	0.0103
1.0	0.0012

CO-ORDINATES OF HIGH SPEED MODEL PRESSURE PORTS			
$X_{c/C}$	$Y_{upper/C}$	$X_{c/C}$	$Y_{lower/C}$
0.011	0.0177	0.011	0.0182
0.024	0.0235	0.025	0.024
0.048	0.0321	0.05	0.0326
0.077	0.0381	0.074	0.0375
0.098	0.0418	0.098	0.0418
0.152	0.0491	0.151	0.049
0.2	0.0534	0.2	0.0535
0.251	0.0563	0.25	0.0562
0.299	0.0579	0.299	0.0579
0.35	0.0595	0.35	0.0595
0.398	0.06	0.402	0.06
0.448	0.0596	0.449	0.0595
0.499	0.0583	0.5	0.0582
0.549	0.0562	0.552	0.0561
0.599	0.0532	0.601	0.0531
0.649	0.0494	0.649	0.0495
0.698	0.0449	0.702	0.0445
0.749	0.0395	0.751	0.0393
0.799	0.0334	0.801	0.0311
0.848	0.0266	0.85	0.0263
0.902	0.0184	0.9	0.0187
0.949	0.0105	0.95	0.0102

TABLE 2 SUMMARY OF SSWT STREAMLINED WALL DATA

Reference No.	Run No.	Model α	Iterations from straight walls	Iterations from contoured walls	Δα from contoured walls	Remarks
1	180	+12°	-	3	+2°	-
2	216	+12°	-	1	-	L.E. fences fitted
3	221	+12°	3	-	-	" " with downstream flow area adjustment.
4	223	+12°	-	1	-	T.E. fences fitted.
5	192	+11°	-	2	+1°	-
6	176	+10°	3	-	-	-
7	182	+9°	-	1	+1°	-
8	185	+8°	-	2	-1°	-
9	188	+7°	-	2	-1°	-
10	209	+6°	-	2	+2°	-
11	206	+4°	-	1	+2°	-
12	198	+2°	-	1	+2°	-
13	196	0°	3	-	-	-
14	172	-4°	4	-	-	-
15	167	-4°	-	1	+2°	-
16	165	-6°	4	-	-	-

TABLE 3

Co-ordinates of the NPL-9510 Section

X_c	Y_{upper}	Y_{lower}
.0	-.0001	-.0001
.0024	.0235	-.0238
.0096	.0456	-.0477
.0150	.0565	-.0586
.0300	.0766	-.0812
.0600	.1002	-.1108
.0900	.1153	-.1321
.1200	.1260	-.1499
.1500	.1343	-.1652
.1800	.1414	-.1790
.2400	.1532	-.2033
.3000	.1633	-.2243
.3600	.1723	-.2426
.4200	.1804	-.2586
.4800	.1877	-.2728
.5400	.1945	-.2852
.6000	.2006	-.2964
.7200	.2118	-.3159
.8400	.2216	-.3455
.9600	.2303	-.3668
1.0800	.2382	-.3804
1.2000	.2454	-.3863
1.3200	.2523	-.3845
1.4400	.2589	-.3748
1.5600	.2650	-.3577
1.6800	.2704	-.3332
1.8000	.2755	-.3021
1.9200	.2801	-.2657
2.0400	.2845	-.2257
2.1600	.2884	-.1842
2.2800	.2920	-.1424
2.4000	.2950	-.1023
2.5200	.2975	-.0638
2.6400	.2994	-.0302
2.7600	.3008	-.0028
2.8800	.3016	+.0175
3.0000	.3019	+.0285
3.1200	.3017	+.0291
3.2400	.3010	+.0193
3.3600	.2997	+.0001
3.4800	.2982	
3.6000	.2958	
3.7200	.2927	
3.8400	.2891	
3.9600	.2845	
4.0800	.2793	
4.2000	.2726	
4.3200	.2649	
4.4400	.2558	
4.5600	.2456	
4.6800	.2341	
4.8000	.2214	
4.9200	.2075	
5.0400	.1923	
5.1600	.1760	
5.2800	.1585	
5.4000	.1402	
5.5200	.1205	
5.6400	.0993	
5.7600	.0767	
5.8800	.0533	
6.0000	.0294	

(All Co-ordinates in Inches)

TABLE 4

Measured Co-ordinates of Pressure Ports

NPL 9510 Section

X_c	Y_{upper}	X_c	Y_{lower}
0.0	0.0	0.0	0.0
.0451	.0925	.0598	-.1100
.0605	.1027	.1061	-.1417
.0986	.1207	.3158	-.2292
.1202	.1282	.6137	-.2986
.1591	.1386	.9160	-.3407
.1845	.1444	1.2122	-.3675
.2186	.1513	1.6622	-.3861
.3108	.1671	2.2539	-.3690
.4613	.1876	2.7041	-.3255
.6111	.2036	3.1540	-.2602
.9106	.2288	3.6039	-.1839
1.2116	.2482	4.0529	-.1062
1.5111	.2646	4.3038	-.0662
1.8109	.2780	5.1044	+.0215
2.4109	.2975	5.4057	+.0302
2.7116	.3024	5.7046	+.0227
3.0117	.3039	6.0000	+.0147
3.1617	.3035		
3.3121	.3024		
3.4621	.3005		
3.6122	.2976		
3.7617	.2937		
3.9116	.2886		
4.0621	.2822		
4.2118	.2740		
4.5098	.2522		
4.8102	.2223		
5.1116	.1847		
5.4070	.1412		
5.7108	.0884		
6.0000	.0147		

(All Co-ordinates in Inches)

TABLE 5 SUMMARY OF SELECTED TSWT RUNS

STREAMLINED WALLS

Reference No.	Run No.	Model α	Mach No.	Iterations from straight walls	Iterations from contoured walls	Changes from contoured walls		E_{AV}	Max. residual error	Grit on
						Δα	ΔM		ΔC_L	
1	184	4.0	0.890	-	Three	0	0.02	.0138	.0034	Yes
2	176	2.0	0.891	-	Two	0	0.025	.0190	-.0021	Yes
3	108(M)	0	0.866	-	Two	0	0.112	.0123	.0031	No
4	168	4.5	0.846	-	Two	0.5	0	.0057	.0024	No
5	170	4.5	0.849	-	Two	0	0	.0068	.0035	Yes
6	172	2.0	0.848	-	Two	2.0	0	.0061	.0027	Yes
7	162	2.0	0.839	-	Two	2.0	0	.0067	.0043	No
8	100	2.0	0.84	-	Two	0	0.05	.008	.0072	No
9	136	0	0.84	-	One	-2.0	0	.0082	-.0032	Yes
10	119/96	2.0	0.81	-	Two	0	0.1	.0063	.0047	No
11	188(S)*	0	0.796	-	Two	0	-0.05	.0078	-.0043	Yes
12	105(M)	0	0.753	Three	-	-	-	.0072	.0032	No
13	*72	4.0	0.706	Four	-	-	-	.0062	.0013	No
14	*63	4.0	0.702	-	Two	1.0	0	.0035	.0037	No
15	*69	3.0	0.701	Four	-	-	-	.0045	.0026	No
16	*65	2.0	0.703	-	One	-2.0	0	.0043	-.0049	No
17	93	2.0	0.712	-	One	0	0.2	.0075	.0032	No
18	122	0	0.698	-	Three	-2.0	-0.1	.0088	.008	No
19	115	6.0	0.506	-	Two	2.0	0	.0069	.0061	No
20	112	4.0	0.507	-	Two	2.0	0	.0045	.0051	No
21	91	2.0	0.508	-	One	0	0.2	.0045	.0009	No
22	109	2.0	0.504	-	Three	2.0	0	.005	-.0046	No
23	105	0	0.506	Four	-	-	-	.0077	.0072	No
24	89	2.0	0.306	Three	-	-	-	.006	.0047	No
Special Cases				Remarks						
25	*224	4.0	0.882	Rerun of Run 184 with local hollow in top wall.				.0266	.0293	Yes
26	*208	-	0.889	Empty test section upper imaginary flowfield simulation for Run 184.				E_{TOP} .0065	-	-
27	*215	-	0.841	Flowfield sim. for Run 162				E_{AV} .0058	-	-
28	*219	-	0.708	Flowfield sim. for Run 72				.0052	-	-
29	*195	-	0.899	Empty test section				.0052	-.0037	-
30	* 30	-	0.303	Empty test section				.0038	.0042	-
				ΔC_L due to camber				.0016 / .0042		

* No plot of wall δ* contours available.

TABLE 6 SUMMARY OF TSWT 'STRAIGHT WALL' DATA

Reference No.	Run No.	Model α	Mach No.	Model Data		Residual Interferences			E_{TOP}	E_{BOT}
				C_L'	C_D'	Δα	ΔC_L	ΔM		
1	66	4°	.706	.5466	.032	+.5	.0649	.041	.1318	.0665
2	56	3°	.697	.3854	.0027	+.26	.0557	.029	.0897	.0431
3	55	2°	.693	.2352	-.004	+.15	.033	.025	.069	.0417
4	54	0°	.683	-.1111	-.0109	-.115	-.0684	.023	.042	.0573
5	68	-2°	.701	-.4636	.0013	-.413	-.0491	.033	.0462	.1031
6	67	-4°	.701	-.6624	.0505	-.654	-.0534	.051	.089	.1742
7	40	4°	.520	.4089	-.003	.255	.0629	.015	.0751	.0236
8	53	3°	.505	.2697	-.006	.302	.0692	.011	.0665	.0194
9	39	2°	.516	.1755	-.0098	.863	.0288	.013	.0499	.0271
10	36	0°	.505	-.0728	-.0136	-.097	-.0057	.012	.0290	.0406
11	52	-2°	.499	-.3195	-.0136	-.222	-.0424	.013	.0195	.0609
12	51	-3°	.505	-.4415	-.0124	-.298	-.0591	.014	.018	.0724
13	50	-4°	.504	-.5467	-.0092	-.363	-.0742	.015	.0182	.0857
14	44	10°	.301	.9753	.0565	.719	.1432	.013	.1485	.0473
15	43	8°	.298	.8317	.0363	.637	.1186	.011	.1253	.0385
16	42A	6°	.299	.5872	.0133	.411	.0877	.009	.093	.024
17	42	4°	.304	.3658	-.0058	.221	.0583	.008	.0654	.0193
18	41	2°	.296	.1608	-.0109	.103	.0237	.007	.045	.0217
19	40A	0°	.293	-.0695	-.0131	-.067	-.0094	.006	.0265	.0385
20	45	-2°	.297	-.2801	-.0119	-.207	-.0394	.007	.0153	.0573
21	46	-4°	.296	-.4871	-.0052	-.4	-.0631	.008	.0181	.0856
22	47	-6°	.300	-.7399	.0095	-.53	-.1012	.009	.0338	.1078
23	48	-8°	.296	-.9106	.0261	-.563	-.1301	.013	.0378	.1396
24	49	-10°	.301	-1.052	.0517	-.567	-.1509	.015	.045	.1688

TABLE 7 SUMMARY OF TSWT WAKE TRAVERSE DATA

M_∞ (approx)	α (Deg.)	Streamlined Walls			Straight Walls	
		C_D	Y_T (Inches)	Y_C (Inches)	Y_T (Inches)	Y_C (Inches)
.7	0	.0064	.545	+. 06	.0375	+.108
.7	2	.0079	.552	+.0417	0.55	+.042
.7	4	.0124	.825	-. 133	1.446	+.244
.6	0	.0063	-342	+. 058	-	-
.6	4	.0088	.692	-. 196	-	-
.5	0	.0056	.408	+. 067	.437	+.035
.5	2	.0066	.392	-. 029	.579	-.035
.5	4	.0085	.596	-. 181	.537	-.102
.3	0	.0049	.317	+. 008	-	-
.3	4	.0083	.4625	-. 198	-	-

TABLE 8

Summary of TSWT Data

NPL 9510 (Transition free)

Ref. No.	Run No.	Model α (deg)	Mach No.	Iterations from straight walls	Iterations from contoured walls	Change from start contours		A3	E_{AV}	C_L
						Δα	ΔM			
1	340	0.0	.853	-	7	0	0.05	.5	.0108	.0899
2	350	3.0	.805	-	4	1.0	0	.5	.016	.8167
3	345	2.0	.804	-	4	2.0	0	.5	.012	.6273
4	353	1.0	.798	-	2	-1.0	0	.5	.007	.3172
5	332	0.0	.809	-	2	0	0.07	.5	.0052	.1084
6	329	0.0	.739	-	2	-4.0	0.14	.7	.0065	.1437
7	313	4.0	.699	-	2	1.0	0	.5	.0084	.7421
8	302	3.0	.7	-	3	1.0	0	.5	.0088	.6061
9	296	2.0	.702	-	1	1.0	0	.8	.0068	.4589
10	280	2.0	.702	-	3	2.0	0	.8	.0042	.4478
11	294	1.0	.699	-	3	1.0	0	.8	.0048	.2957
12	275	0.0	.702	4	-	-	-	.8	.0072	.1702
13	316	4.0	.599	-	2	0	-0.1	.5	.0097	.6524
14	318	4.0	.588	-	1	0	-.05	.8	.0092	.6456
15	324	6.0	.5	-	2	1.0	0	.7	.0032	.7621
16	321	5.0	.505	-	1	1.0	0	.7	.0048	.6743
17	306	4.0	.502	-	1	1.0	0	.8	.0068	.6047
18	304	3.0	.502	-	1	0	-0.2	.8	.0036	.5144
19	301	2.0	.503	-	1	2.0	0	.8	.0068	.4086
20	356	1.0	.497	-	2	1.0	0	.7	.0039	.2744
21	288	0.0	.506	3	-	-	-	.8	.0073	.1679

TABLE 9

Summary of TSWT Data

NPL 9510 (Transition fixed)

Ref. No.	Run No.	Model α (deg)	Mach No.	Iterations from straight walls	Iterations from contoured walls	Change from start contours		A3	E_{AV}	C_L	Residual α error (deg)
						Δα	ΔM				
22	398	2.0	.87	-	0	0	0.02	.7	.0056	.4635	-.051
23	396	2.0	.849	-	-	1.0	0.005	.7	.0054	.512	-.0055
24	395	1.0	.844	-	-	1.0	0	.7	.0052	.2581	.0075
25	394	0.0	.837	-	-	-5.0	0.237	.7	.0073	.0274	-.0059
26	389	3.0	.804	-	4	1.0	0	.6	.0068	.7073	-.0045
27	388	2.0	.802	-	4	1.0	0	.6	.0061	.5011	-.0088
28	387	1.0	.802	-	2	1.0	0	.6	.0035	.2654	.0095
29	386	0.0	.801	-	-	-	-	.6	.0074	.099	.0058
30	393	0.0	.753	-	1	0	0.01	.7	.0048	.15	-.0121
31	391	3.0	.758	-	3	1.0	0	.7	.0053	.6694	.01
32	403	2.0	.749	-	2	2.0	0	.6	.004	.4675	.0006
33	402	0.0	.743	-	2	0	0.043	.7	.0044	.1603	-.0021
34	384	4.0	.696	-	3	1.0	0	.6	.0027	.7026	-.0068
35	383	3.0	.696	-	3	1.0	0	.6	.0042	.5884	.0103
36	382	2.0	.701	-	2	1.0	0	.6	.006	.4292	.0174
37	381	1.0	.697	-	4	1.0	0	.6	.0025	.2873	-.0084
38	380	0.0	.704	-	1	0	0.1	.6	.006	.1499	-.011
39	390	0.0	.704	-	-	0	0	.6	.0028	.1376	-.0079
40	374	5.0	.602	-	3	0	0.1	.6	.0065	.7097	.0018
41	375	4.0	.598	-	1	-1.0	0	.6	.005	.6203	.0061
42	376	3.0	.605	-	3	-1.0	0	.6	.0035	.5359	-.0127
43	377	2.0	.598	-	1	-1.0	0	.6	.0069	.3942	.0096
44	378	1.0	.6	-	2	-1.0	0	.6	.0039	.2799	.0075
45	379	0.0	.595	-	1	-1.0	0	.6	.0054	.155	.0069
46	371	5.0	.508	-	2	1.0	0	.6	.0053	.6927	.0045
47	373	4.9	.501	-	2	-1.0	0	.6	.004	.6828	.0069
48	370	4.0	.501	-	2	1.0	0	.6	.005	.6339	.0068
49	369	3.0	.493	-	2	1.0	0	.6	.0045	.493	.0044
50	368	2.0	.5	-	1	1.0	0	.6	.0056	.406	.012
51	367	1.0	.498	-	1	1.0	0	.6	.0056	.2658	-.0086
52	366	0.0	.496	4	-	-	-	.5	.051	.1431	.0008

SELF-STREAMLINING WIND TUNNEL (SSWT)

(Southampton, UK)

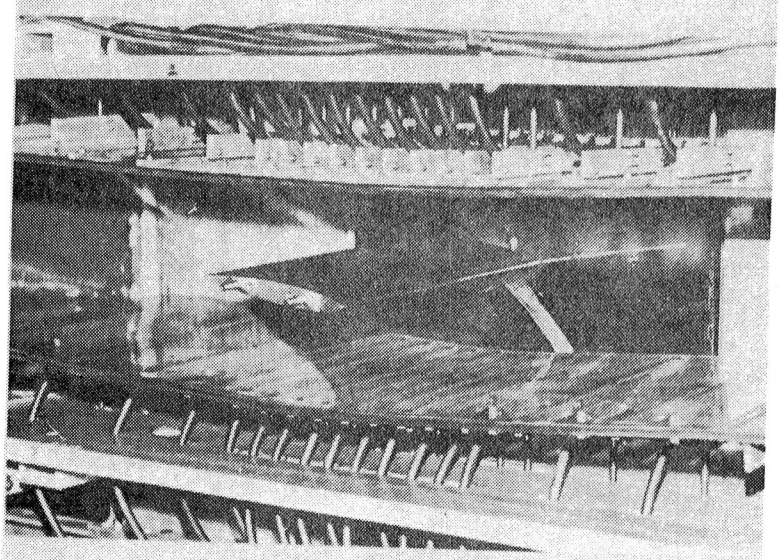

FLEXIBLE WALLED CASCADE RIG

(Southampton, UK)

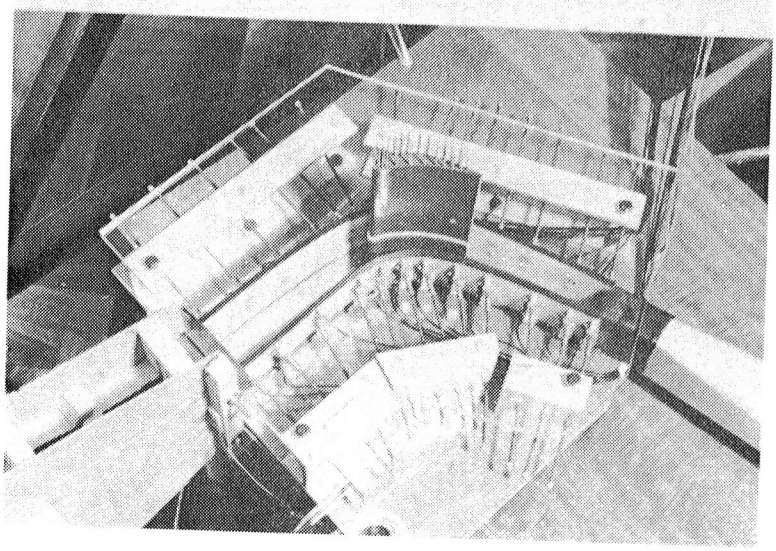

FIG. 1.1 LOW SPEED FLEXIBLE WALLED TEST SECTIONS AT THE UNIVERSITY OF SOUTHAMPTON.

(Southampton, UK)

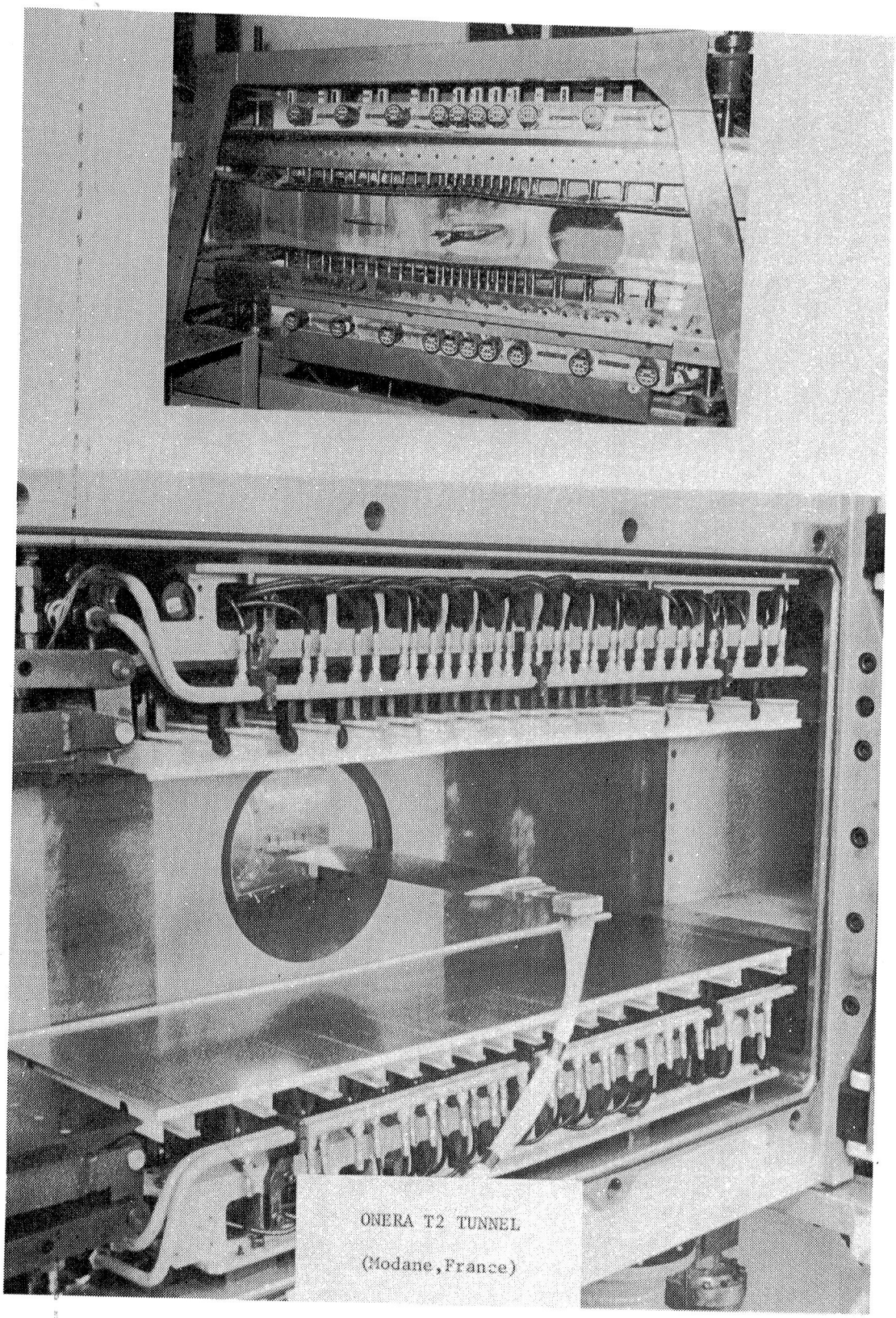

FIG. 1.2(a) TRANSONIC FLEXIBLE WALLED TEST SECTIONS OPERATIONAL IN EUROPE

TRANSONIC WIND TUNNEL

(Berlin, West Germany)

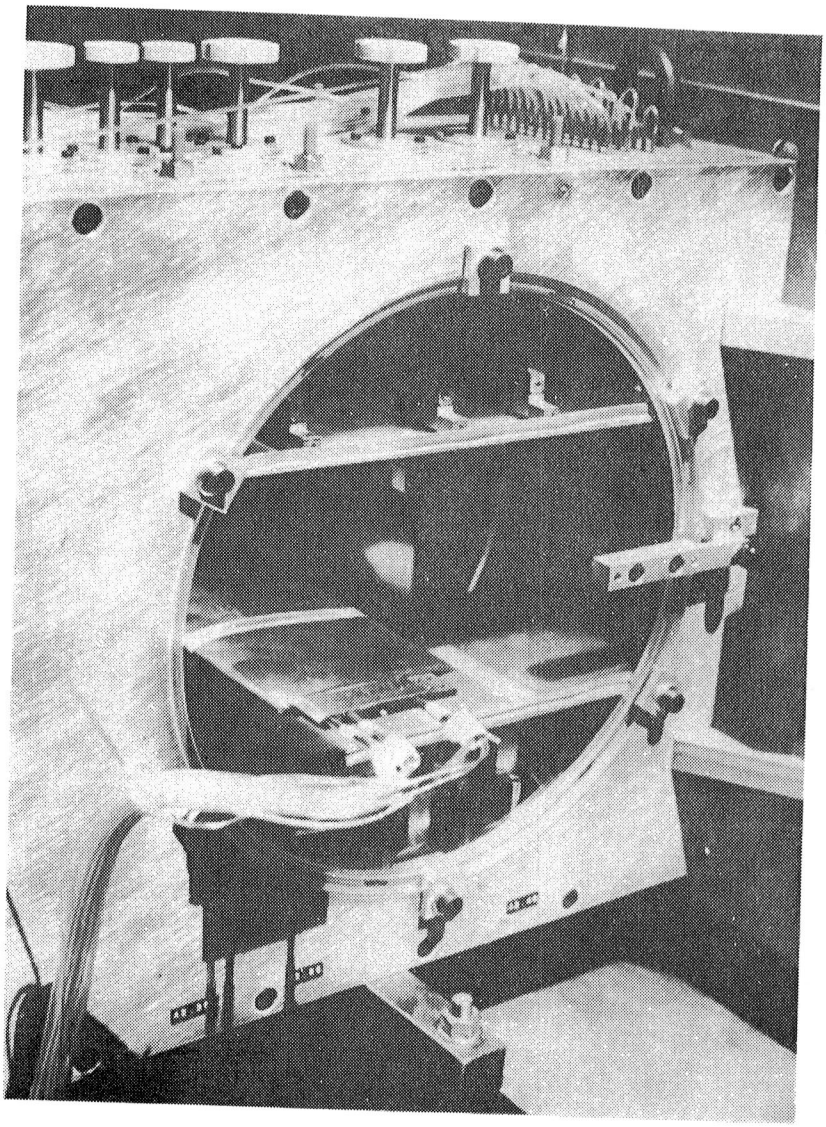

FIG. 1.2(b) TRANSONIC FLEXIBLE WALLED TEST SECTIONS OPERATIONAL IN EUROPE (Continued).

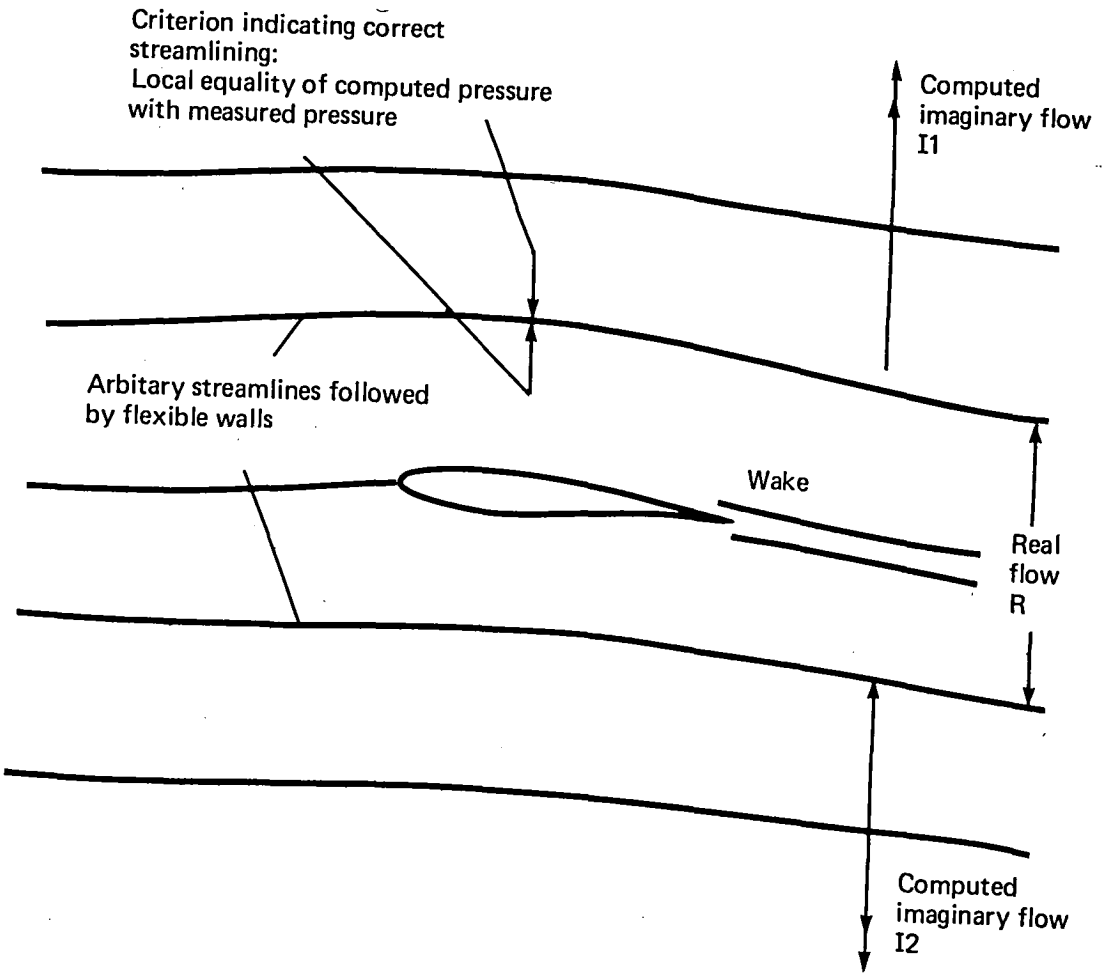

FIG. 2.1. A TWO-DIMENSIONAL FLOWFIELD ILLUSTRATING THE PRINCIPLE OF TEST SECTION STREAMLINING.

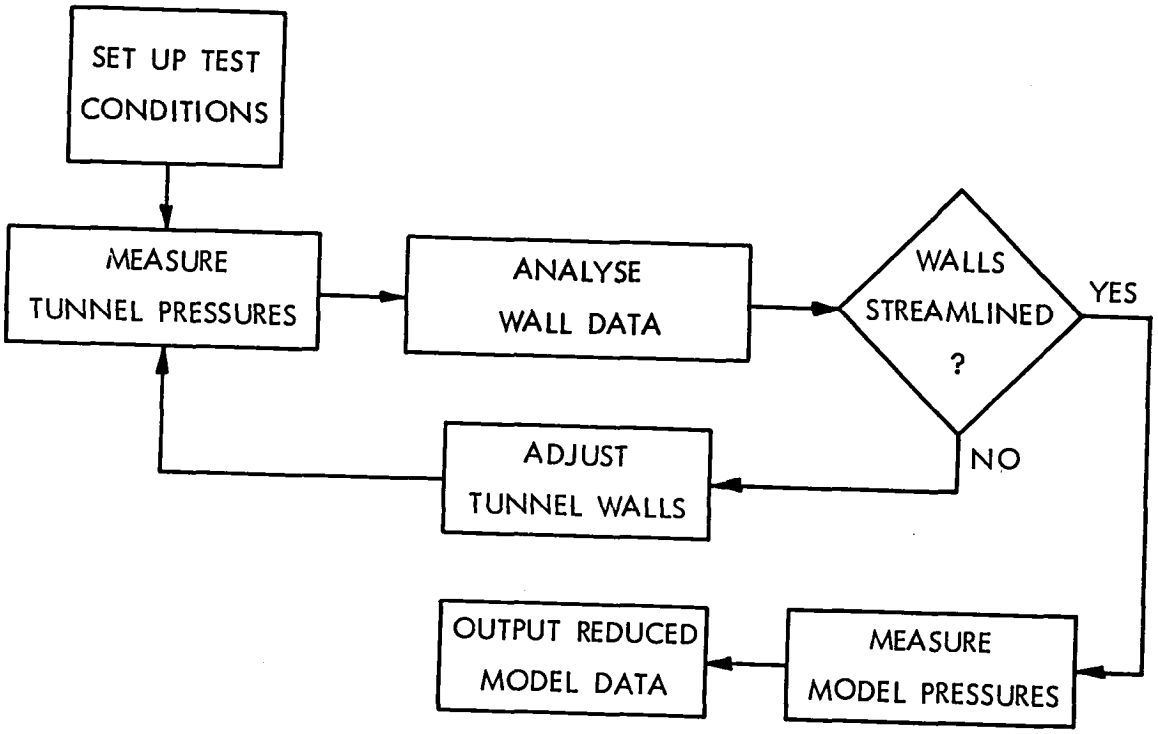

FIG. 2.2 SELF-STREAMLINING OPERATING PROCEDURE

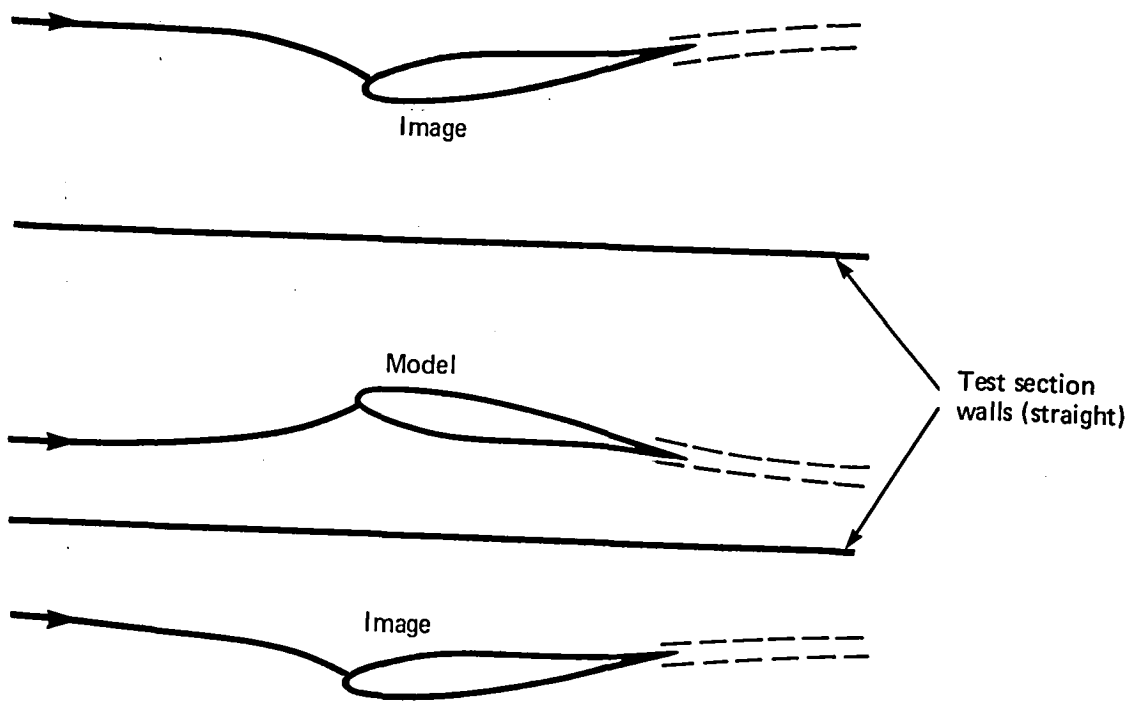

(a) Closed tunnel mode

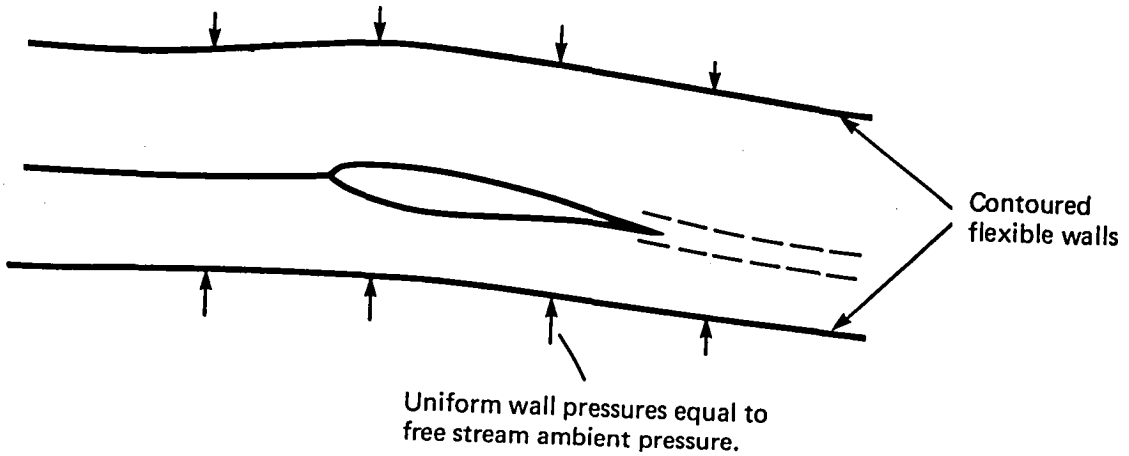

(b) Open jet mode.

FIG. 2.3. ILLUSTRATIONS OF SIX OPERATIONAL MODES OF A SELF-STREAMLINING WIND TUNNEL.

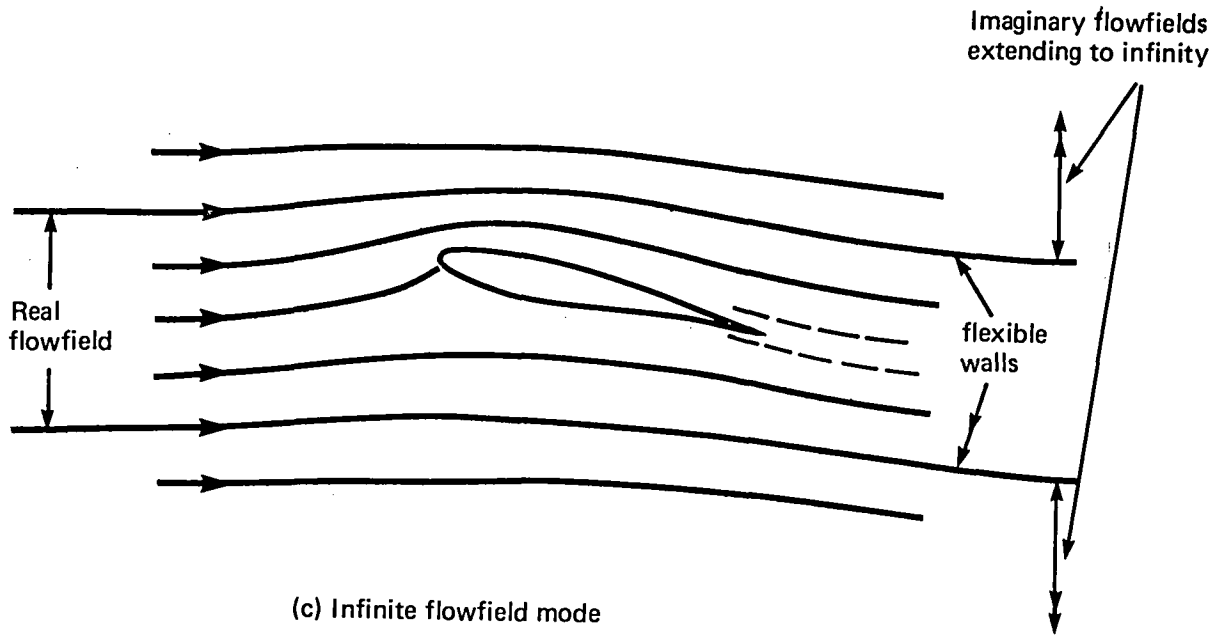

(c) Infinite flowfield mode

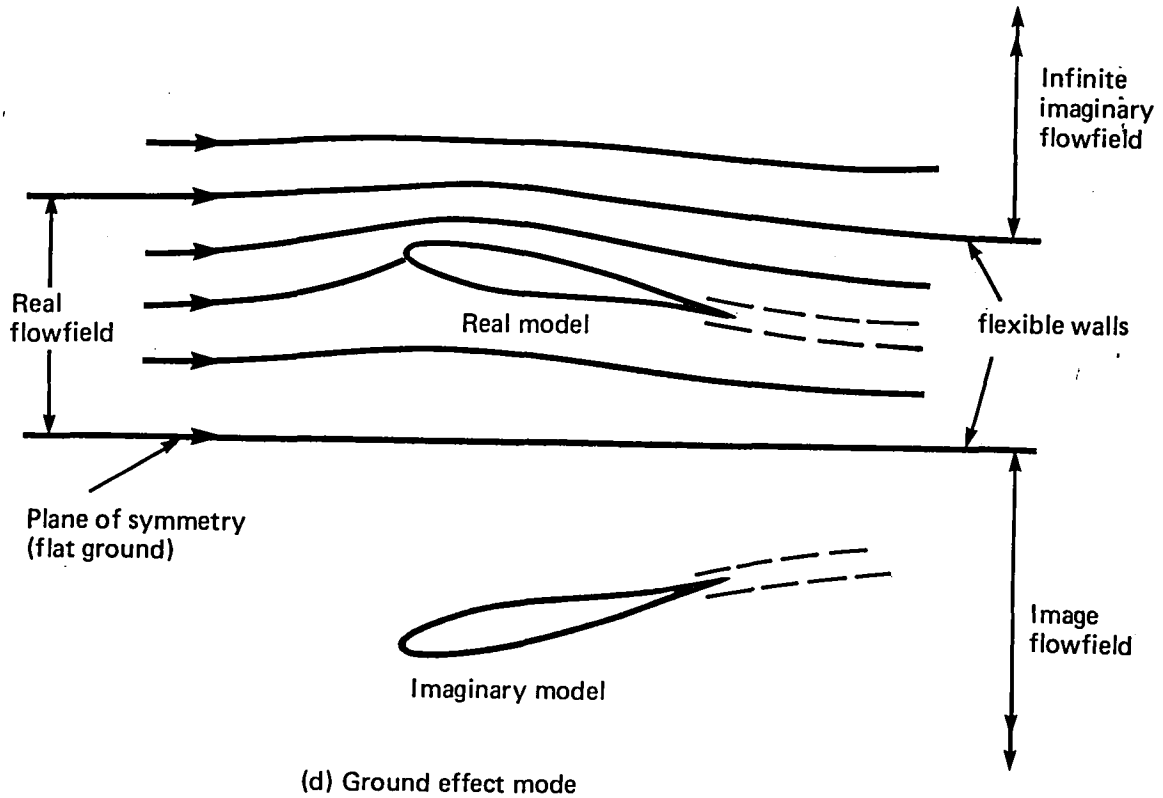

(d) Ground effect mode

FIG. 2.3. ILLUSTRATIONS OF SIX OPERATIONAL MODES OF A SELF-STREAMLINING WIND TUNNEL (CONTINUED.)

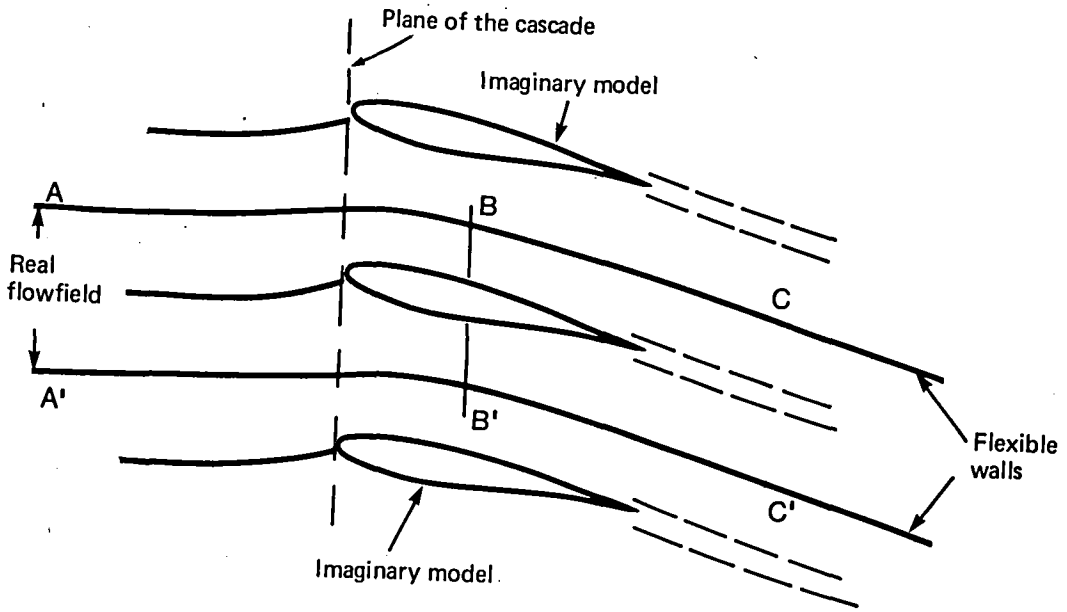

(e) Cascade mode.

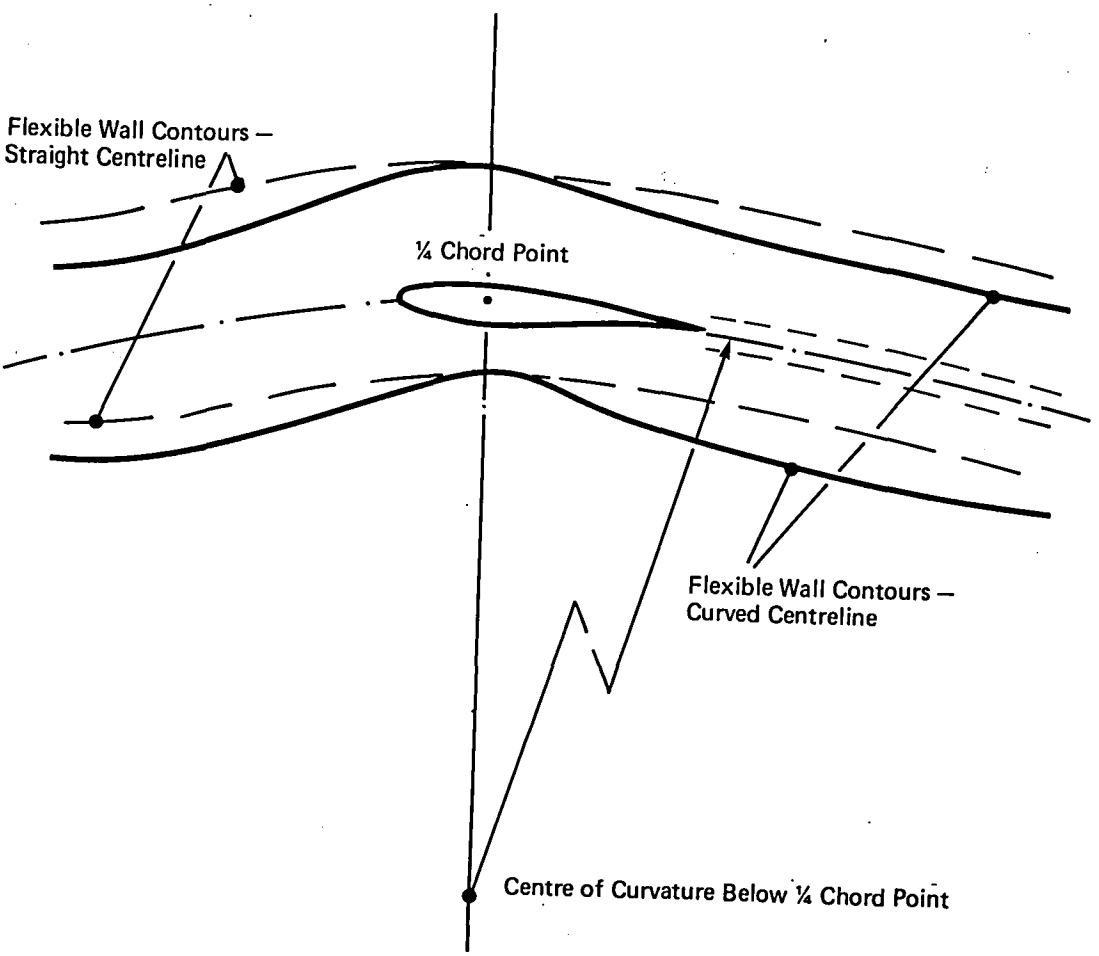

(f) Steady pitching mode

FIG. 2.3. ILLUSTRATIONS OF SIX OPERATIONAL MODES OF A SELF-STREAMLINING WIND TUNNEL (CONCLUDED.)

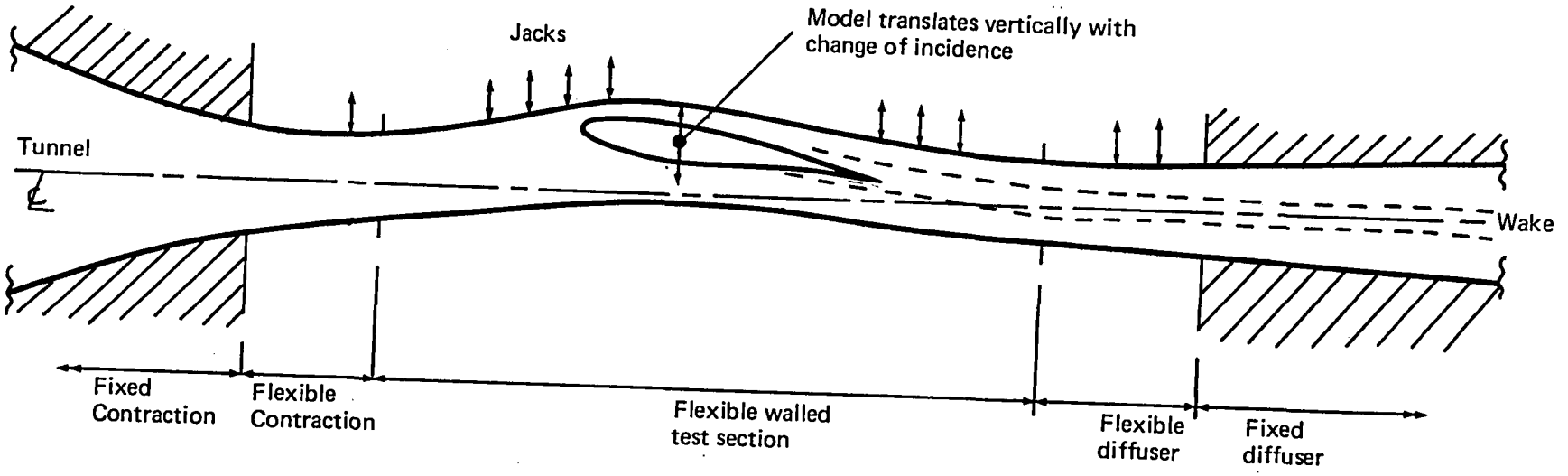

FIG. 4.1 A TWO-DIMENSIONAL FLEXIBLE WALLED TEST SECTION DESIGN CONCEPT.

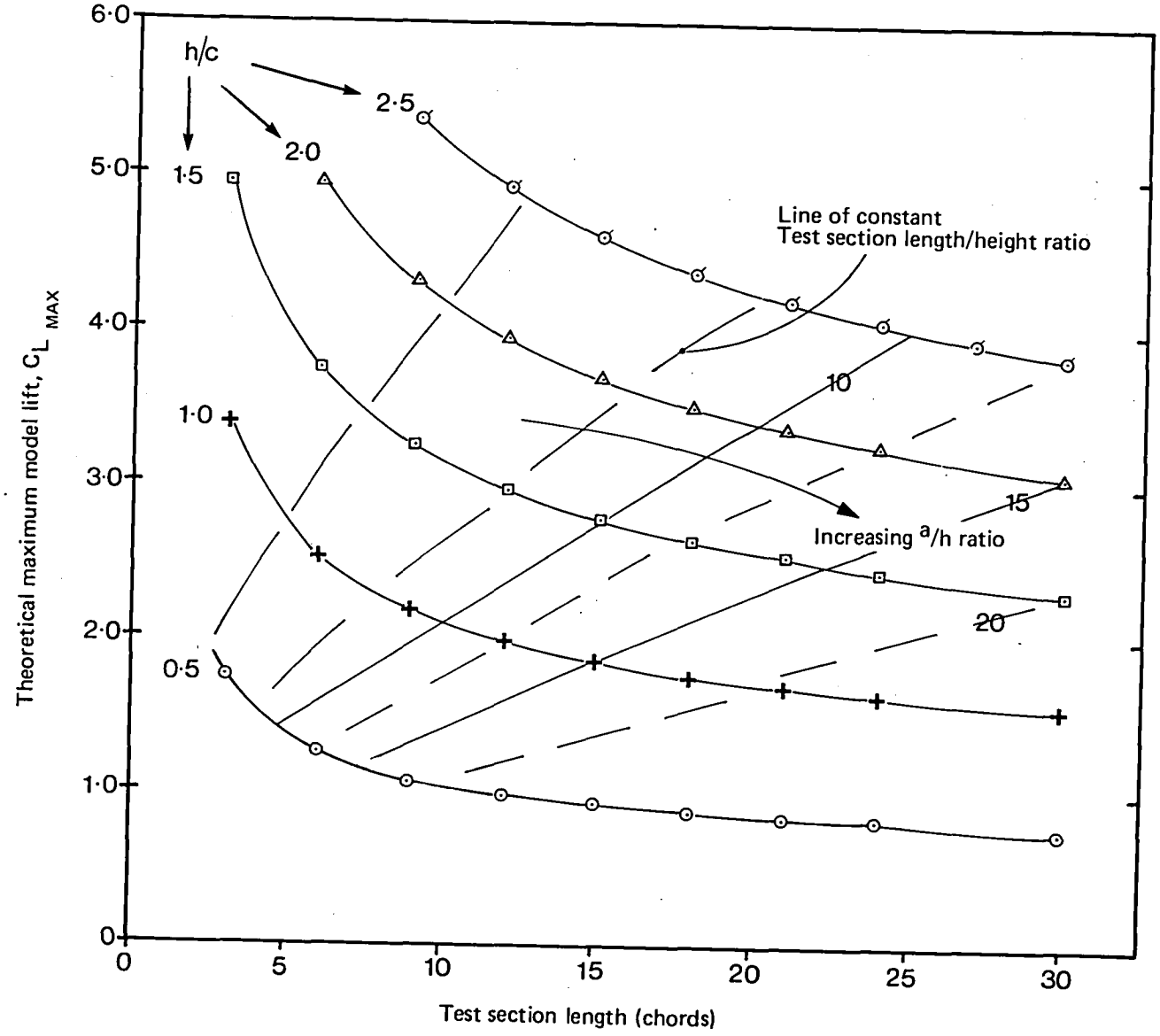

FIG. 4.2 VARIATION OF THEORETICAL $C_{L_{MAX}}$ WITH TEST SECTION LENGTH FOR DIFFERENT TEST SECTION HEIGHTS.

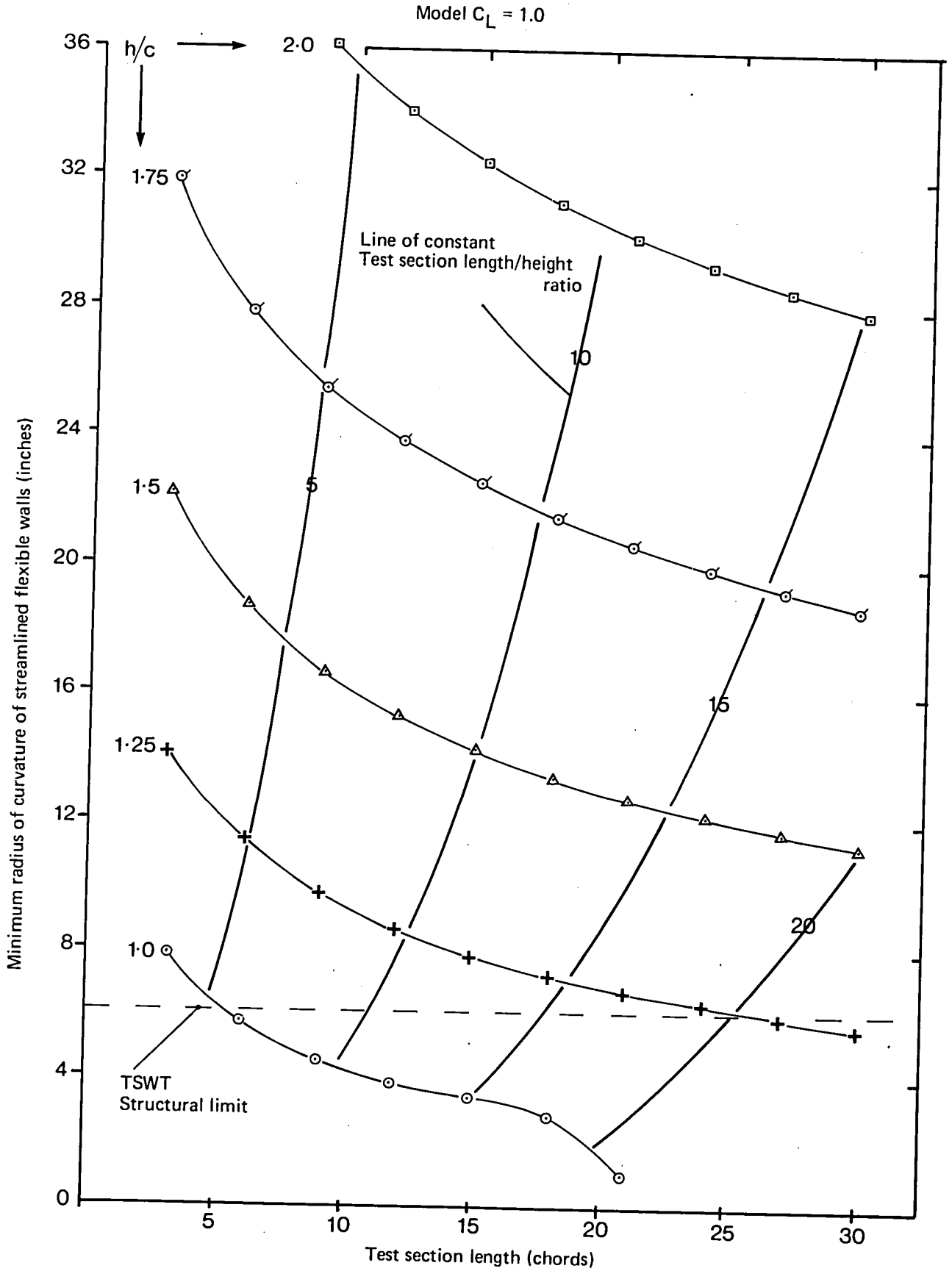

FIG. 4.3. VARIATION OF WALL MINIMUM RADIUS OF CURVATURE WITH TEST SECTION LENGTH FOR DIFFERENT TEST SECTION HEIGHTS

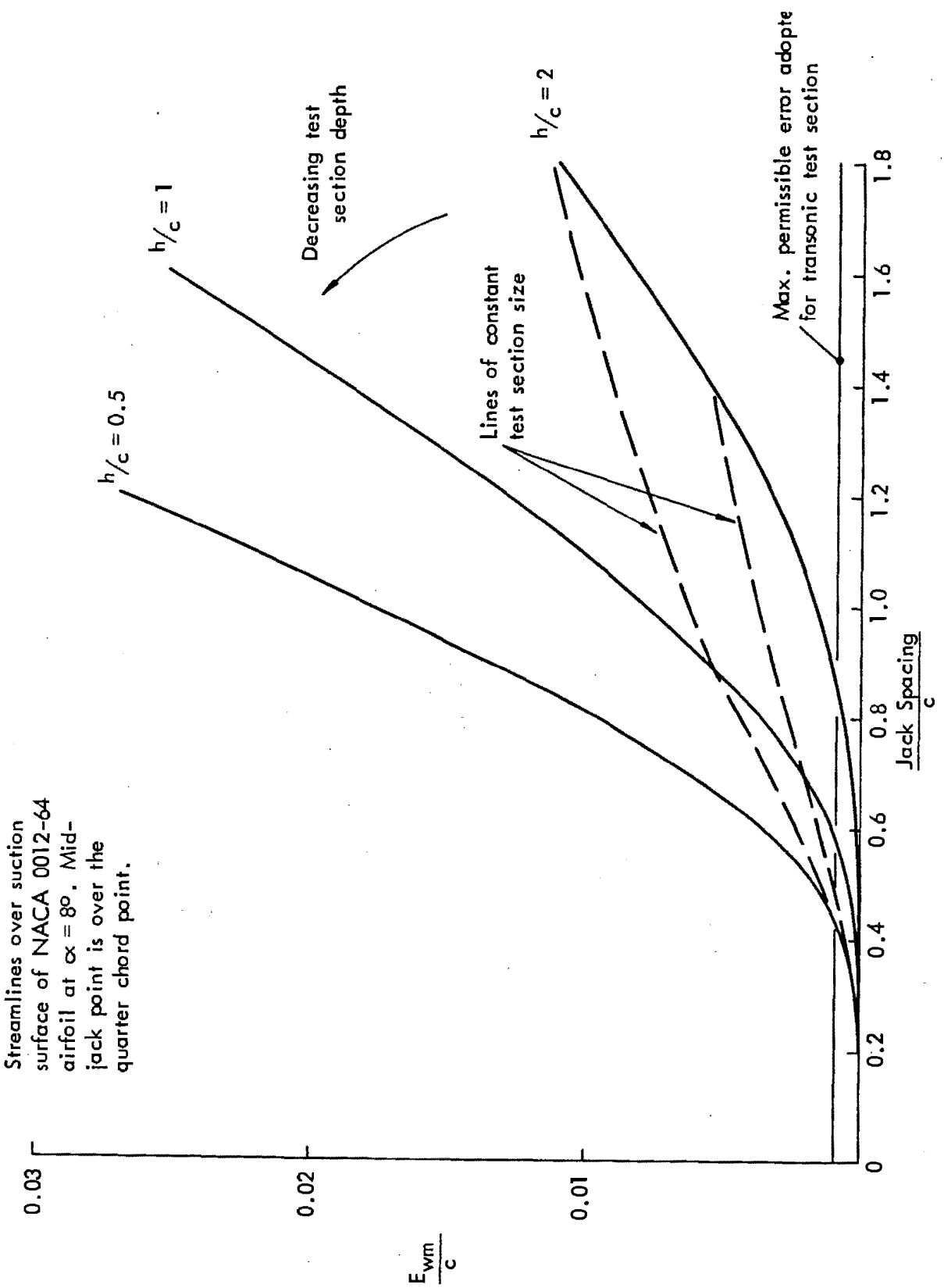

FIG. 4.4(a) MAXIMUM ERRORS BETWEEN AIRFOIL STREAMLINES AND AN ELASTIC STRUCTURE.

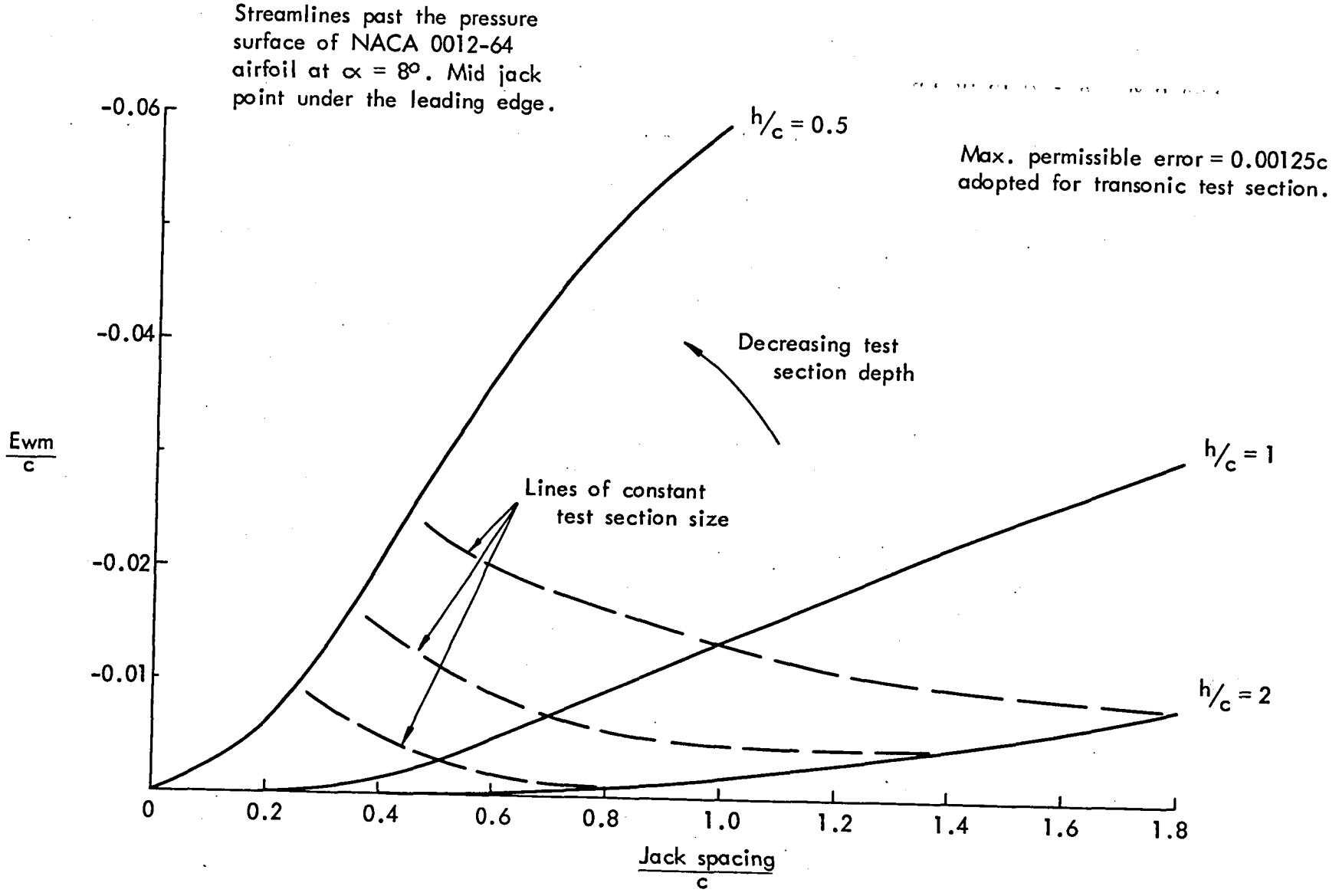

FIG. 4.4(b) MAXIMUM ERRORS BETWEEN AIRFOIL STREAMLINES AND AN ELASTIC STRUCTURE.

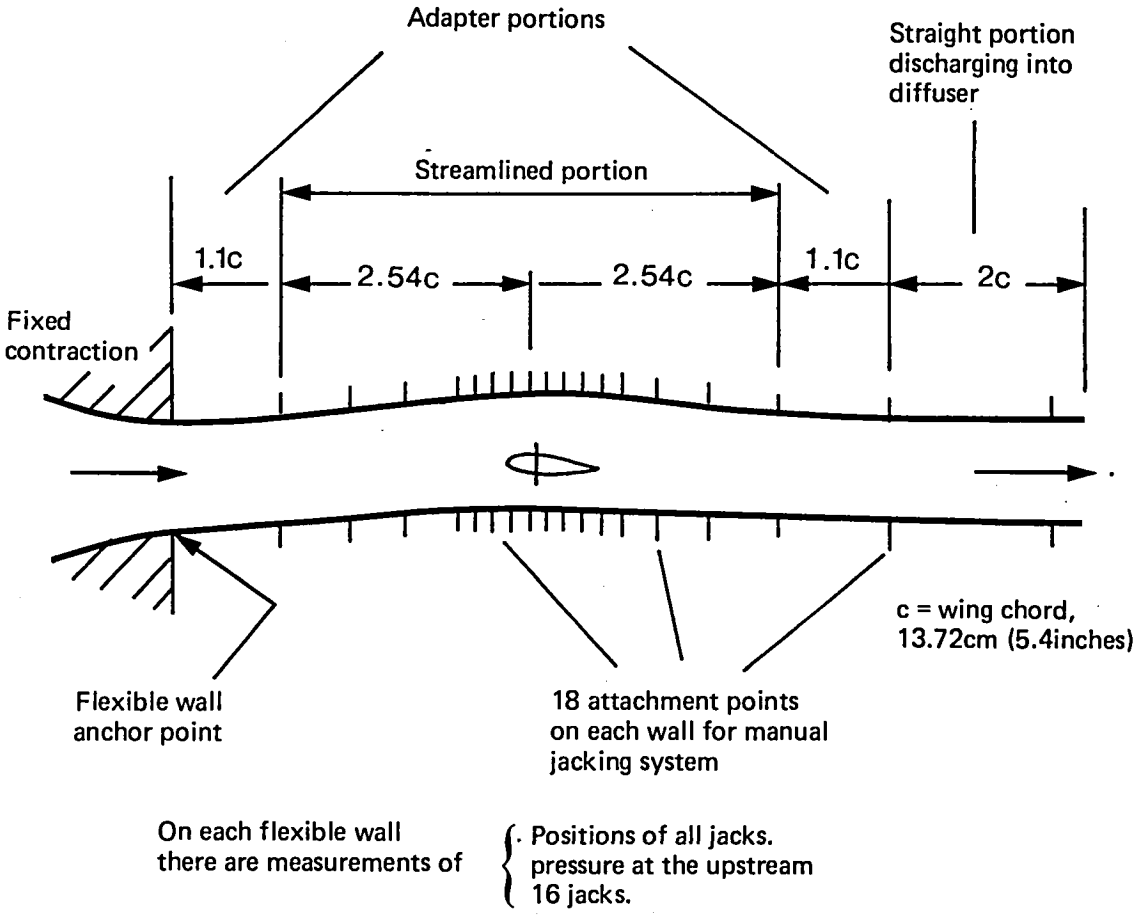

FIG. 5.1 A SCHEMATIC DIAGRAM OF THE LOW SPEED TWO-DIMENSIONAL SELF-STREAMLINING TEST SECTION.

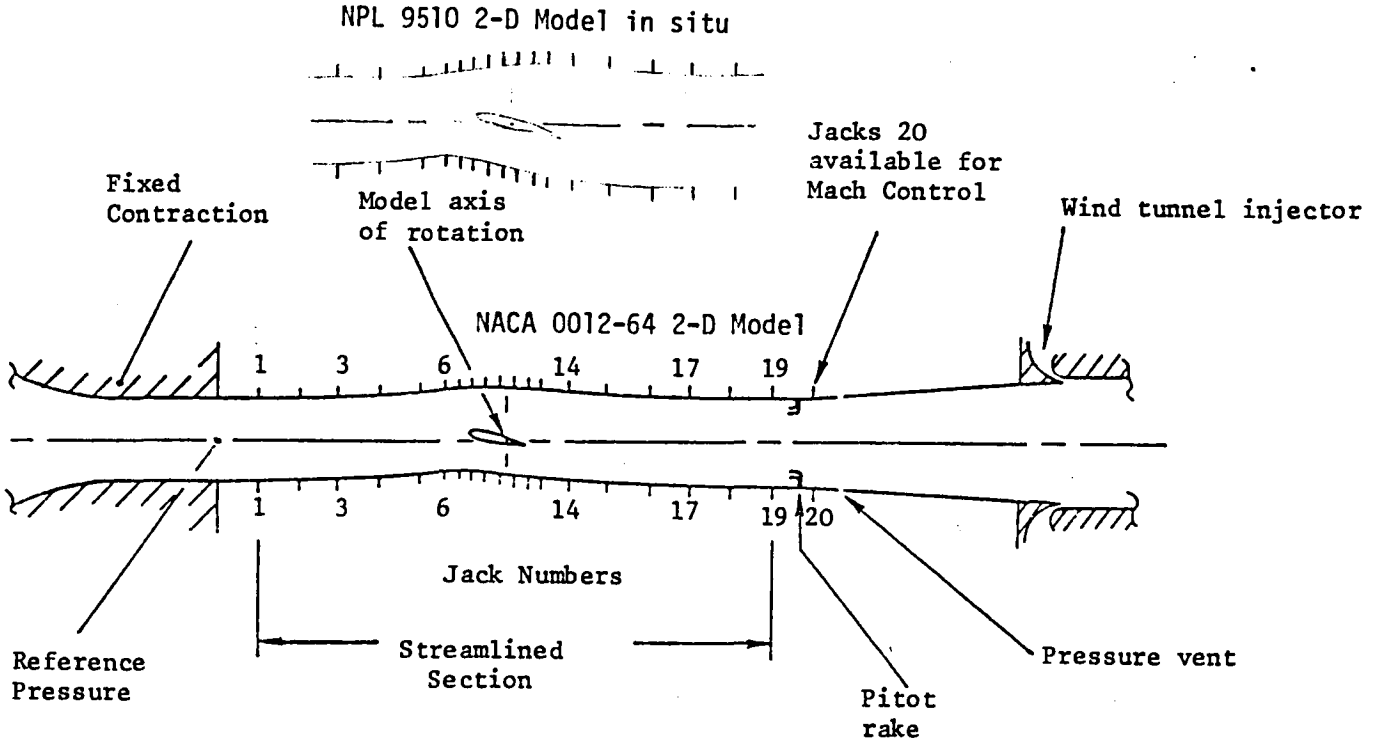

FIG. 6.1 Transonic flexible walled test section layout

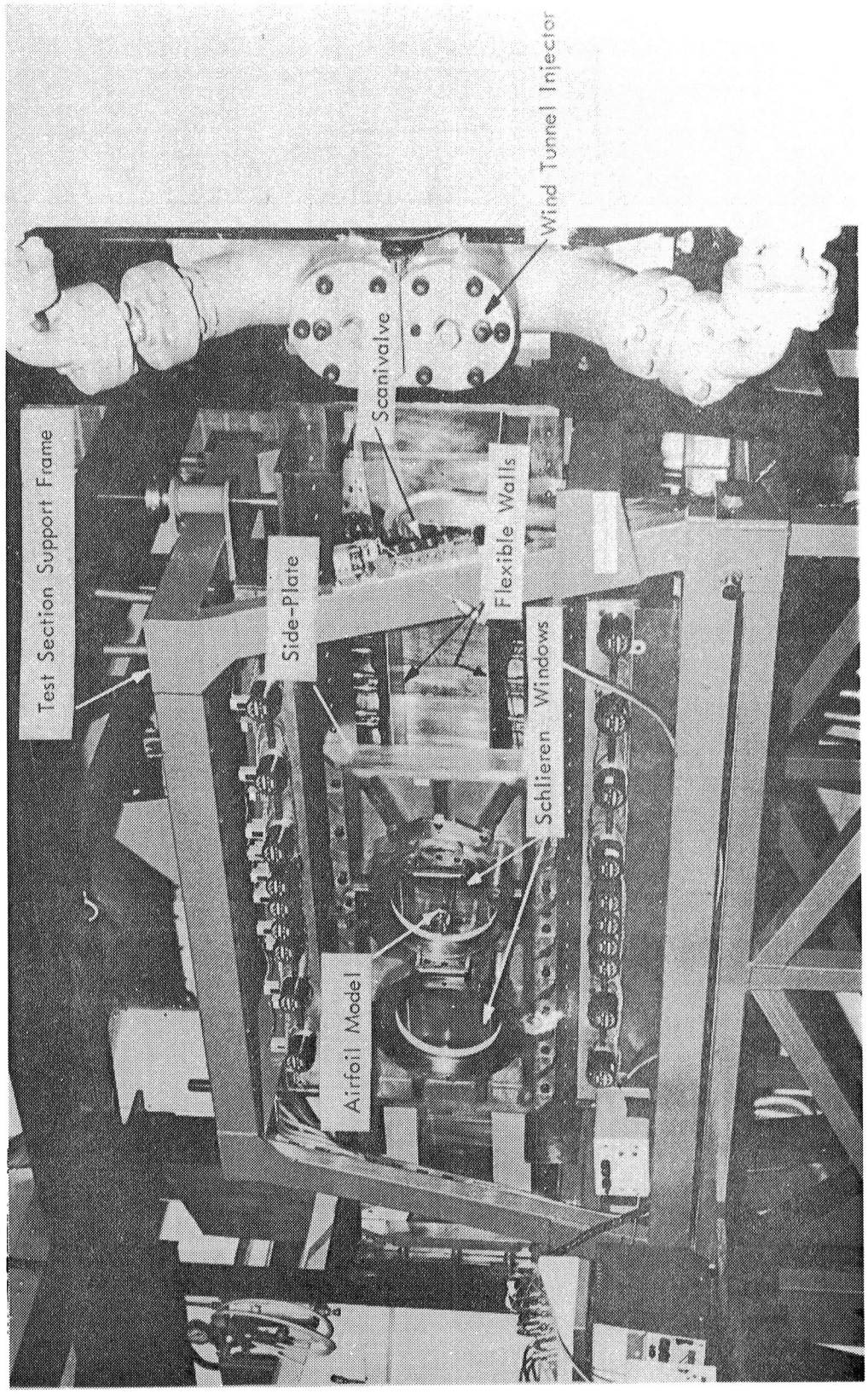

FIG . 6.2 TRANSONIC SELF STREAMLINING TEST SECTION

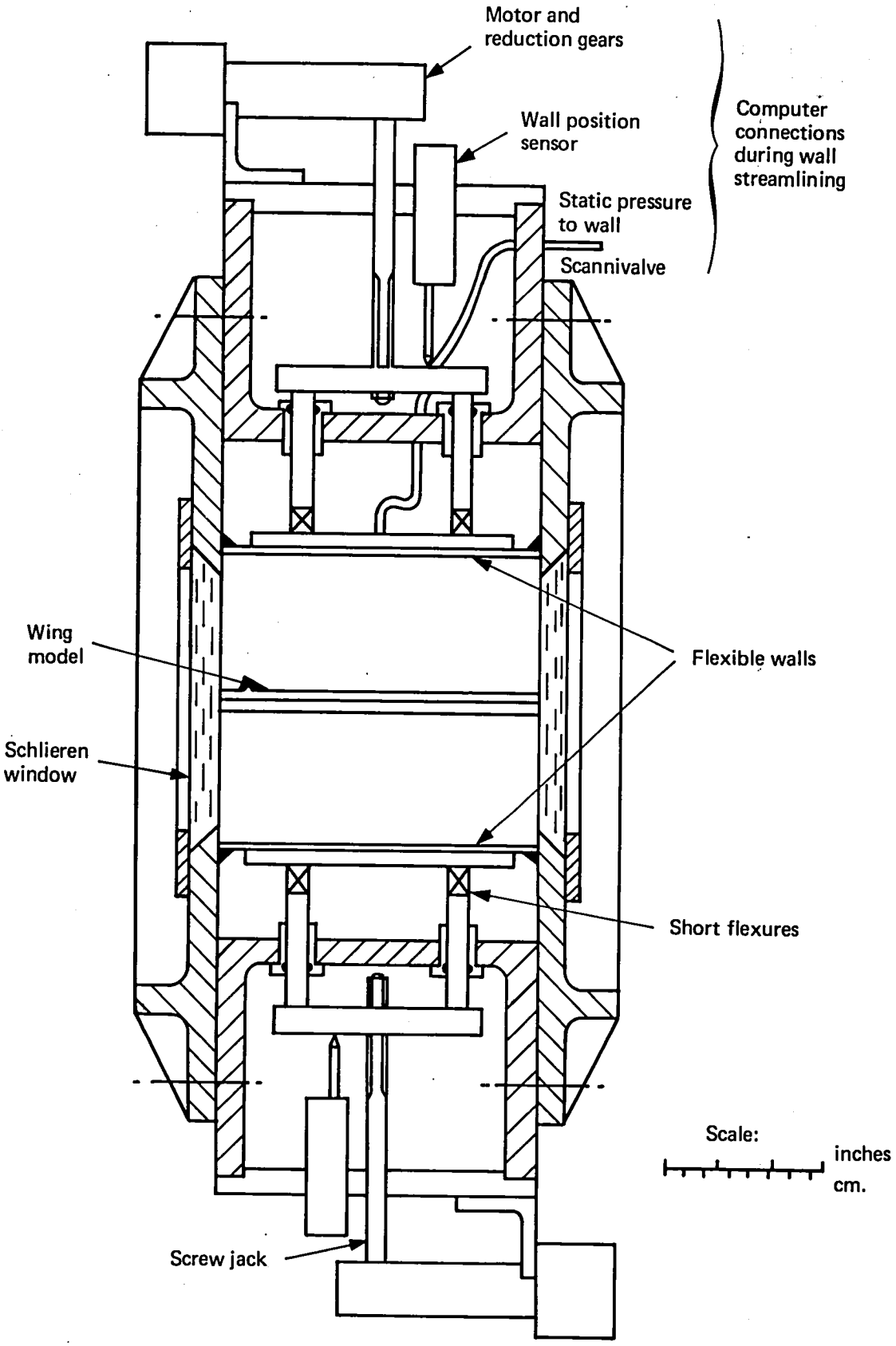

FIG. 6.3 TRANSONIC SELF-STREAMLINING TEST SECTION DESIGN - A VERTICAL CROSS SECTION LOOKING ALONG THE FLOW.

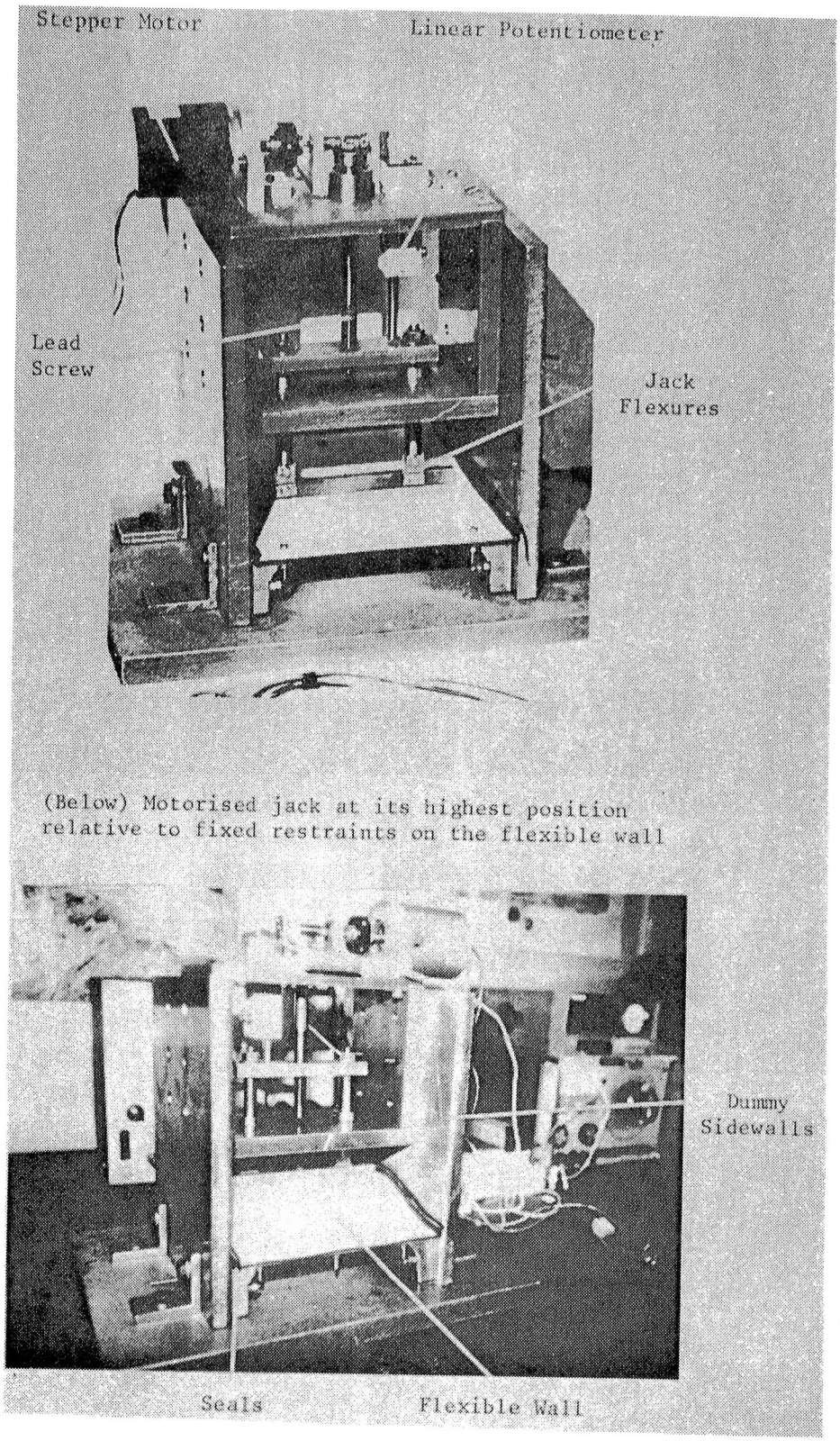

FIG. 6.4 PROTOTYPE WALL JACK RIG.

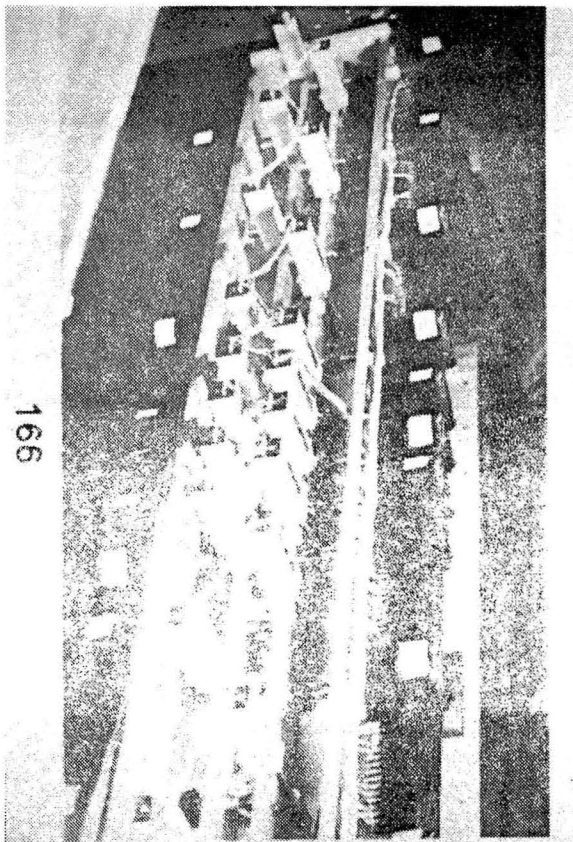

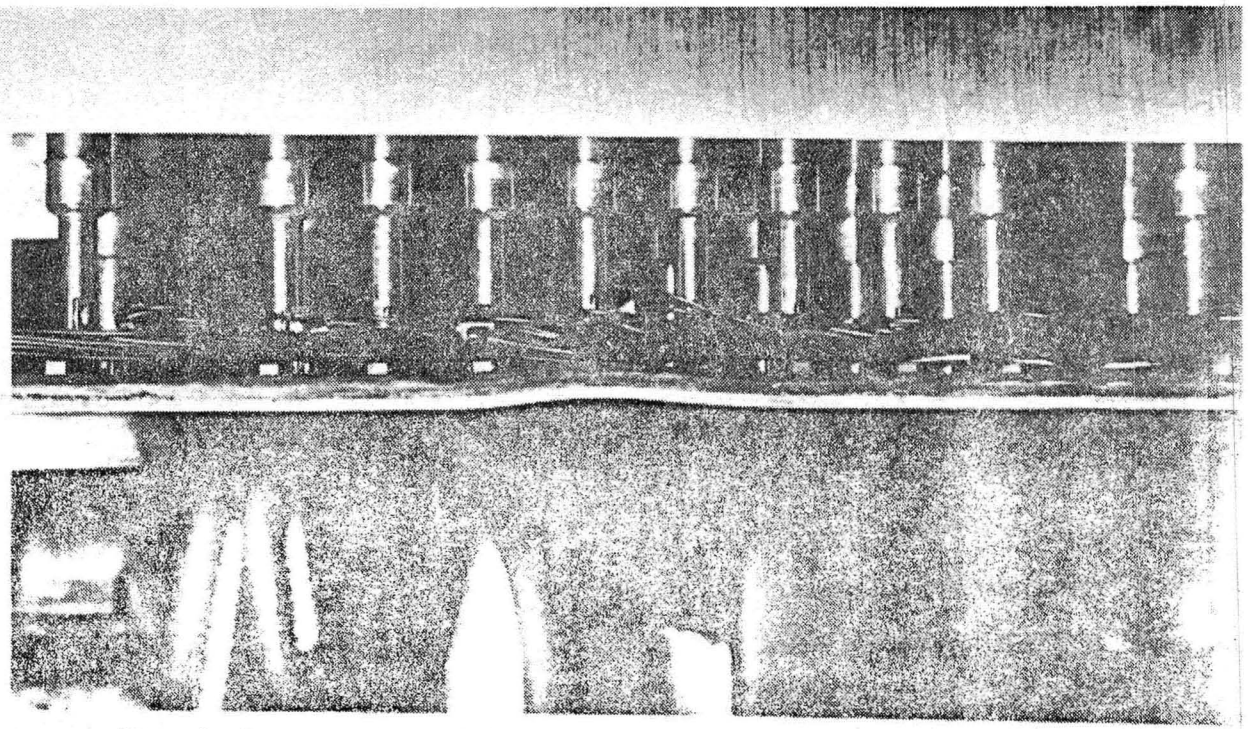

(Above) Close-up view of the wall jacks on the top wall adjacent to the model. A severe bump has been introduced in the wall contour. (Left) General view from above the test section which shows the compact layout of the jacking mechanisms and linear potentiometers.

FIG. 6.5 TSWT WALL JACKS.

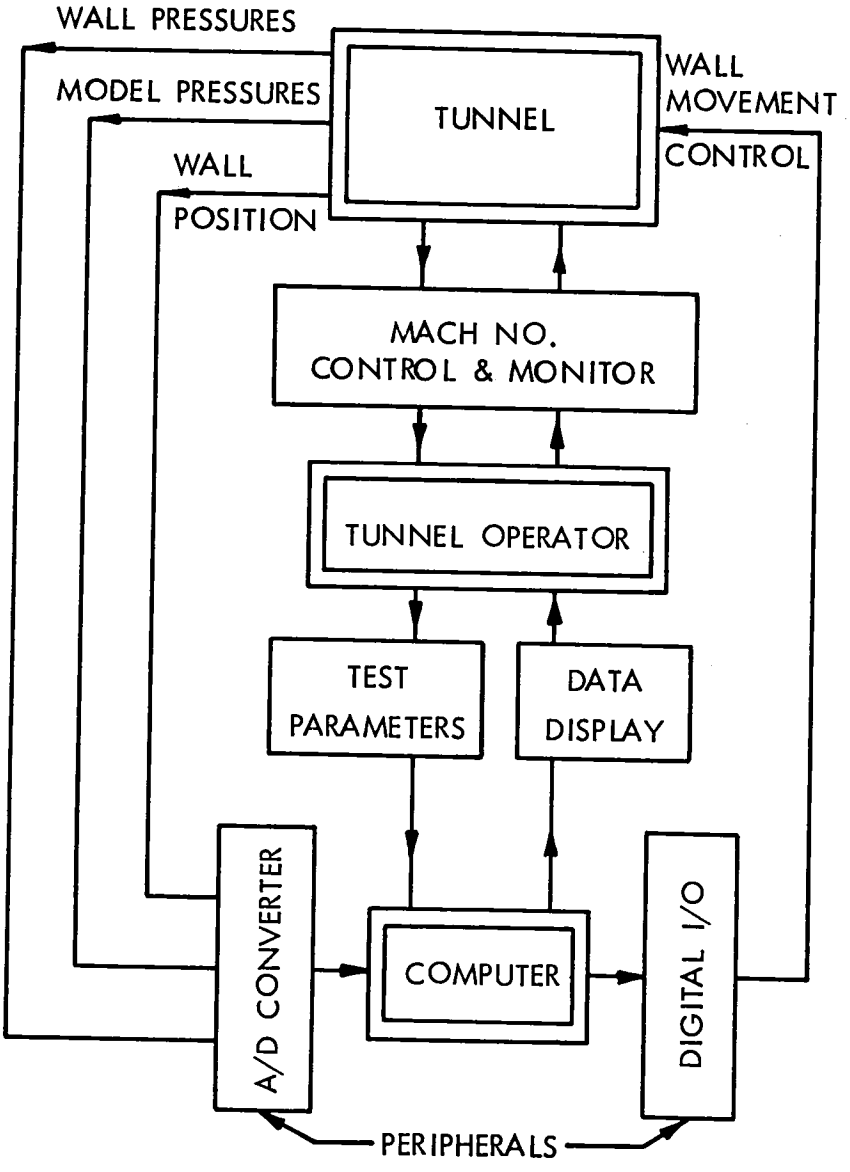

FIG. 6.6 TSWT CONTROL SYSTEM OUTLINE

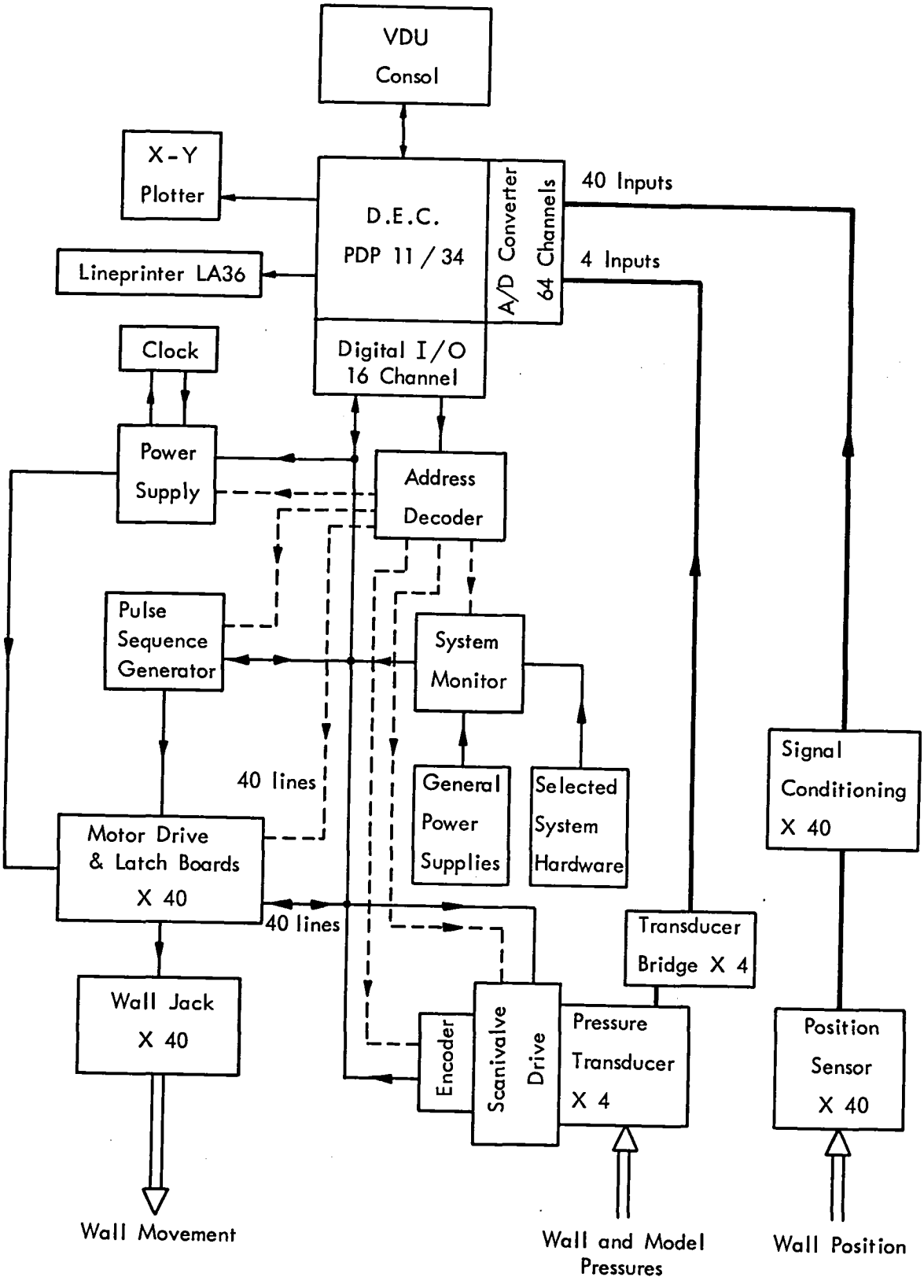

FIG.6.7 T.S.W.T. CONTROL SYSTEM HARDWARE

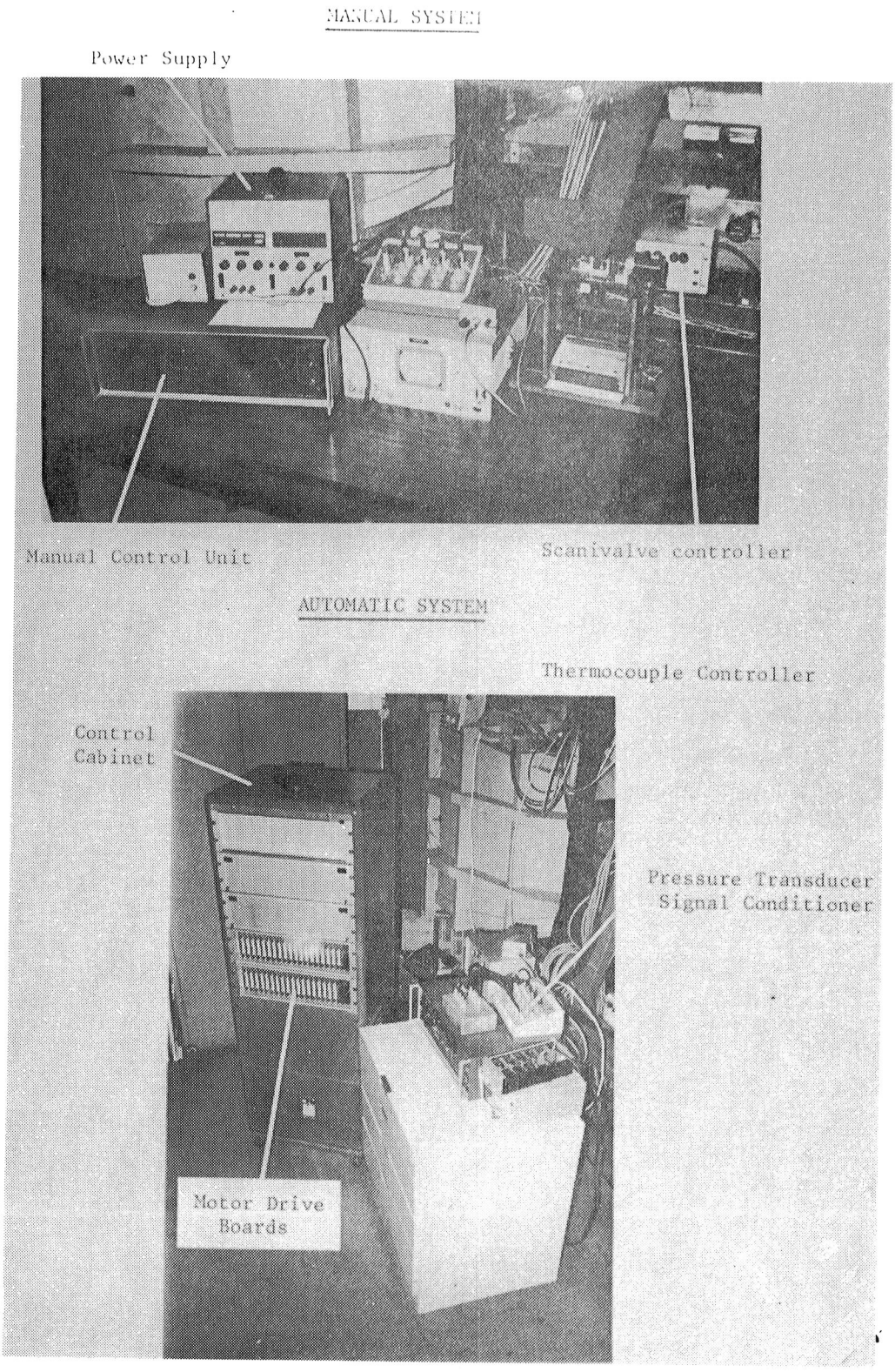

FIG. 6.8 TSWT CONTROL HARDWARE ADJACENT TO THE TSWT TEST SECTION.

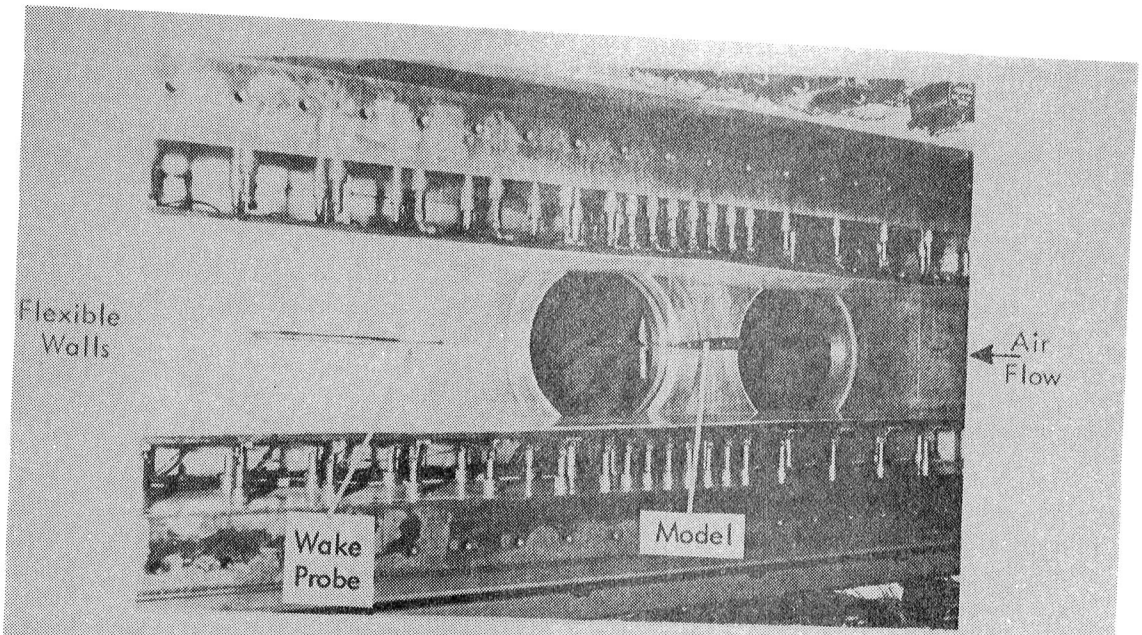

The wake probe mounted in TSWT downstream of a NACA 0012-64 schlieren model (above) with the walls streamlined for the test case of $M_\infty = .7$; $\alpha = 4^o$.

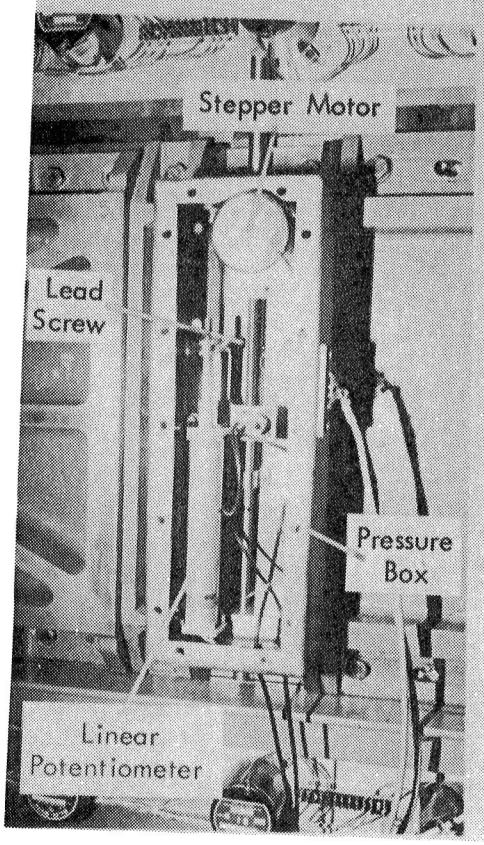

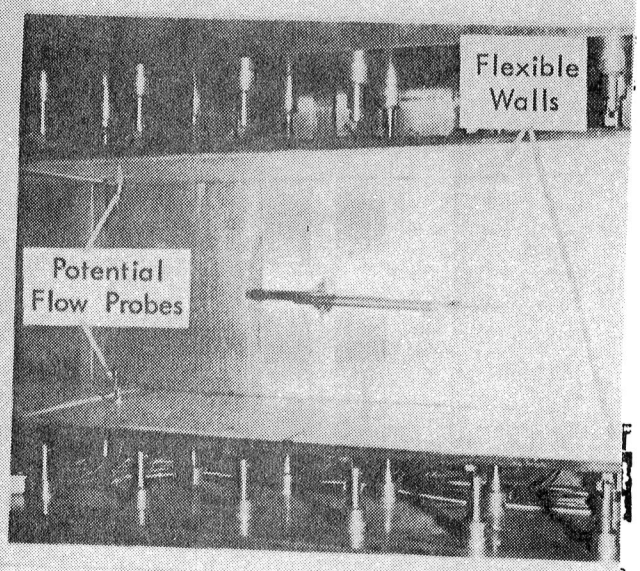

The wake traverse mechanism is mounted on a rigid sidewall plate (left with the pressure box open). The probe is connected by stainless steel tubes to a sliding plate flush with the sidewall of the test section (above).

FIG. 6.9 WAKE TRAVERSE HARDWARE IN SITU

WAKE PROBE

(Disc - Static Type)

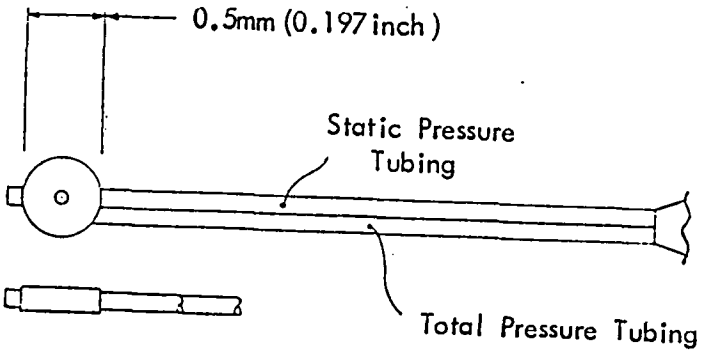

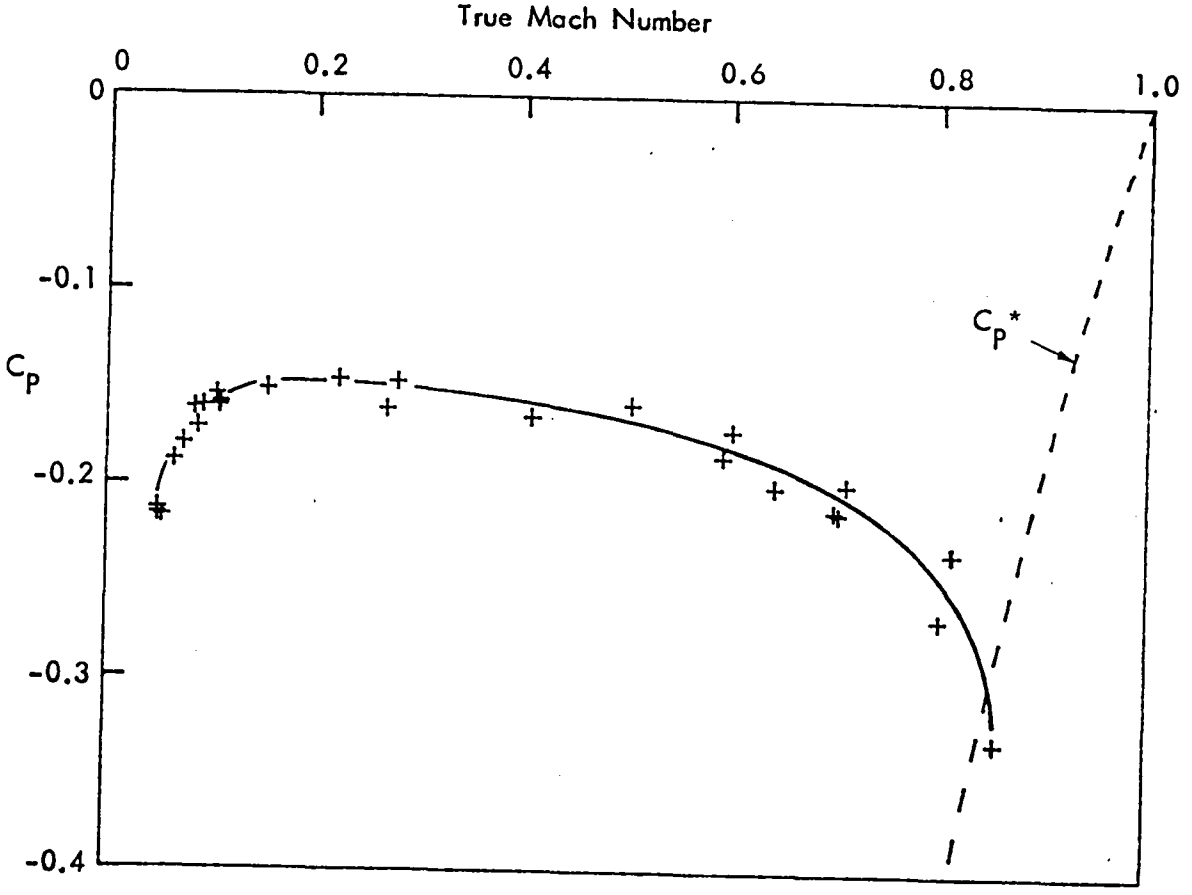

FIG. 6.10 WAKE PROBE CALIBRATION

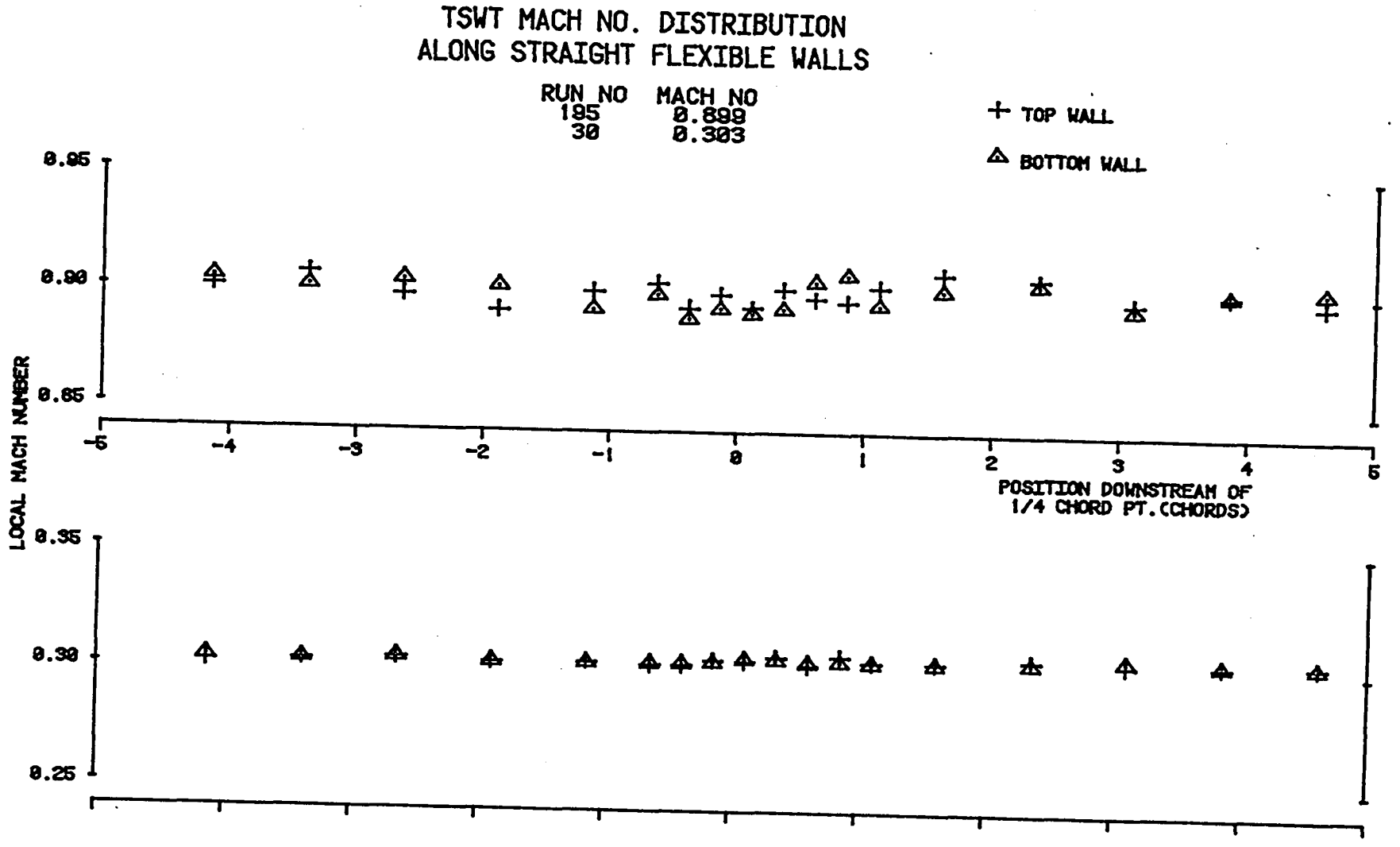

FIG. 6.11 COMPARISON OF STRAIGHT WALL MACH NUMBER DISTRIBUTIONS FOR $M_\infty \simeq 0.3$ AND $M_\infty \simeq 0.9$

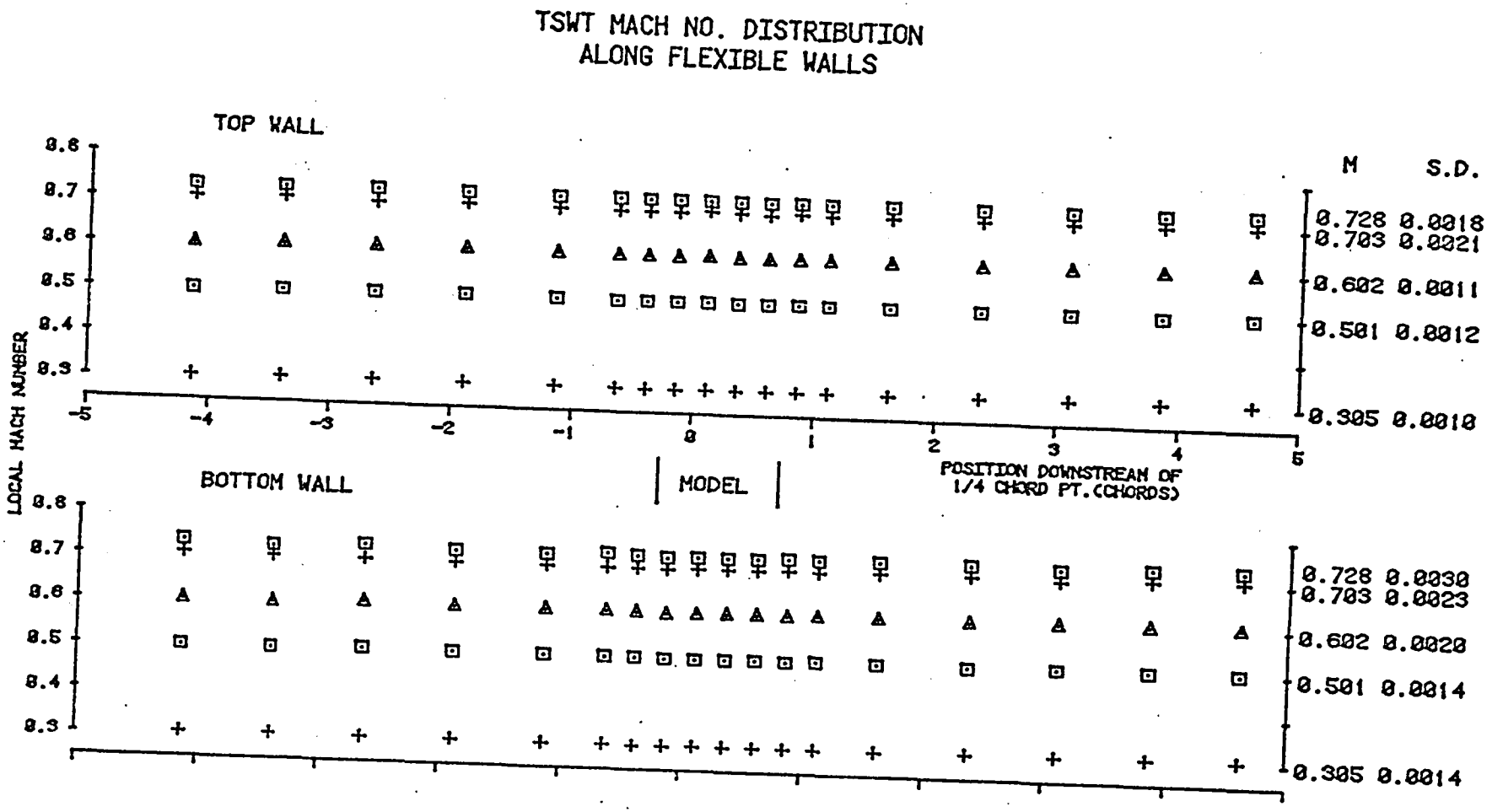

FIG. 6.12 MACH NUMBER DISTRIBUTION ALONG FLEXIBLE WALLS SET TO 'A' CONTOUR

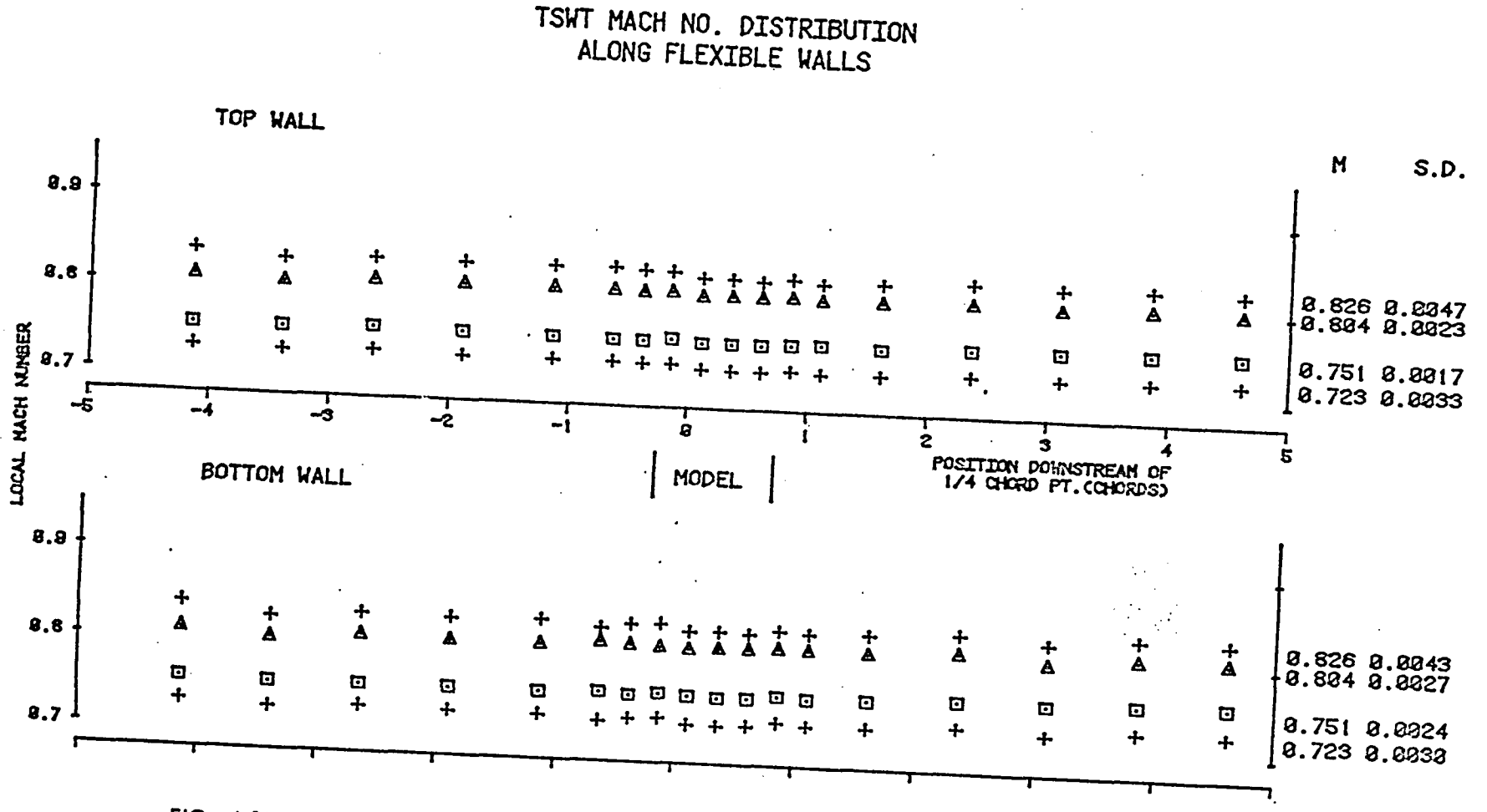

FIG. 6.13 MACH NUMBER DISTRIBUTION ALONG FLEXIBLE WALLS SET TO 'B' CONTOUR

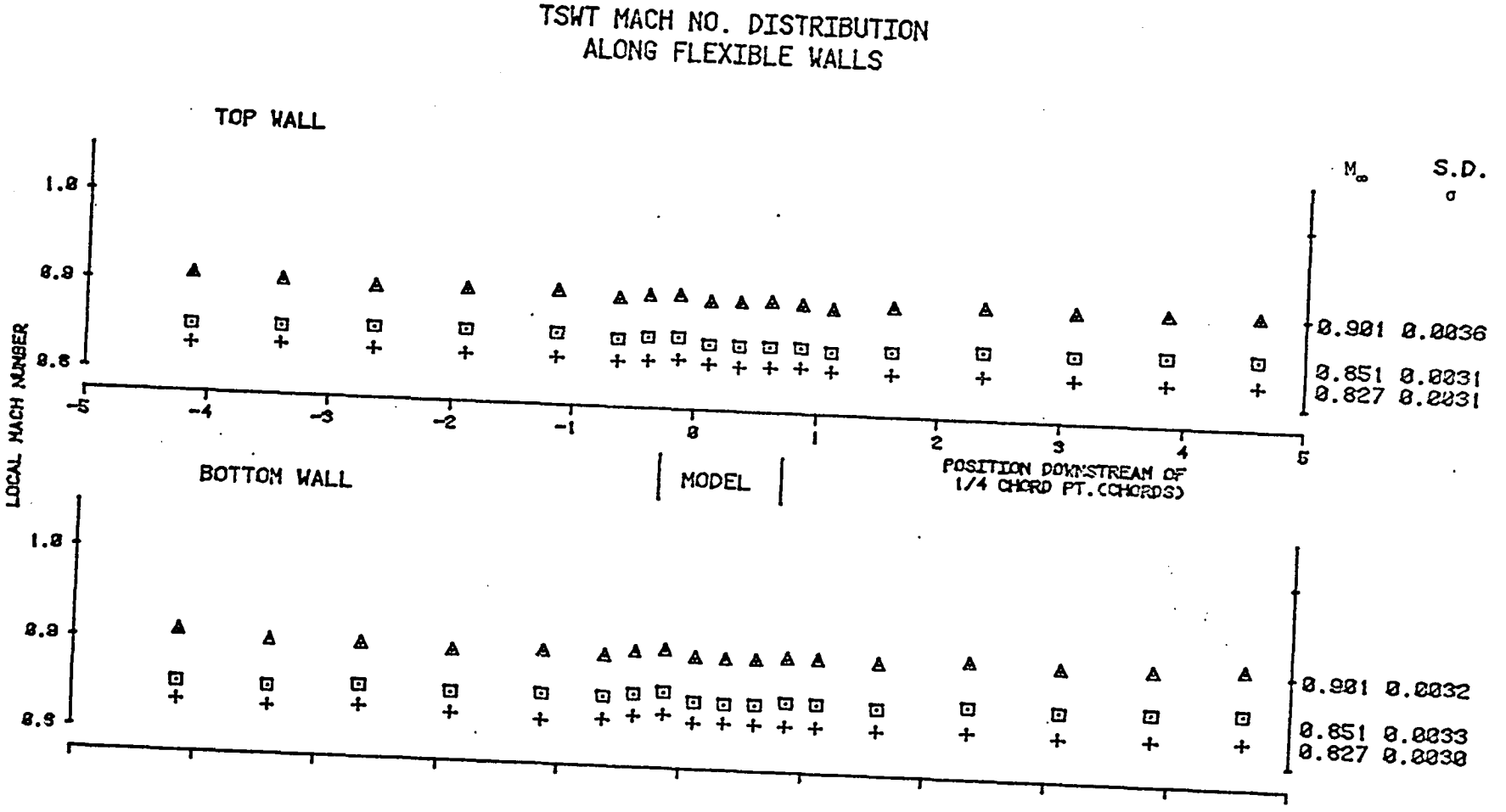

FIG. 6.14 MACH NUMBER DISTRIBUTIONS ALONG FLEXIBLE WALLS SET TO 'C' CONTOUR

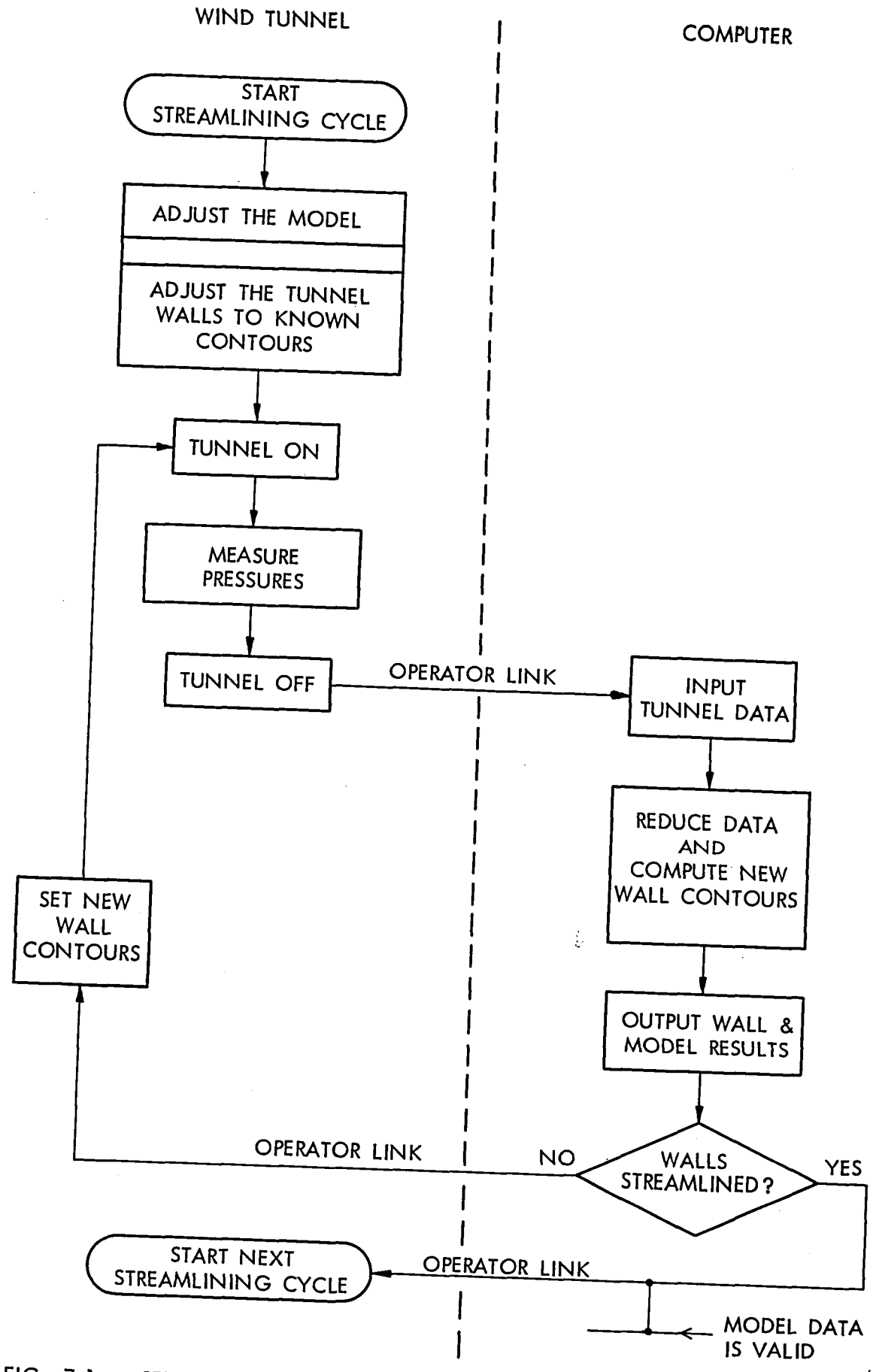

FIG. 7.1 SELF STREAMLINING WIND TUNNEL MANUAL OPERATING PROCEDURE

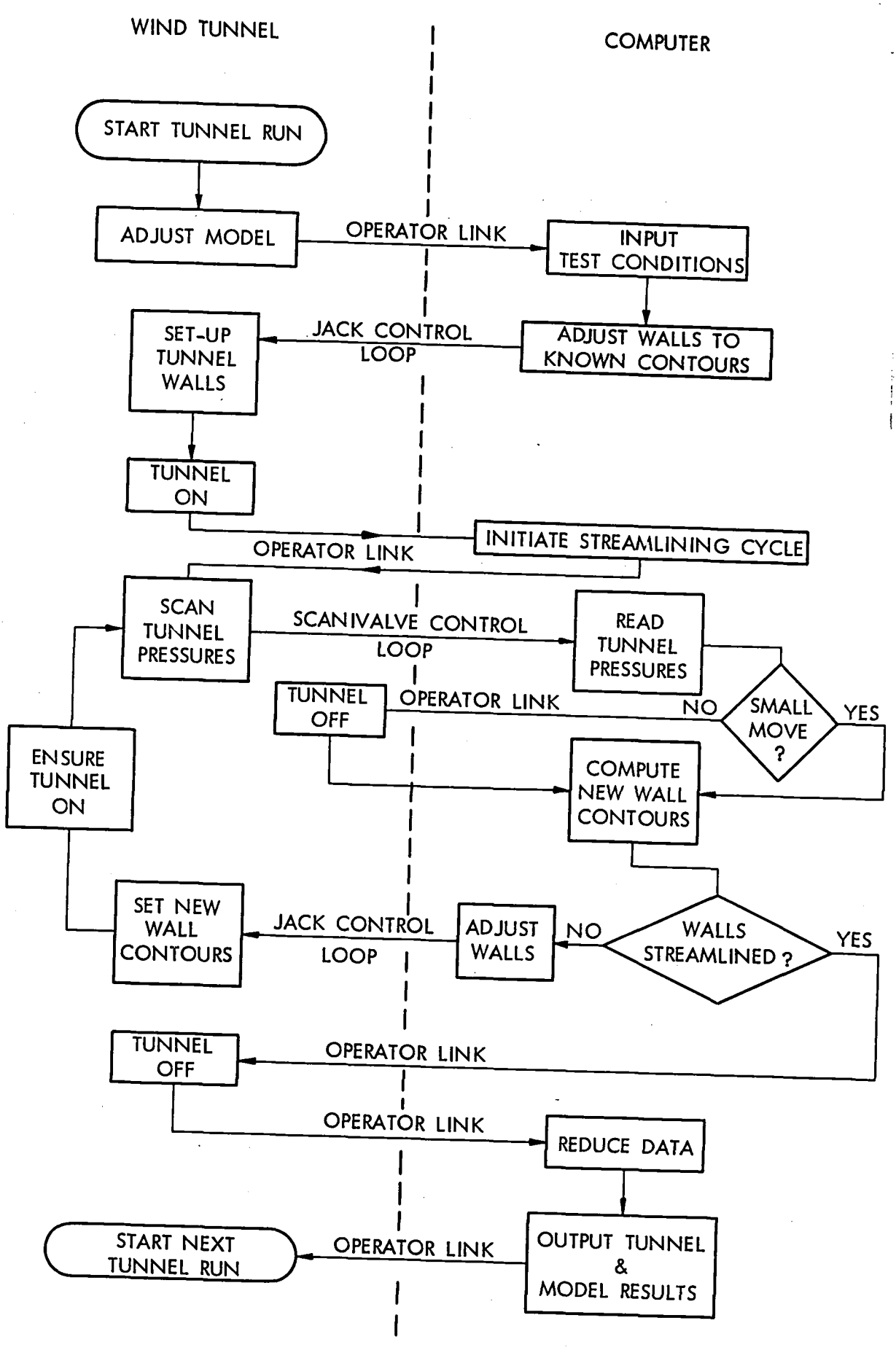

FIG. 7.2 SELF STREAMLINING WIND TUNNEL AUTOMATIC OPERATING PROCEDURE

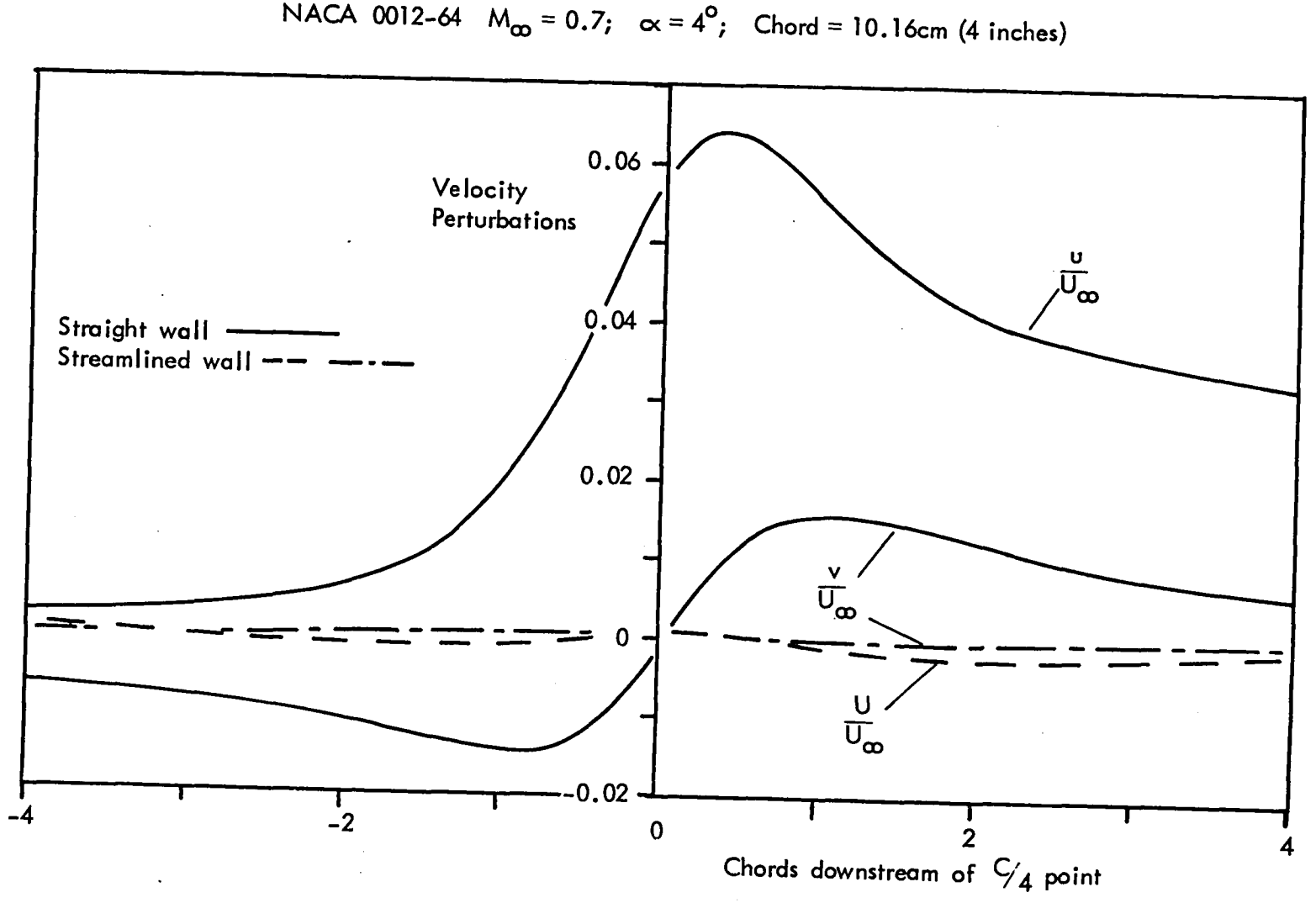

FIG. 7.3 WALL INDUCED VELOCITY PERTURBATIONS ALONG TSWT CENTRELINE.

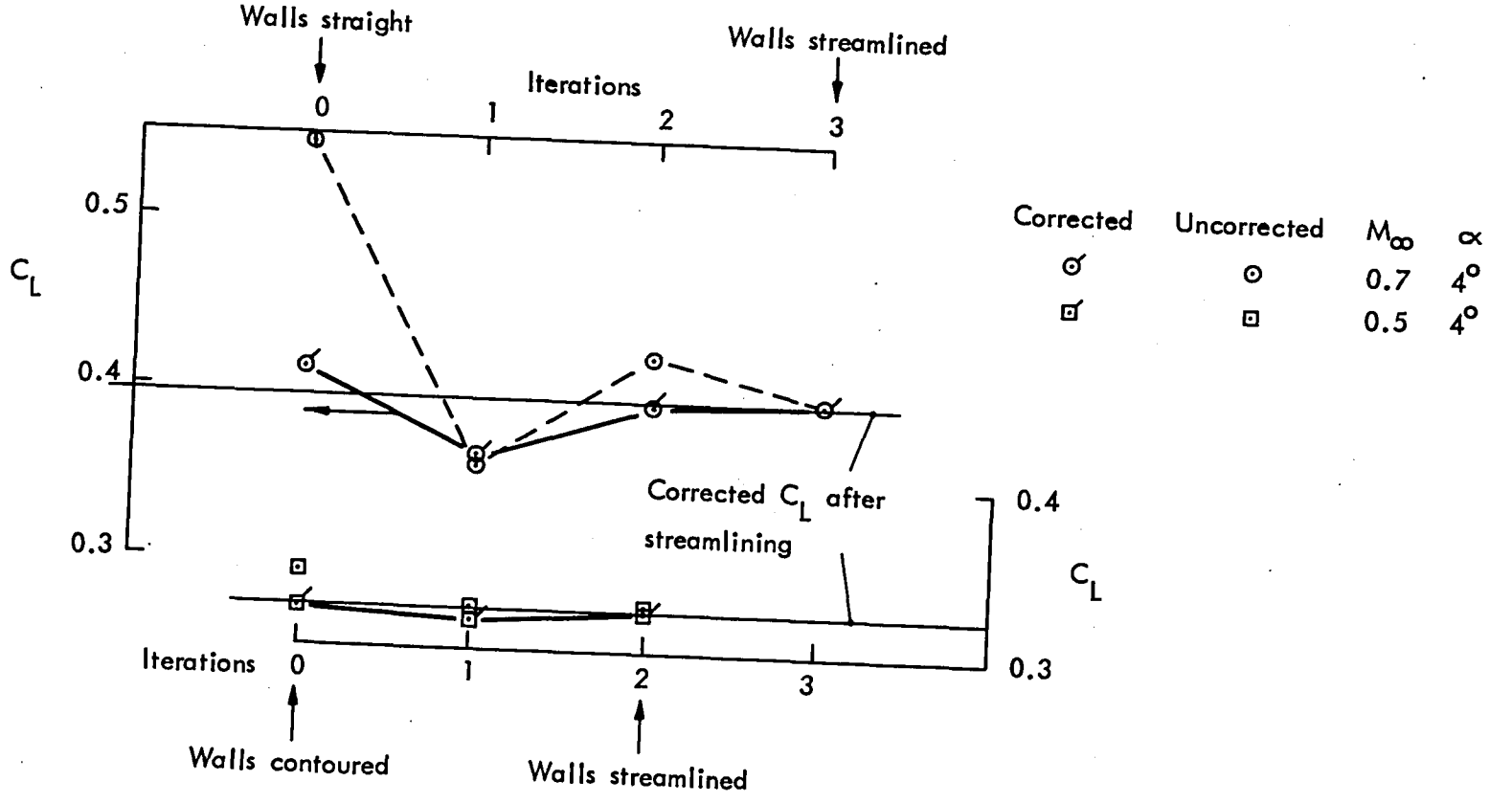

FIG. 7.4 VARIATION OF CORRECTED AND UNCORRECTED MODEL C_L DURING TYPICAL STREAMLINING CYCLES

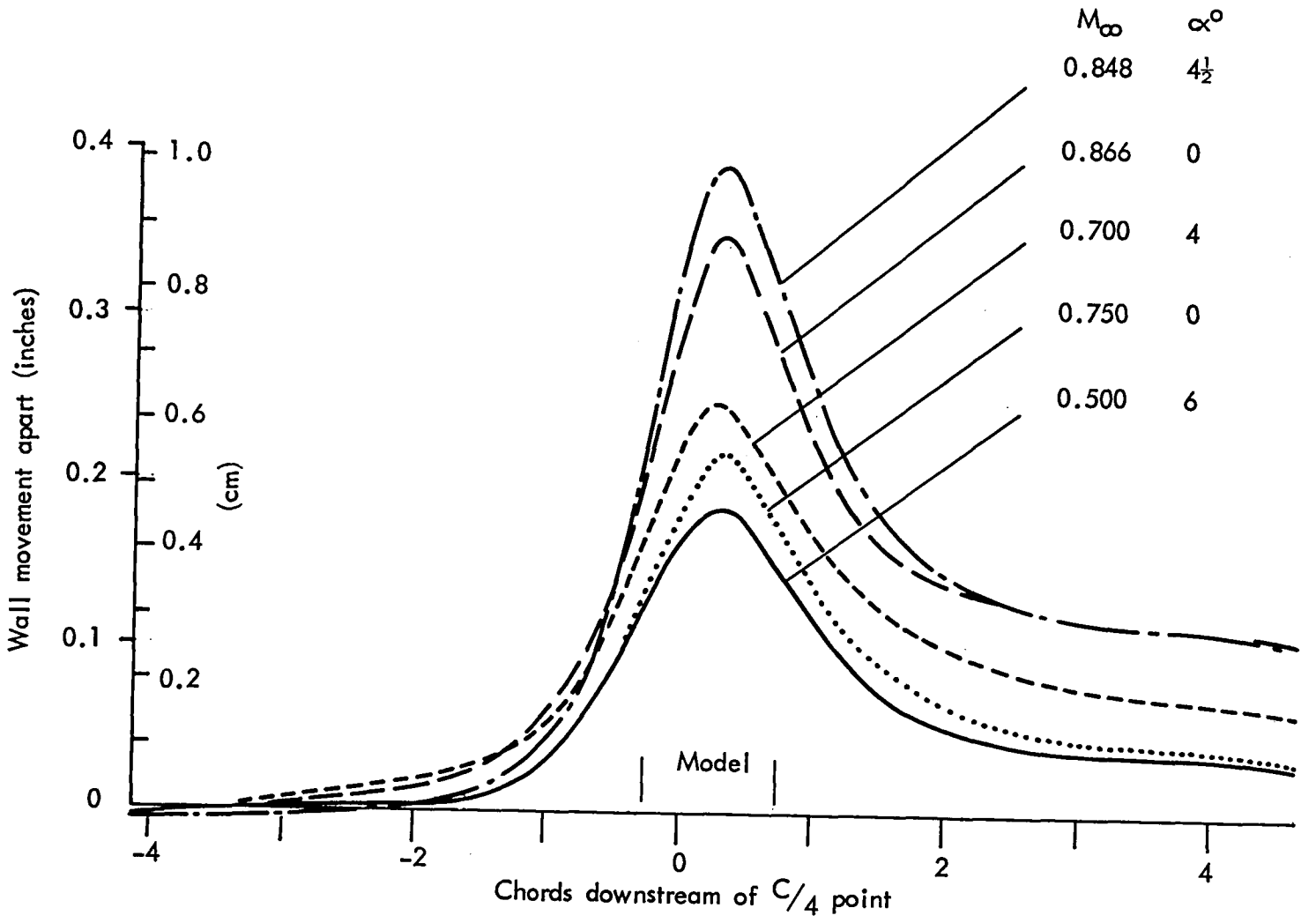

FIG. 7.5 RELATIVE SEPARATION OF STREAMLINED WALLS FOR VARIOUS MODEL ATTITUDES AND MACH. NUMBERS

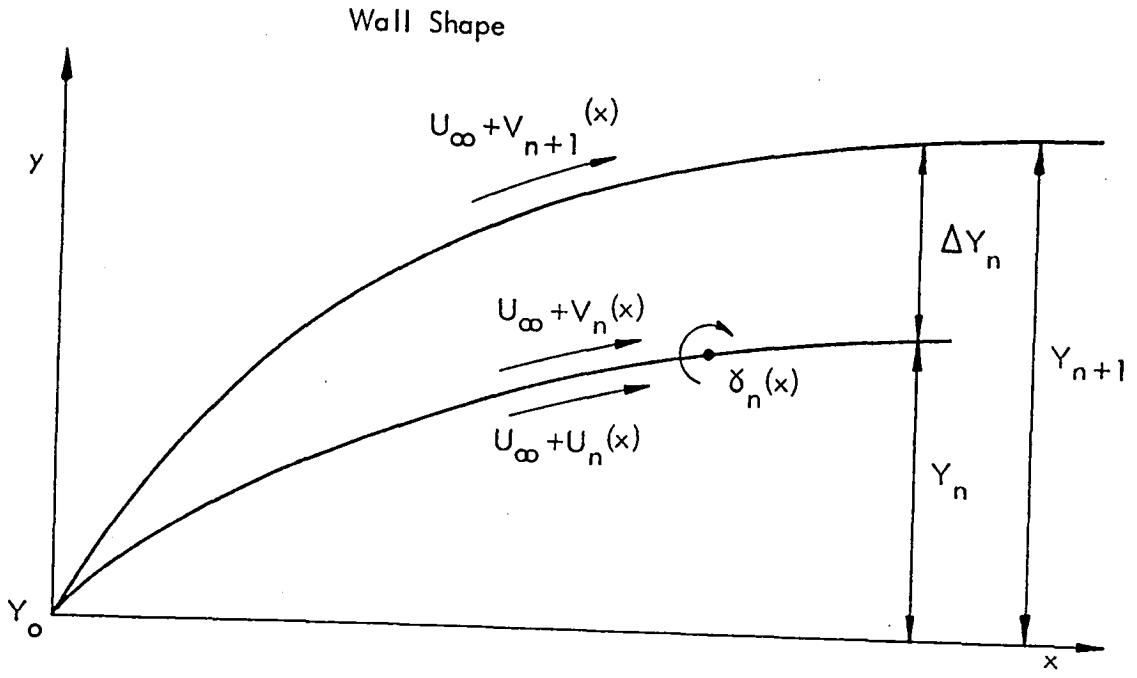

FIG. 8.1 WALL SETTING STRATEGY CONCEPT

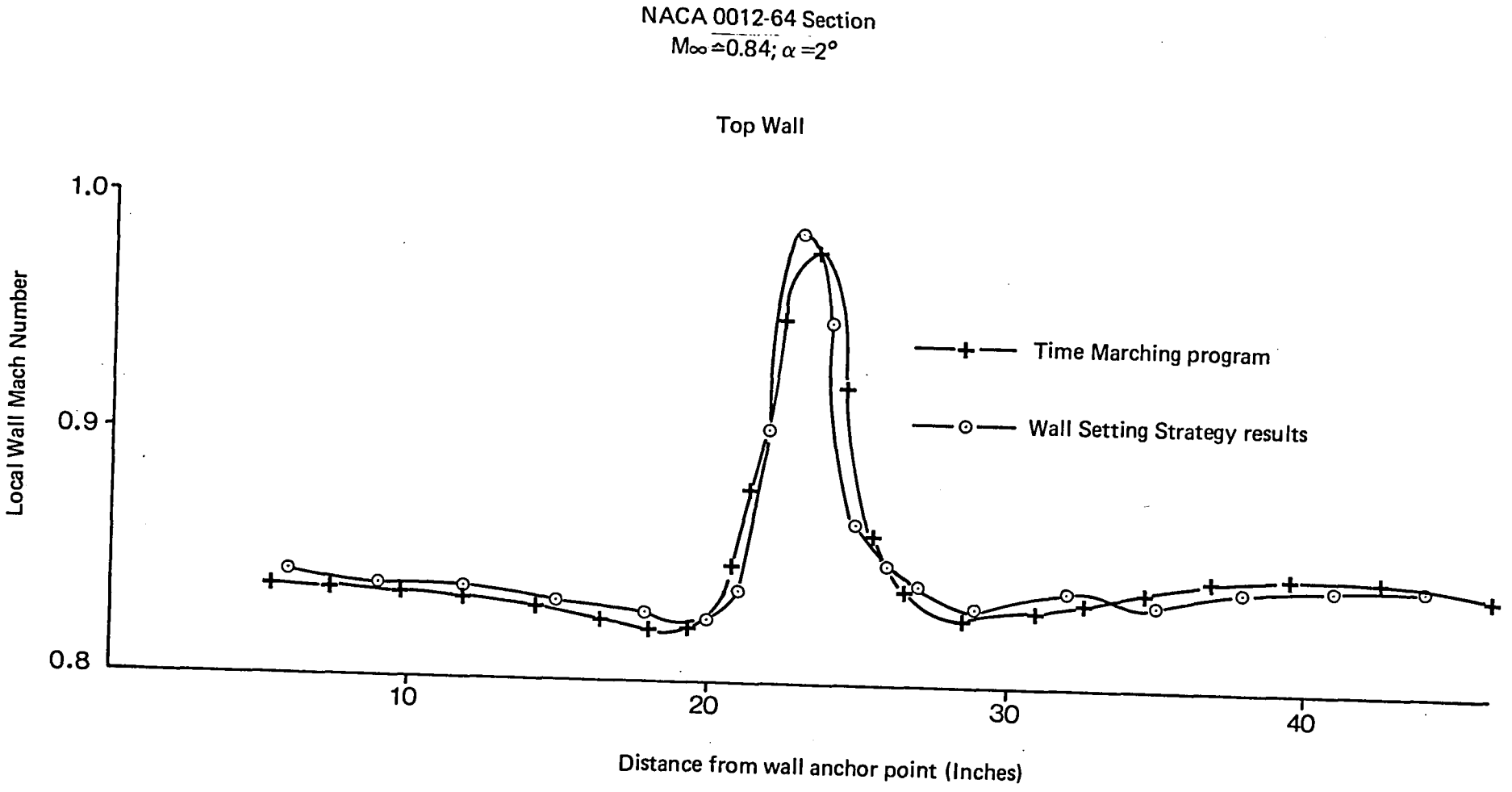

FIG. 8.2 COMPARISON OF IMAGINARY WALL MACH NUMBER DISTRIBUTIONS CALCULATED FROM THE TSWT WALL SETTING STRATEGY AND A TIME MARCHING PROGRAM.

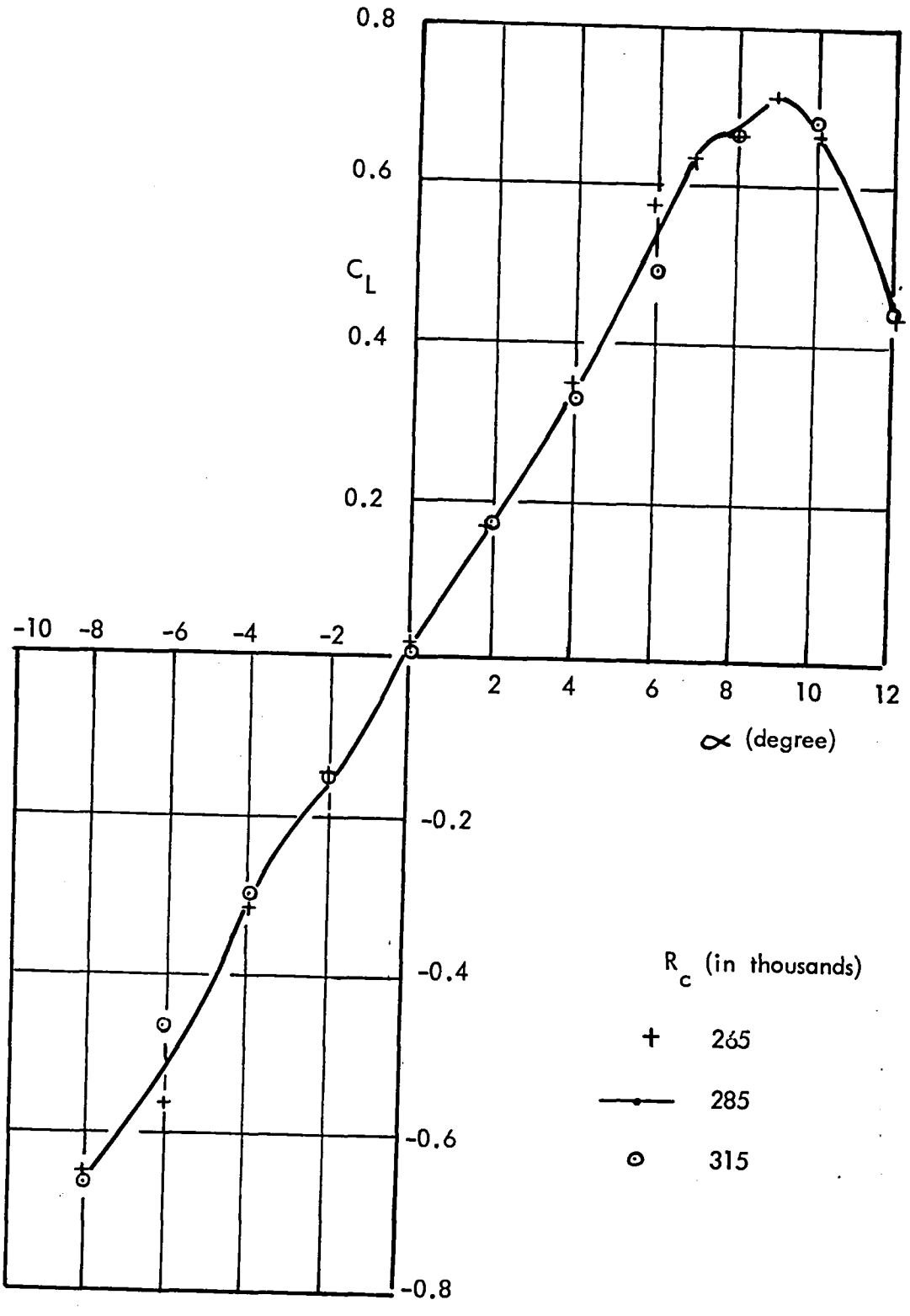

FIG . 9.1 SUMMARY OF LTPT LIFT COEFFICIENT DATA

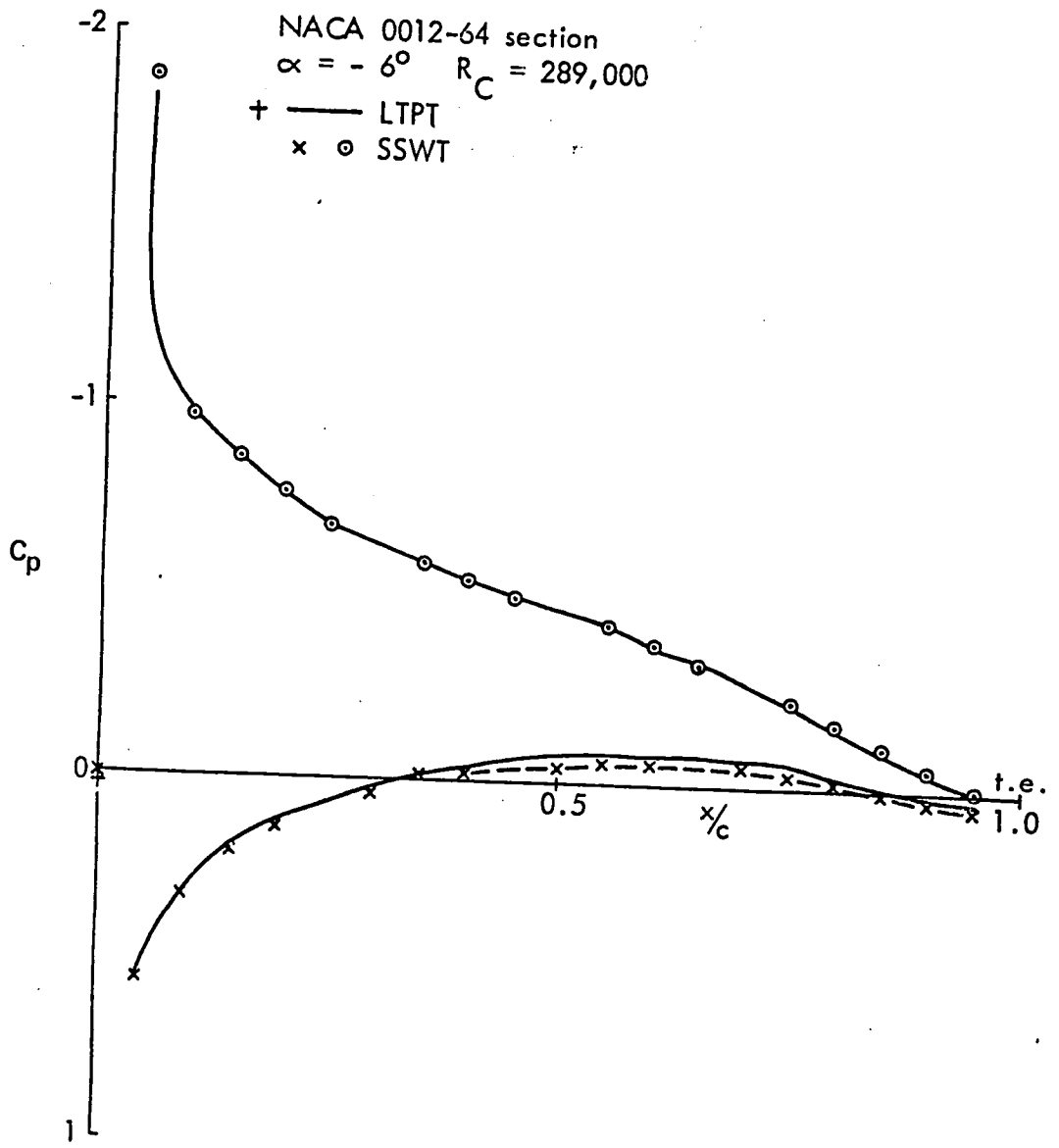

FIG. 9.2(a) NACA 0012-64 PRESSURE DISTRIBUTION

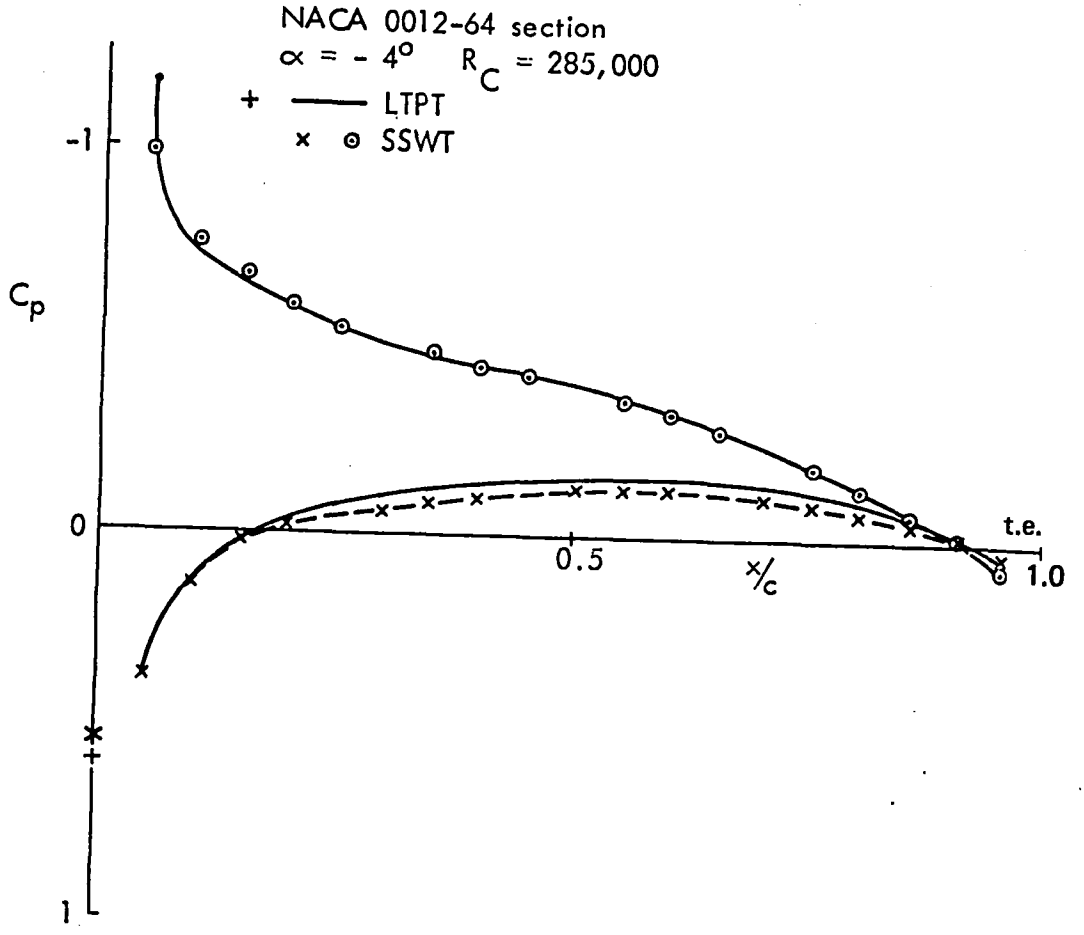

FIG. 9.2(b) NACA 0012-64 PRESSURE DISTRIBUTION

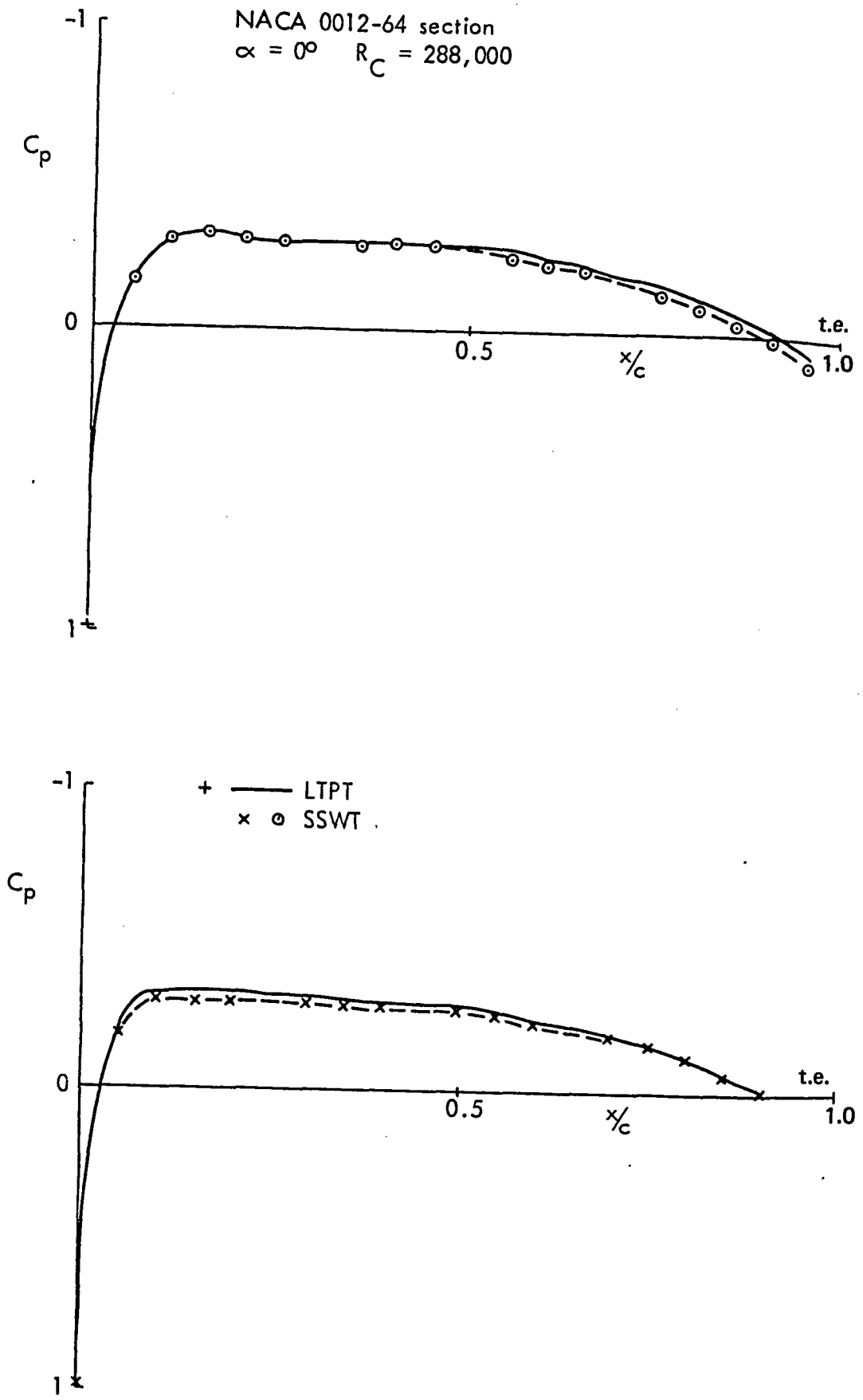

FIG. 9.2(c) NACA 0012-64 PRESSURE DISTRIBUTION

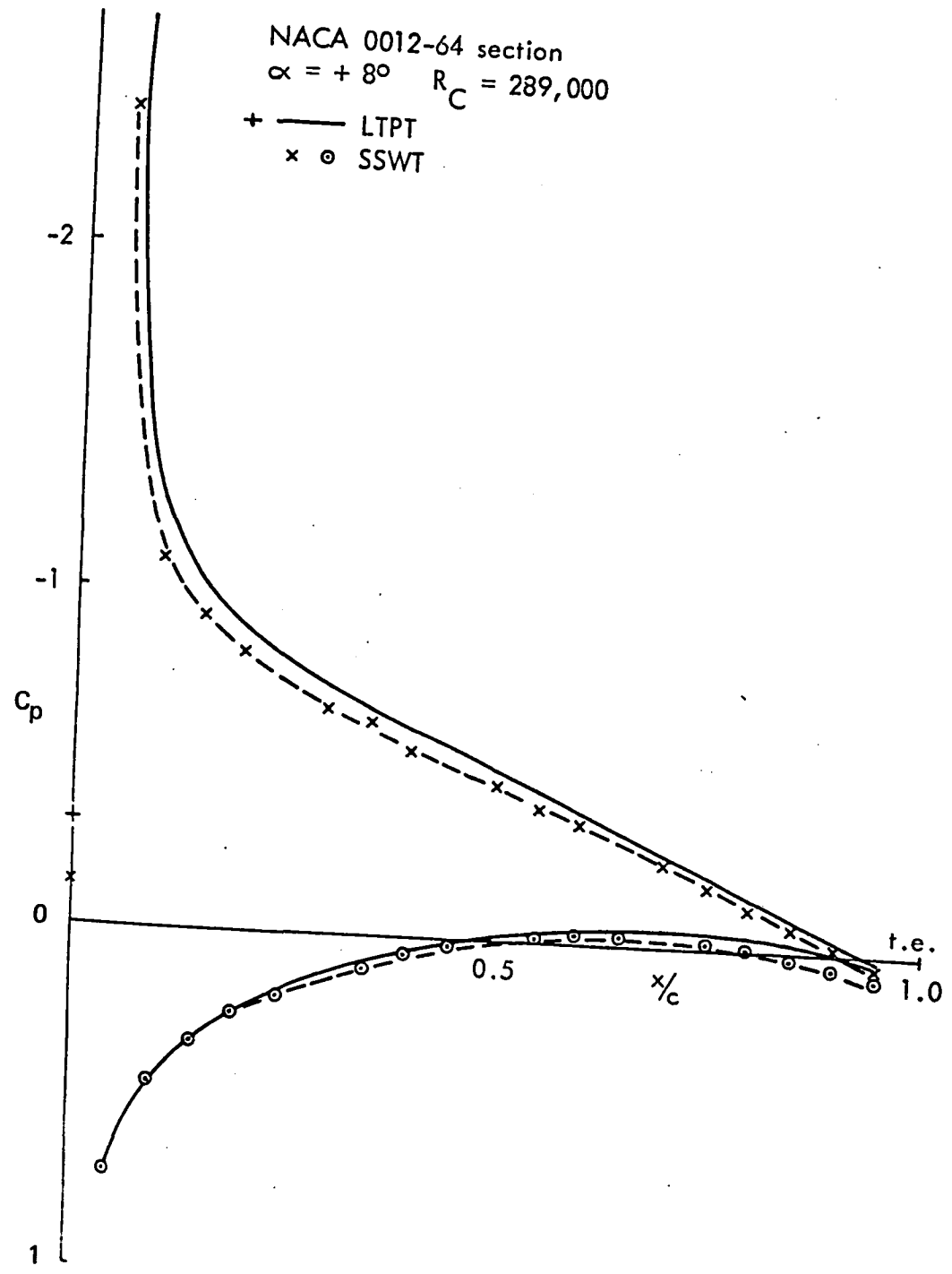

FIG. 9.2(d) NACA 0012-64 PRESSURE DISTRIBUTION

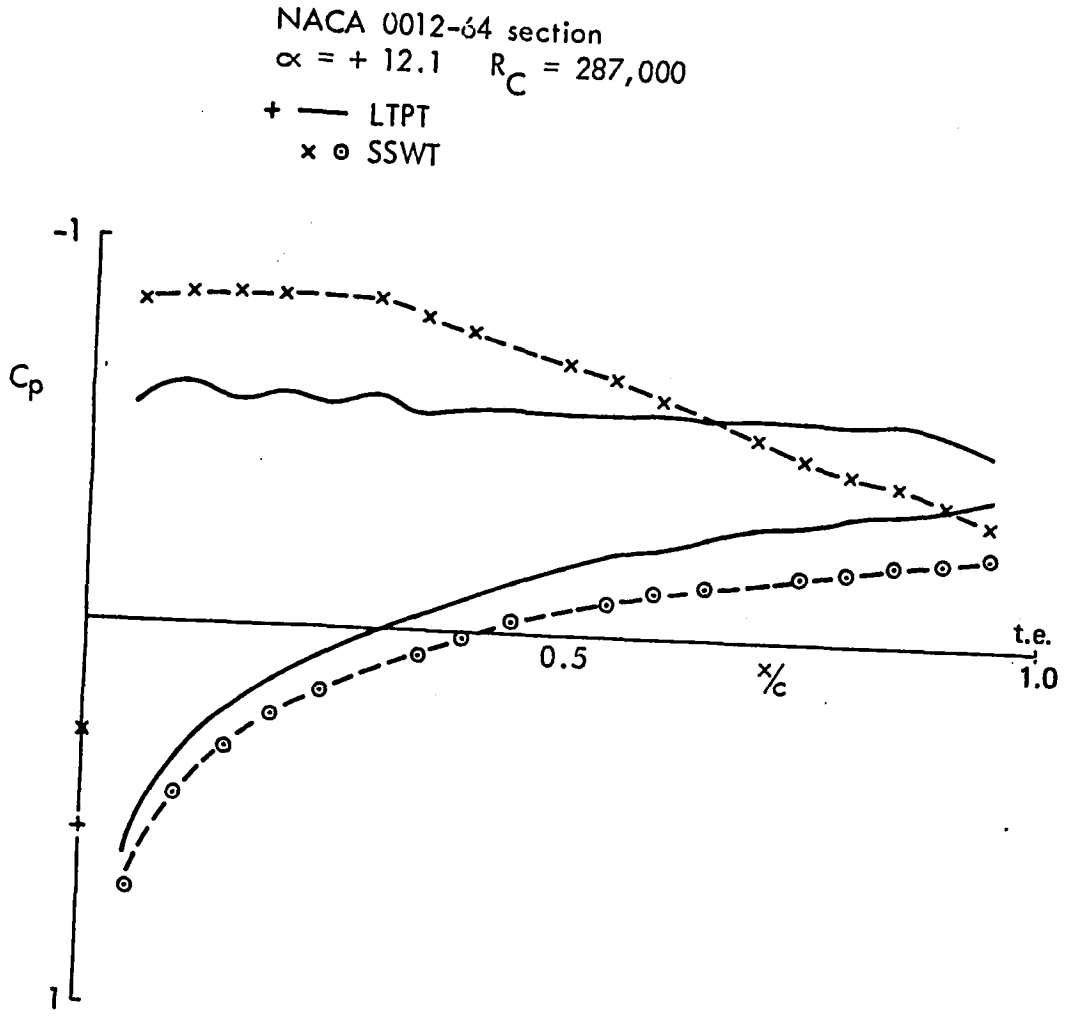

FIG. 9.2(e) NACA 0012-64 PRESSURE DISTRIBUTION

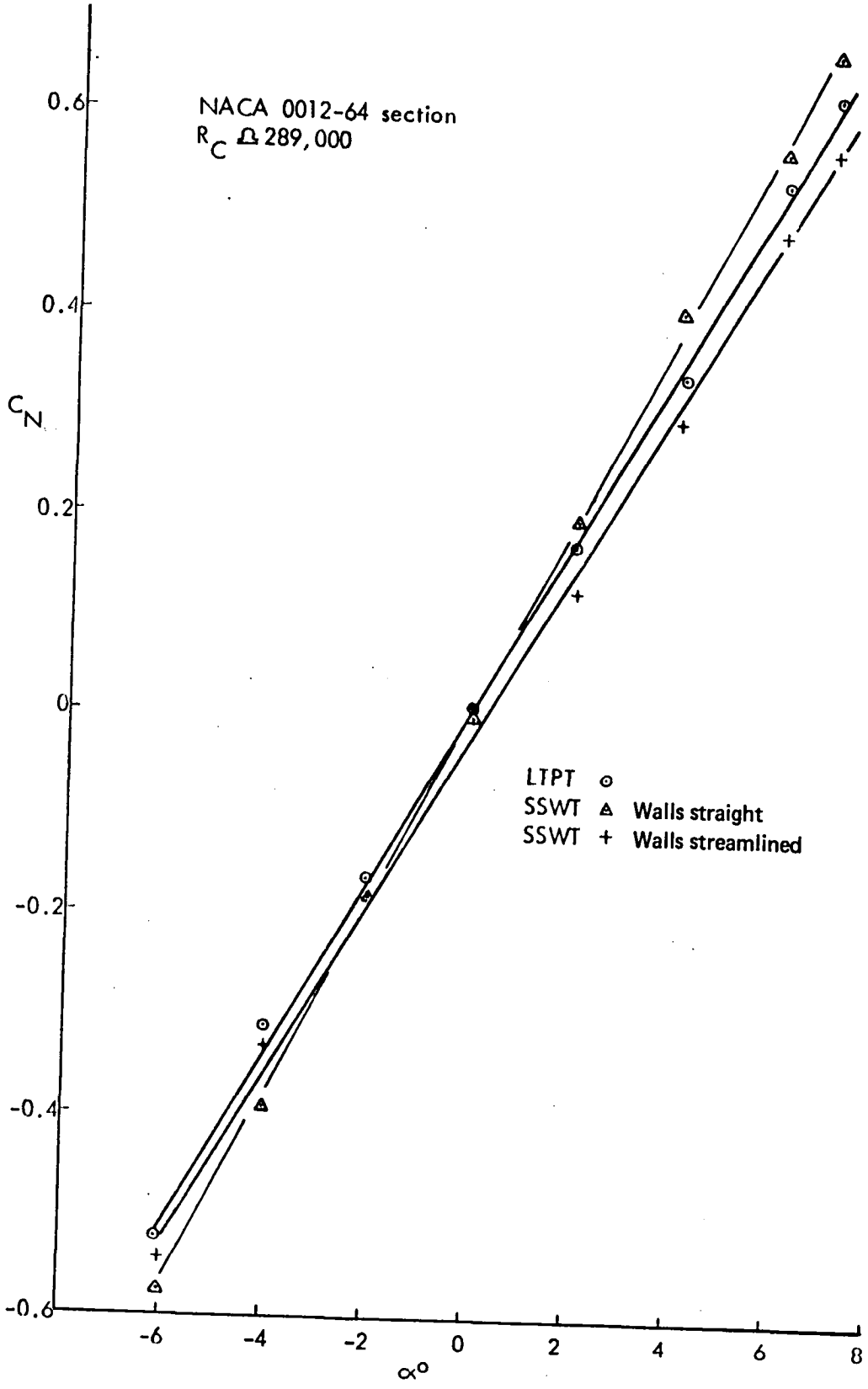

FIG. 9.3(a) C_N-α DATA FROM LTPT AND THE SELF STREAMLINING WIND TUNNEL.

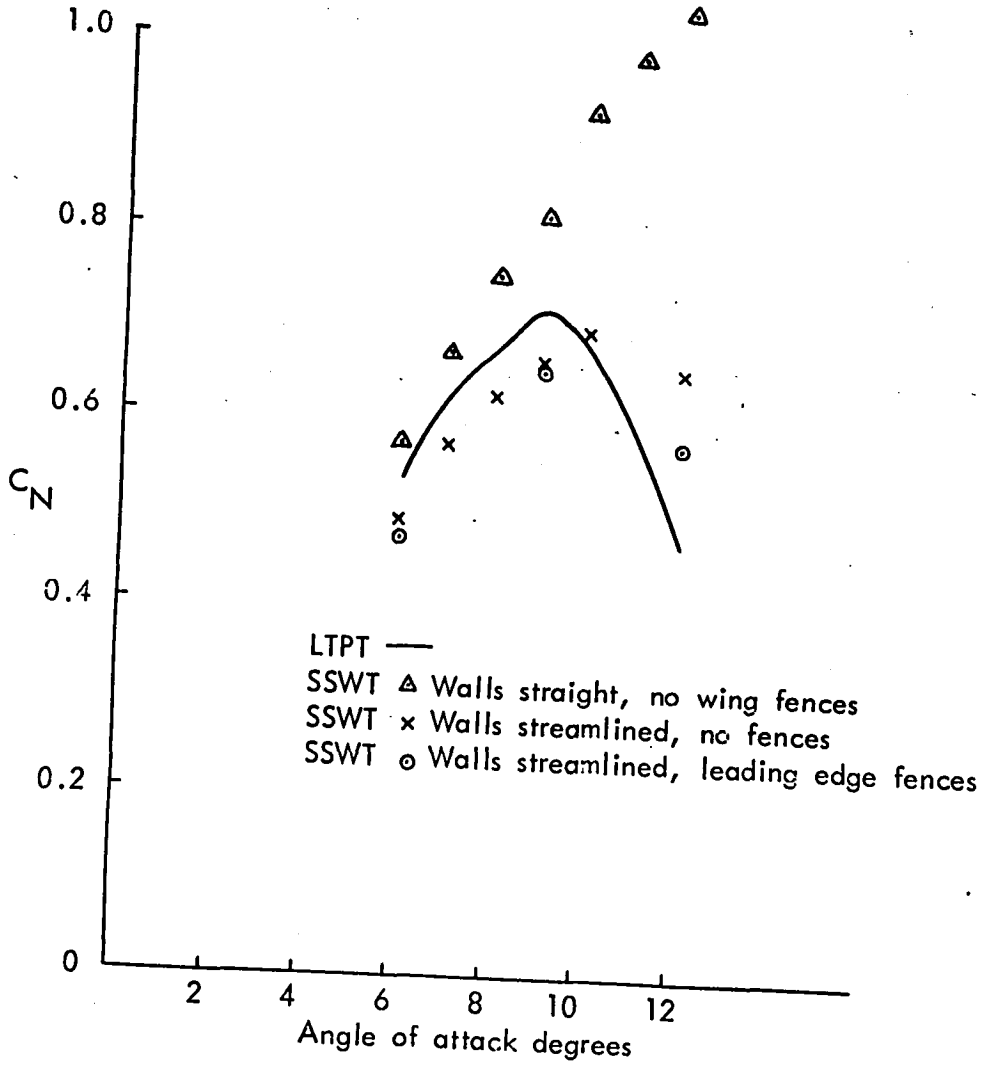

FIG. 9.3(b) VARIATION OF C_N WITH ANGLE OF ATTACK IN STALL REGIME

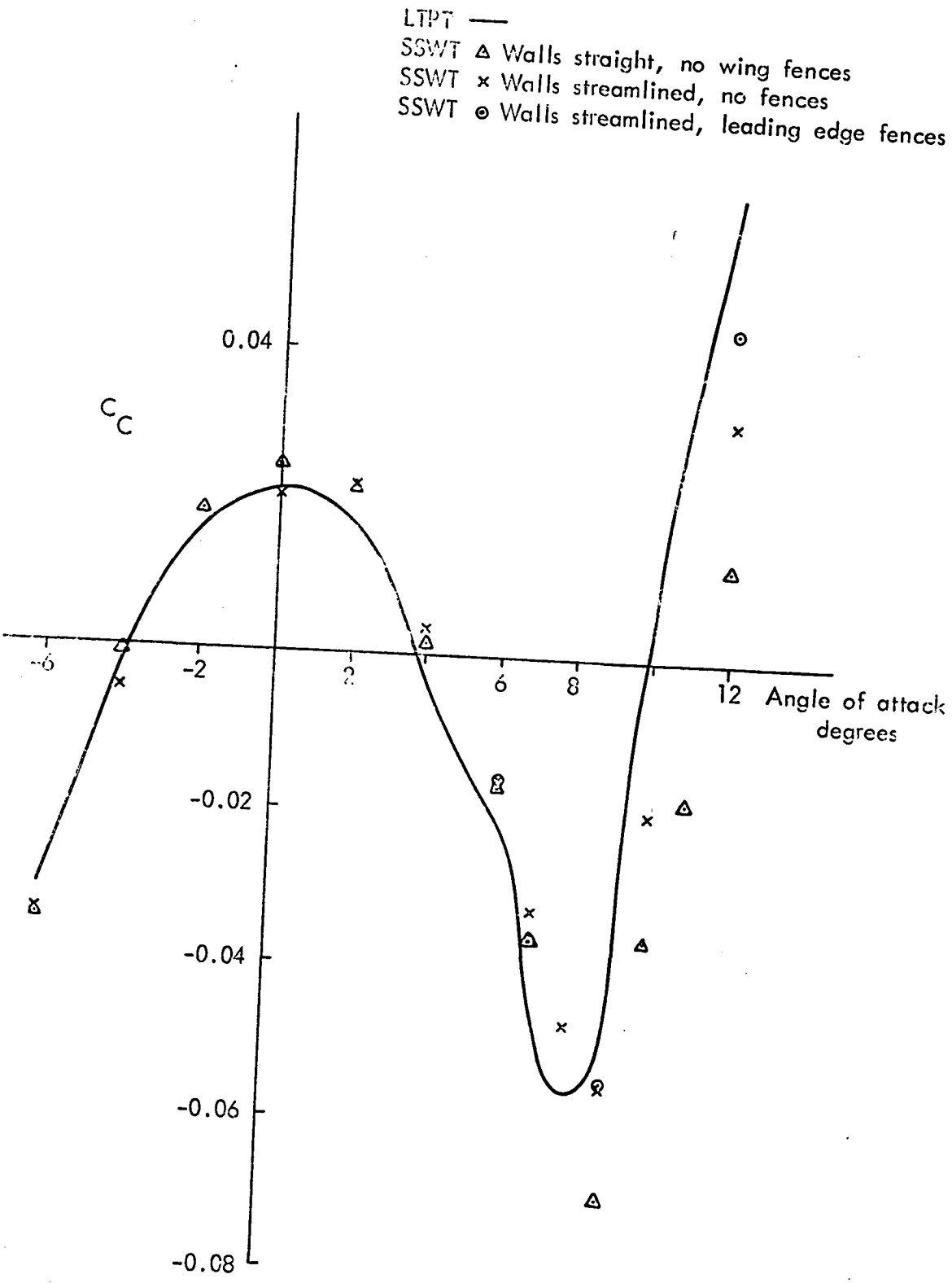

FIG. 9.4 $C_C - \alpha$ DATA FROM LTPT AND SSWT

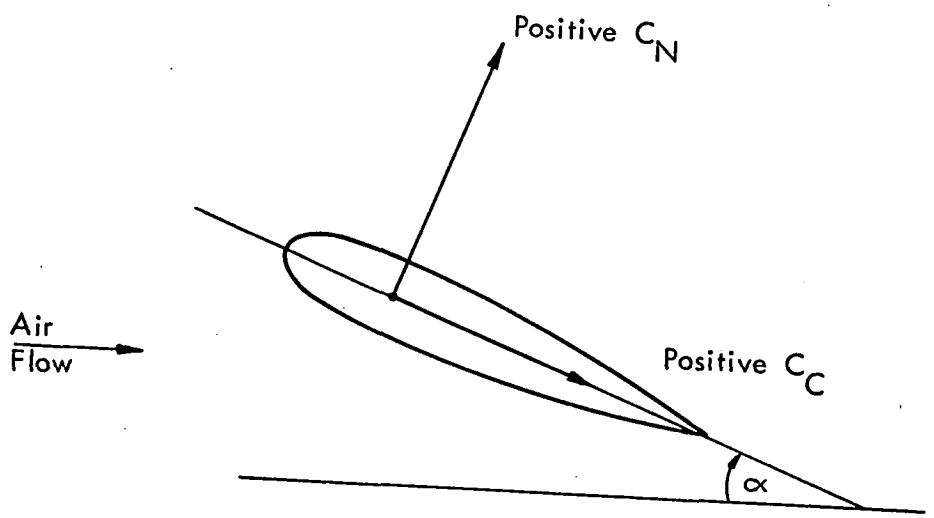

FIG. 9.5 FRAME OF REFERENCE FOR C_N AND C_C DATA

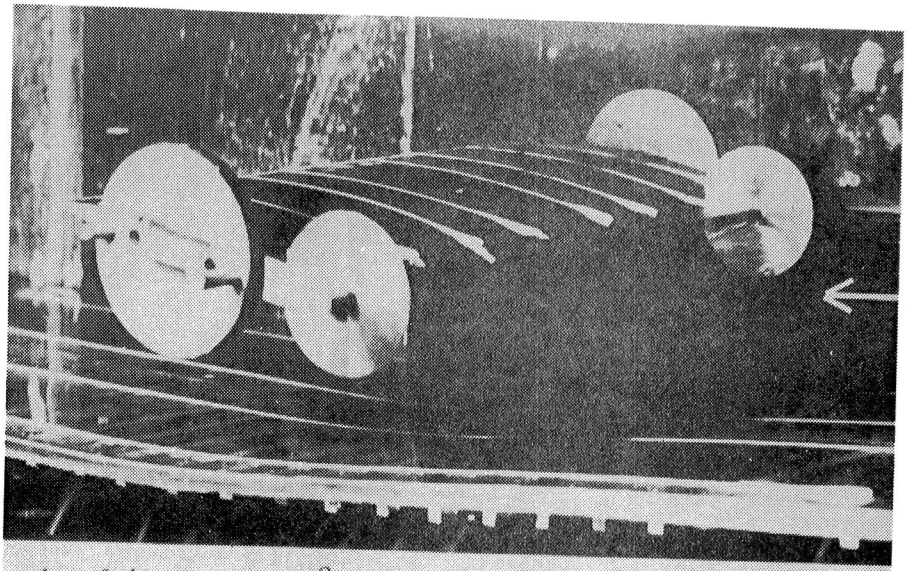

Air Flow

Aerofoil at $\alpha = +12^{o}$ (model mounted upside-down) showing uniform flow on the upper (pressure) surface and on the flexible floor of the test section.

Aerofoil Mounting Trunion

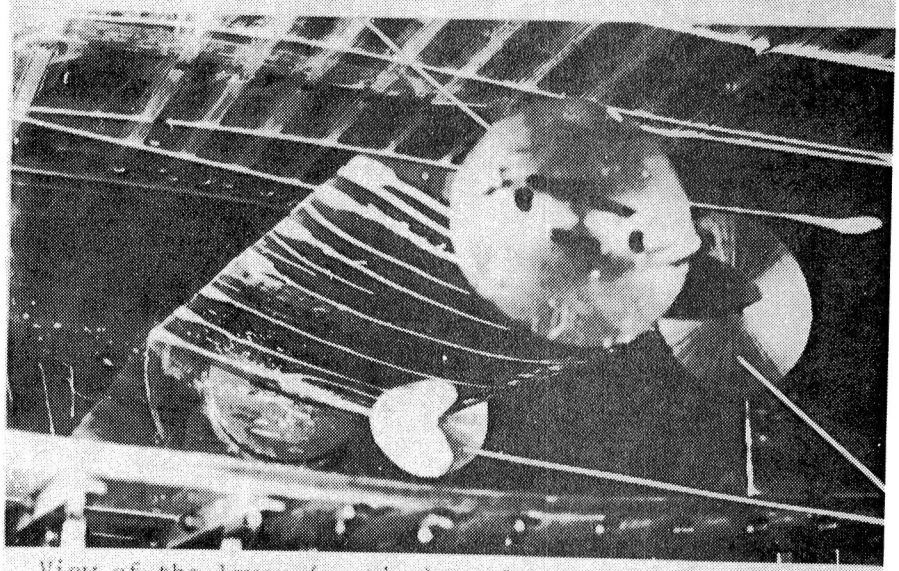

Leading Edge Fences

View of the lower (suction) surface of the aerofoil. The dye streaks show large reverse flow regions with three dimensional patterns.

FLOW VISUALISATION ON A NACA 0012-64 AEROFOIL WITH LEADING EDGE FENCES FITTED.

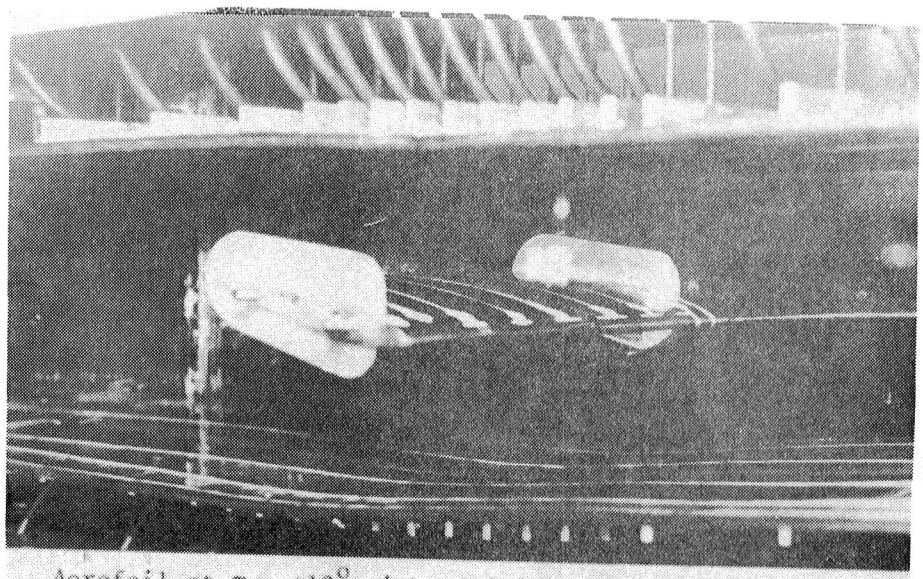

Aerofoil at $\alpha = +12^{\circ}$ with trailing edge fences fitted. The dye streaks show uniform flow over the upper (pressure) surface.

Trailing Edge Fences

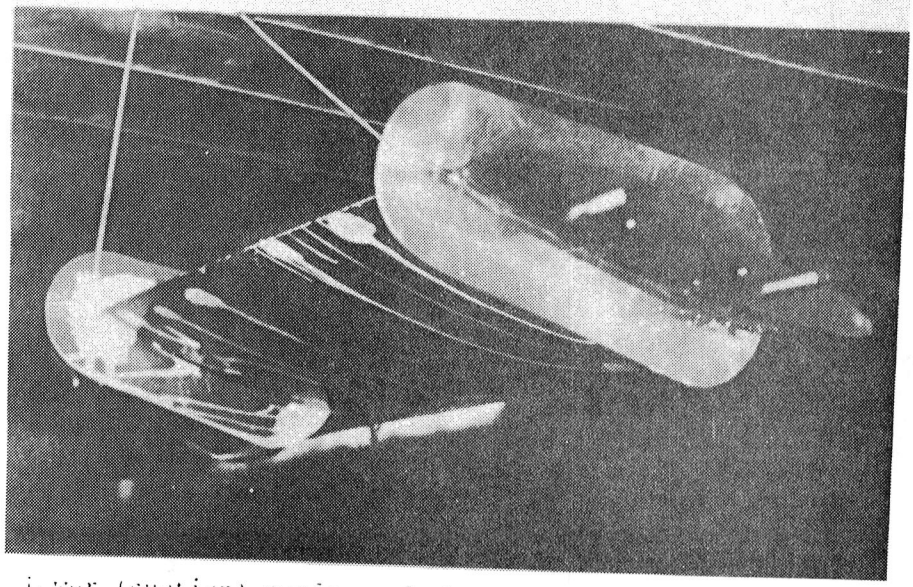

lower (suction) surface of the aerofoil shows evidence two-dimensional reverse flow. Separation is indicated the wing fences.

VISUALISATION OF A NACA 0[illegible]

194

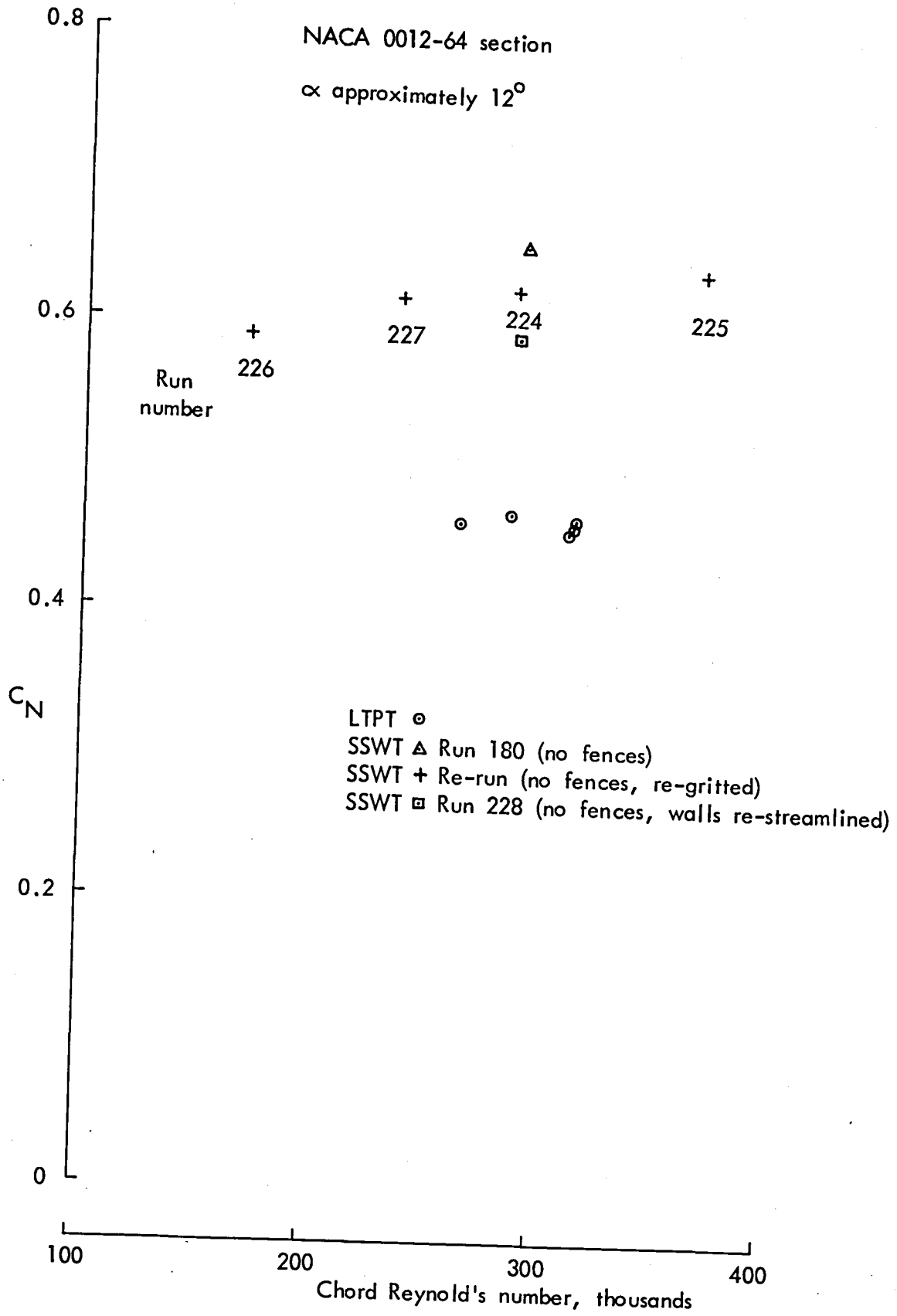

Figure 9.8(a) VARIATION OF AIRFOIL C_N WITH R_c.

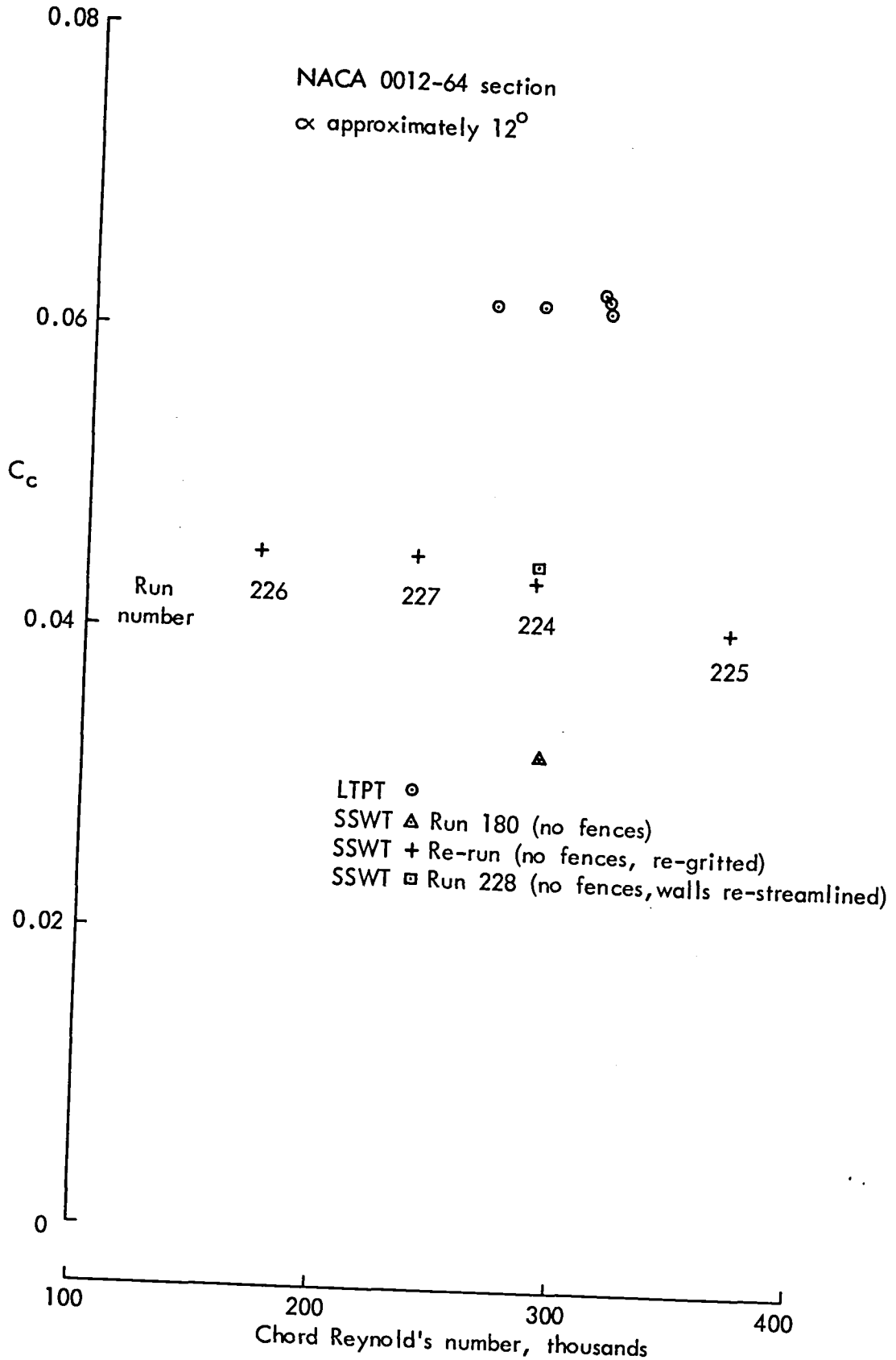

Figure 9.8(b) VARIATION OF AIRFOIL C_c WITH R_c

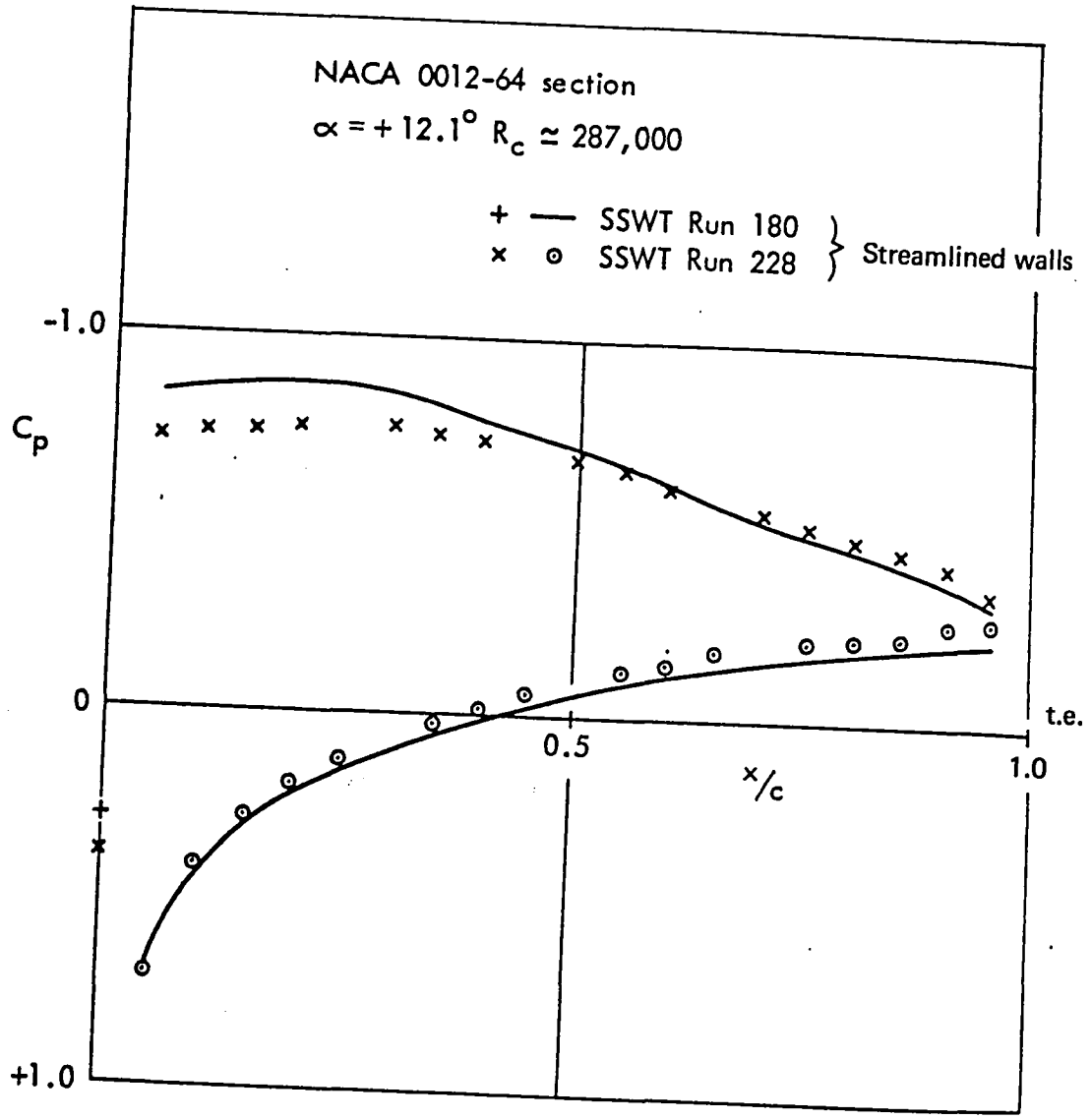

FIG. 9.9 NACA 0012-64 PRESSURE DISTRIBUTION

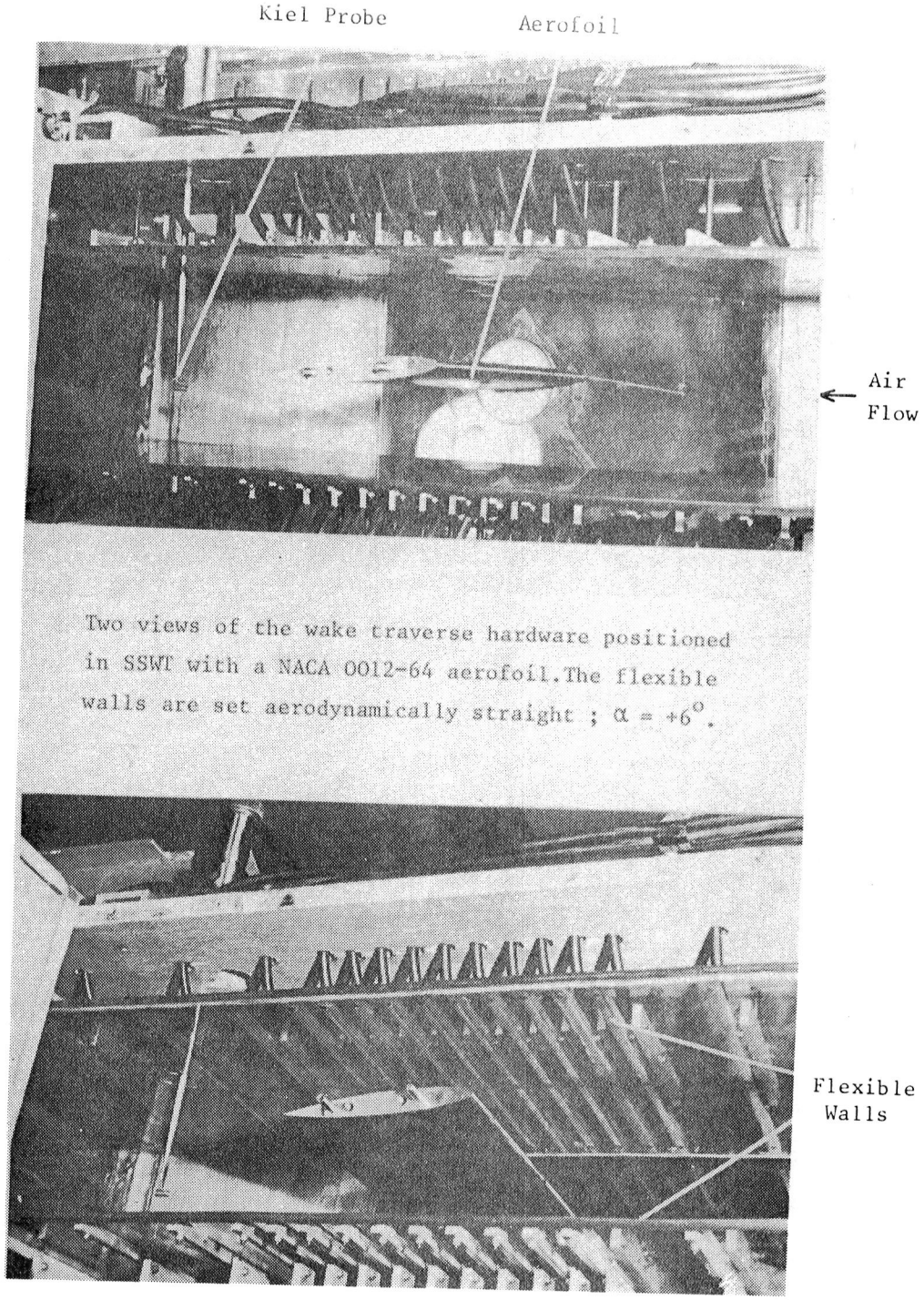

Two views of the wake traverse hardware positioned in SSWT with a NACA 0012-64 aerofoil. The flexible walls are set aerodynamically straight ; $\alpha = +6^{o}$.

FIG. 9.10 WAKE TRAVERSE HARDWARE IN SSWT

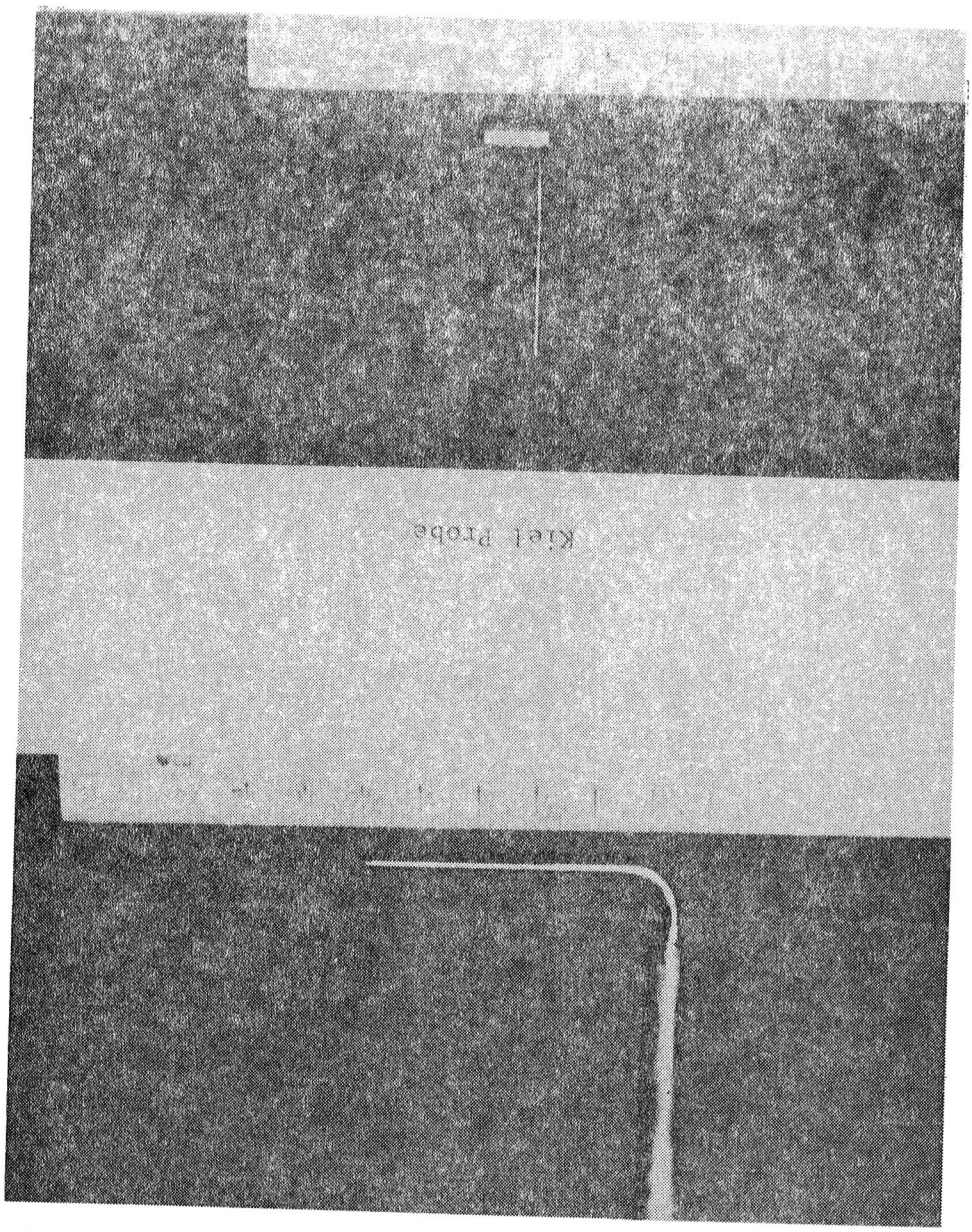

STATIC PROBE AND KIEL PROBE USED IN LOW SPEED WAKE TRAVERSES.

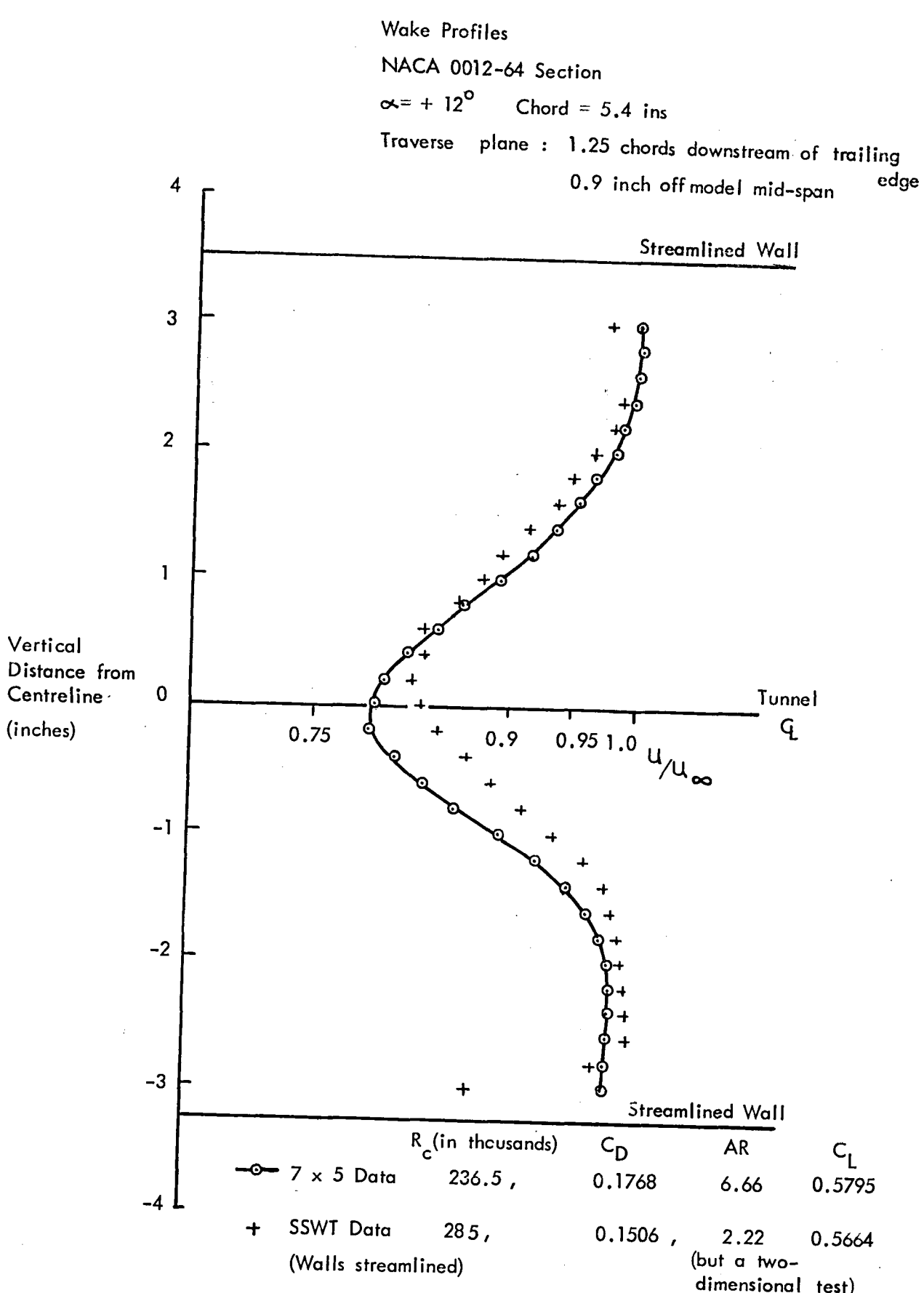

FIG. 9.12 COMPARISON OF WAKE PROFILES FROM 7 x 5 and SSWT, $\alpha = +12^\circ$.

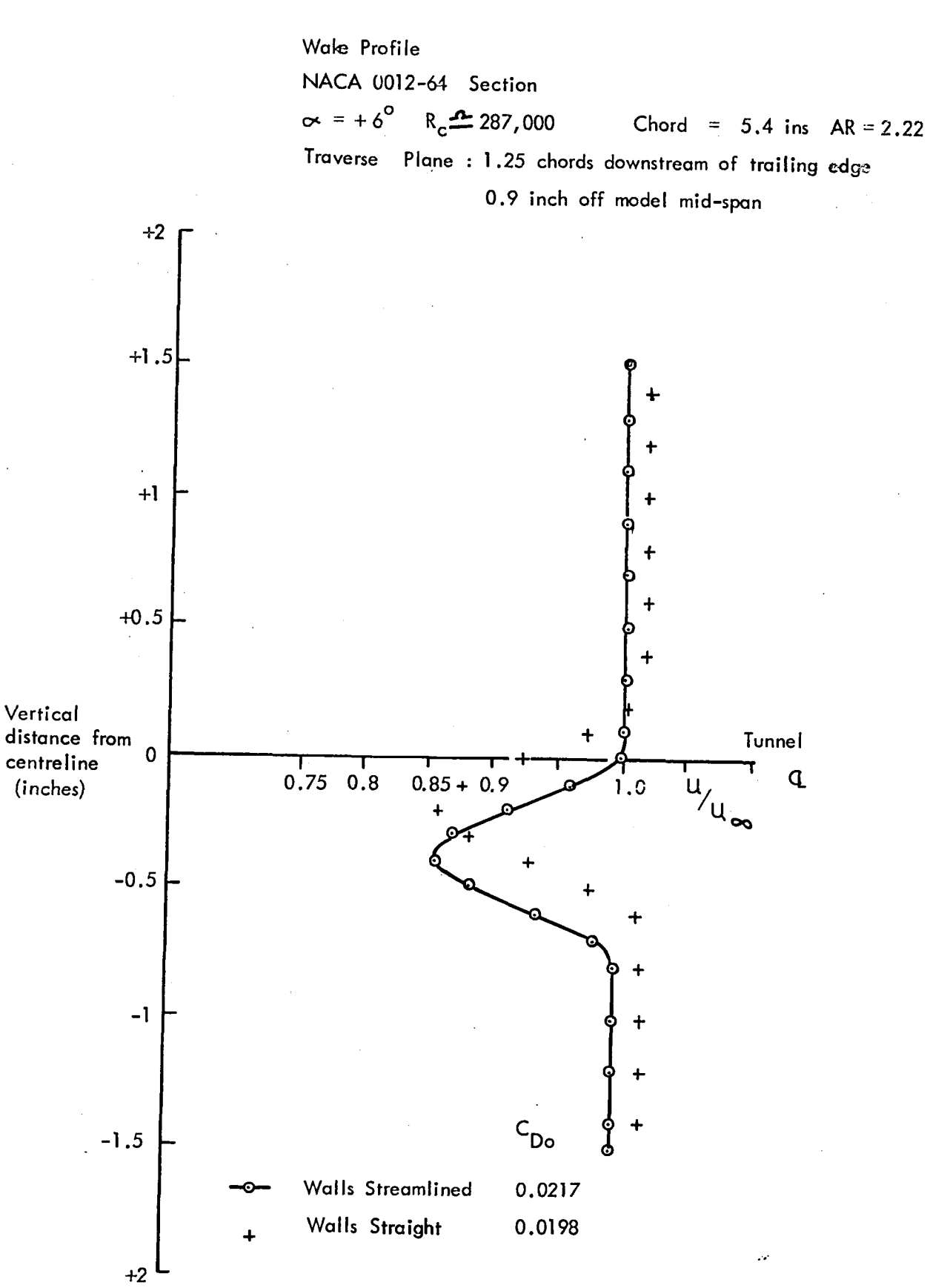

FIG. 9.13 SSWT WAKE PROFILES FOR NACA 0012-64 SECTION $\alpha = +6^\circ$

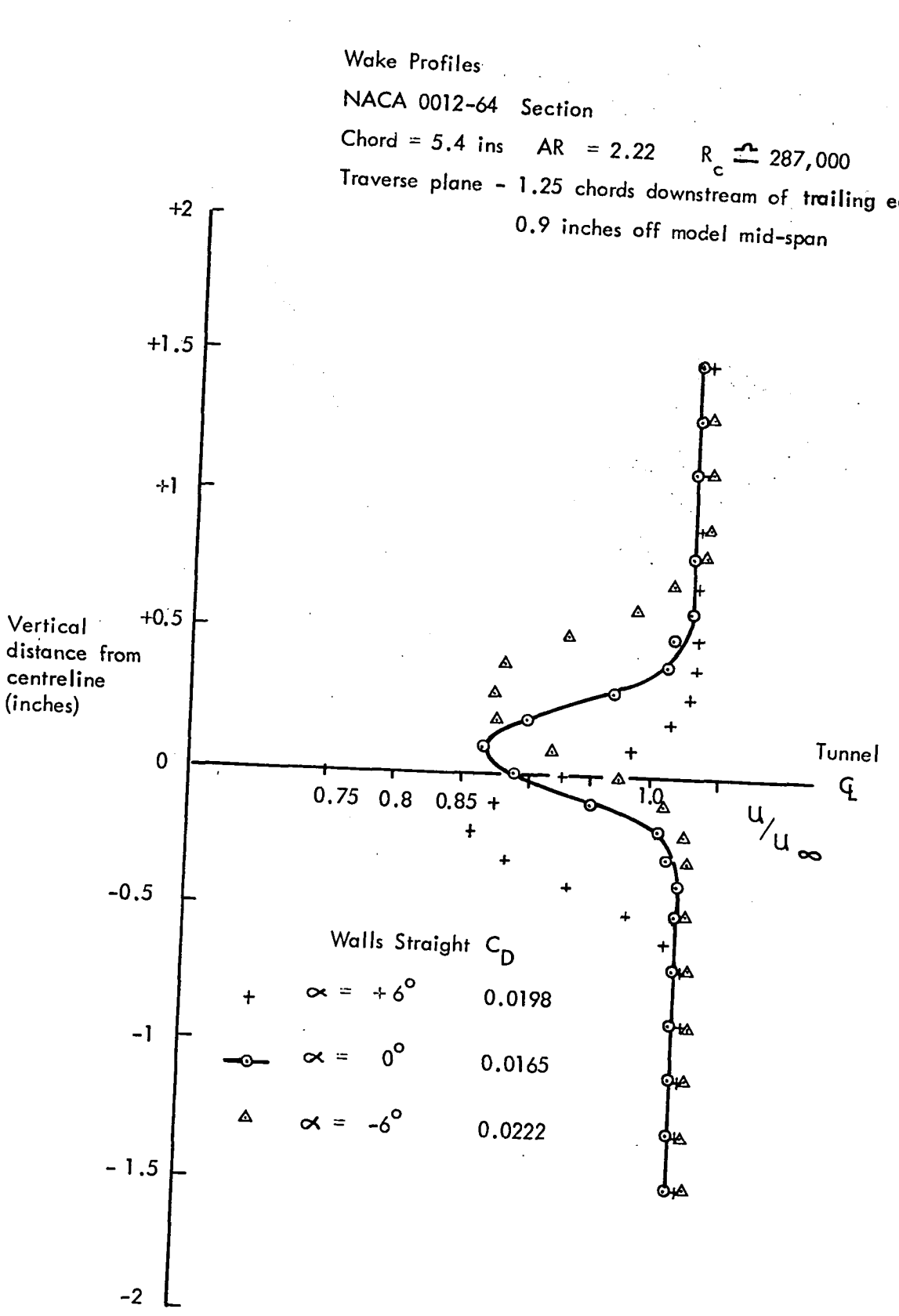

FIG. 9.14 SSWT WAKE PROFILES FOR NACA 0012-64 SECTION, UNSTALLED.

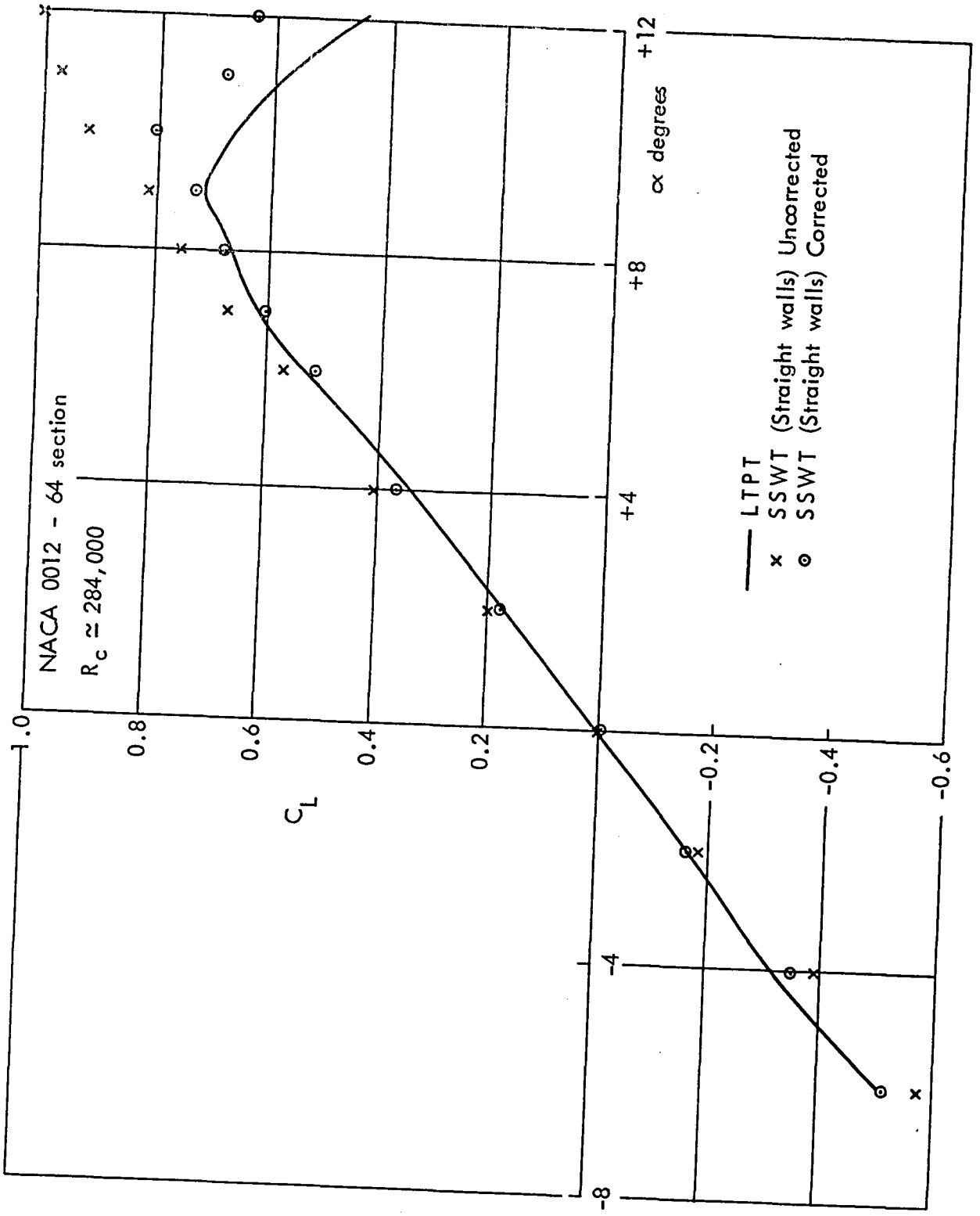

FIG. 9.15(a) C_L DATA FROM THE STRAIGHT WALL SSWT AND LTPT.

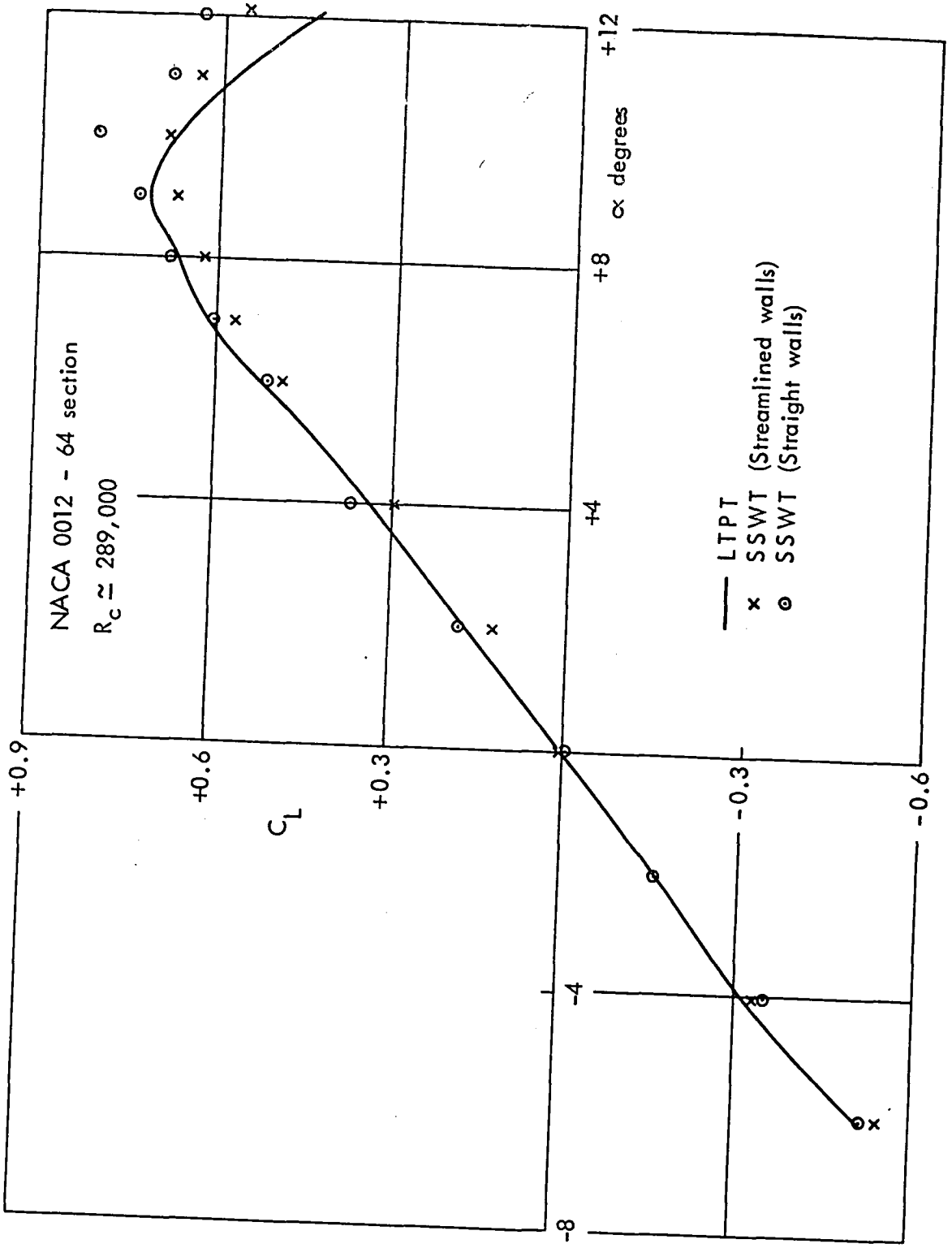

FIG. 9.15(b) COMPARISON OF STREAMLINED WALL SSWT AND STRAIGHT WALL SSWT CORRECTED C_L DATA

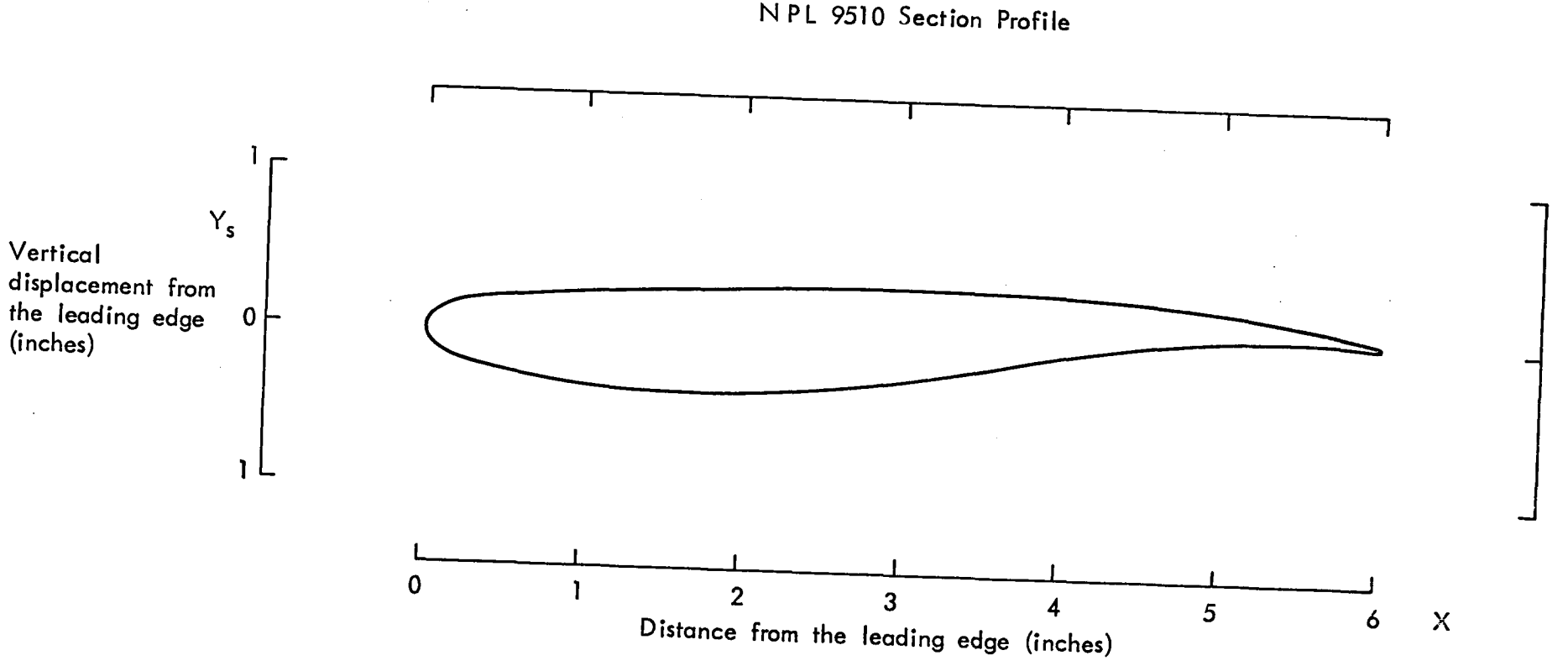

FIG. 9.16 MODEL PROFILE

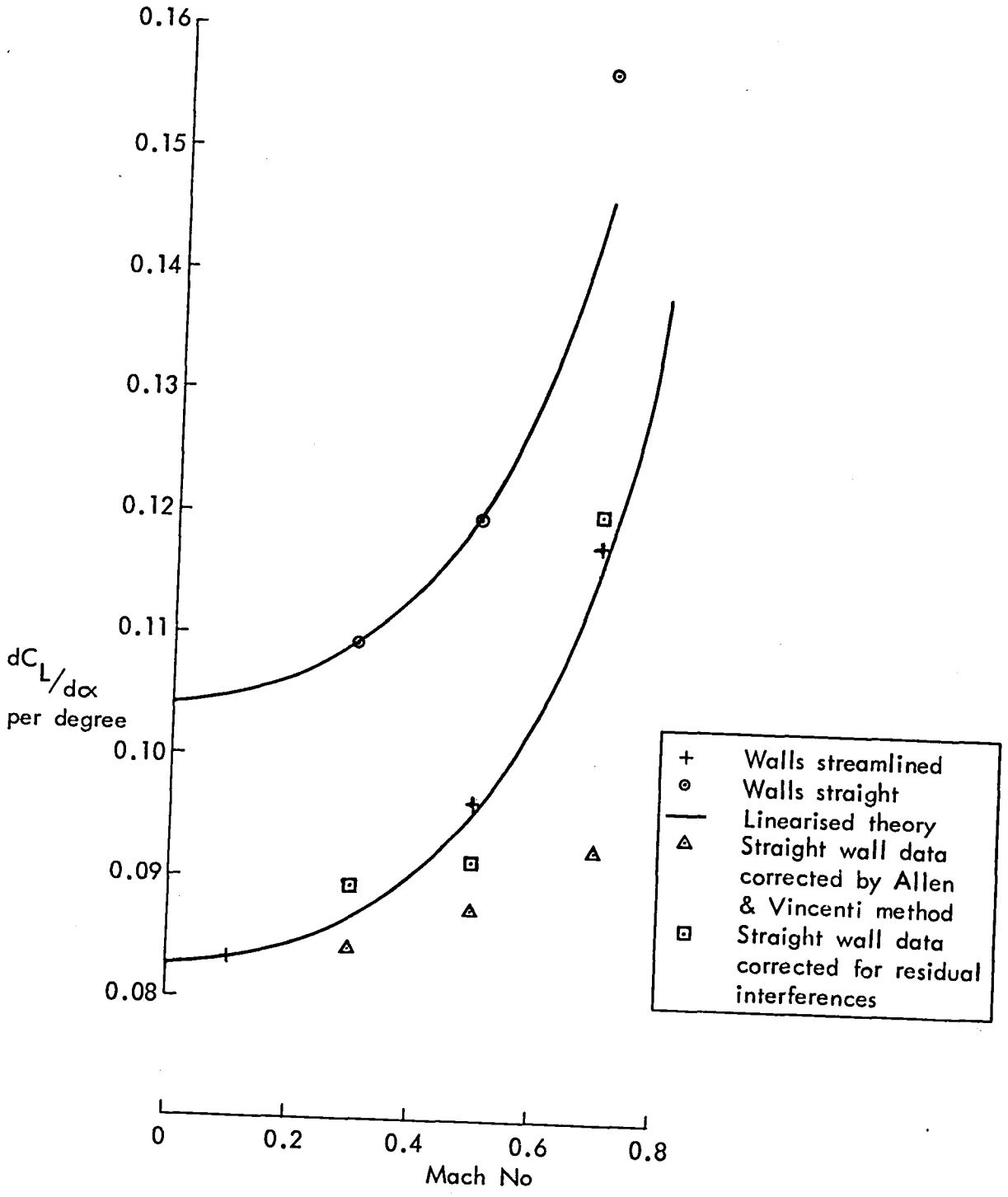

FIG. 9.17 SUMMARY OF MODEL DATA FROM FLEXIBLE WALLED WIND TUNNELS BELOW MACH 0.8

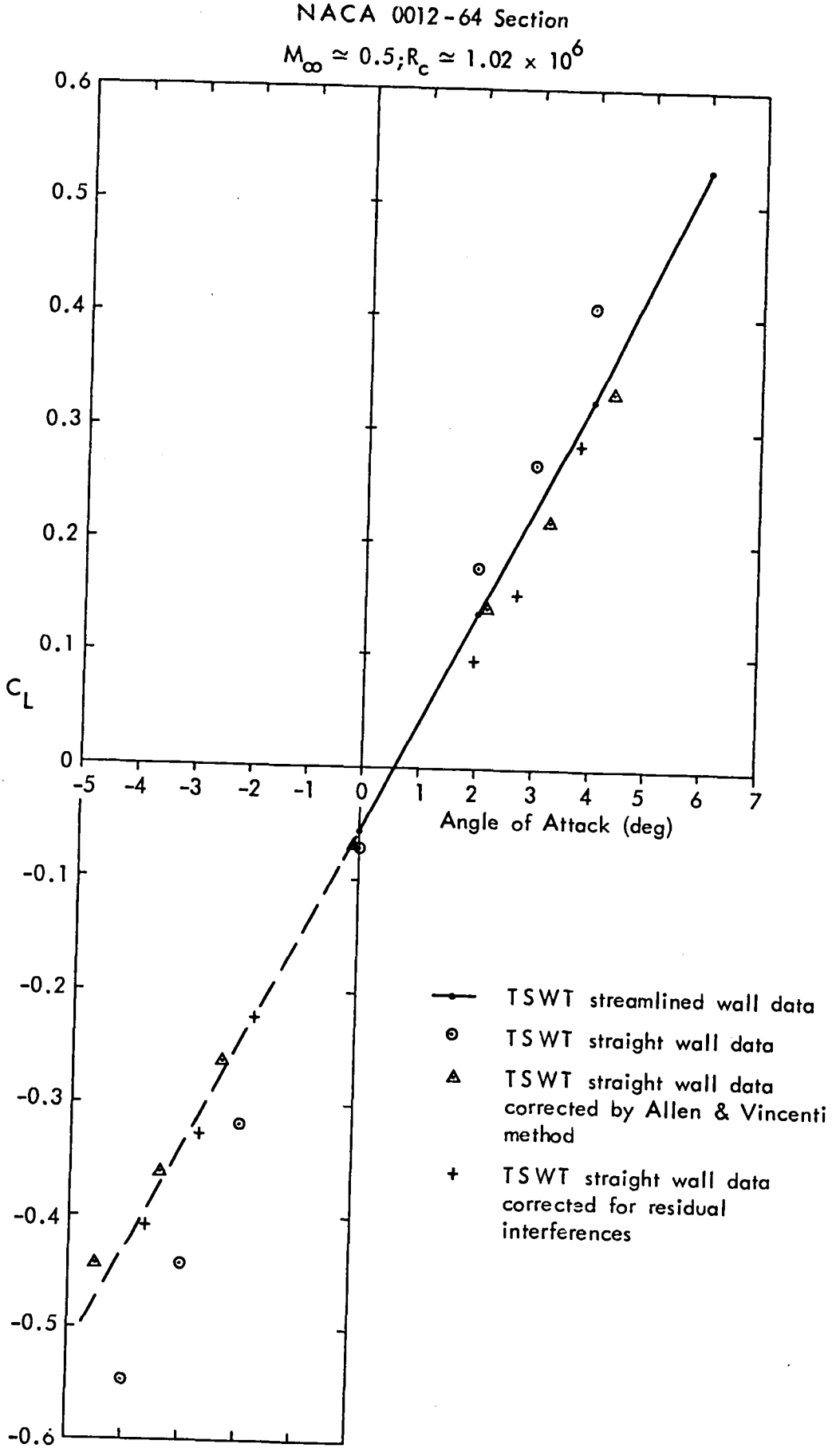

FIG. 9.18(a) LIFT CURVE SLOPES ; $M_\infty \simeq 0.5$

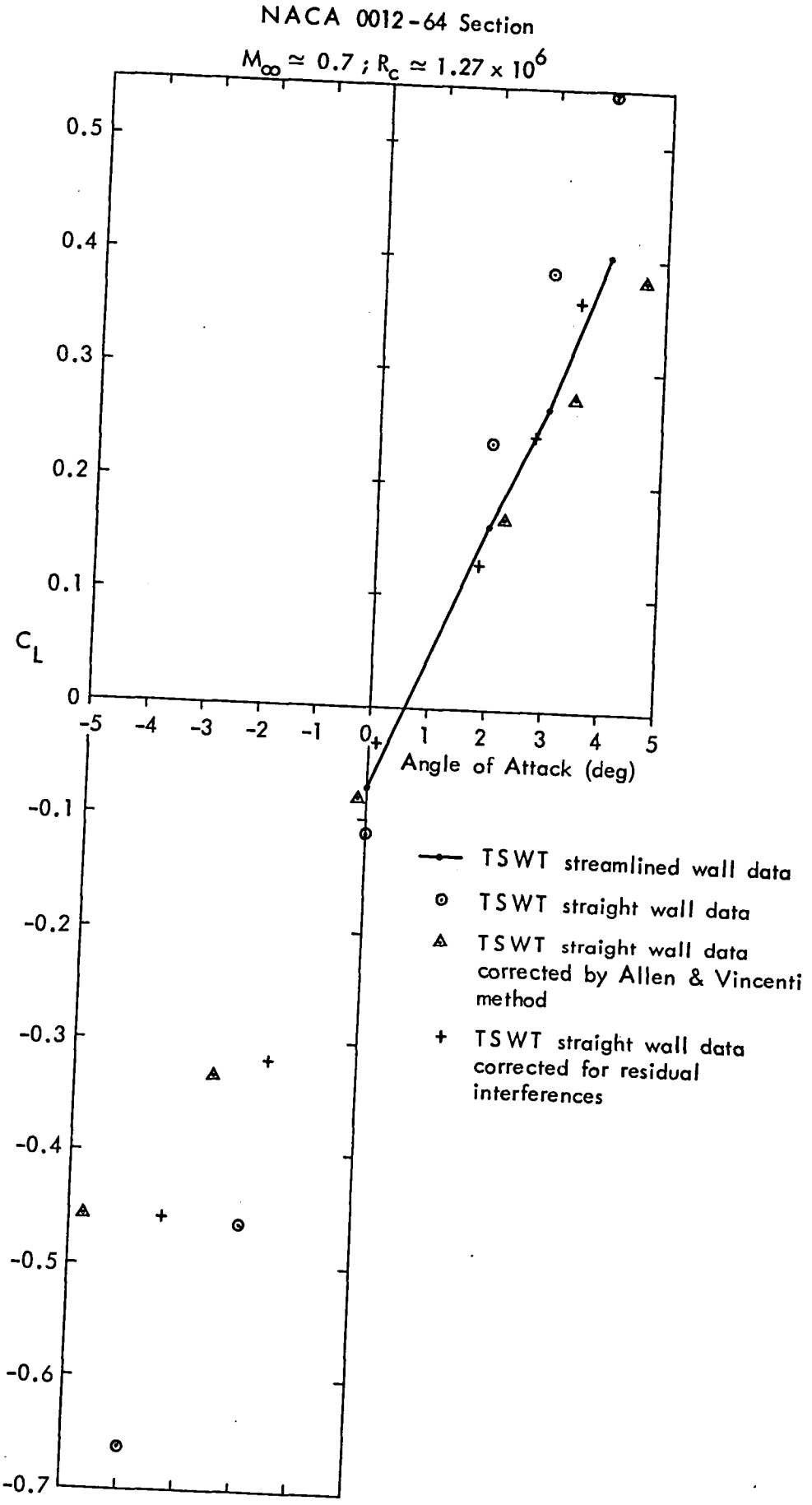

FIG. 9.18(b) LIFT CURVE SLOPES; $M_\infty \simeq 0.7$

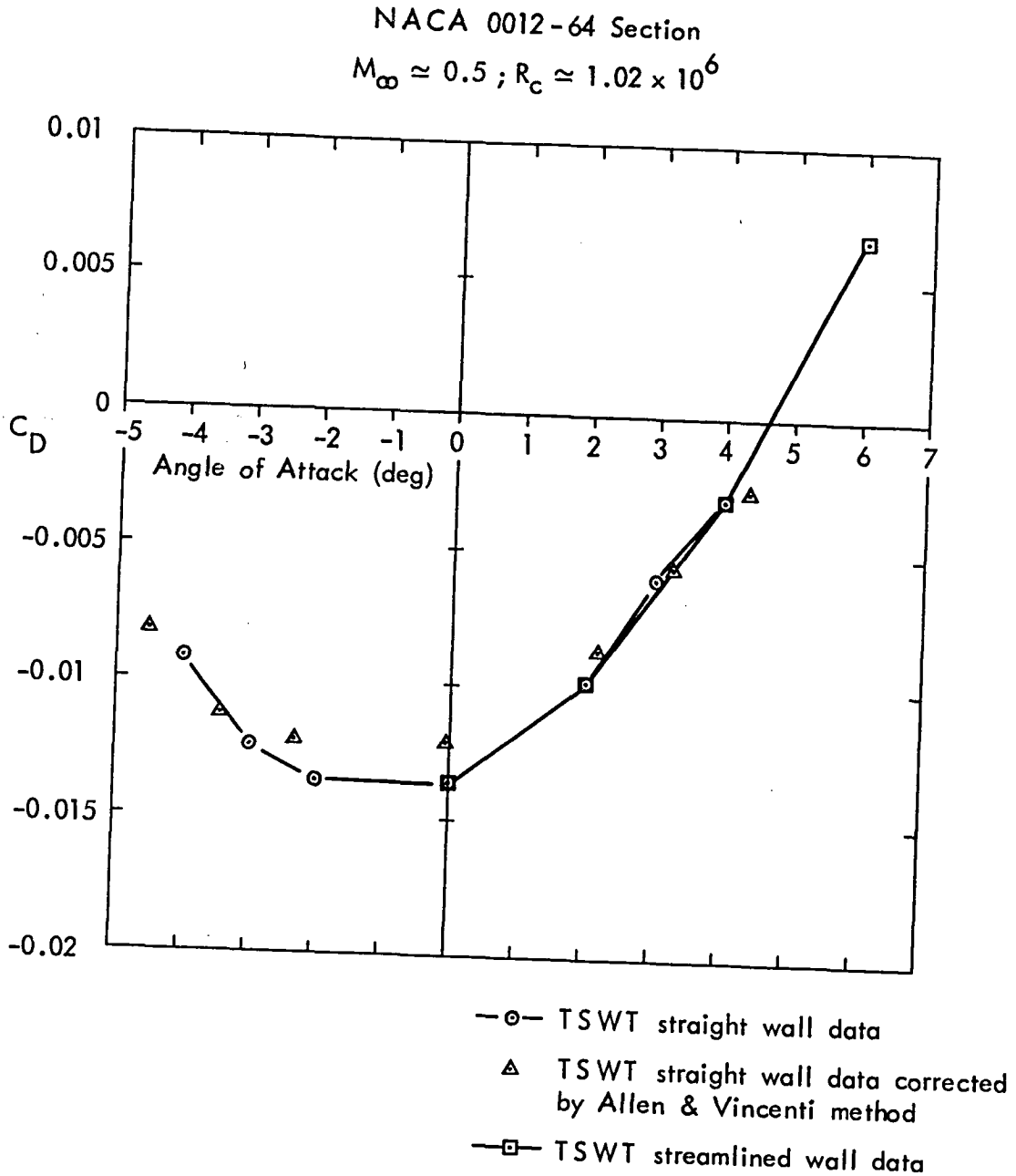

FIG. 9.19(a) VARIATION OF MODEL PRESSURE DRAG WITH ANGLE OF ATTACK ; $M_\infty \simeq 0.5$

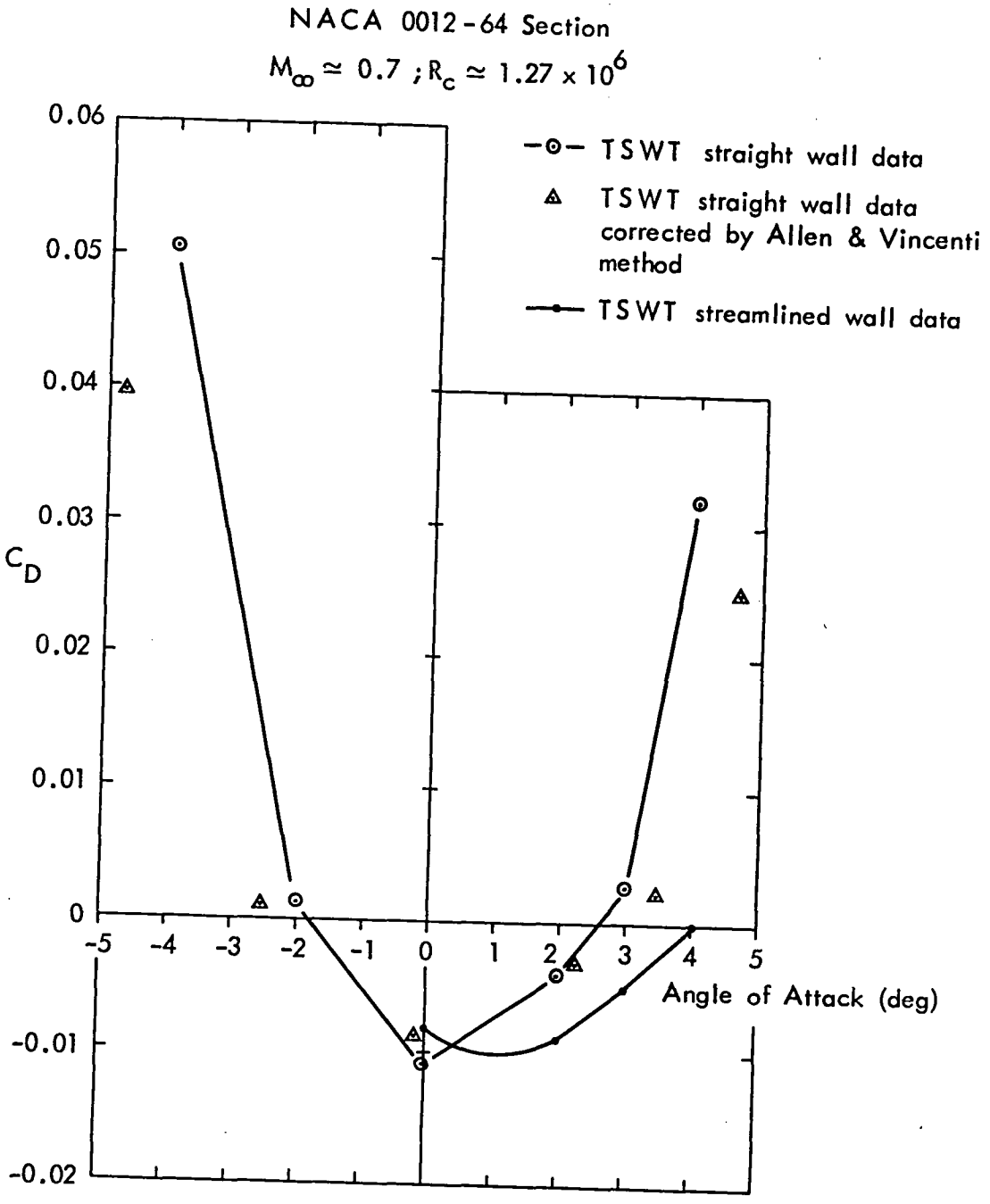

FIG. 9.19(b) VARIATION OF MODEL PRESSURE DRAG WITH ANGLE OF ATTACK ; $M_\infty \simeq 0.7$

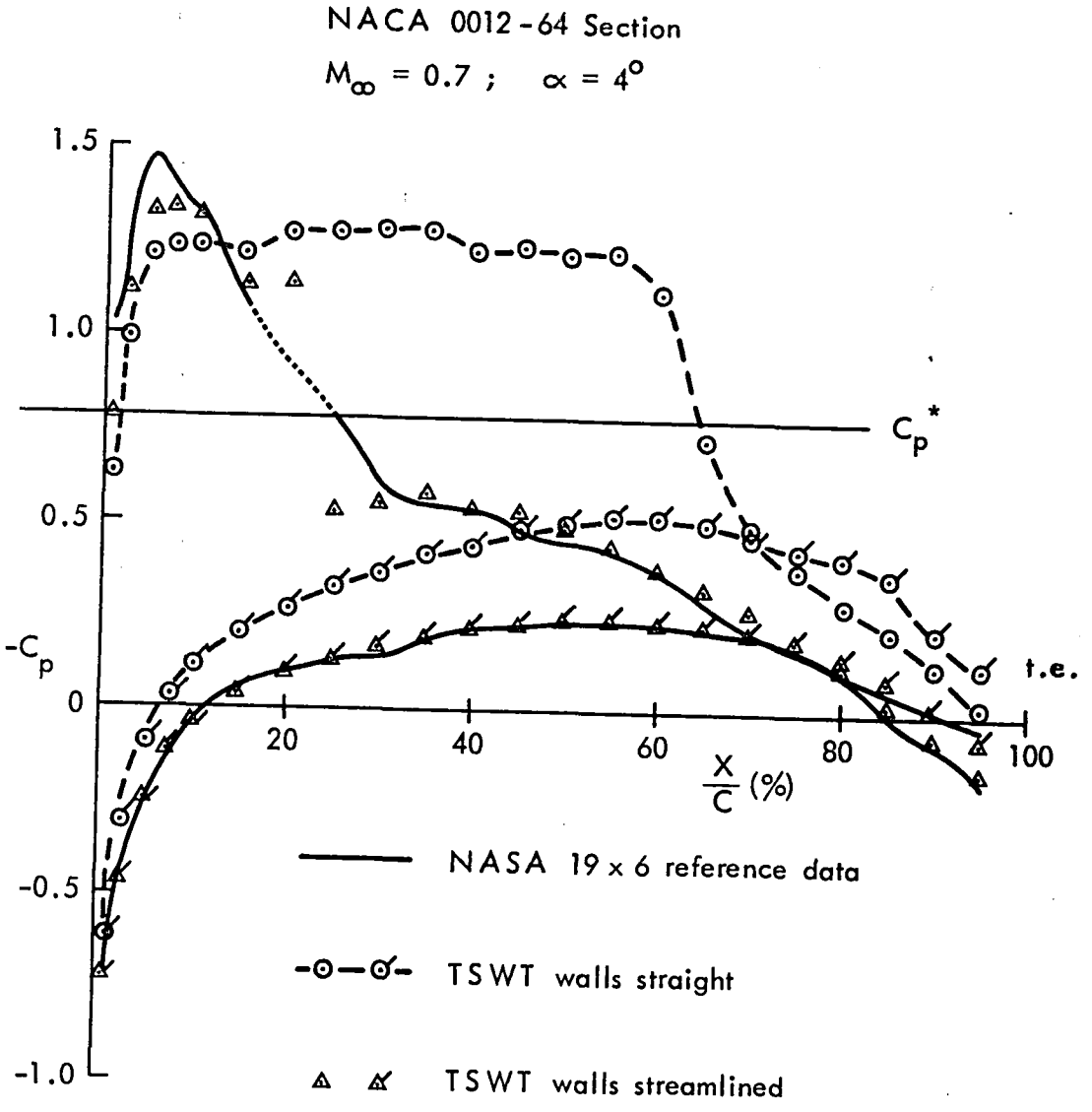

FIG. 9.20 MODEL PRESSURE DISTRIBUTION WITH WALLS STRAIGHT AND STREAMLINED COMPARED WITH REFERENCE DATA ; $M_\infty = 0.7$

NACA 0012-64 Section

$M_\infty = 0.7$; $\alpha = +4^0$

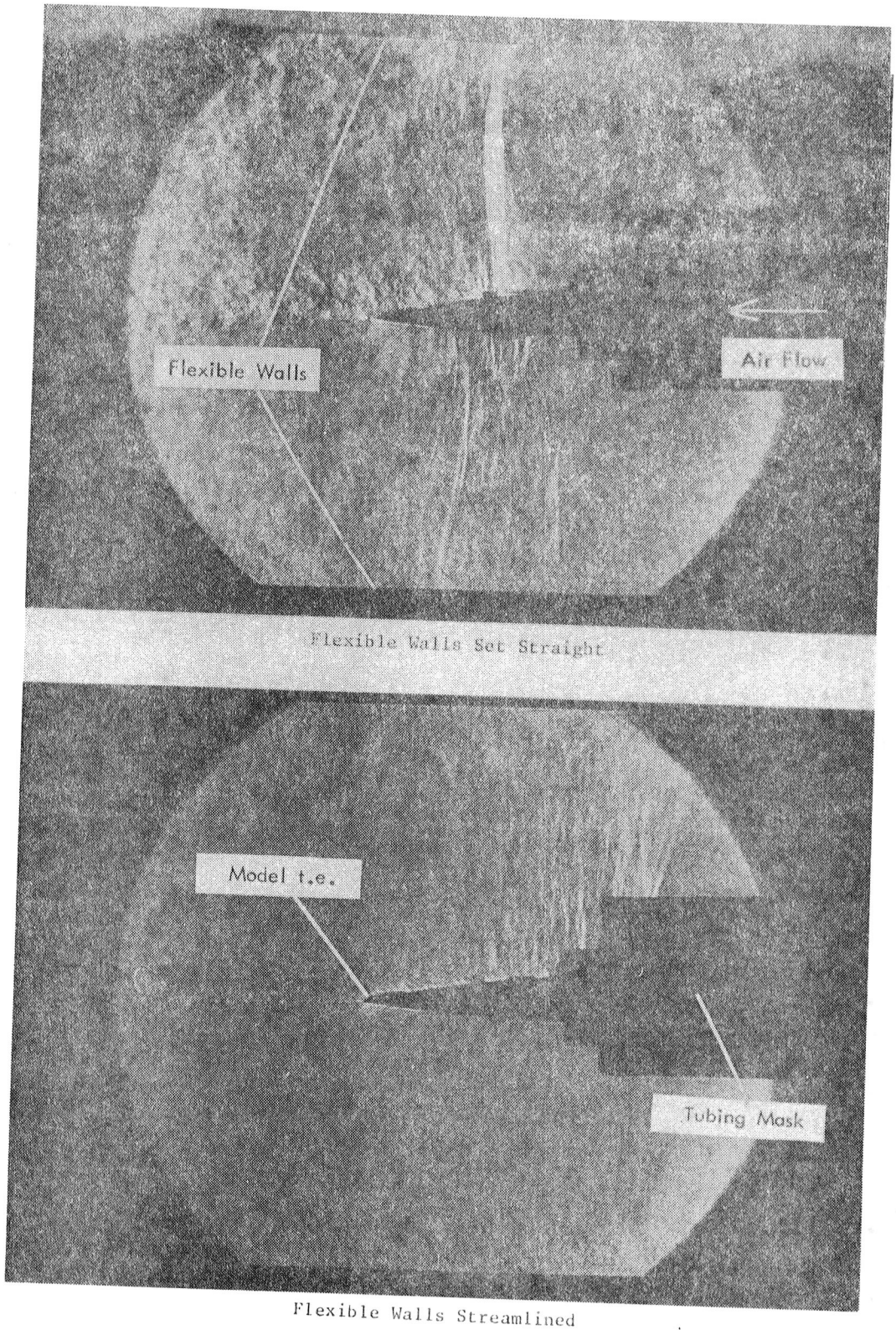

FIG. 9.21 SPARK SCHLIEREN PICTURES SHOW THE EFFECTS OF WALL STREAMLINING.

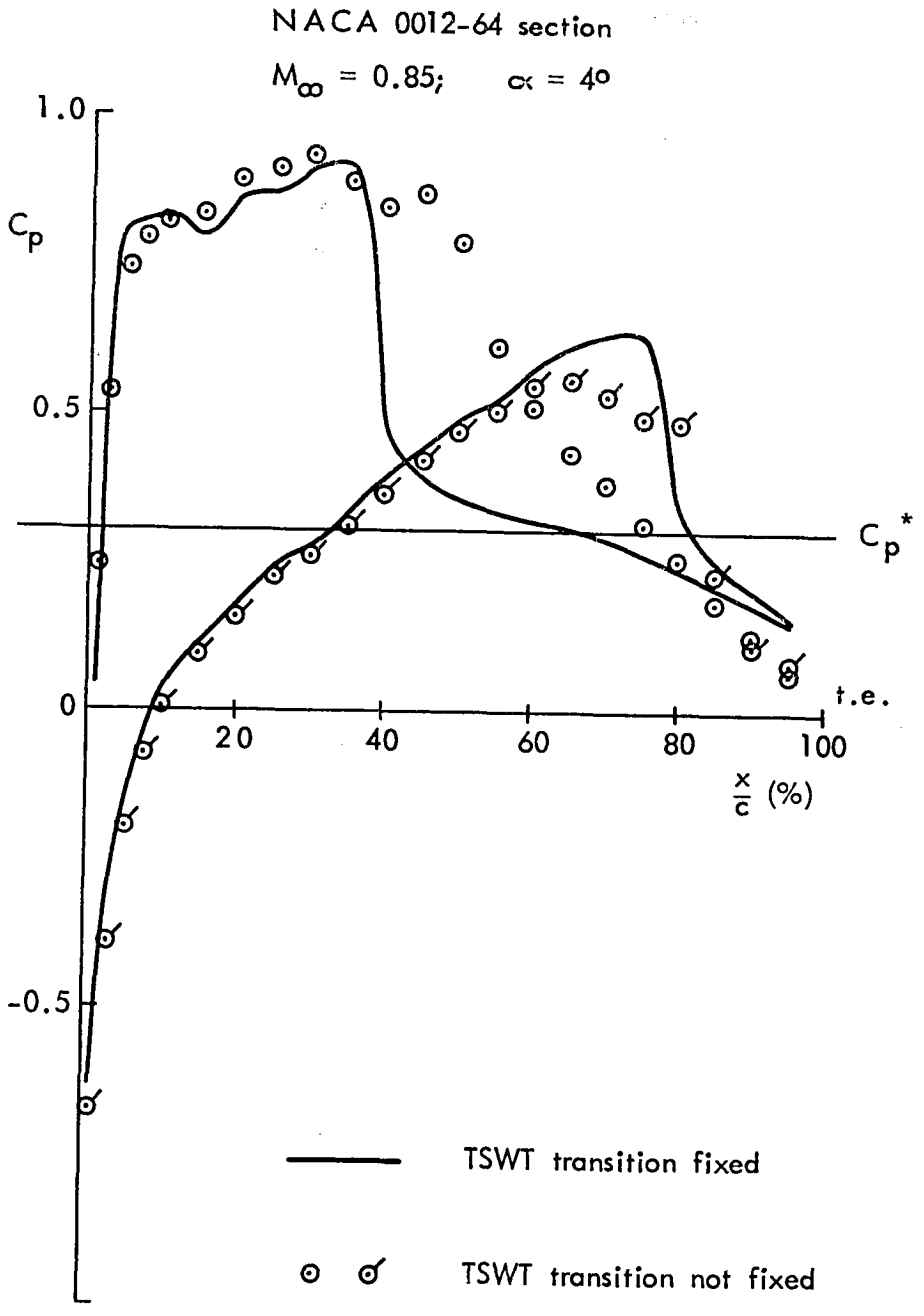

FIG. 9.22 EFFECTS OF TRANSITION FIXING ON MODEL PRESSURE DISTRIBUTION; M_∞ = 0.85

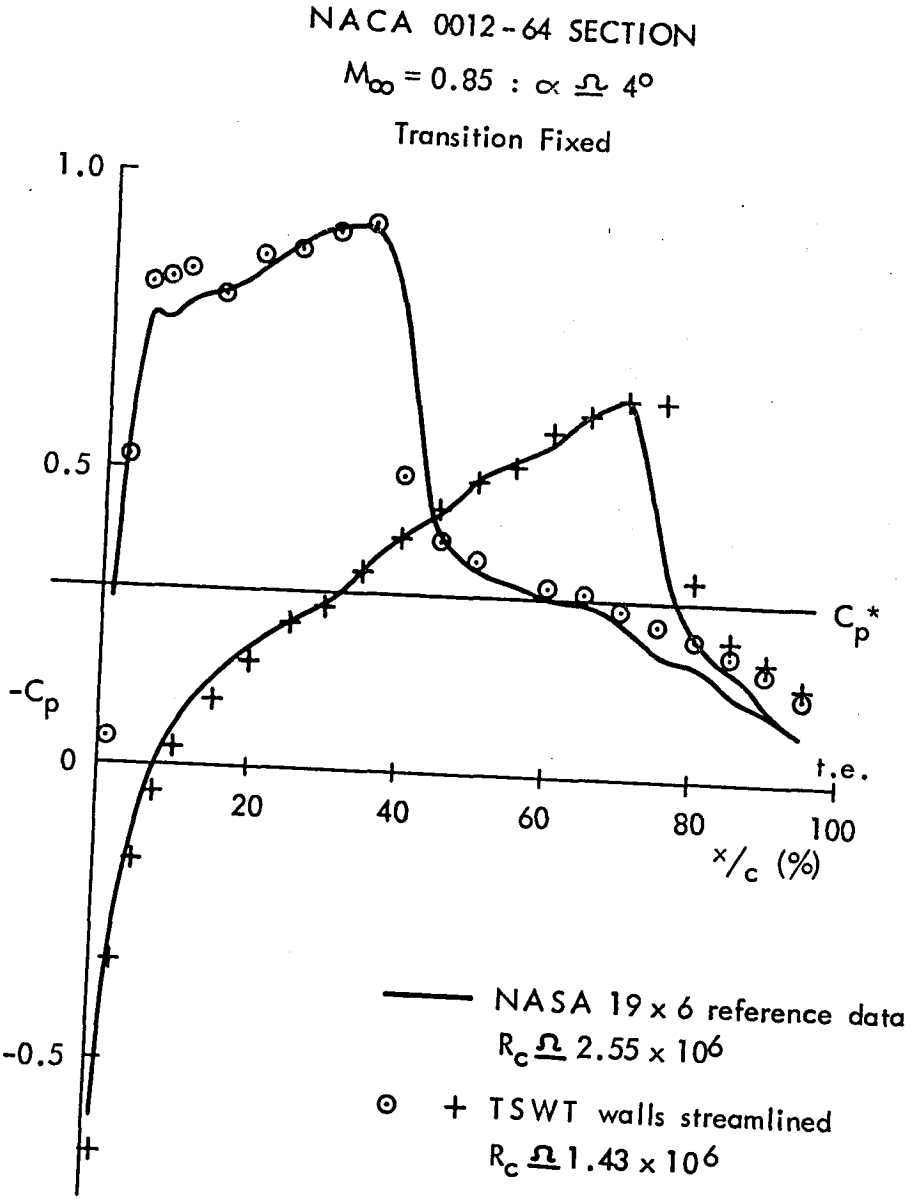

FIG. 9.23 COMPARISON OF MODEL PRESSURE DISTRIBUTION WITH REFERENCE DATA, $M_\infty = 0.85$

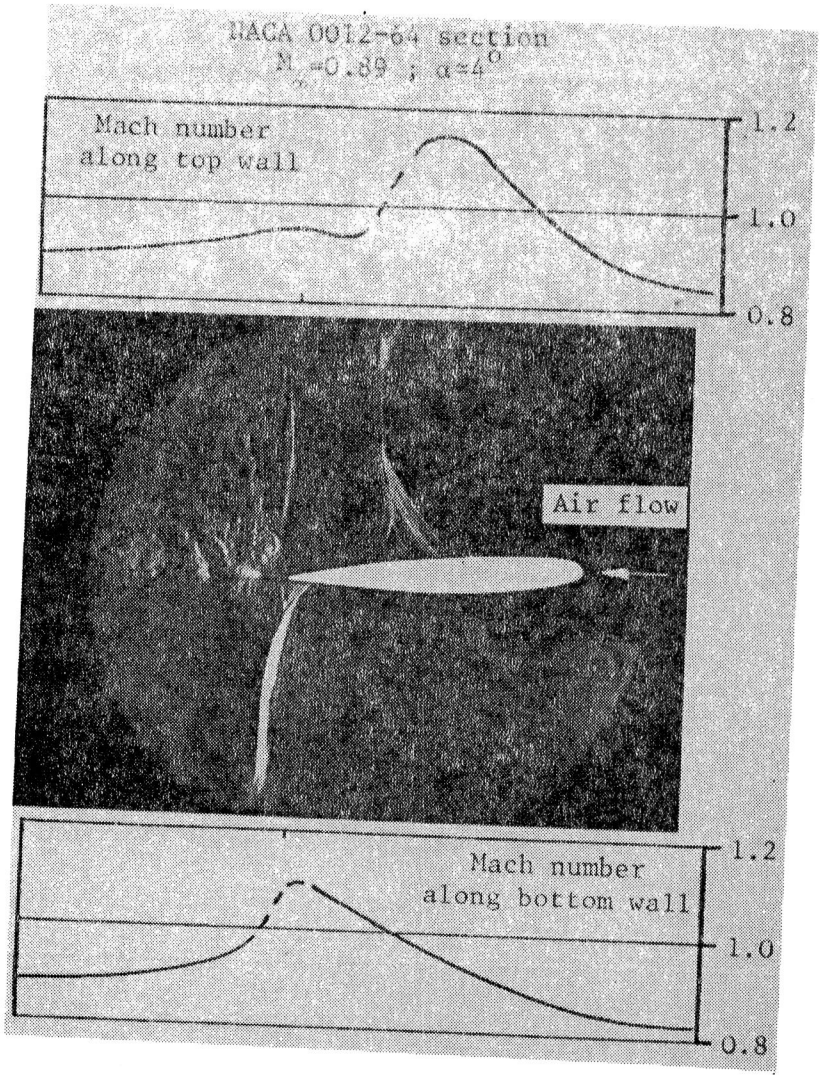

FIG. 9.24 SPARK SCHLIEREN PICTURE WITH WALL MACH NUMBER DISTRIBUTION; $M_\infty = 0.89$

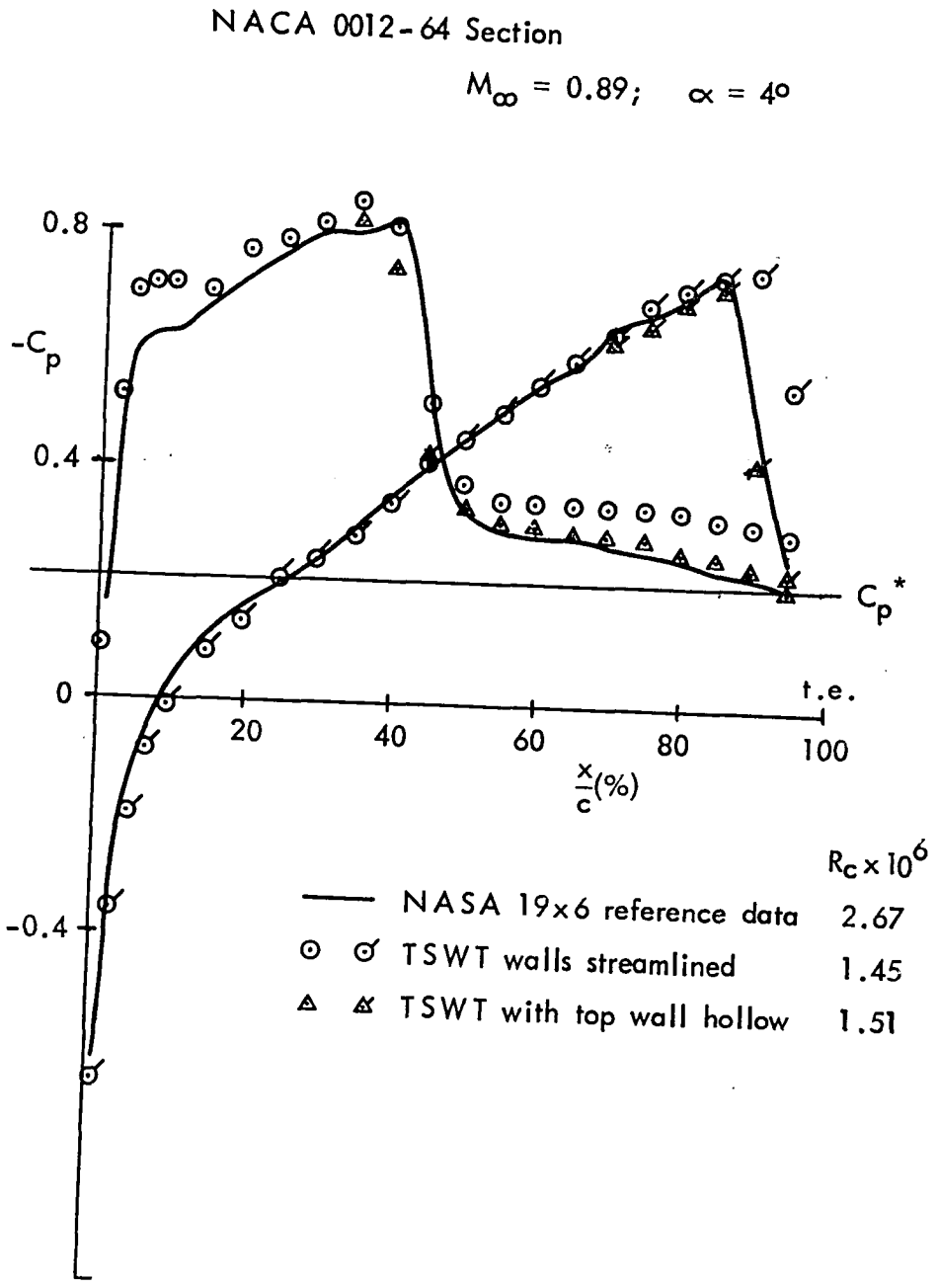

FIG. 9.25 EFFECTS OF ALLOWANCE FOR SHOCK/WALL BOUNDARY-LAYER INTERACTION ON MODEL PRESSURE DISTRIBUTIONS COMPARED WITH REFERENCE DATA, $M_\infty = 0.89$

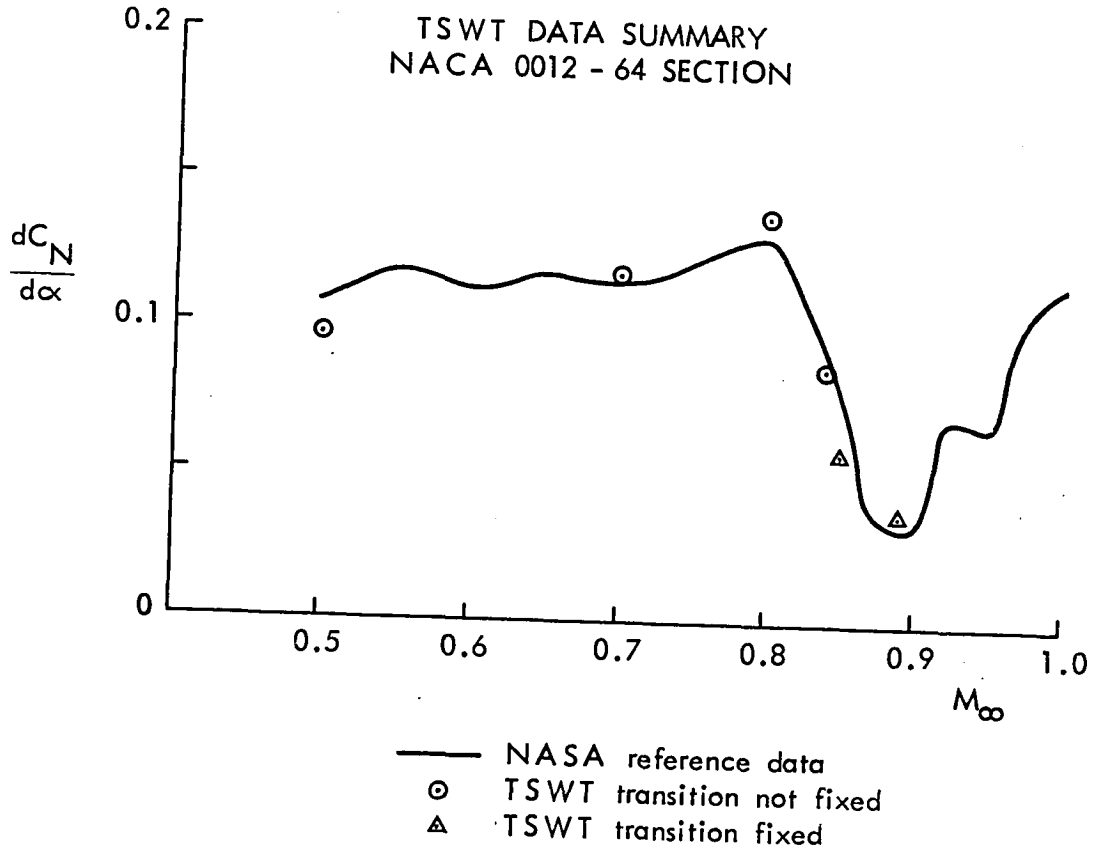

FIG. 9.26 COMPARISON OF TSWT NORMAL FORCE SLOPE WITH REFERENCE DATA OVER M_∞ RANGE

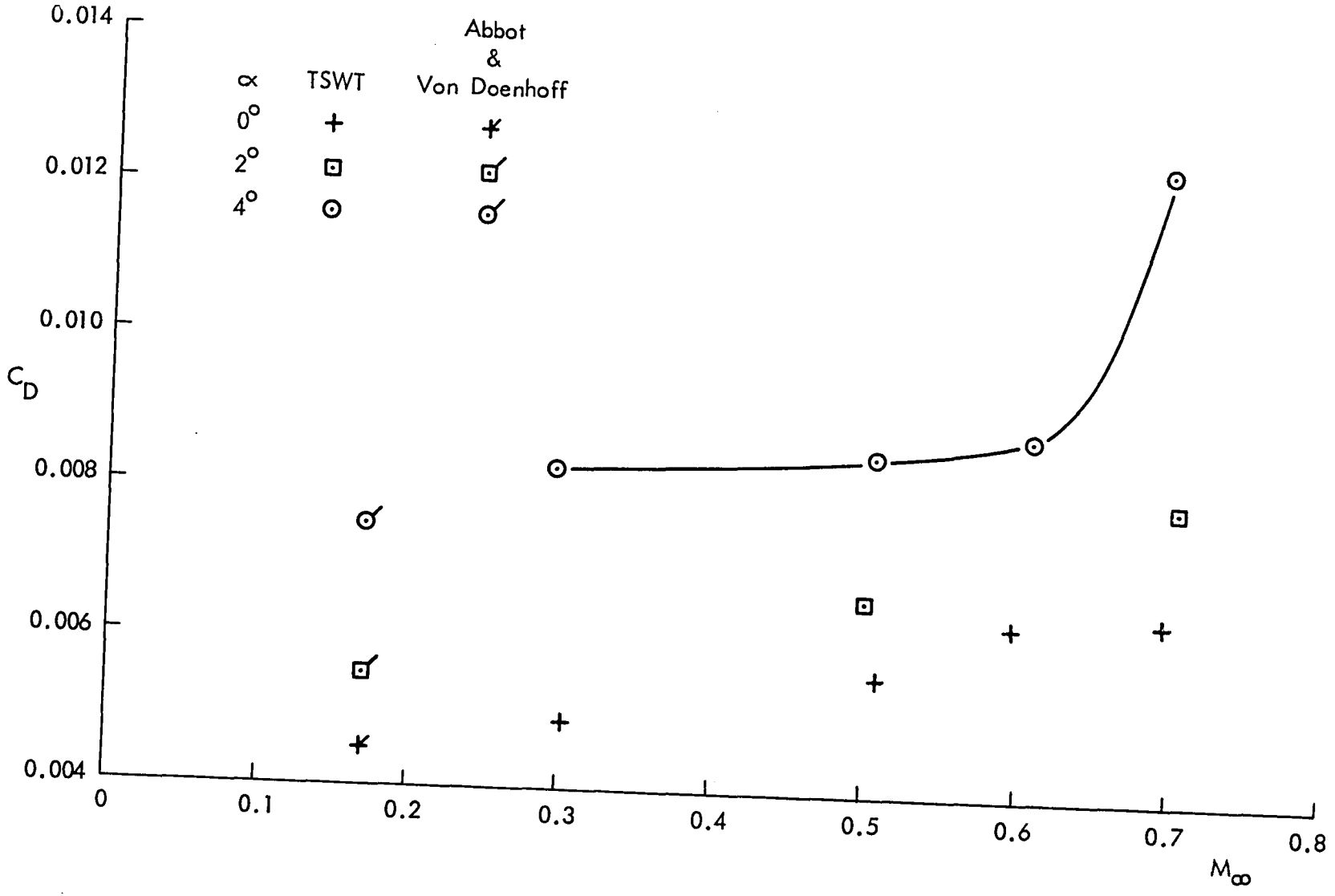

FIG. 9.27 NACA 0012-64 WAKE TRAVERSE DATA. WALLS STREAMLINED

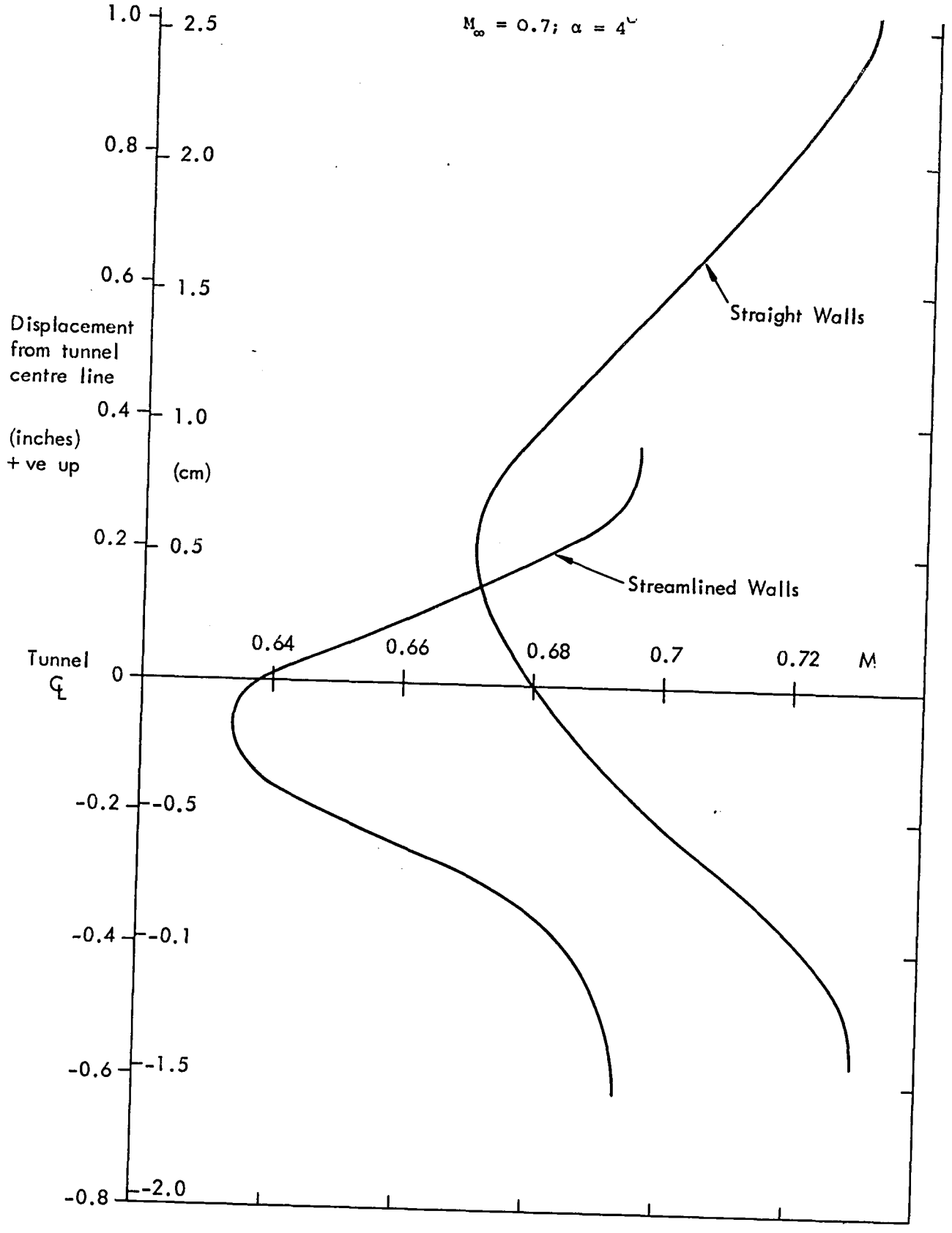

FIG. 9.28 COMPARISON OF NACA 0012-64 SECTION WAKES WITH THE TEST SECTION WALLS SET STRAIGHT AND STREAMLINED :

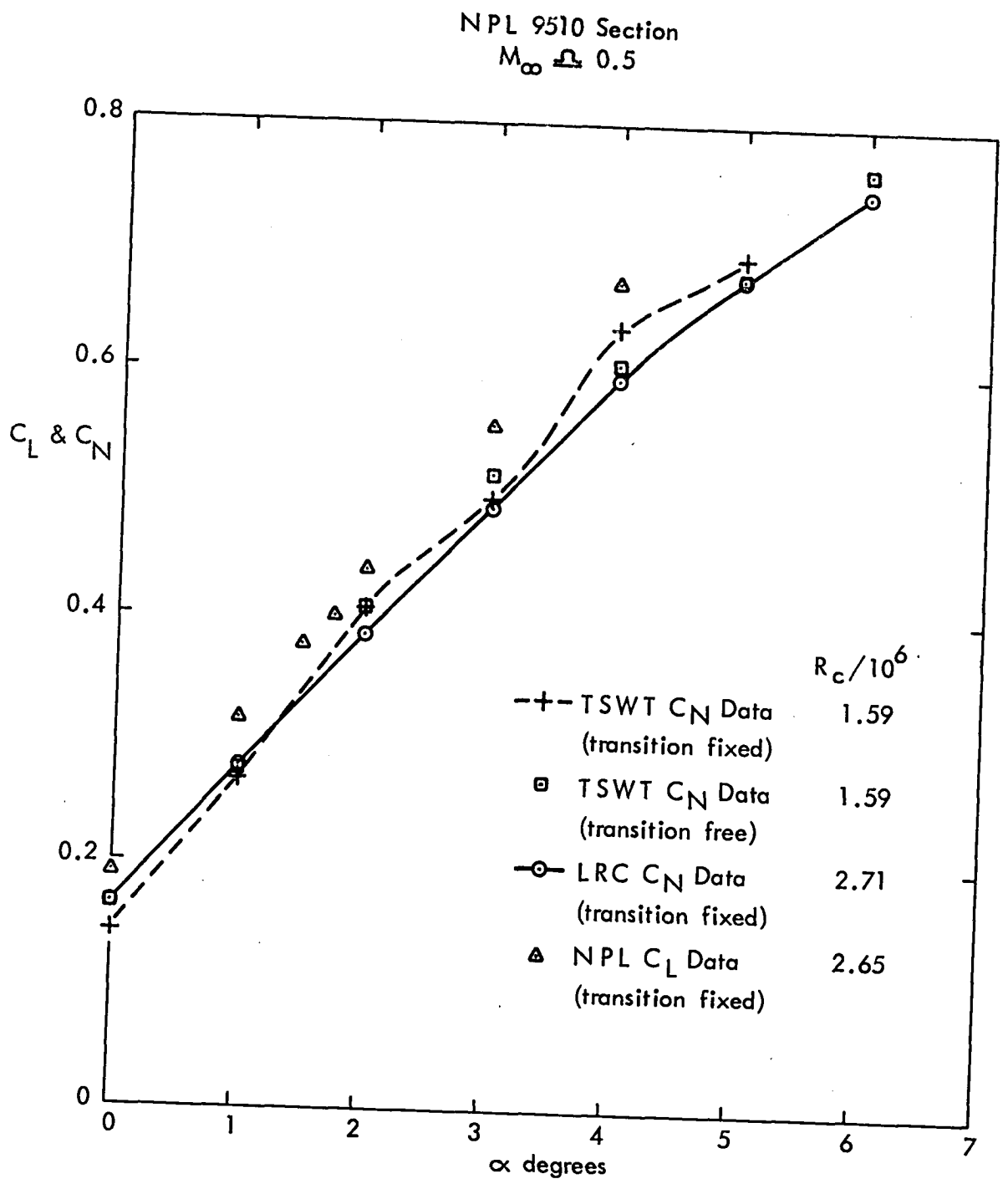

FIG. 9.29(a) VARIATIONS OF C_L AND C_N WITH ANGLE OF ATTACK; $M_\infty \triangleq 0.5$

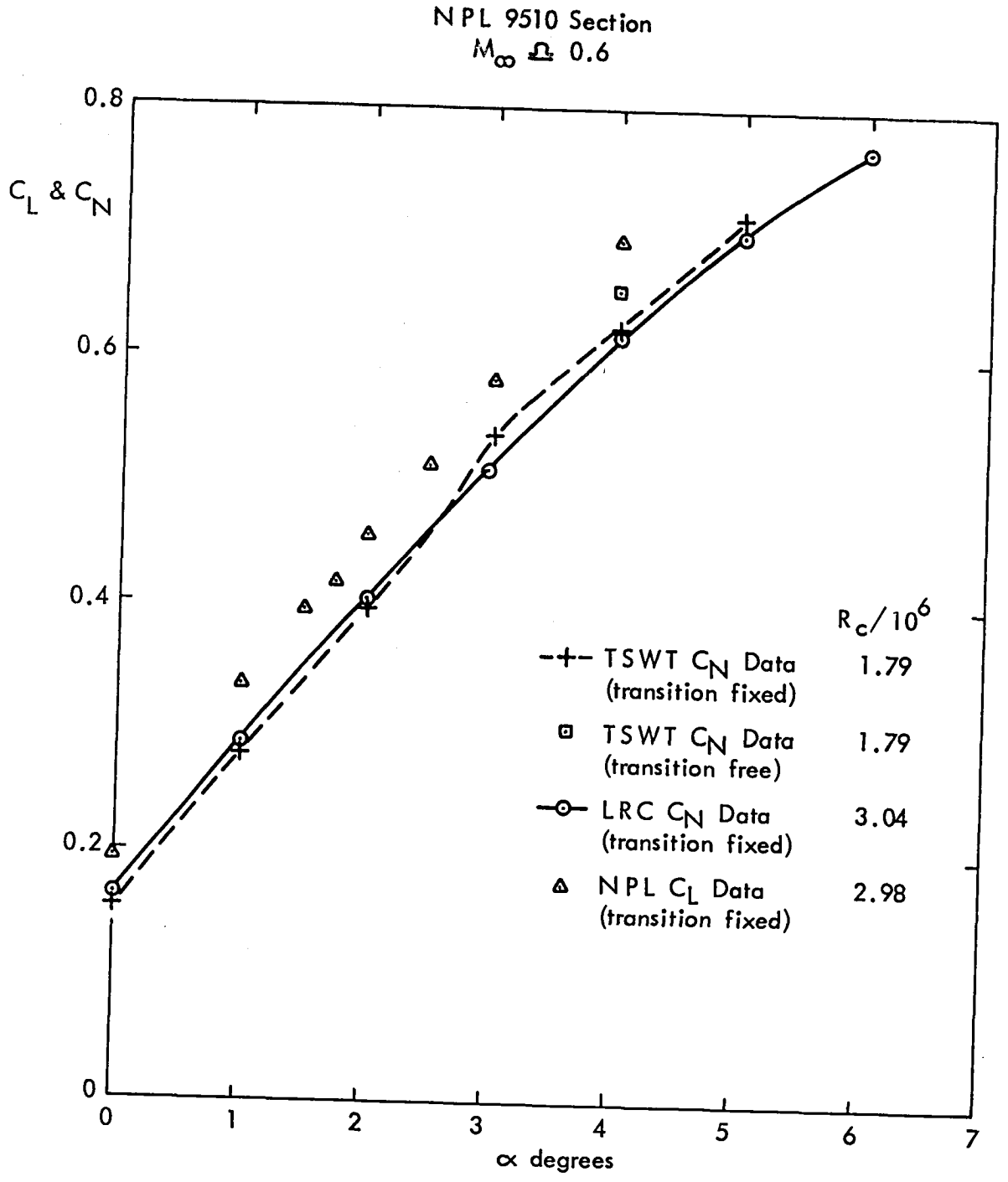

FIG.9.29(b) VARIATIONS OF C_L AND C_N WITH ANGLE OF ATTACK; $M_\infty \triangleq 0.6$

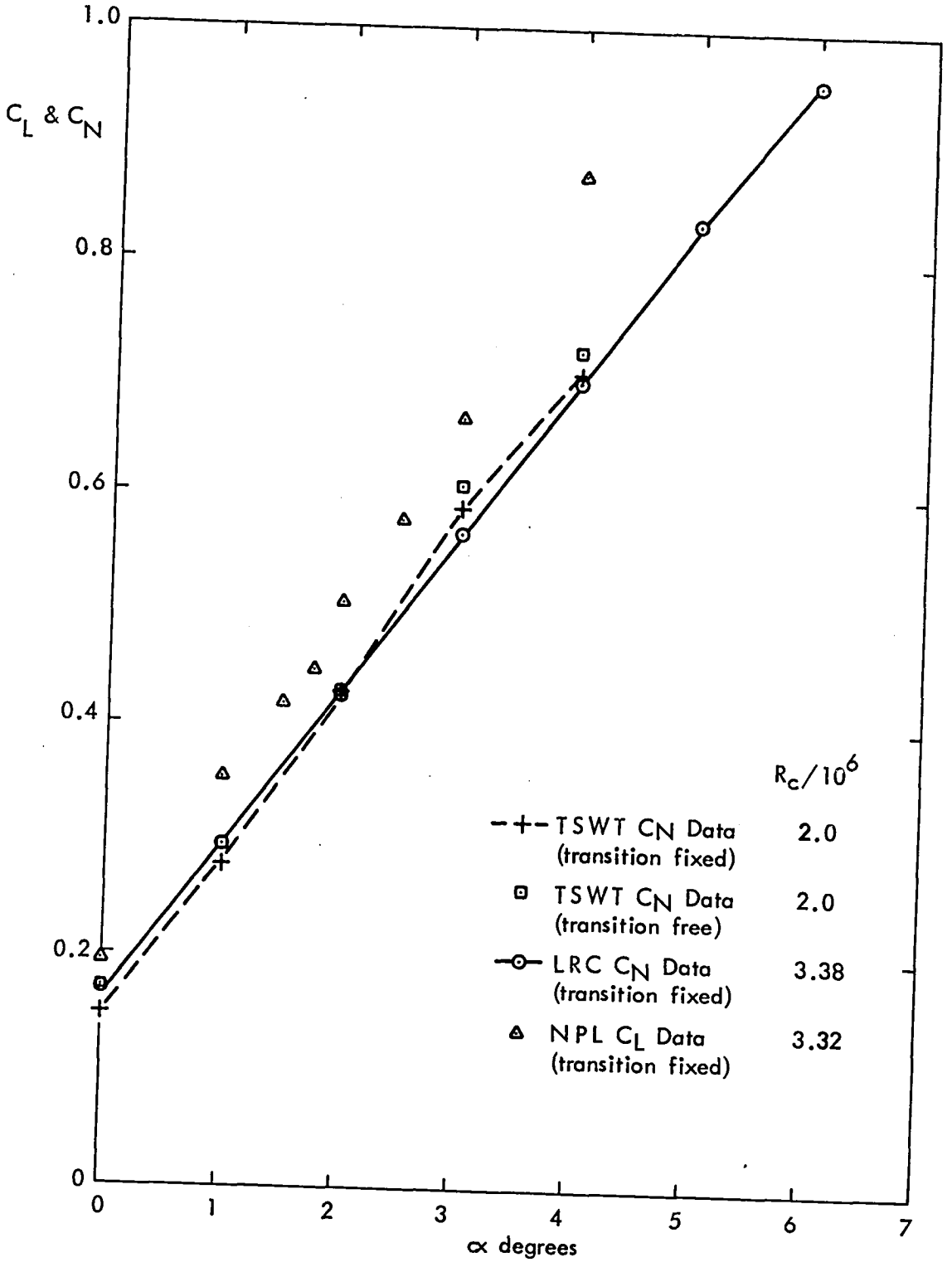

FIG.9.29(c) VARIATIONS OF C_L AND C_N WITH ANGLE OF ATTACK; $M_\infty \triangleq 0.7$

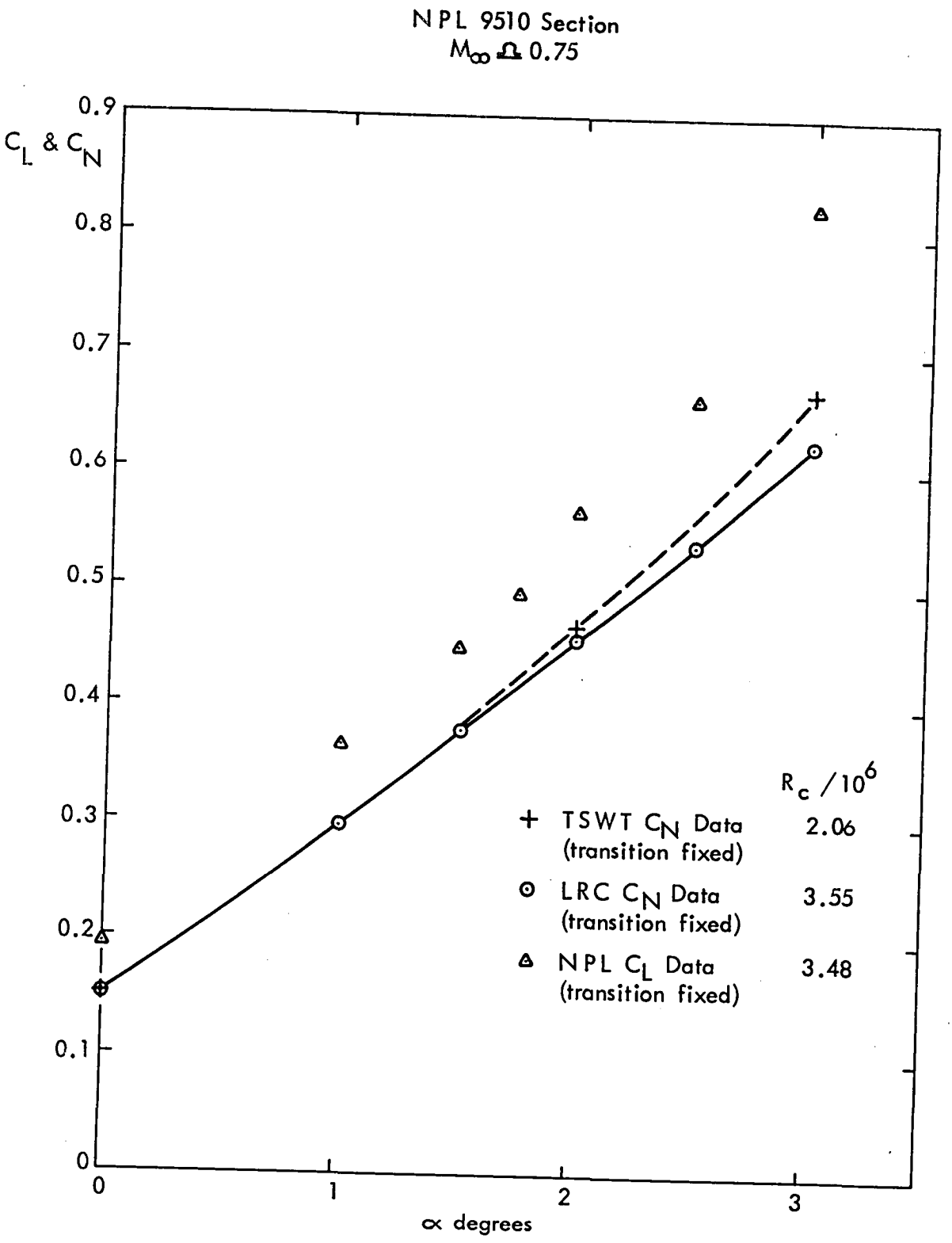

FIG. 9.29(d) VARIATIONS OF C_L AND C_N WITH ANGLE OF ATTACK; $M_\infty \triangleq 0.75$

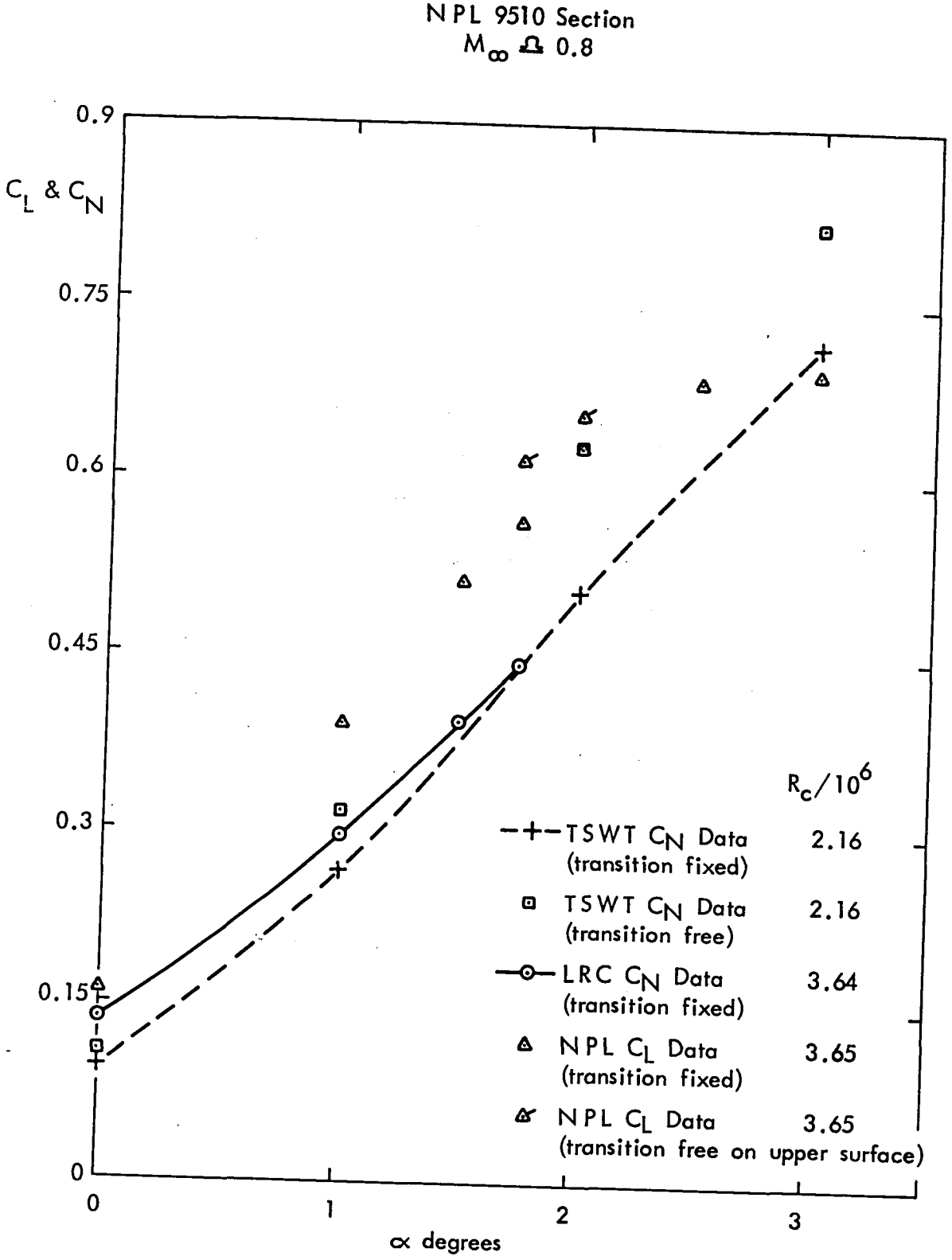

FIG. 9.29(e) VARIATIONS OF C_L AND C_N WITH ANGLE OF ATTACK; $M_\infty \triangleq 0.8$

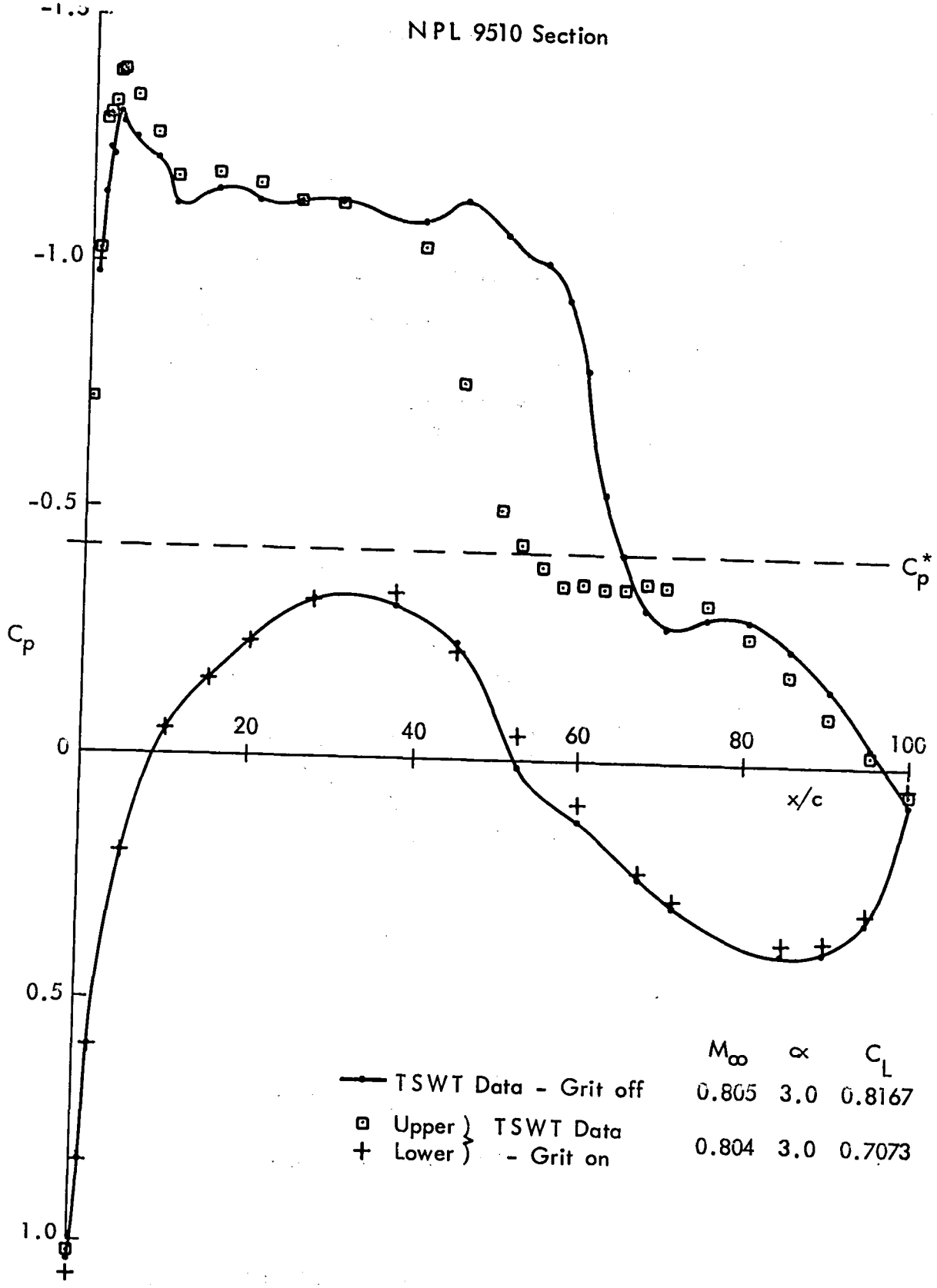

FIG. 9.30 COMPARISON OF MODEL PRESSURE DISTRIBUTIONS WITH TRANSITION FIXED AND TRANSITION FREE : $M_\infty \triangleq 0.8$; $\alpha = 3^\circ$

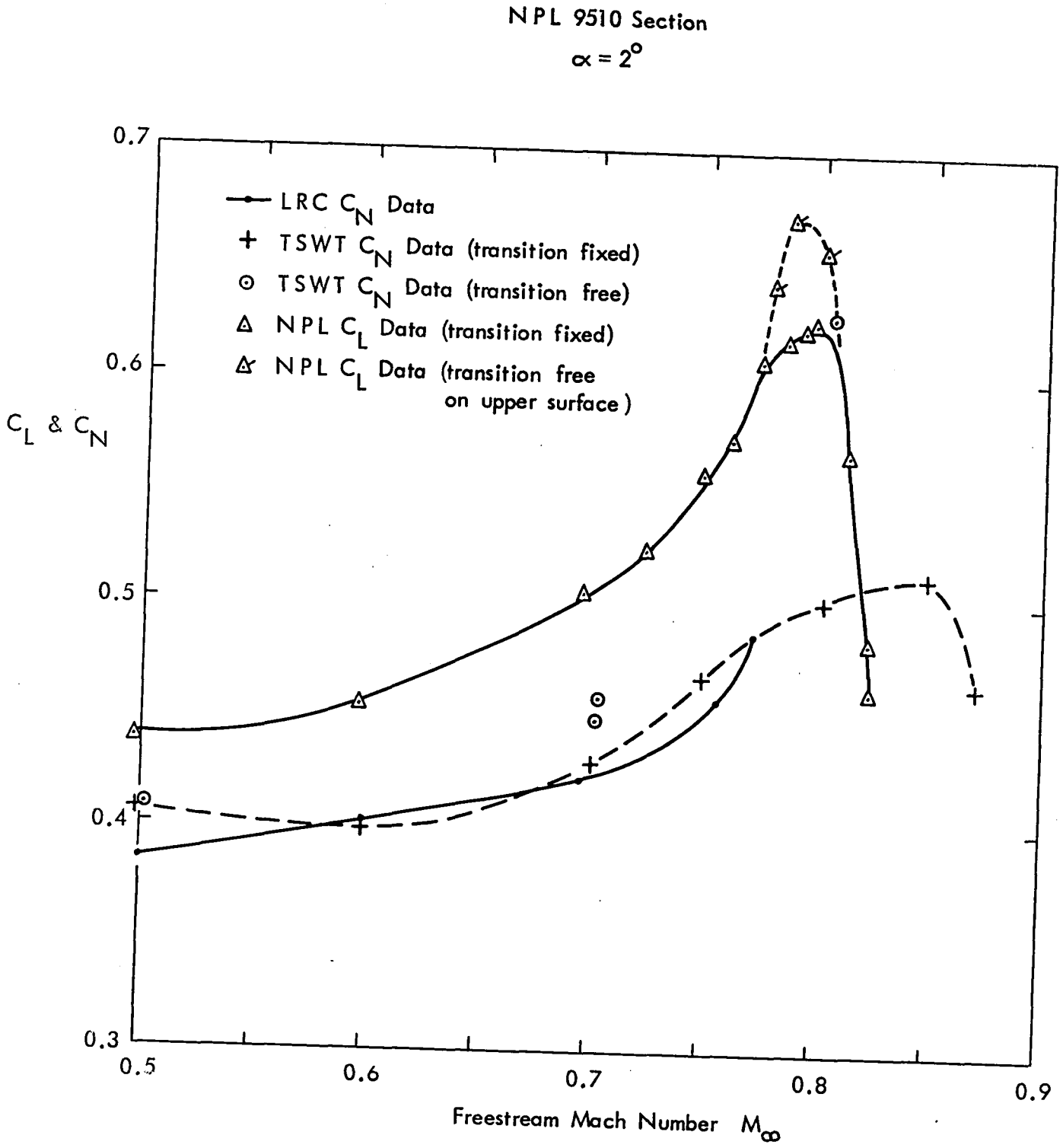

FIG.9.31 VARIATION OF NORMAL FORCE WITH MACH NUMBER; $\alpha = 2^\circ$

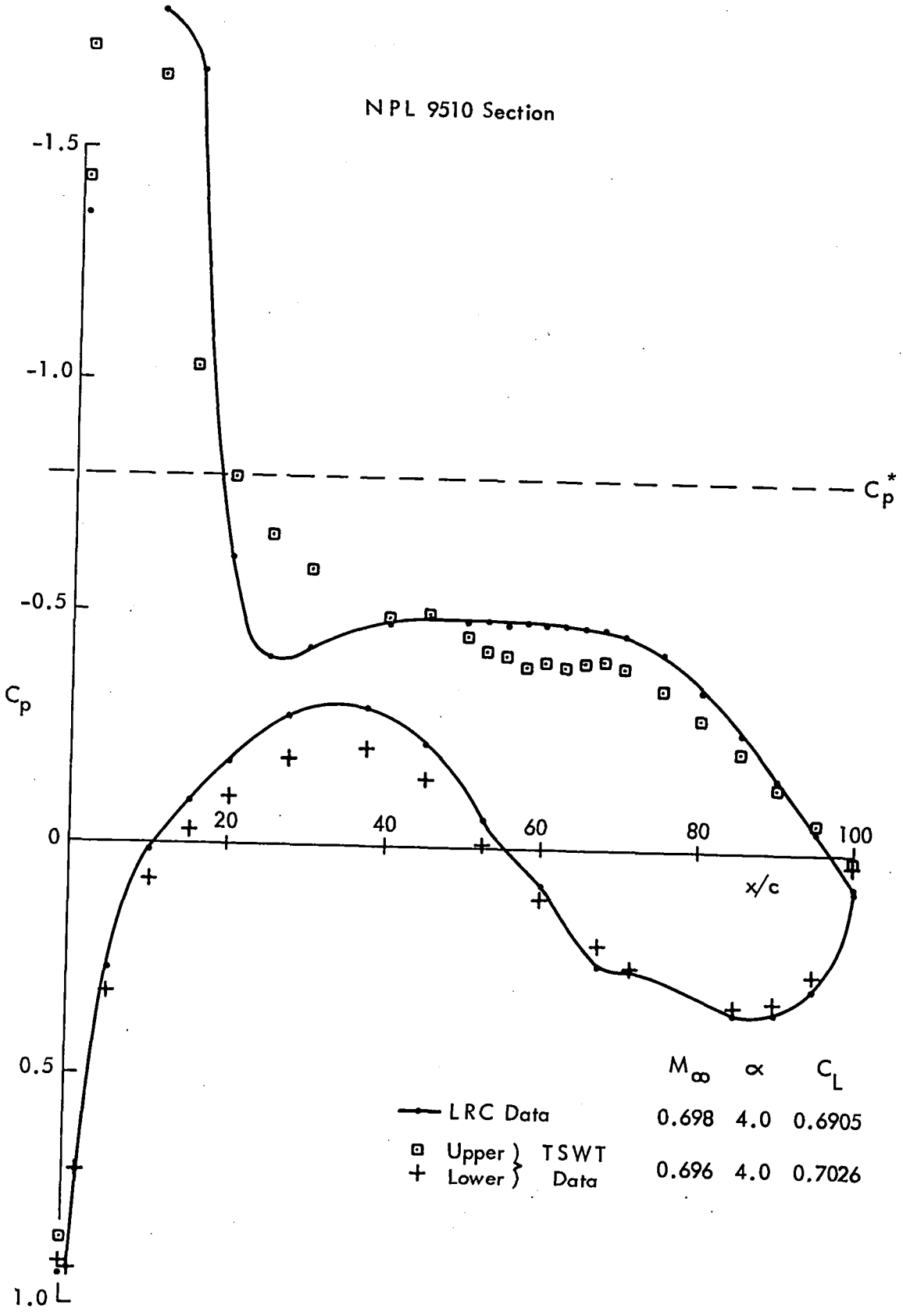

FIG. 9.32 COMPARISON OF TSWT AND LRC MODEL PRESSURE DISTRIBUTIONS ; $M_\infty \triangleq 0.7$; $\alpha \triangleq 4°$

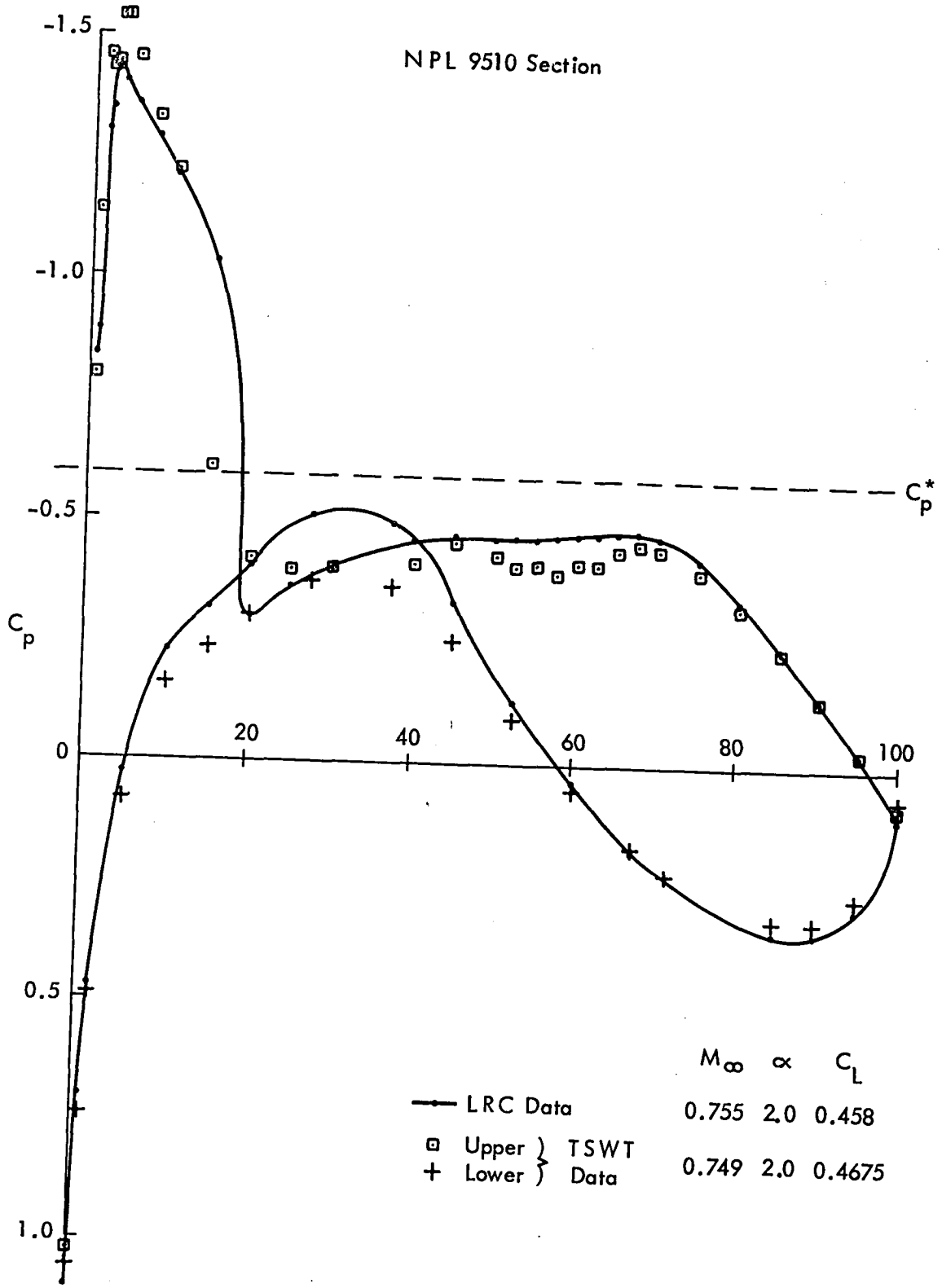

FIG. 9.33 COMPARISON OF TSWT AND LRC MODEL PRESSURE DISTRIBUTIONS : $M_\infty \triangleq 0.75$; $\alpha \triangleq 2^\circ$

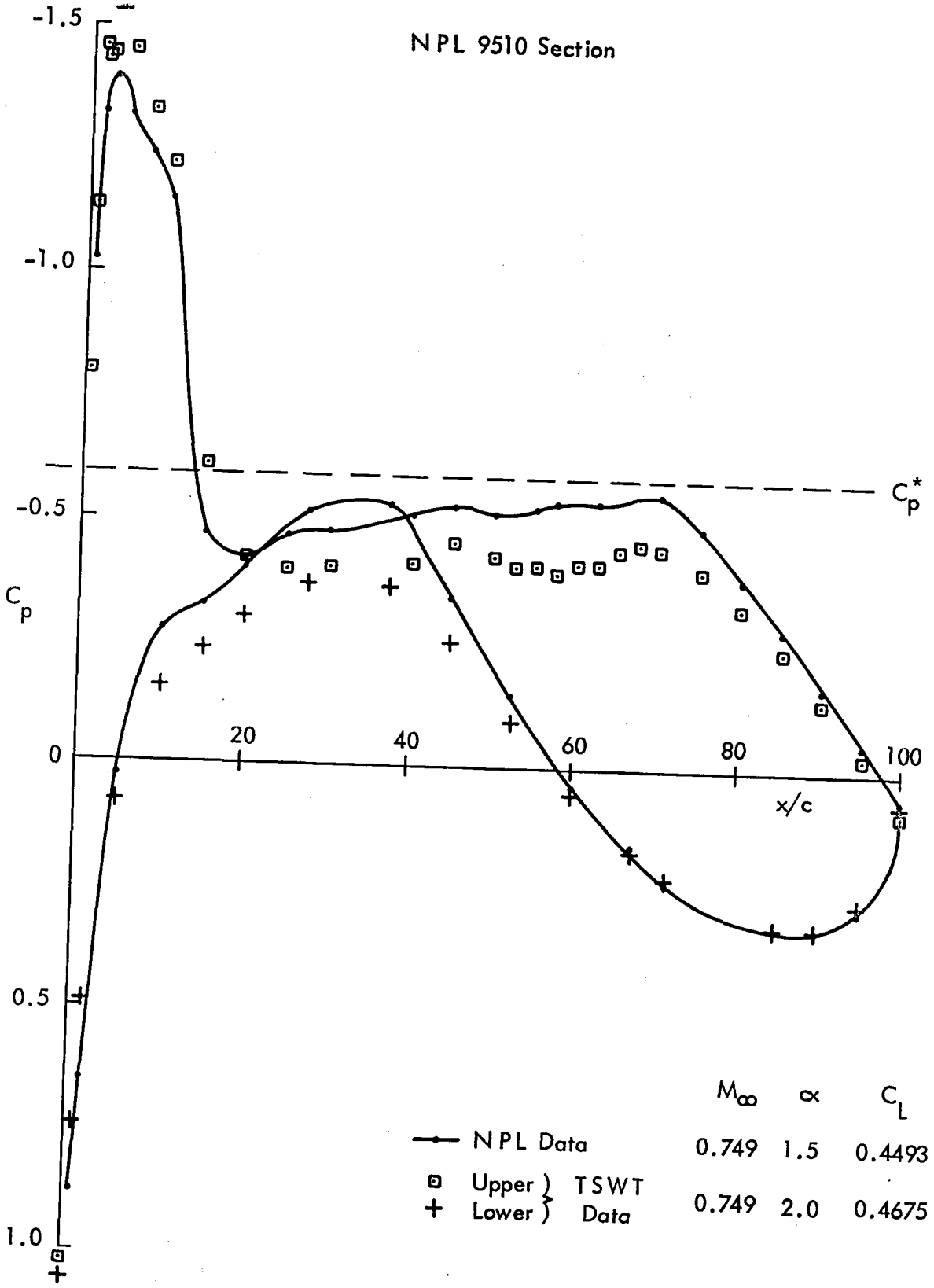

FIG. 9.34 COMPARISON OF TSWT AND NPL MODEL PRESSURE DISTRIBUTIONS : $M_\infty \simeq 0.75$; $\alpha \simeq 2°$

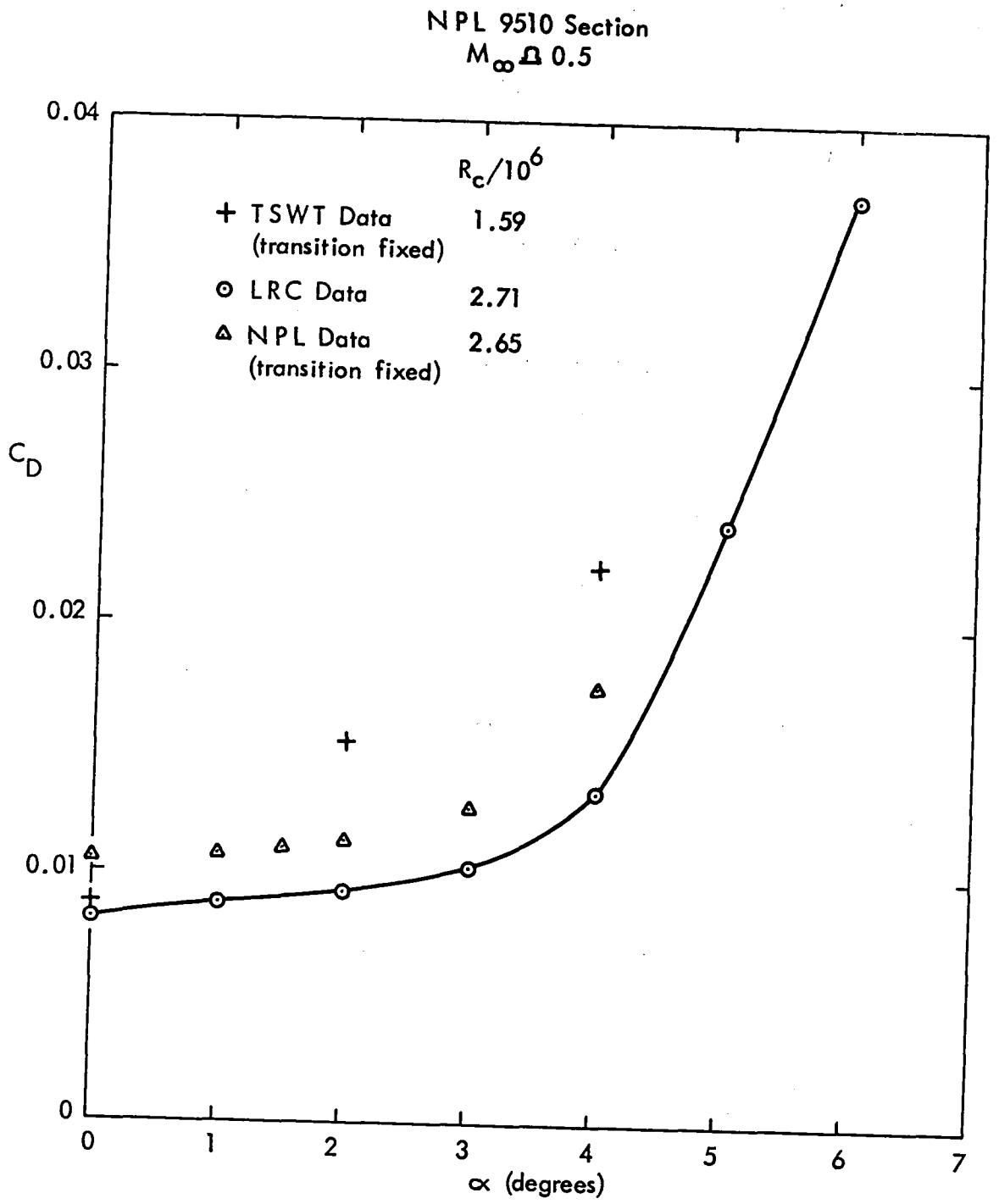

FIG. 9.35(a) VARIATION OF DRAG COEFFICIENT WITH ANGLE OF ATTACK: $M_\infty \Omega$ 0.5

NPL 9510 Section
$M_\infty \triangleq 0.6$

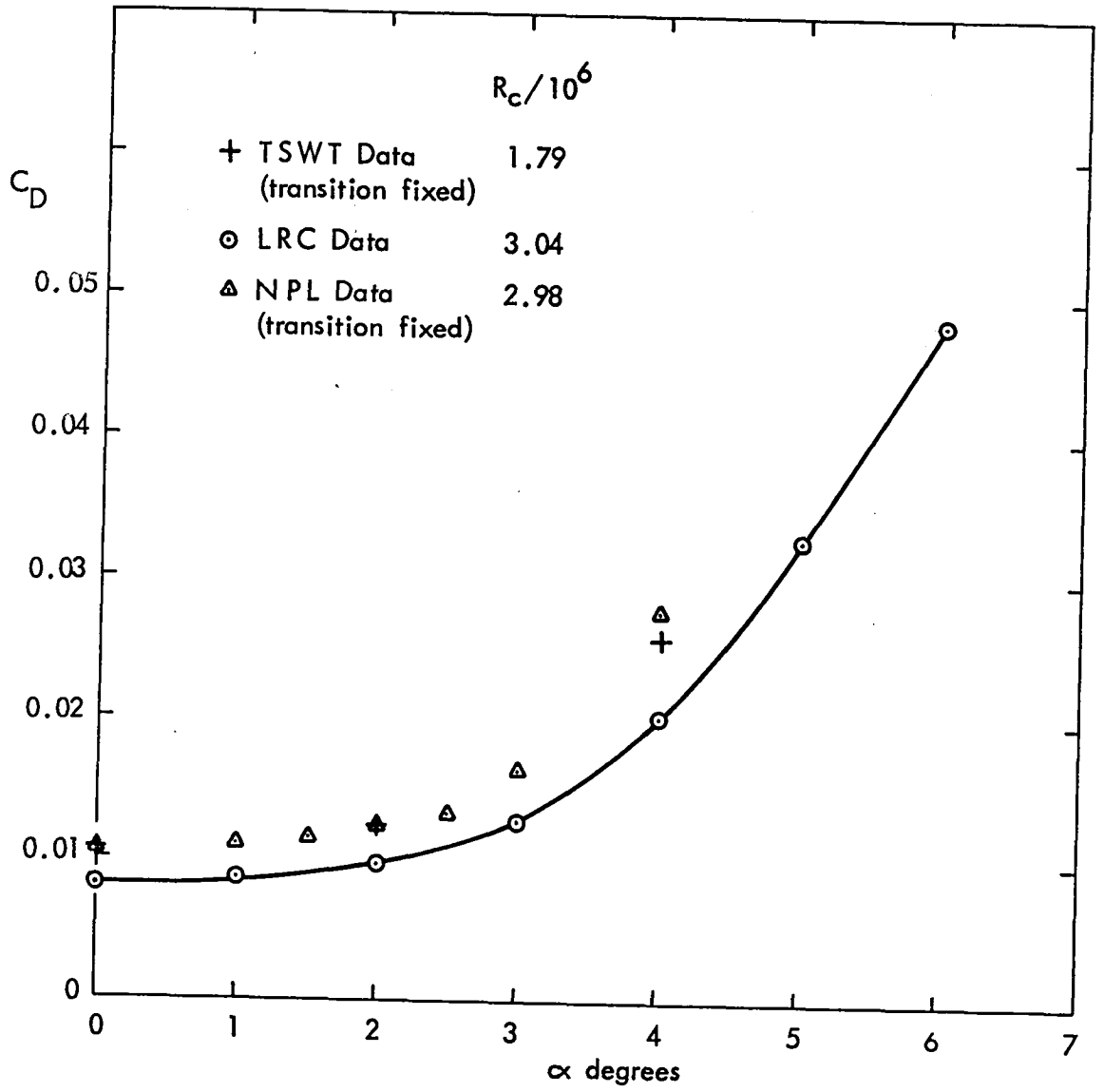

FIG. 9.35(b) VARIATION OF DRAG COEFFICIENT WITH ANGLE OF ATTACK: $M_\infty \triangleq 0.6$

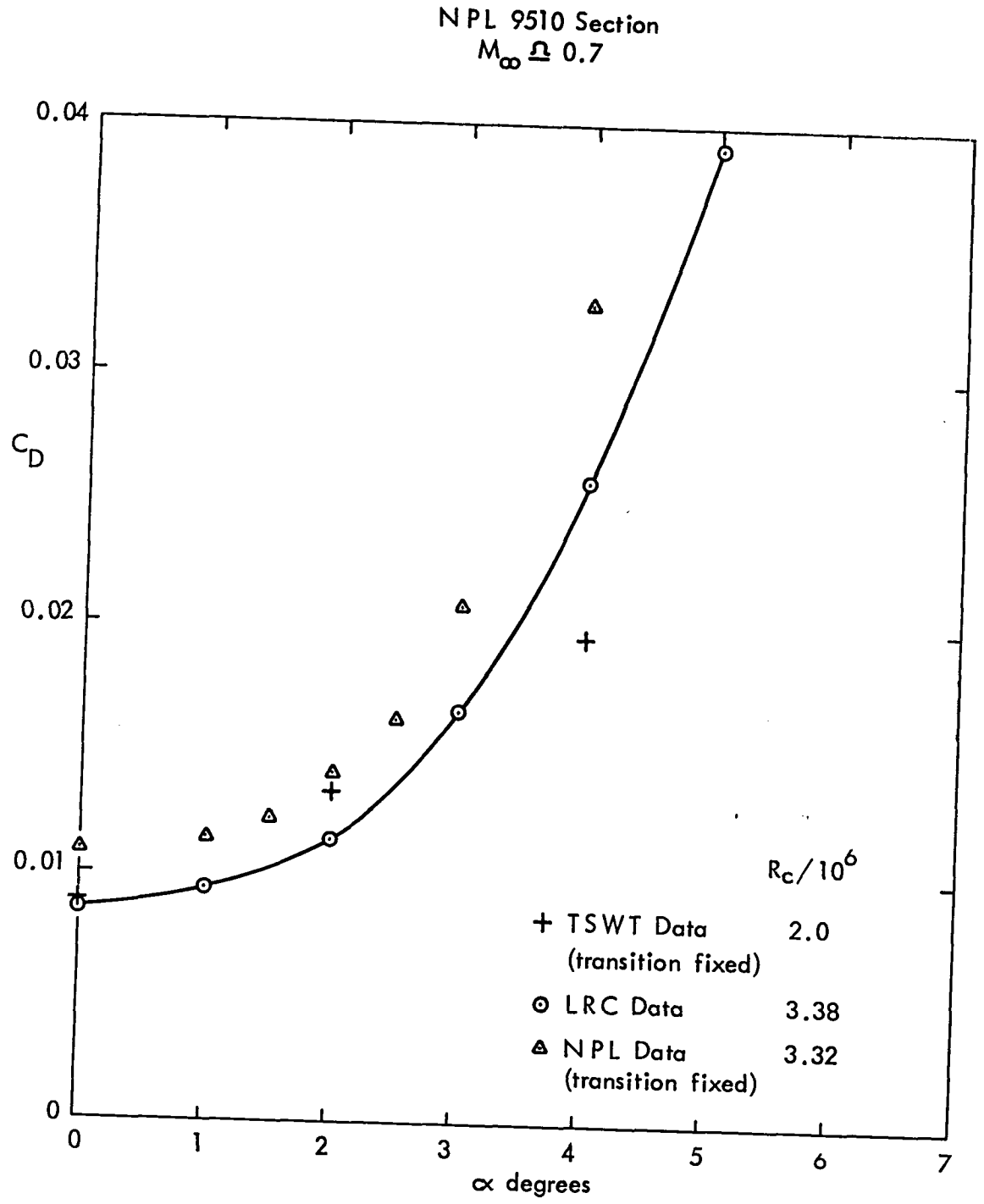

FIG. 9.35(c) VARIATION OF DRAG COEFFICIENT WITH ANGLE OF ATTACK: $M_\infty \triangleq 0.7$

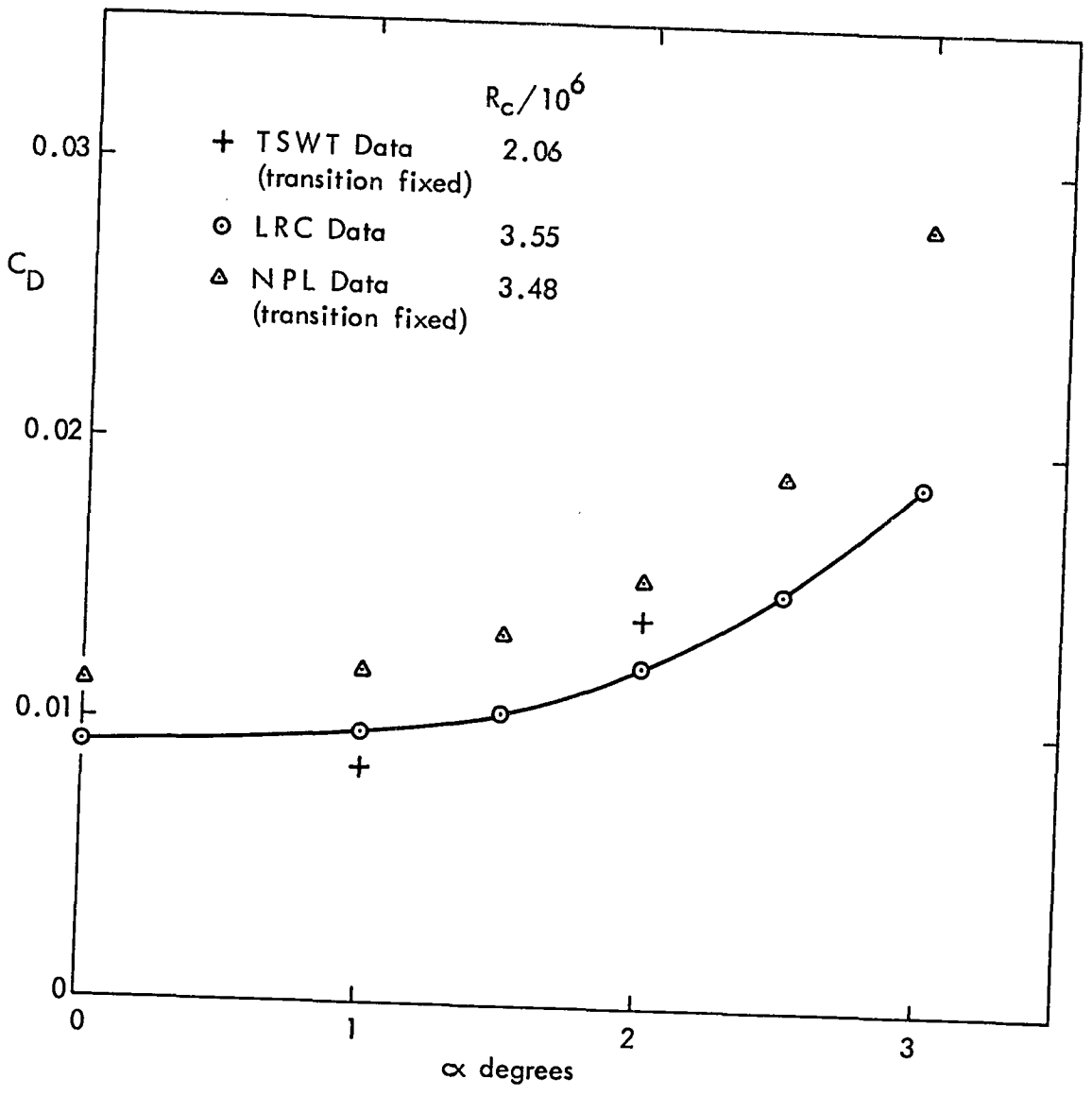

FIG. 9.35(d) VARIATION OF DRAG COEFFICIENT WITH ANGLE OF ATTACK: $M_\infty \Omega 0.75$

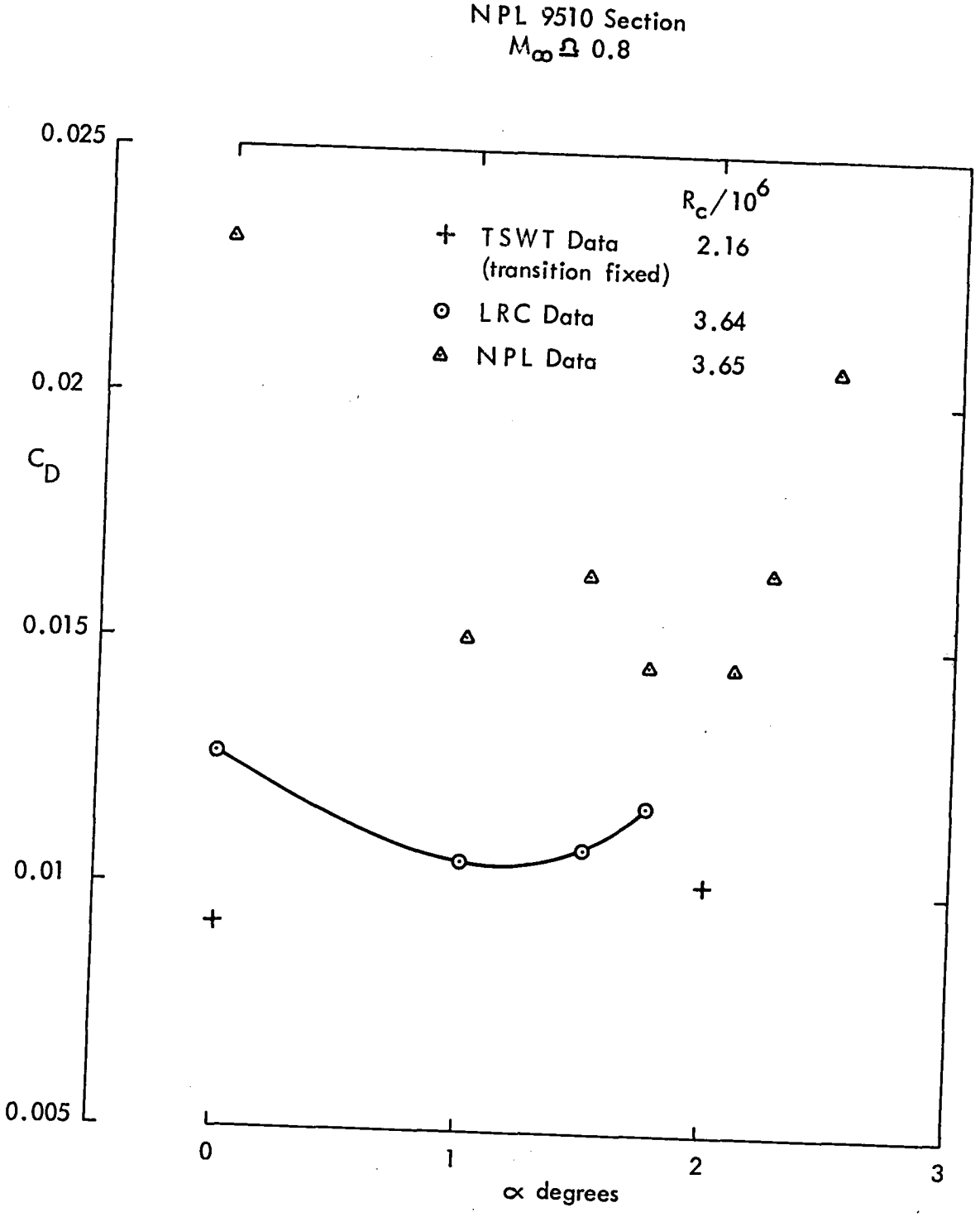

FIG.9.35(e) VARIATION OF DRAG COEFFICIENT WITH ANGLE OF ATTACK: $M_\infty \Omega$ 0.8

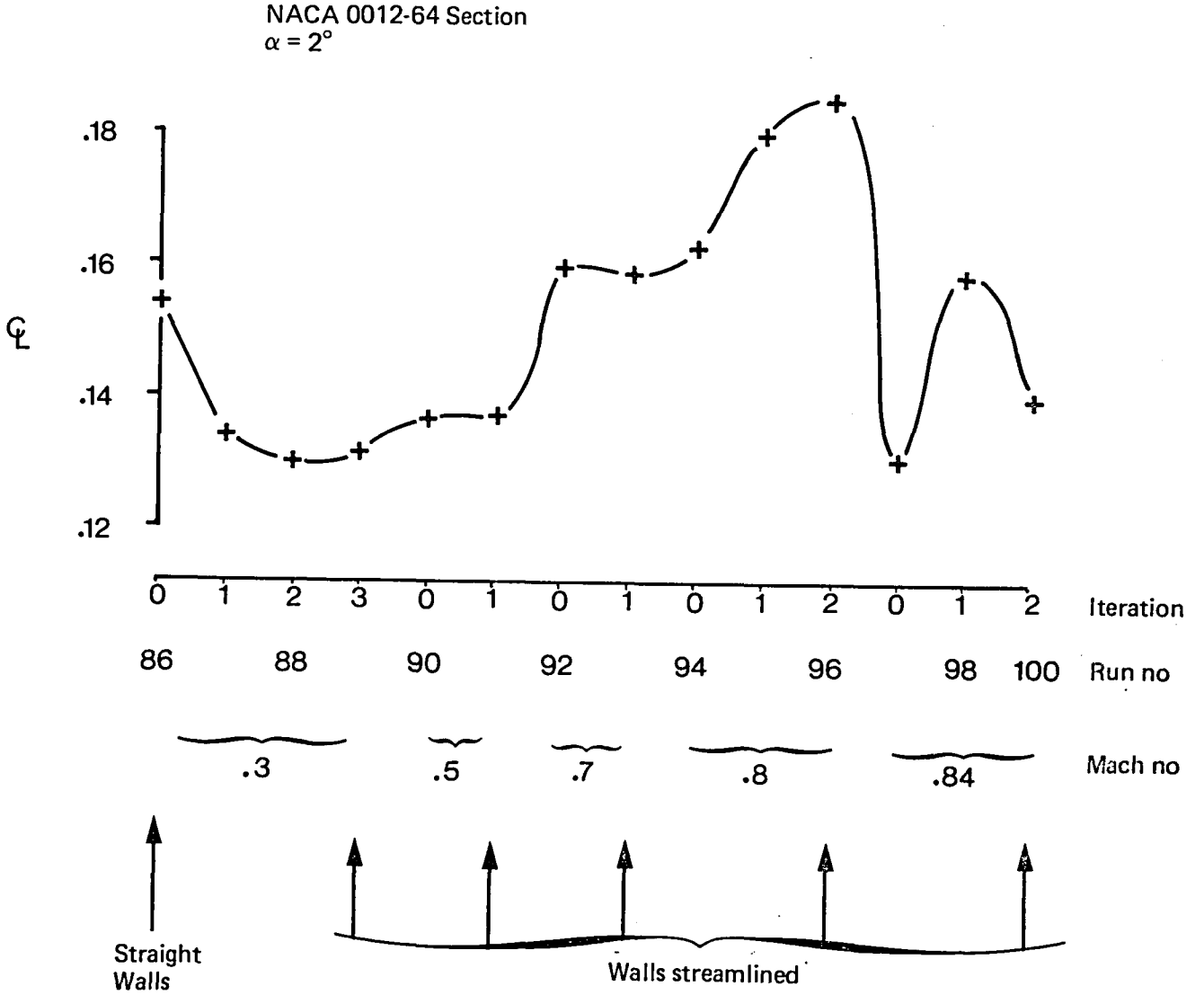

FIG. 10.1 MODEL LIFT COEFFICIENT VARIATION DURING SUCCESIVE STREAMLINING CYCLES OVER THE MACH NUMBER RANGE FROM 0.3 to 0.84

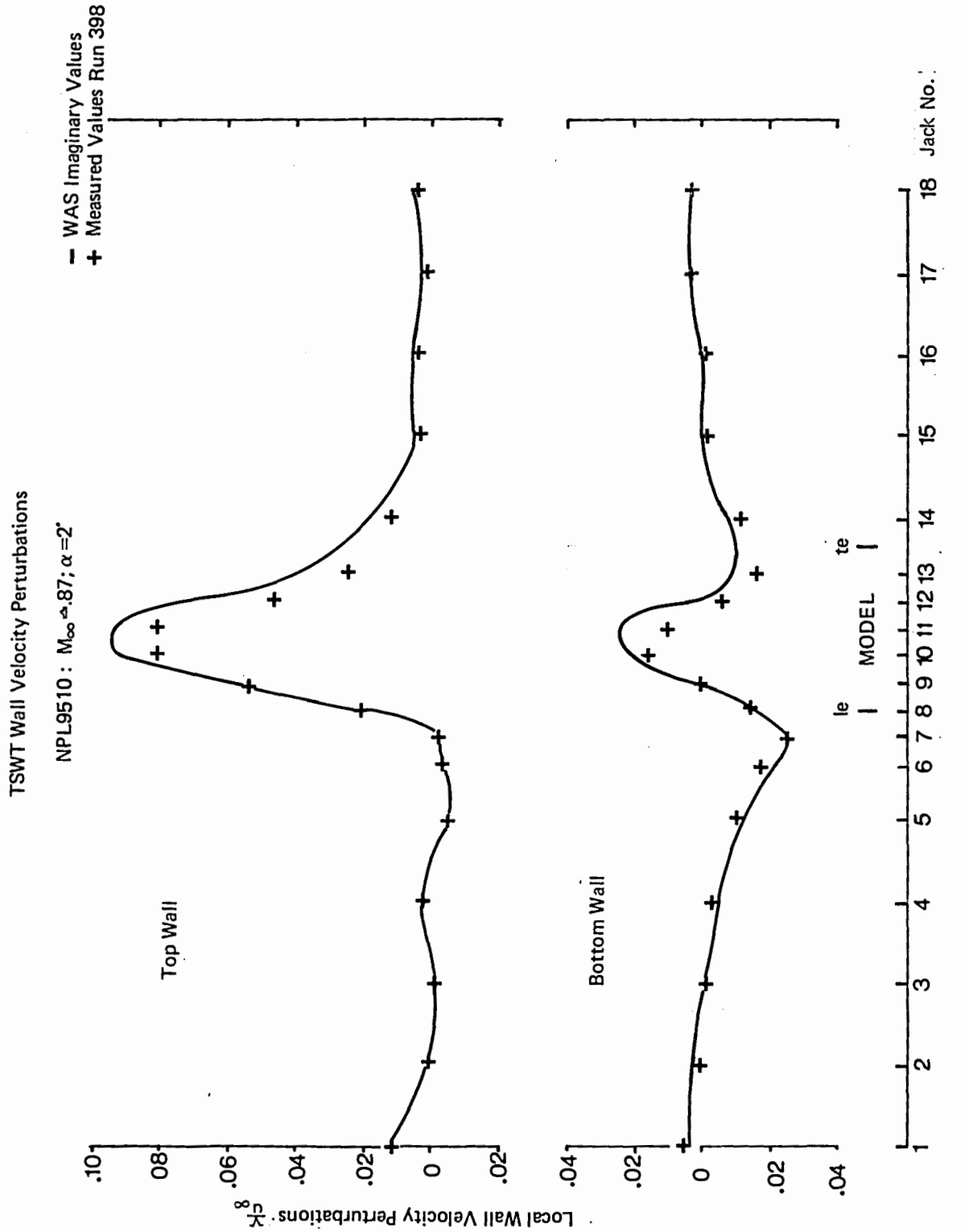

FIG. 10.2 COMPARISON OF REAL AND IMAGINARY WALL VELOCITY PERTURBATIONS ALONG EACH WALL.

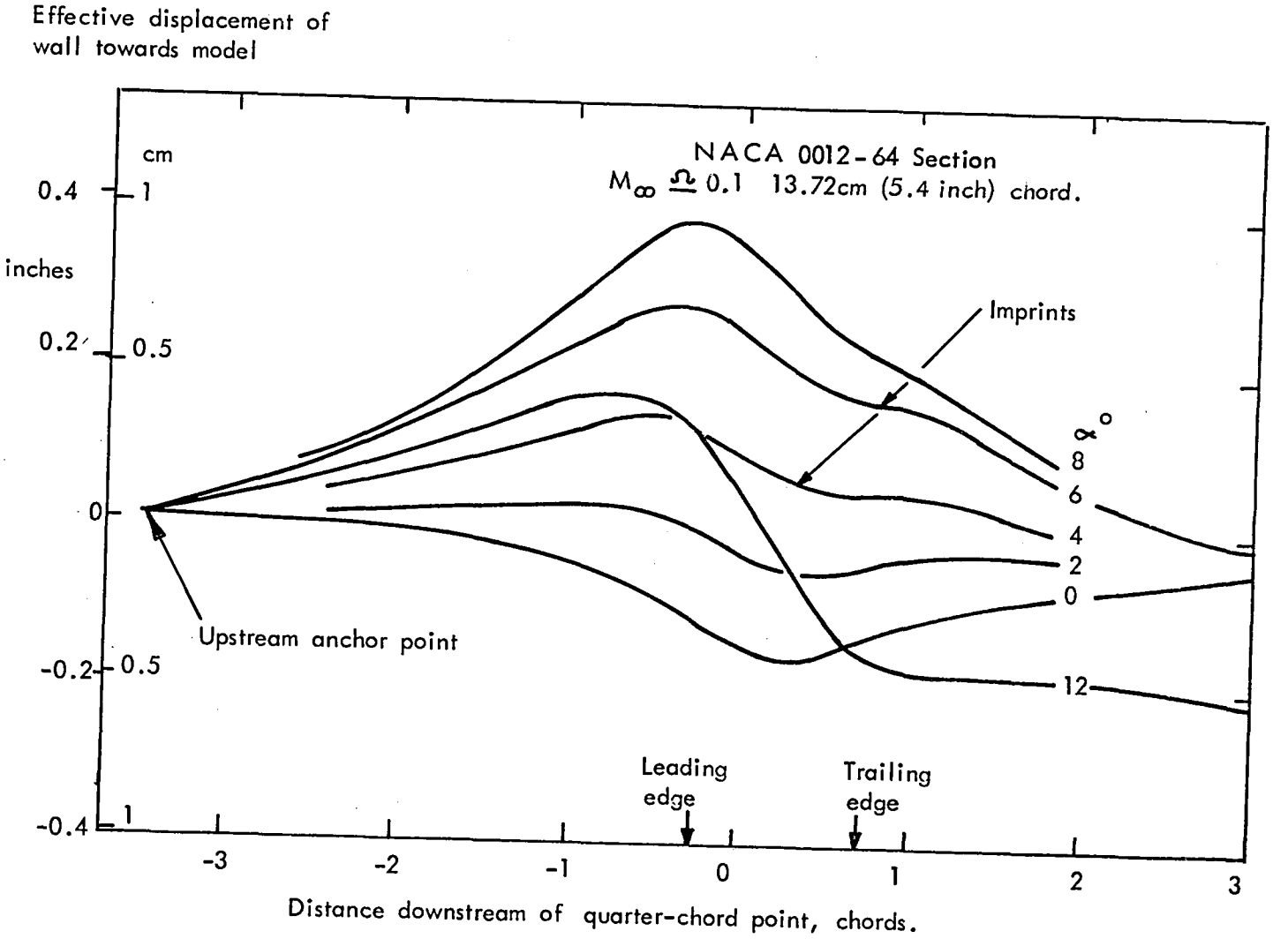

FIG. 10.3 EFFECTIVE CONTOURS OF SSWT WALL UNDER AIRFOIL MODEL AT SELECTED ANGLES OF ATTACK.

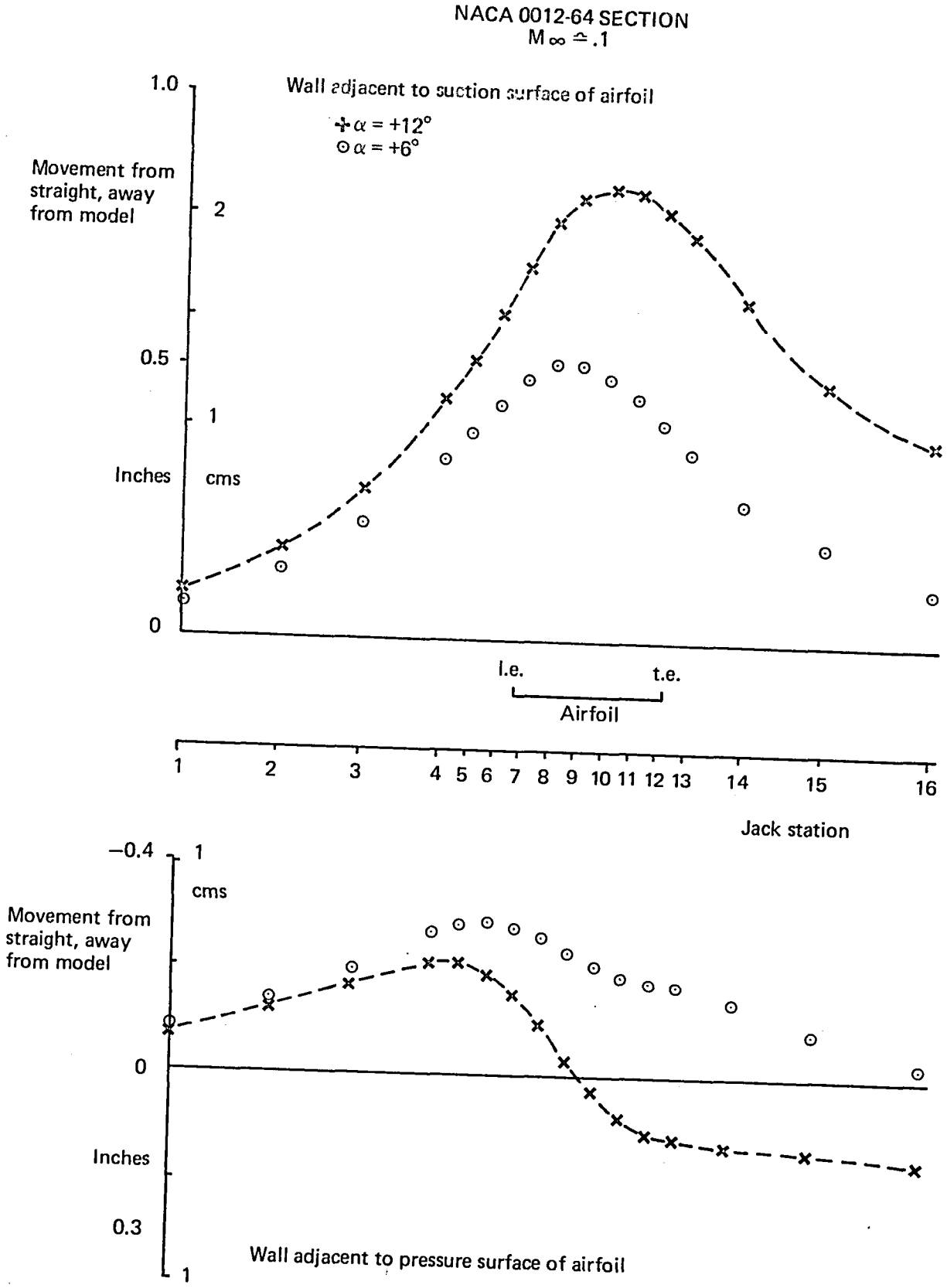

FIG. 10.4 TYPICAL STREAMLINED FLEXIBLE WALL CONTOURS IN SSWT.

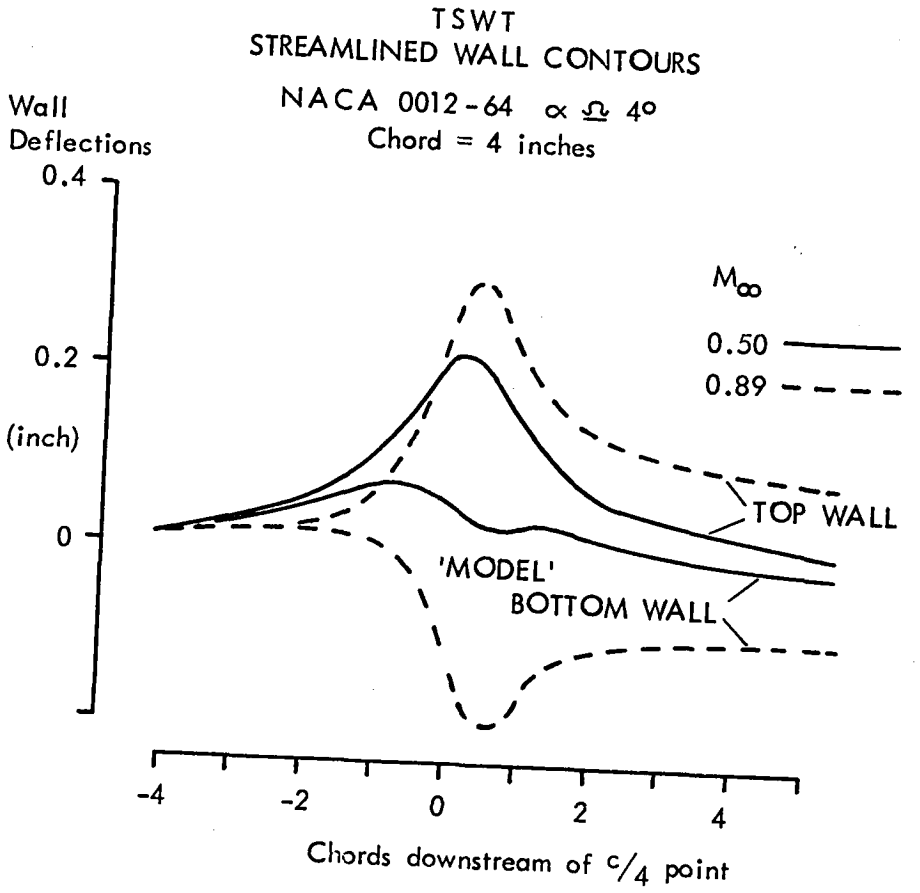

FIG. 10.5 COMPARISON OF TSWT STREAMLINED WALL CONTOURS FOR $M_\infty \triangleq 0.5$ AND $M_\infty = 0.89$

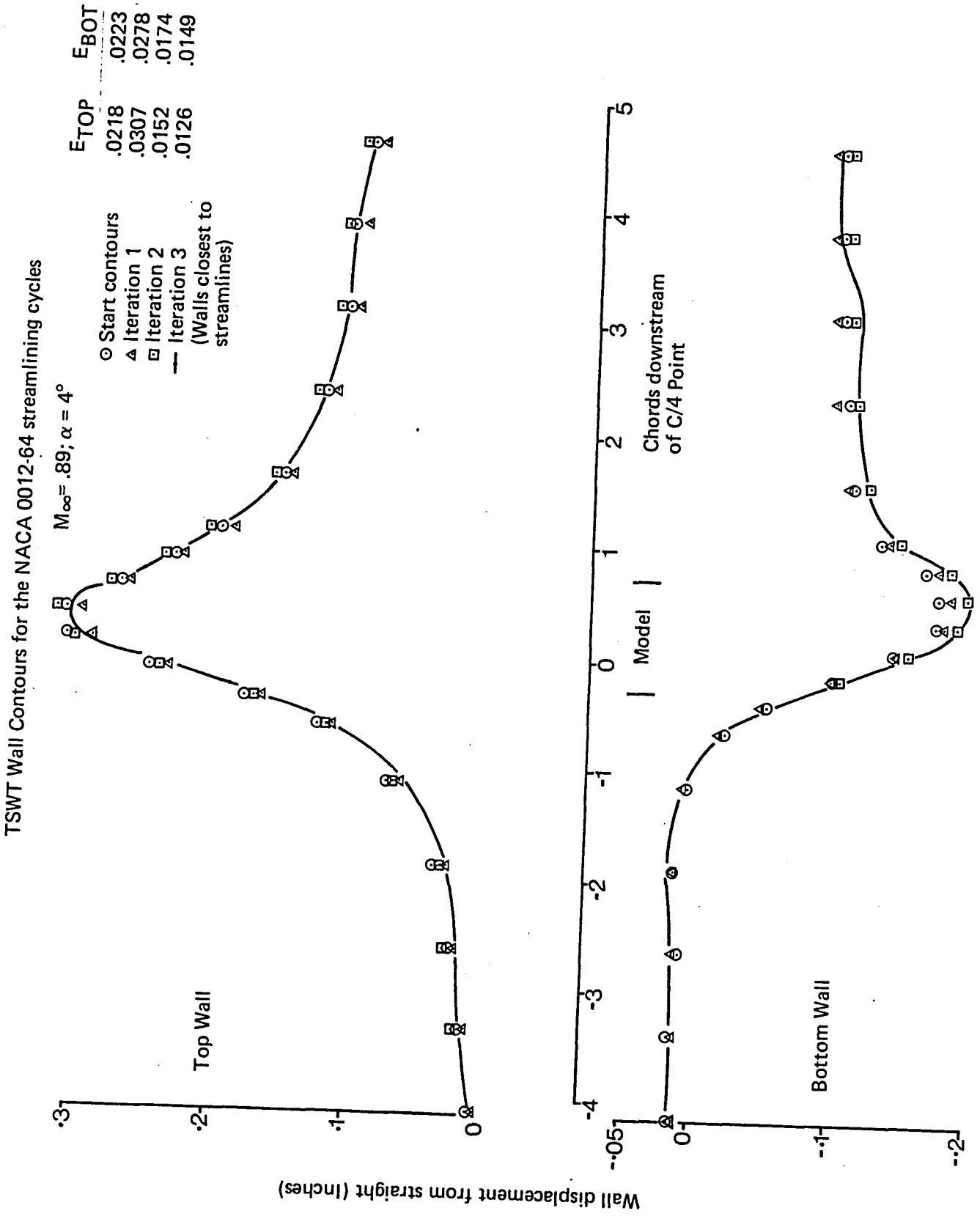

FIG. 10.6 WALL CONTOURS SET DURING A STREAMLINING CYCLE; M_∞ = 0.89; α = 4°

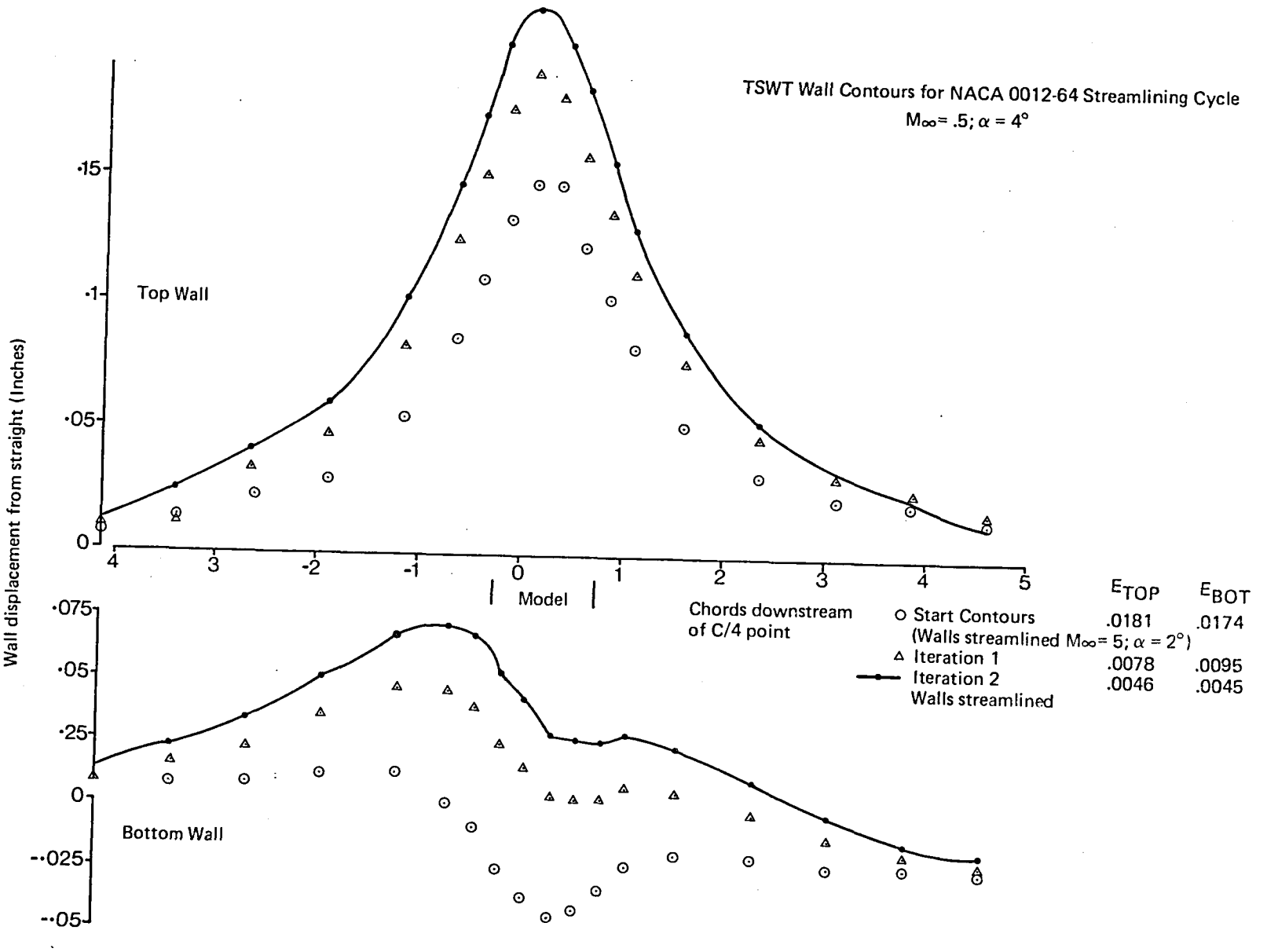

FIG. 10.7 WALL CONTOURS SET DURING A STREAMLINING CYCLE; $M_\infty = 0.5$; $\alpha = 4^\circ$

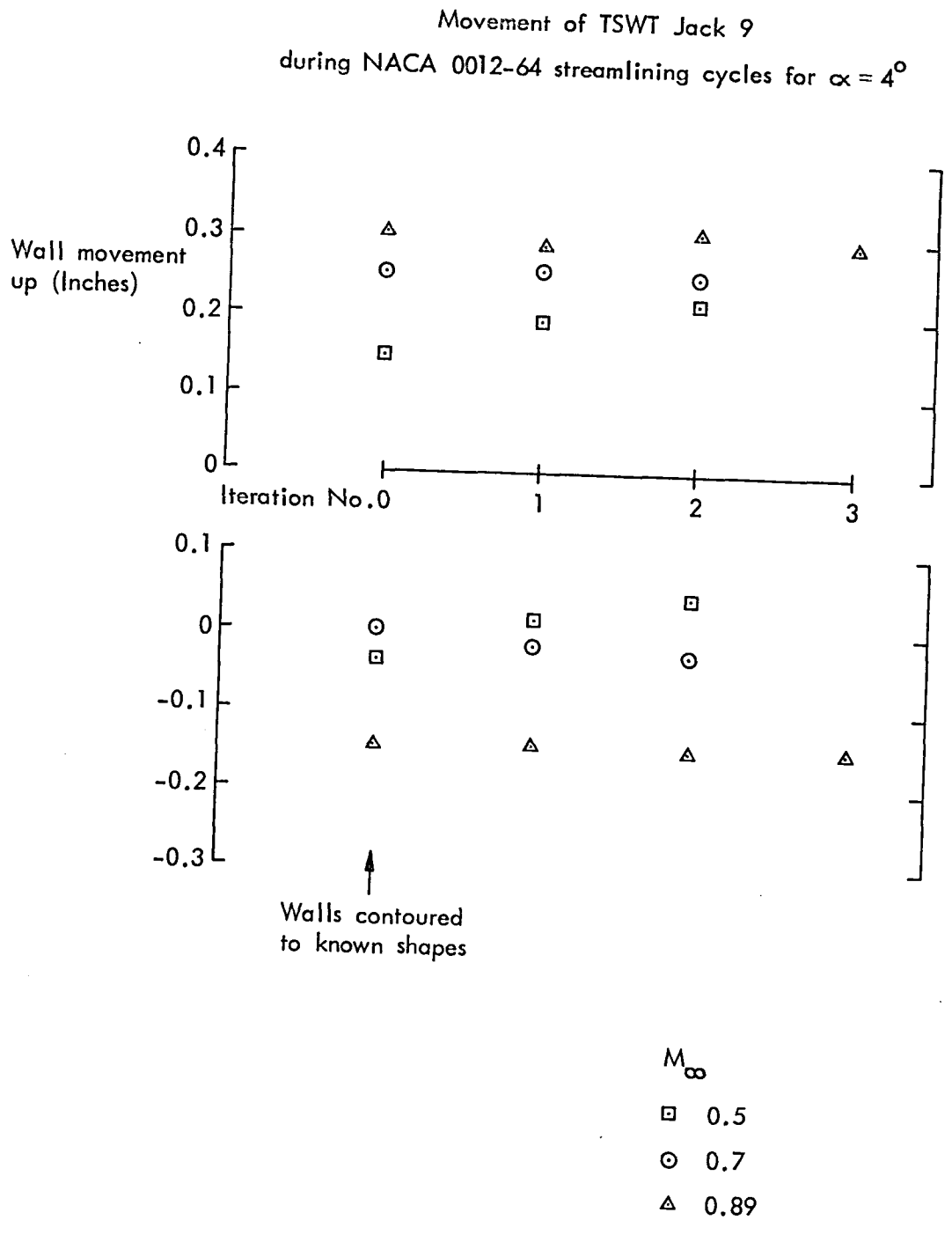

FIG. 10.8 WALL MOVEMENT ADJACENT TO THE MODEL QUARTER CHORD DURING A STREAMLINING CYCLE.

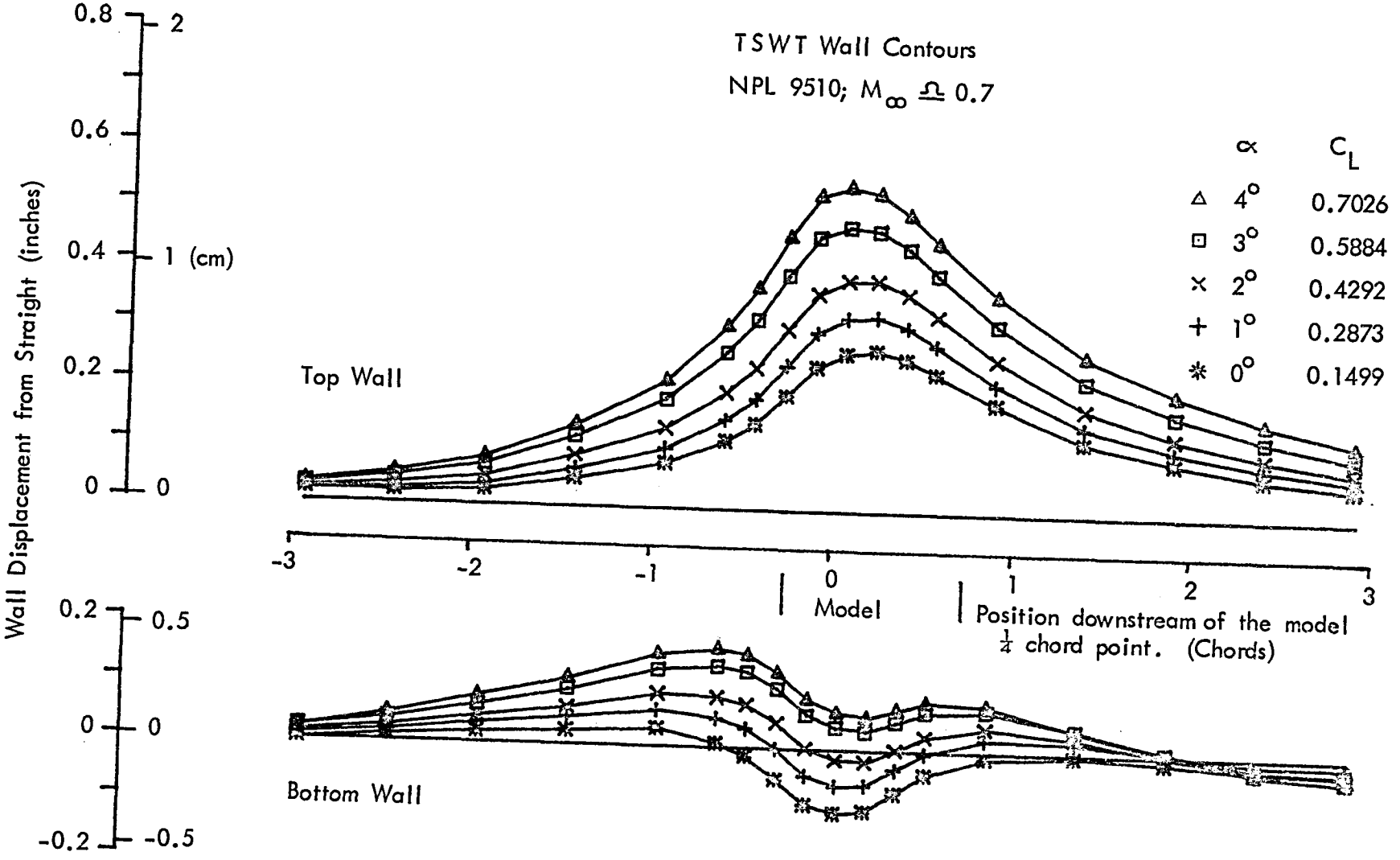

FIG. 10.9 WALL CONTOURS FOR VARYING ANGLE OF ATTACK AT $M_\infty \triangleq 0.7$

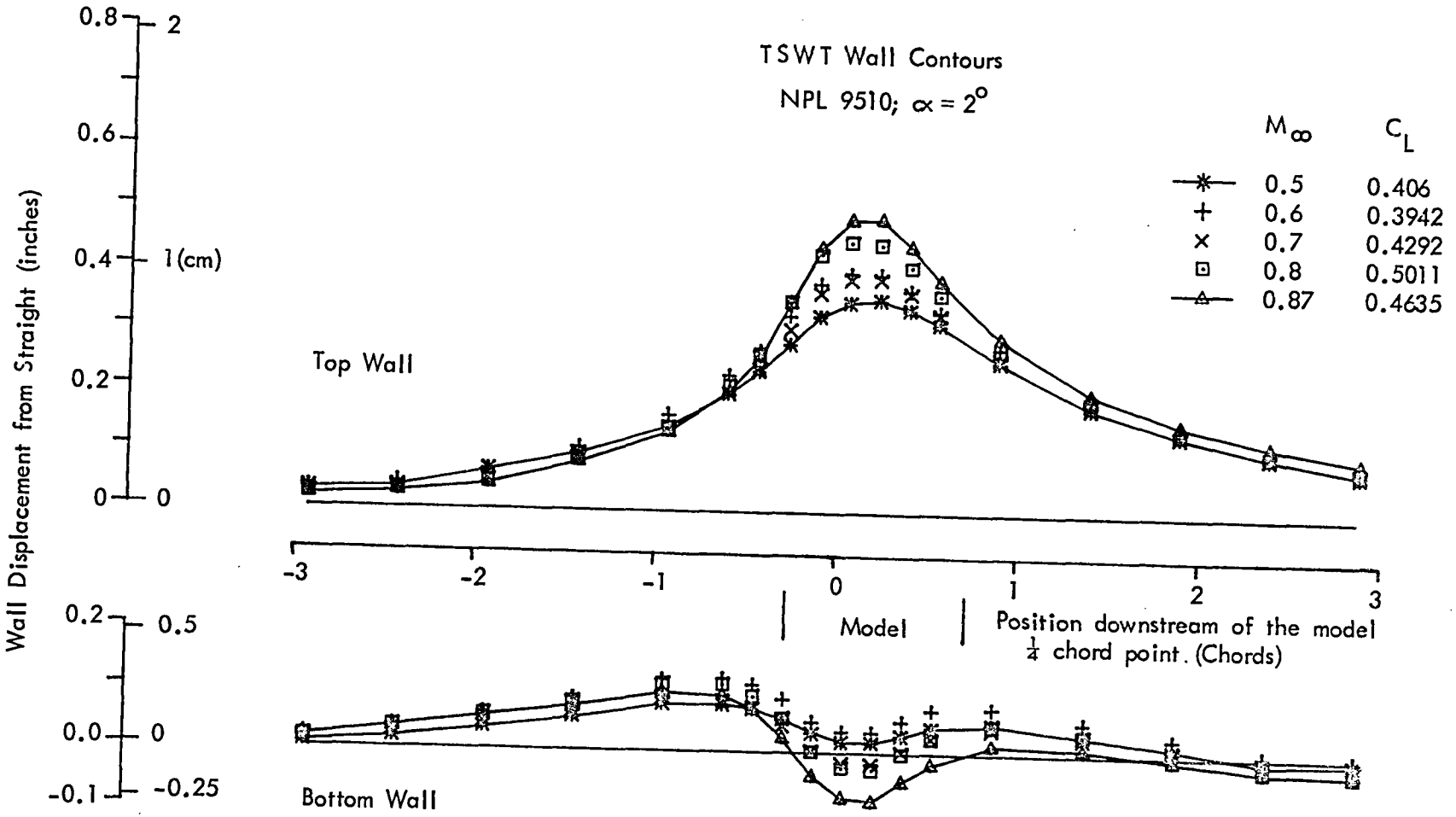

FIG. 10.10 WALL CONTOUR VARIATIONS WITH MACH NUMBER, $\alpha = 2^\circ$

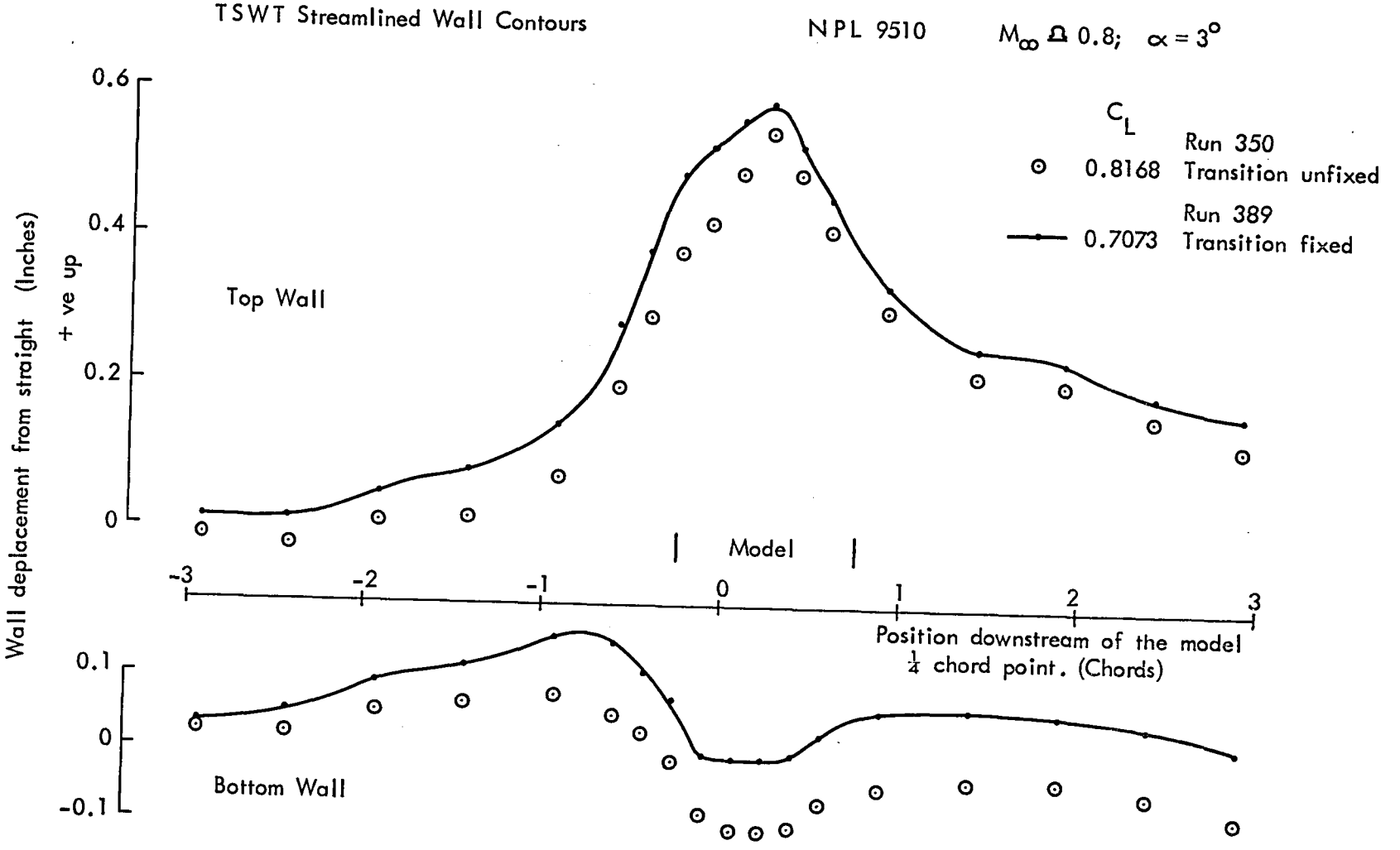

FIG. 10.11 COMPARISON OF TSWT WALL CONTOURS WITH MODEL TRANSITION FIXED AND UNFIXED

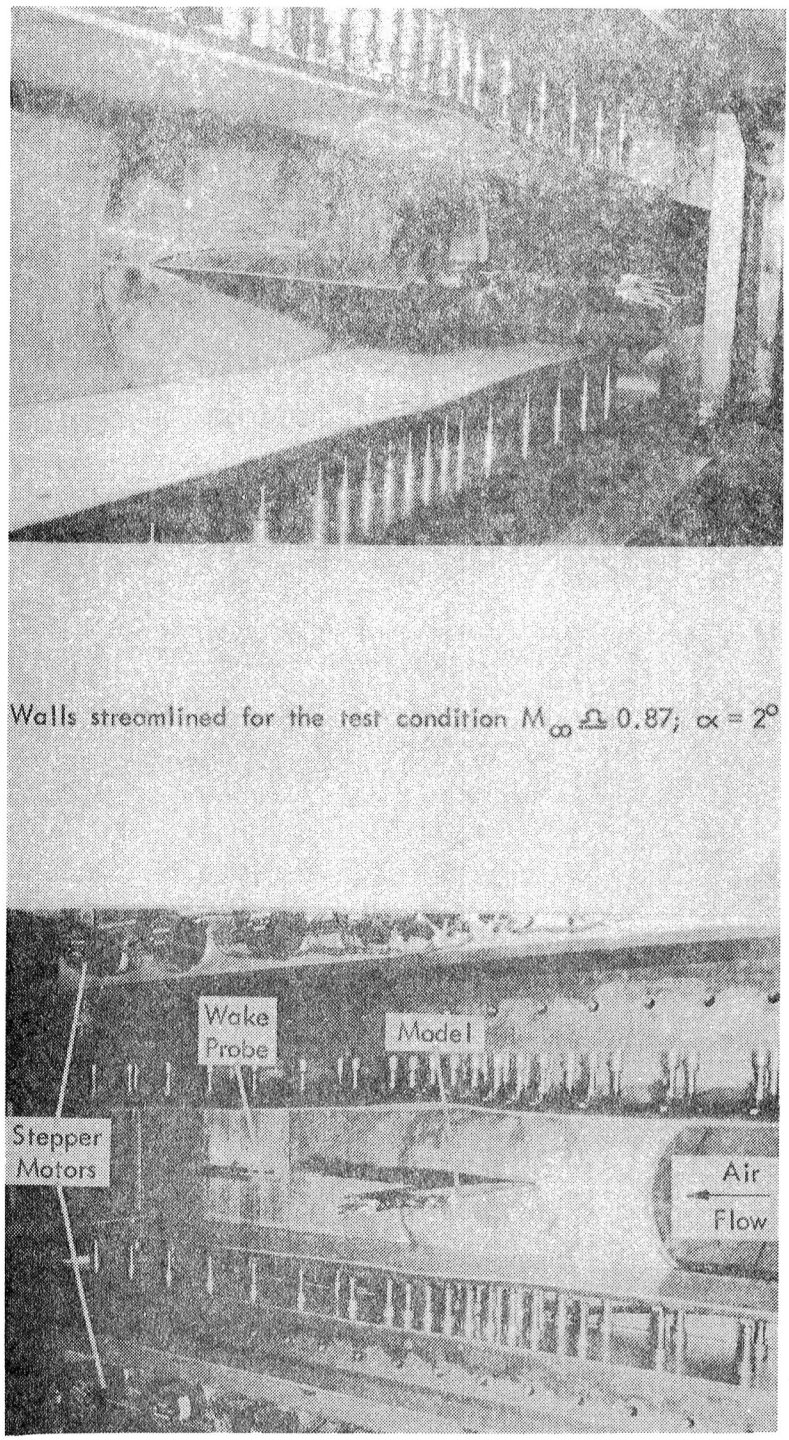

FIG. 10.12 TSWT STREAMLINED AROUND AN NPL 9510 AEROFOIL

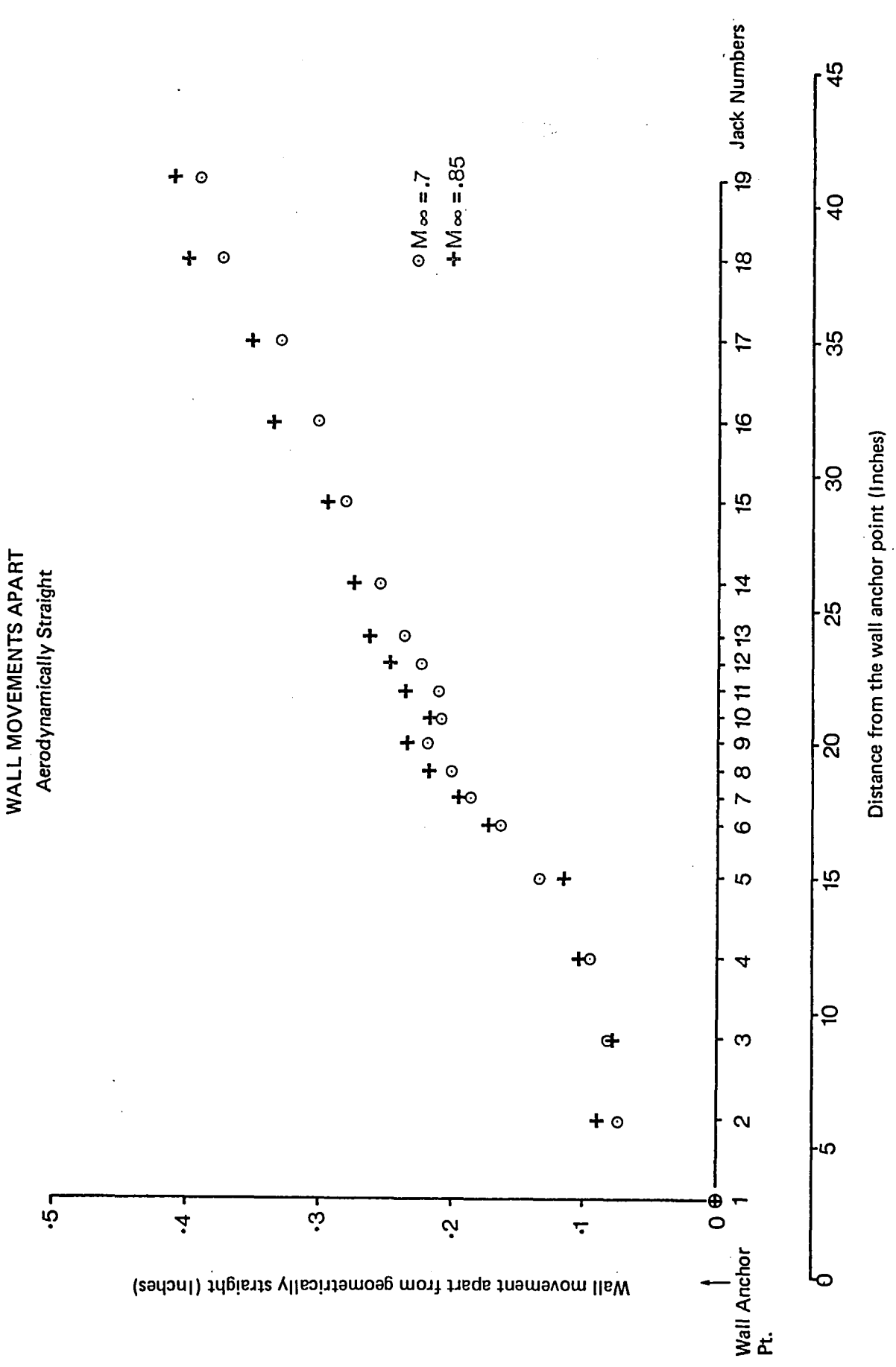

FIG. 10.13 FLEXIBLE WALL MOVEMENTS APART FOR AERODYNAMICALLY STRAIGHT CONTOURS.

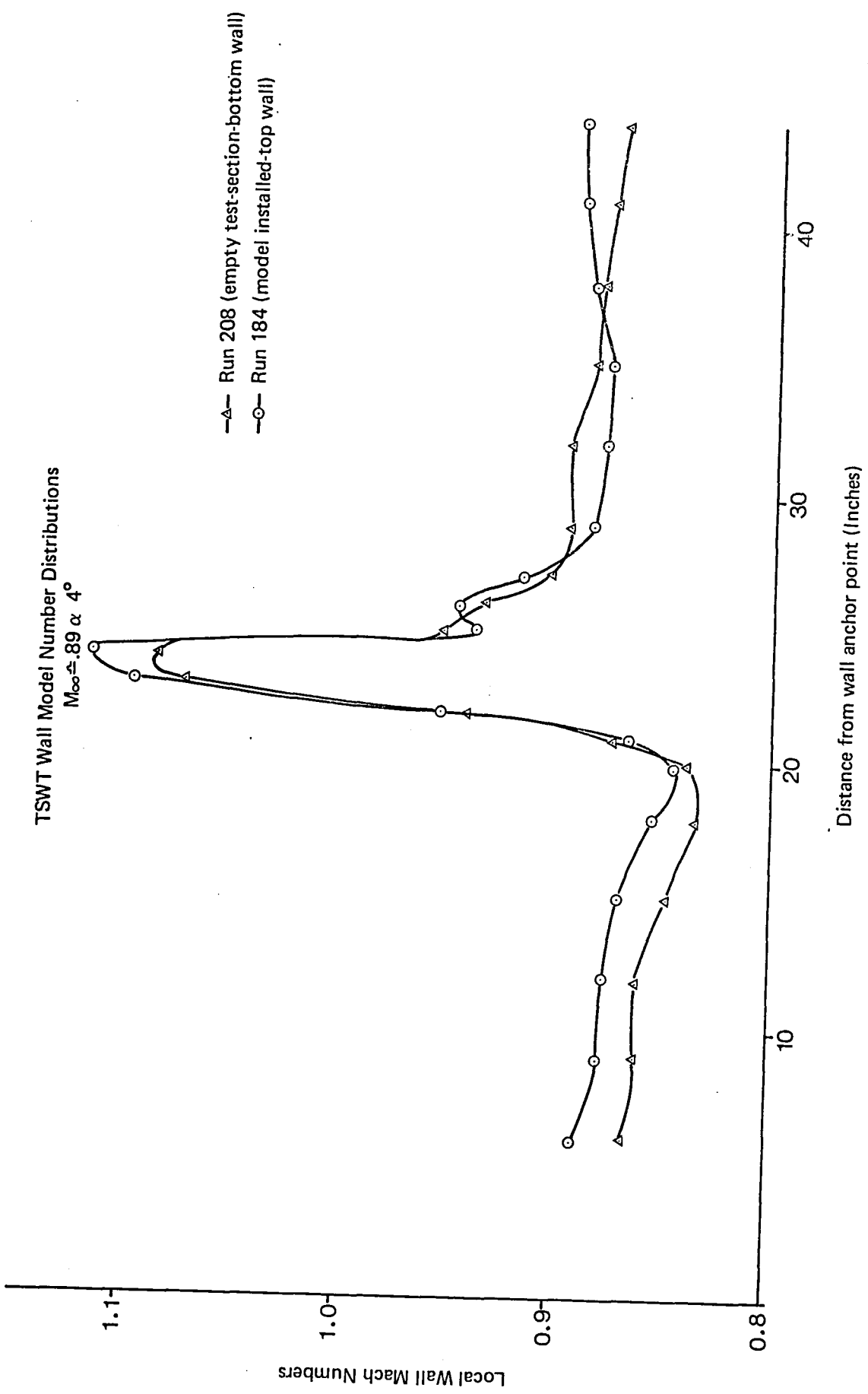

FIG. 10.14 COMPARISON OF WALL MACH NUMBER DISTRIBUTIONS FOR RUN 184 (Top Wall) AND RUN 208 (Bottom Wall)

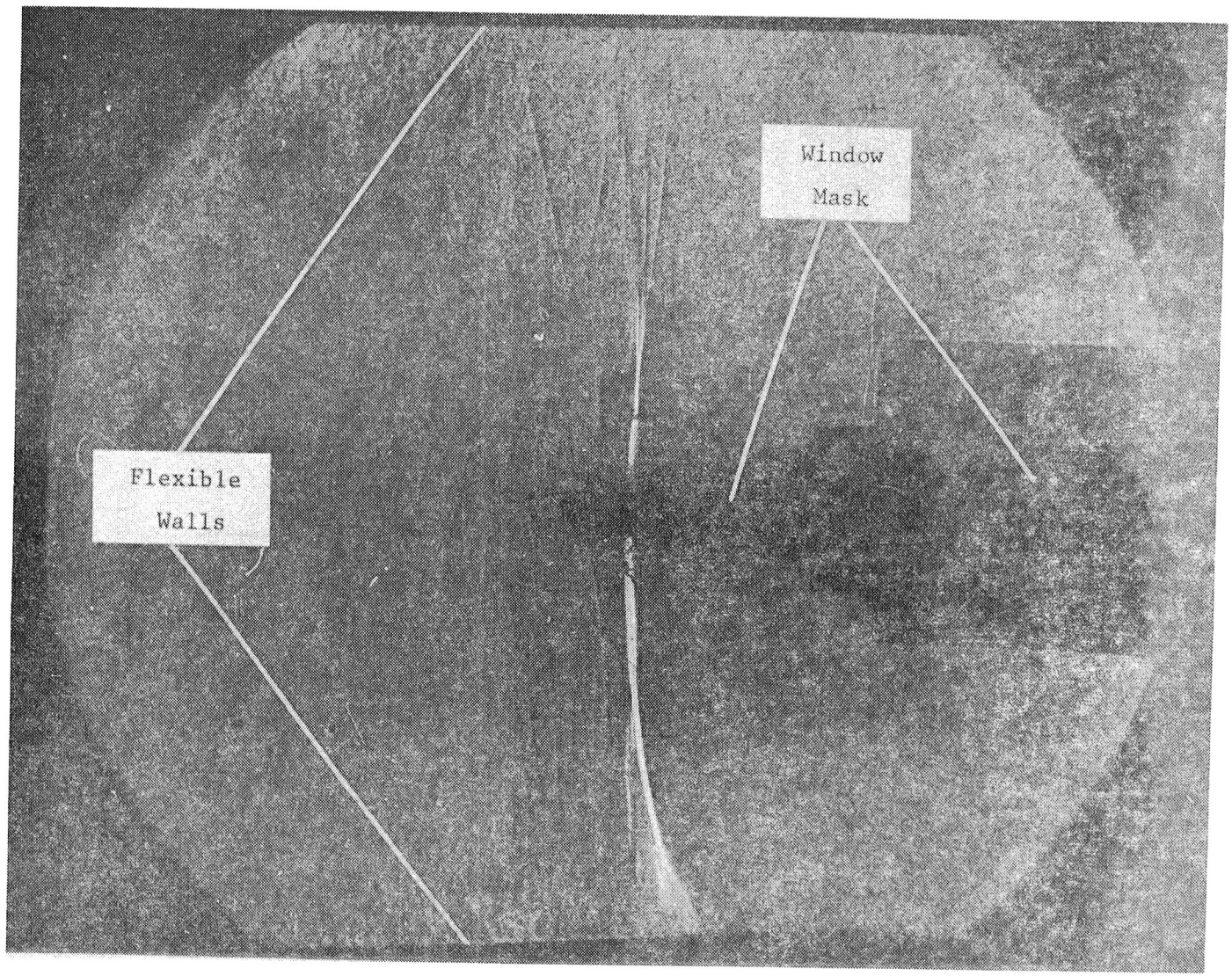

FIG. 10.15 IMAGINARY FLOWFIELD SIMULATION USING AN EMPTY TEST SECTION; $M_\infty = 0.89$

APPENDIX A

EXTRACT FROM

ANALYTICAL WORK IN SUPPORT OF THE DESIGN AND OPERATION OF TWO-DIMENSIONAL SELF-STREAMLINING TEST SECTIONS

NASA CR 145019 JULY 1976

CHAPTER 3. INTERFERENCE EFFECTS OF WALL POSITION ERRORS

3.1 The Nature of the Problem

It is recognised that the flexible-walls can only be positioned by the jacks within some set tolerance, and in this chapter is outlined a method by which the interference introduced by such errors may be estimated. In any given test section of this type there are likely to be many jacks along each wall. In the existing low speed test section there are 15. Position errors are likely to arise in a random manner, both in location and magnitude, within the tolerance band.

While the designer is to a large extent free to choose this tolerance, he must bear in mind that complexity and therefore cost will increase as the tolerance is reduced. Further, since the flexible wall is positioned at a finite number of jacking points there is no control over the shapes of the portions of wall between jacks, which would probably render pointless any endeavour towards levels of precision above some value.

In the existing low speed test section the wall setting accuracy is estimated to be approximately ±0.127mm (±.005 inches) giving a dimensionless tolerance:chord ratio of $\pm 9.3 \times 10^{-4}$, and the same tolerance has been adopted in the following analysis.

In this analysis the wall setting errors are regarded as producing a bump or series of bumps in an otherwise flat walled two-dimensional test section. Even though the bump height would in practice be random, here only the worst case of a maximum error, which is equal to the tolerance, is considered.

In practice a single jack in error along a nominally flat wall might produce a local wall shape similar to a portion of a sinusoid, with the peak or trough of the wave located at the jack. In this analysis such a wall contour disturbance is represented by an equal strength source/sink pair lying on the wall line, with a minimum pair spacing equal to the jack spacing. The strengths of the source and sink were chosen to give an arbitrary bump height equal to 0.00093c. It is recognised that this analytical representation of the effect of a jack error is less than ideal, but it is believed the representation gives reasonable results.

The effects of the presence of the bumps are assessed in the form of three measures of interference in the empty test section at what would be the location of the wing model, assumed central in the test section. The measures of interference are:

a) Angle of attack error at the wing leading edge.

b) Induced camber, which is assumed to be the difference between the flow angles at the leading and trailing edges.

c) Disturbance to free stream velocity, assessed as a dynamic pressure error at the wing quarter-chord point.

Even though the interference effects are quoted for this single but representative value of bump height, since the bumps are small the interference effects are expected to vary linearly with height, allowing simple scaling for other values of wall setting errors.

The interference at the model will depend on the number of jacks in error, on their location, and on the sign of the setting error. With many jacks per wall, any of which can be in error, it is clear that a very large number of different values of interference is possible.

The approach used here is to analyse a simple bump configuration which intuitively gives an interference close to the maximum. The probability of occurrence is then considered.

3.2 Analysis of Simple Bump Configuration

To find values for the worst effects at the model, investigations were made into the nature of each interference, using an inviscid flow model to determine velocity components and distributions.

The flow model for the simple case of a single bump in one flexible wall consists of a source/sink pair combined with a system of images, thereby producing a test section as shown in Figure 3.1. The parameters available in the analysis are test section height h, the approximate bump length d (measured between source and sink) and the bump position x_b (determined by the source location). It would appear logical to non-dimensionalise with respect to tunnel height, but the severity of the interference is a function of model size and therefore wing chord c was used instead.

Typical magnitudes of each interference and their variations with bump location are shown in Figs.3.2a, b and c, for particular values of $^h/_c$ and $^d/_c$. The graphs clearly show that a maximum effect occurs for each interference, as the bump passes underneath the wing model.

The approximate bump positions for the maxima are illustrated in Fig.3.3 for values of $^h/_c$ in the region of 1. The maximum angle of attack error occurs when the leading edge of the wing is over the nose or tail of the bump. The induced camber is a maximum when the wing leading edge is approximately over the nose of the bump or the trailing edge is over the tail. The maximum velocity increment occurs when the quarter chord point is over the bump mid-point. The forms of Figs.3.2a, b and c also suggest that the interferences are significant in most cases for a total range in $^{x_b}/_c$ of about 1.

It is therefore assumed that jack errors outside of a tunnel length of about 2 chords will not produce any significant interference, and it does not matter whether these jacks are in error or not, within the assumed tolerance.

The variations of the three maximum interferences with bump length and model size are shown in Fig.3.4a, b and c. It can be seen that the interferences reach near-maximum values at $^d/_c$ in the region of unity.

It is now possible to consider the probabilities for the occurrence of combinations of jack errors leading to significant interference. It is assumed that each jack error is statistically independent and, in order to obtain a conservative estimate, that the magnitude of each error is equal to the tolerance. In practice, there would be a distribution of errors ranging in magnitude from zero up to the tolerance. Over a tunnel length of two chords near the model, let there be N jacks. The probability of a particular jack being in error (up or down) is 1/N. The probability of all the other jacks being in error in the opposite sense is $1/2^{N-1}$. However, it has already been seen that any single bump will produce a significant interference over a range of about 1 chord and could therefore be produced by any one of N/2 jacks. The probability of a significant interference occurring because of a single jack bump is therefore

$$P_1 = \frac{1}{N} \cdot \frac{1}{2^{N-1}} \frac{N}{2} = \frac{1}{2^N}$$

The probability of a second jack adjacent to the first having an error of the same sign is 1/(N - 1). The probability of a two jack simple bump is therefore

$$P_2 = \frac{1}{N} \left(\frac{1}{N-1}\right) \cdot \frac{1}{2^{N-2}} \frac{N}{2} = \frac{1}{2^{N-1}(N-1)}$$

The probability of an n jack simple bump is

$$P_n = \frac{(N-n)!}{2^{N-n+1}(N-1)!}$$

and the relative probability is

$$\frac{P_n}{P_1} = \frac{2^{n-1}(N-n)!}{(N-1)!}$$

These results are given for various N in Table 1 in the form of the inverse of the probability, i.e. in terms of the likely number of wall adjustments to produce a maximum error.

TABLE 1

	N = 6	N = 12
$1/P_1$	64	4096
$1/P_2$	160	22528
$1/P_3$	320	112640

3.3 A Summary of Interference Effects

Current aims are to use minimum test section depths roughly equal to a wing chord and jack spacings of around $\frac{1}{4}$ chord. The arguments of the previous section and the results in Table 1 suggest that for jack spacings of 3 or 4 per chord, the probability of a multi-jack simple bump is sufficiently high that the maximum error values in Figs.3.4a, b and c should be taken. Therefore it is felt that the interference effects given by such a bump in one wall of a test section with depth of one chord should be adopted in test section design. The interference effects are then

angle of attack error	0.025 degrees
induced camber	0.05 degrees
C_p error	0.0018

These three effects can be related by converting them into equivalent errors in C_L. The conversions have assumed a lift curve slope of 2π for the angle of attack error, thin airfoil theory (similar to that in Section 4.2.1) in converting induced camber, and a uniform C_p error in forming an equivalent C_L error. Note that the latter approximation will lead to a high estimate for the C_L error. The resultant figures are

C_L error due to angle of attack error	0.00275
C_L error due to induced camber	0.00125
C_L error due to C_p error	0.0018

These levels of interference may be considered acceptably small, and therefore it is felt that despite the fact of the analytical model not giving a shape of bump very close to that which might be expected in practice, it is unlikely that a more realistically shaped bump could give a less acceptable level of interference.

If on the other hand the interferences are not acceptable, because it is impossible to apply corrections the tunnel must be designed to reduce the errors. The preceeding reasoning indicates that this may be achieved at lowest cost by installing position monitors of enhanced accuracy only at those jack locations close to the model.

SYMBOLS

a	Tunnel working section semi-length
a_1	Two-dimensional lift curve slope
c	Wing chord
$C_L, \Delta C_{LU}, \Delta C_{LC}$	Lift coefficients
C_p	Pressure coefficient
d	Length of wall bump
$f(\eta)$	Function defined by equation 4.17
h	Tunnel working section height
M	Mach number
$m(x)$	Source strength per unit length of wall
N,n	Indices
P_n	Probability
r_c	Camber ratio
t	Wall setting tolerance
$U,u,v,\bar{u},\bar{v},$	Velocity components
w	Complex potential ($w = \varphi + i\phi$)
$x,y;x_1,y_1$	Coordinates
x_b	Coordinate of the nose of the wall bump relative to the wing quarter chord
Δy	Wall movement relative to the straight
z,z_o	Complex variables ($z = x + iy$)
α_s	Flow turning angle
Γ	Vortex strength
γ_o, γ_{w1}	Wall vorticity distributions
η	Transformation parameter
ξ	Dummy variable

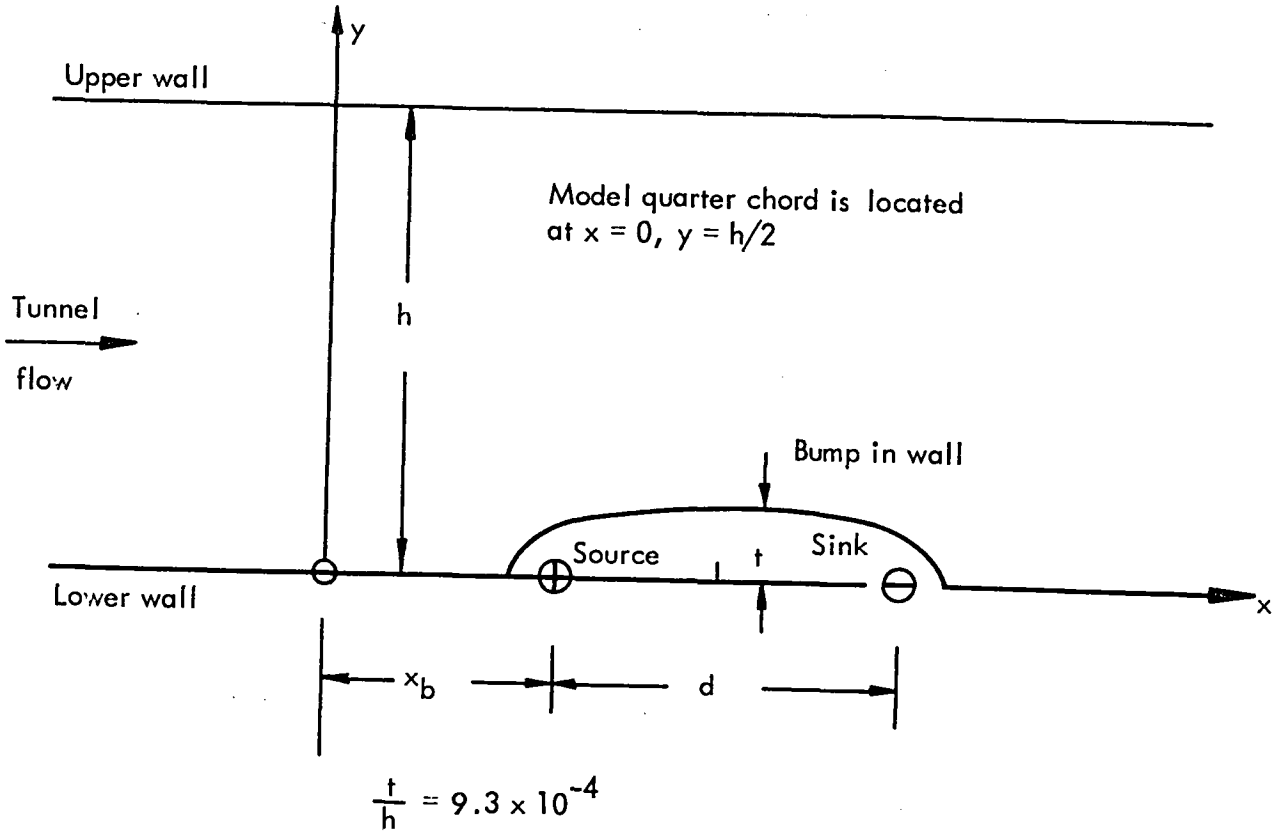

FIG. 3.1. TEST SECTION STREAMLINES TO REPRESENT JACK POSITION ERROR.

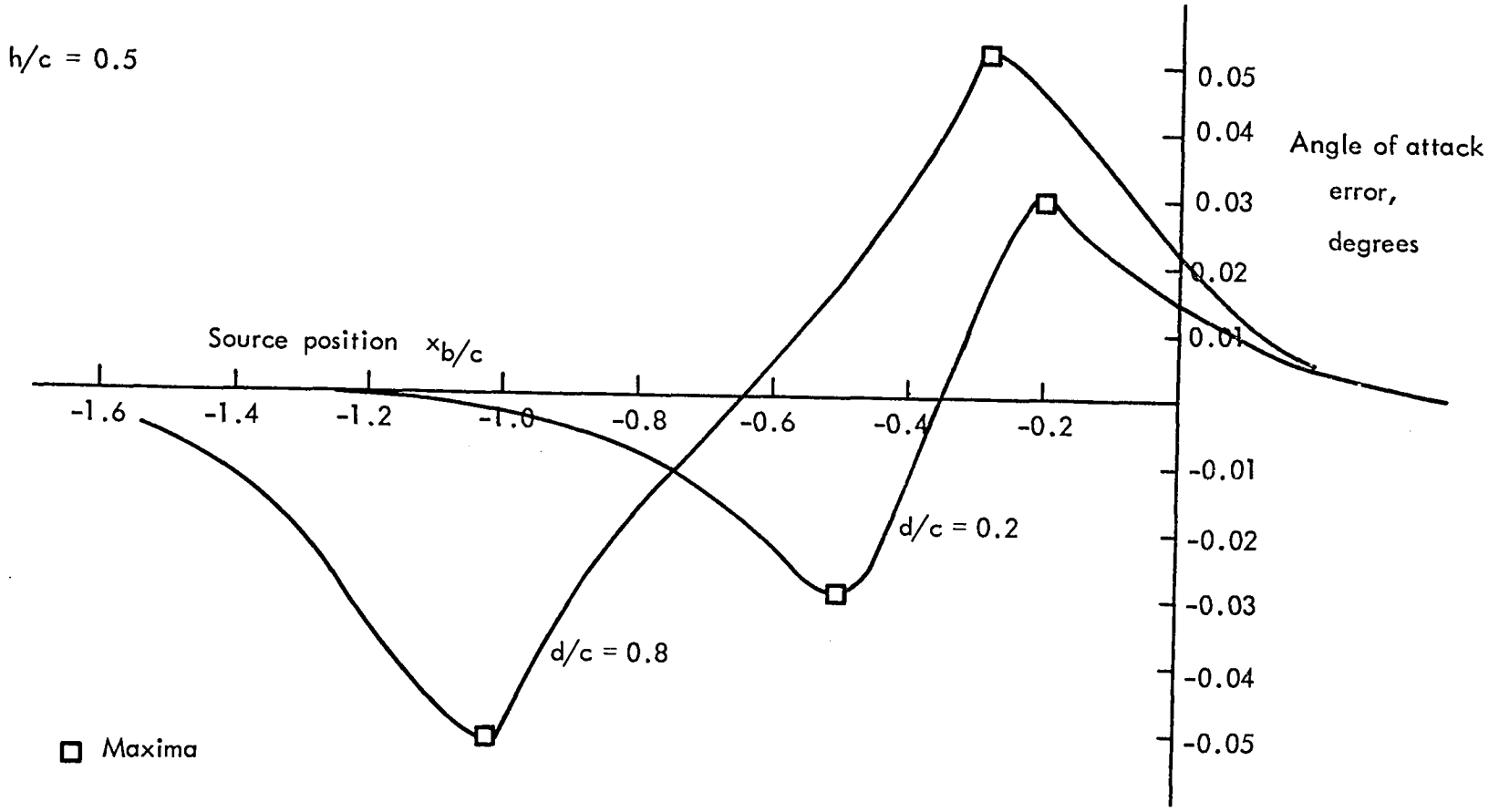

FIG. 3.2a. ANGLE OF ATTACK ERROR AS A FUNCTION OF BUMP POSITION.

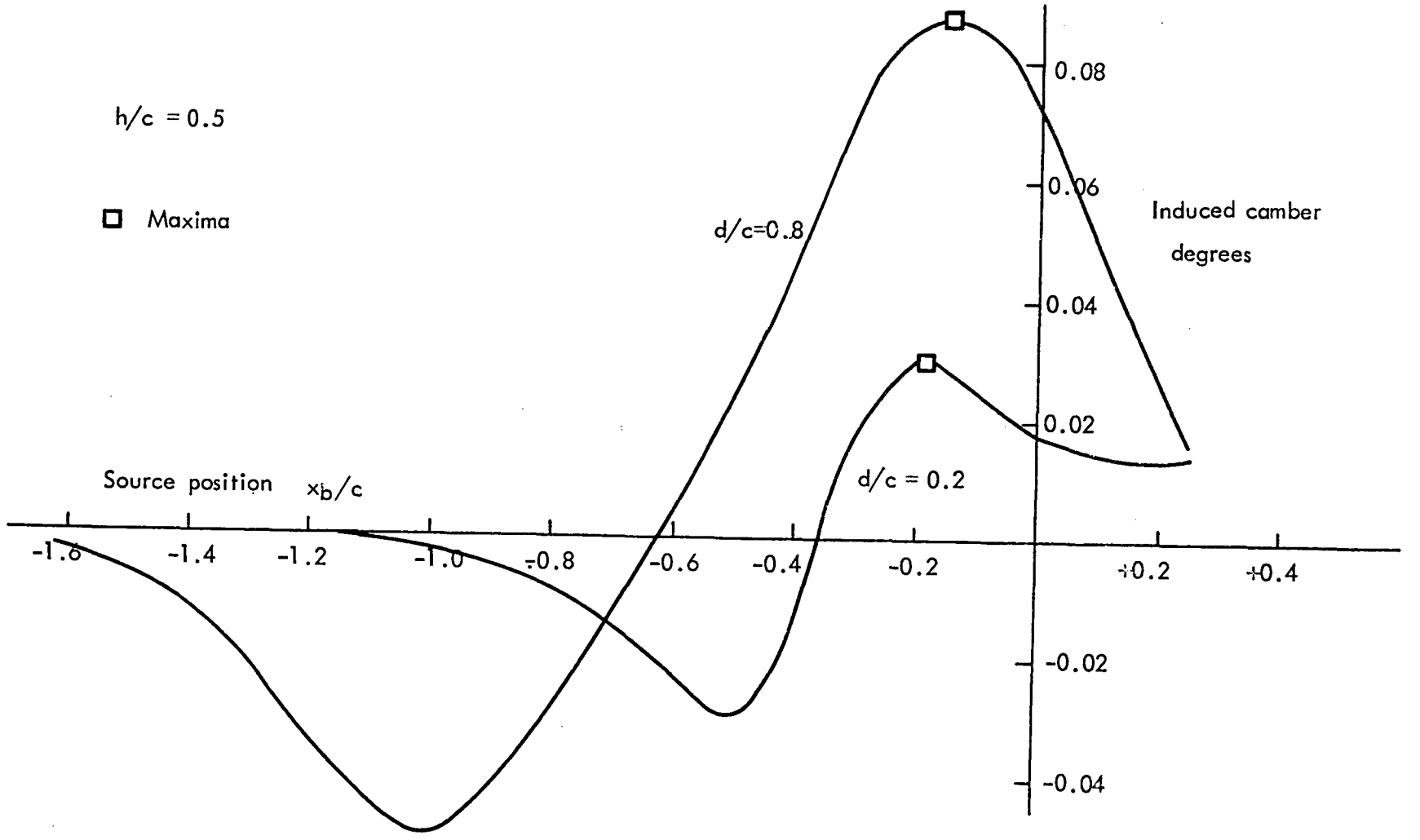

FIG. 3.2b. INDUCED CAMBER AS A FUNCTION OF BUMP POSITION.

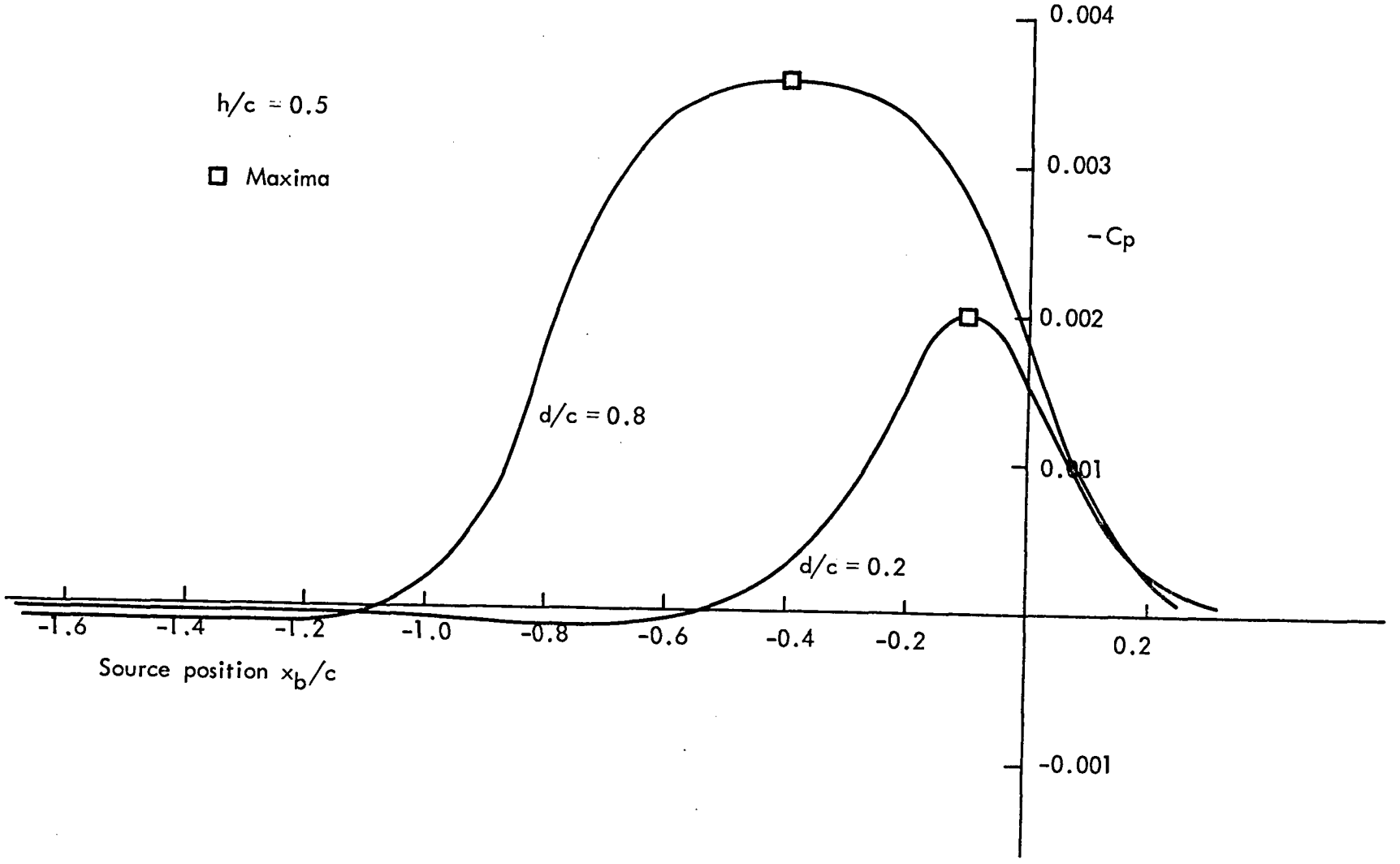

FIG. 3.2c. PRESSURE COEFFICIENT ERROR AS A FUNCTION OF BUMP POSITION.

(a) Angle of attack

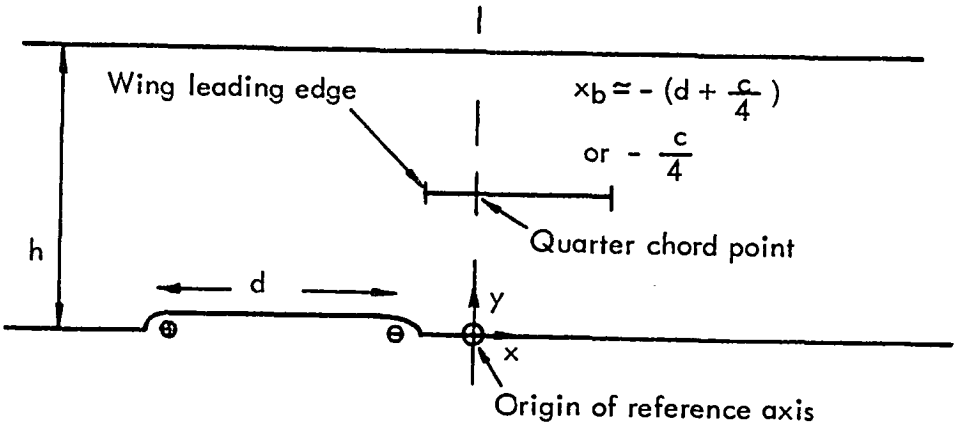

(b) Induced camber

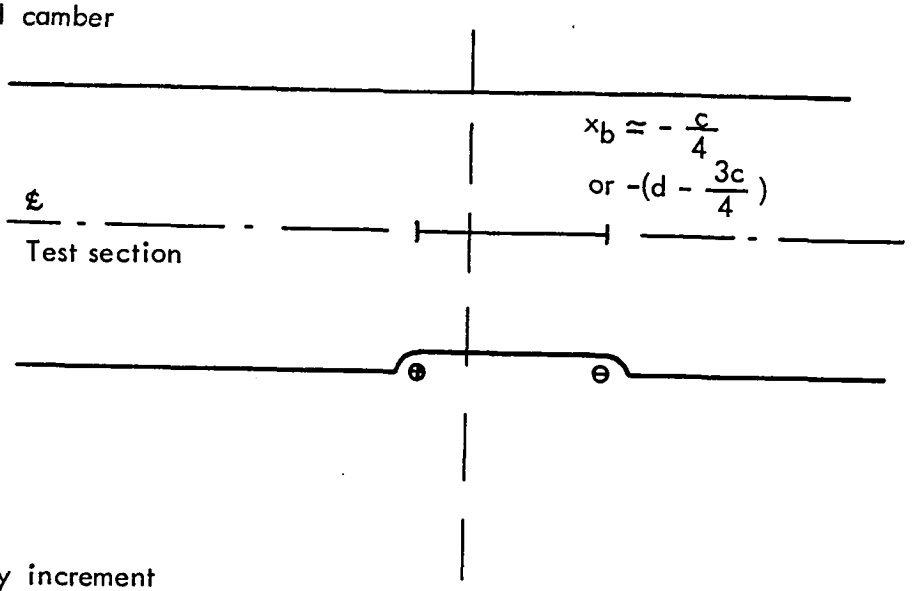

(c) Velocity increment

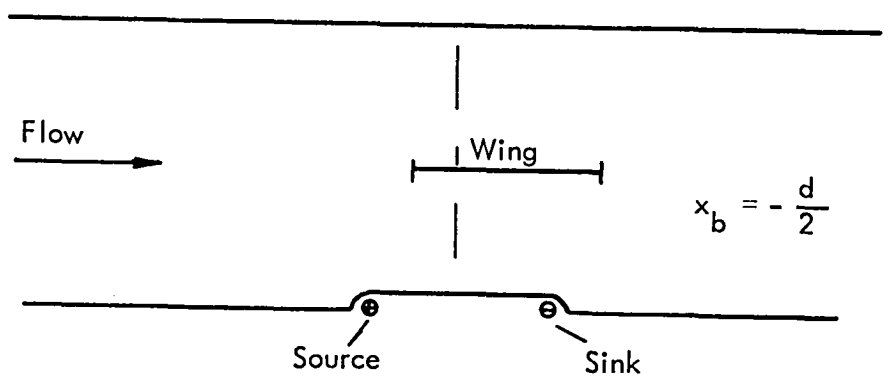

FIG. 3.3. BUMP POSITIONS FOR MAXIMUM INTERFERENCES.

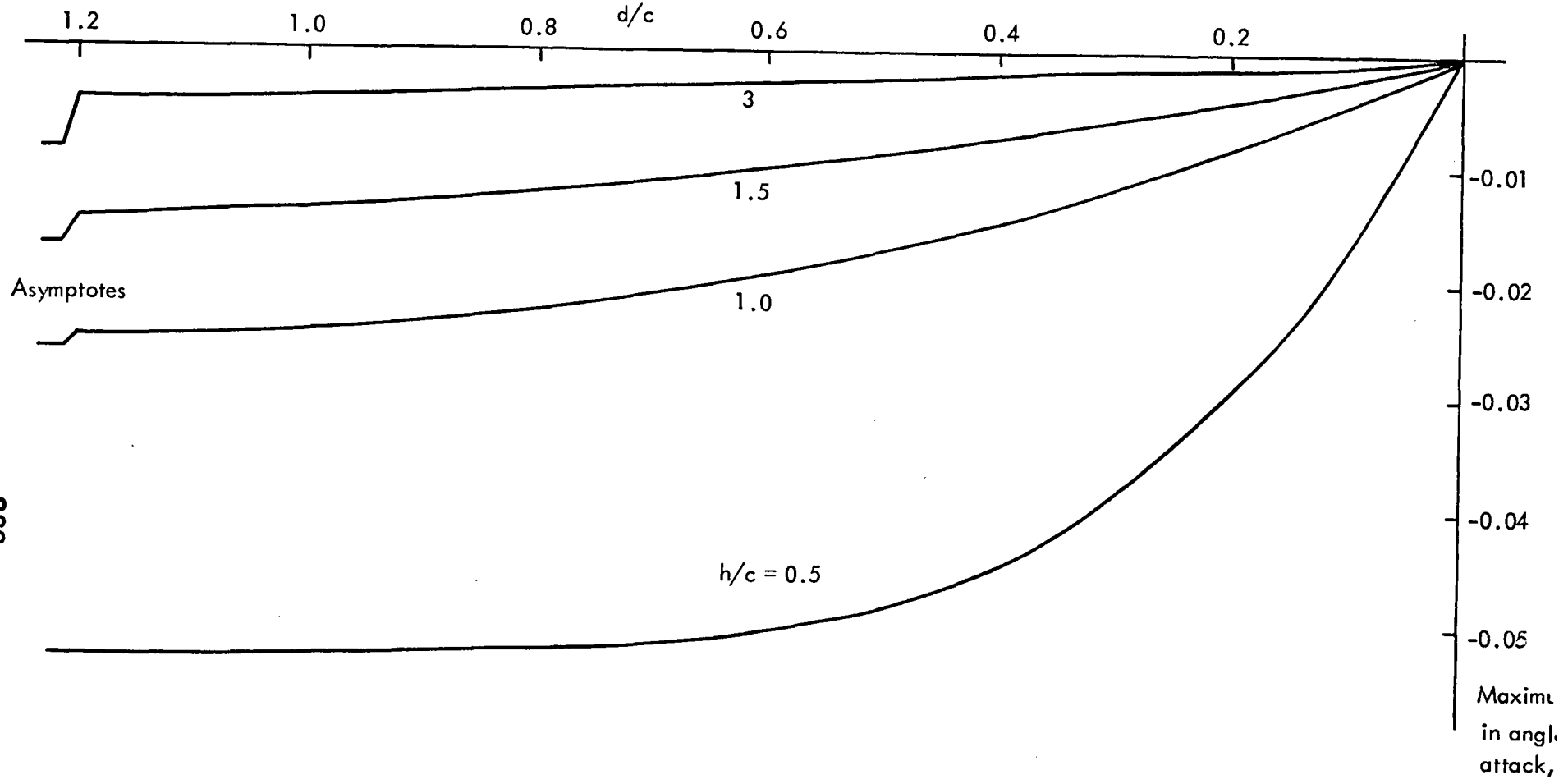

FIG. 3.4a. MAXIMUM ANGLE OF ATTACK INTERFERENCE AS A FUNCTION OF BUMP LENGTH.

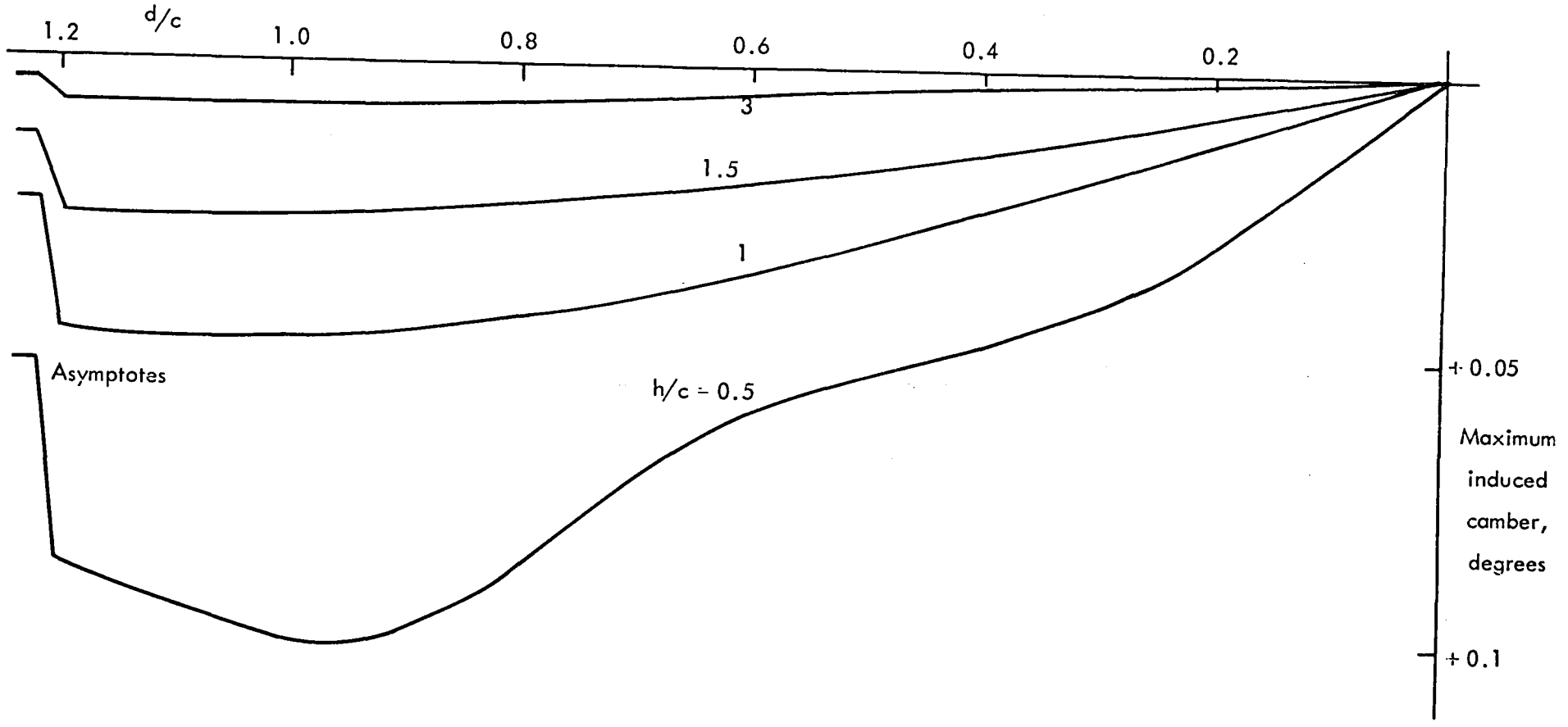

FIG. 3.4b. MAXIMUM INDUCED CAMBER INTERFERENCE AS A FUNCTION OF BUMP LENGTH.

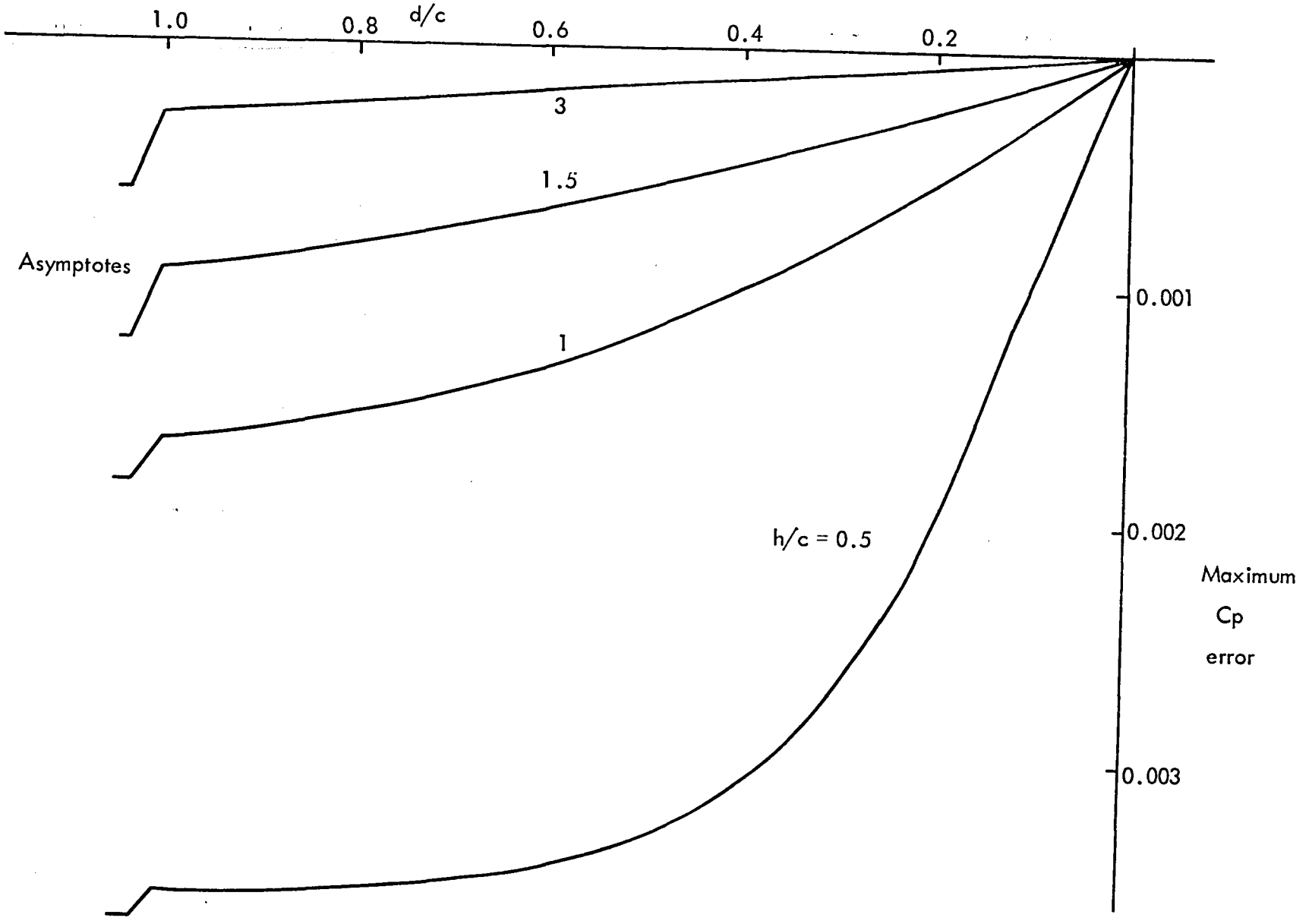

FIG. 3.4c. MAXIMUM PRESSURE COEFFICIENT ERROR AS A FUNCTION OF BUMP LENGTH.

APPENDIX B

EXTRACT FROM

SELF-STREAMLINING WIND TUNNEL -

LOW SPEED TESTING AND TRANSONIC TEST SECTION DESIGN

NASA CR-145257 OCTOBER 1977

CHAPTER 4. FURTHER DESIGN ANALYSIS FOR SELF-STREAMLINING TEST SECTIONS

4.2 Comparisons Between the Contours of Structural Members and Streamlines

A flexible wall is a structural member constrained by the jacks to pass through discrete points on a streamline. The contour of the wall is determined by, among other things, its elastic properties, and will presumably depart from a streamline contour between jacks because its natural elastic contour may not be the same as the streamline contour. Its contour will be modified by stiffnesses in the jack-to-wall attachments, by static pressure differences across the wall, and by friction between the flexible wall and rigid sidewalls. In the two flexible walled test sections so far designed at Southampton University the magnitudes of differences between wall and streamline contours have been minimised b:

1) grouping the jacks closely together, with the closest spacing where the greatest curvature of the wall occurs,

2) employing flexures as jack-to-wall attachments, the stiffness of the flexures being very much lower than that of the wall,

3) arranging for the pressures inside and outside of the flexible walls to be nominally equal,

4) employing feathered-edge rubber seals between the flexible walls and sidewalls.

These design features can only minimise but not eliminate the differences between the achieved contour and the streamline. In particular the natural elastic shape will inevitably differ from the streamline.

Analysis of this problem has begun. Ideally some theoretically determined streamlines likely to be experienced in airfoil testing should be considered. However, as these were not immediately available the analytical methods were developed using streamlines from simple potential flow around a realistically sized bluff body. The method is outlined below and some results given for this simple body and flowfield, but the work continues with the method being applied to the flow around an airfoil, and will be reported later.

The deflection δ produced by a series of concentrated loads acting on a nominally straight beam with its ends simply supported is given by

$$\delta = \frac{1}{EI} \int_0^{\ell} M_1 M_2 dX \qquad 4.1$$

where E = Youngs Modulus of elasticity,

I = Second moment of area of beam cross-section.

M_1 = Bending moment at X due to the applied loads

M_2 = Bending moment at X due to a unit load applied at the point where δ is required.

In this case the deflections of several points along a beam are known but the loads generating them are not. Therefore a set of n equations for the n deflections each in terms of the n unknown loads may be solved for the loads. The deflection of any point on the beam may then be determined.

In the analysis reported here the shape was determined of a beam passing through six equally spaced points along a streamline, (hence n = 4), and the difference between the beam at its mid-point and the streamline examined. The flowfield was that around a lifting cylinder with wake; streamline contours were computed above and below the cylinder for the beam analysis. Variables included the jack spacing and the fore-and-aft position of the mid-point of the beam relative to the cylinder.

The maximum differences between beam mid-points and the streamlines occur when the mid-point is near to the model, and with large jack spacings. On Figure 4.1 is shown an example of this analysis applied to the top and bottom walls, with the beam mid-points above and below the cylinder. The difference between the beam mid-point and the streamline is presented as an error, for each wall, as a function of the ratio

$$\frac{\text{jack spacing}}{\text{test section height}}$$

Shown also is a tolerance band indicating the maximum errors which are being aimed at in the design. In this example the maximum permissible jack spacing would be about 30% of the test section height.

This example is purely illustrative of the method which is currently being applied to walls and streamlines around a lifting airfoil. A study such as this of the difference between beam and streamline contours is fundamental to the design of flexible wall test sections.

4.3 Cancellation of Interference due to Length Truncation

4.3.1 It has been argued[3,4] that the finite lengths of the streamlined walls introduce an interference at a lifting model placed centrally in the test section, the interference having the form of a camber induced by flow curvature. An estimate of magnitude of the error ΔC_{Lc} due to flow curvature is[3,4]

$$\frac{\Delta C_{Lc}}{C_L} = -\left(\frac{c}{h}\right)^2 \frac{a_1}{2\pi} f\left(\frac{a}{h}\right) \qquad 4.2$$

where C_L = lift coefficient

c = wing chord

a_1 = lift curve slope

a = test section semi-length

h = test section depth.

This expression predicts an error in C_L of the order 1% for the low speed test section currently in use.

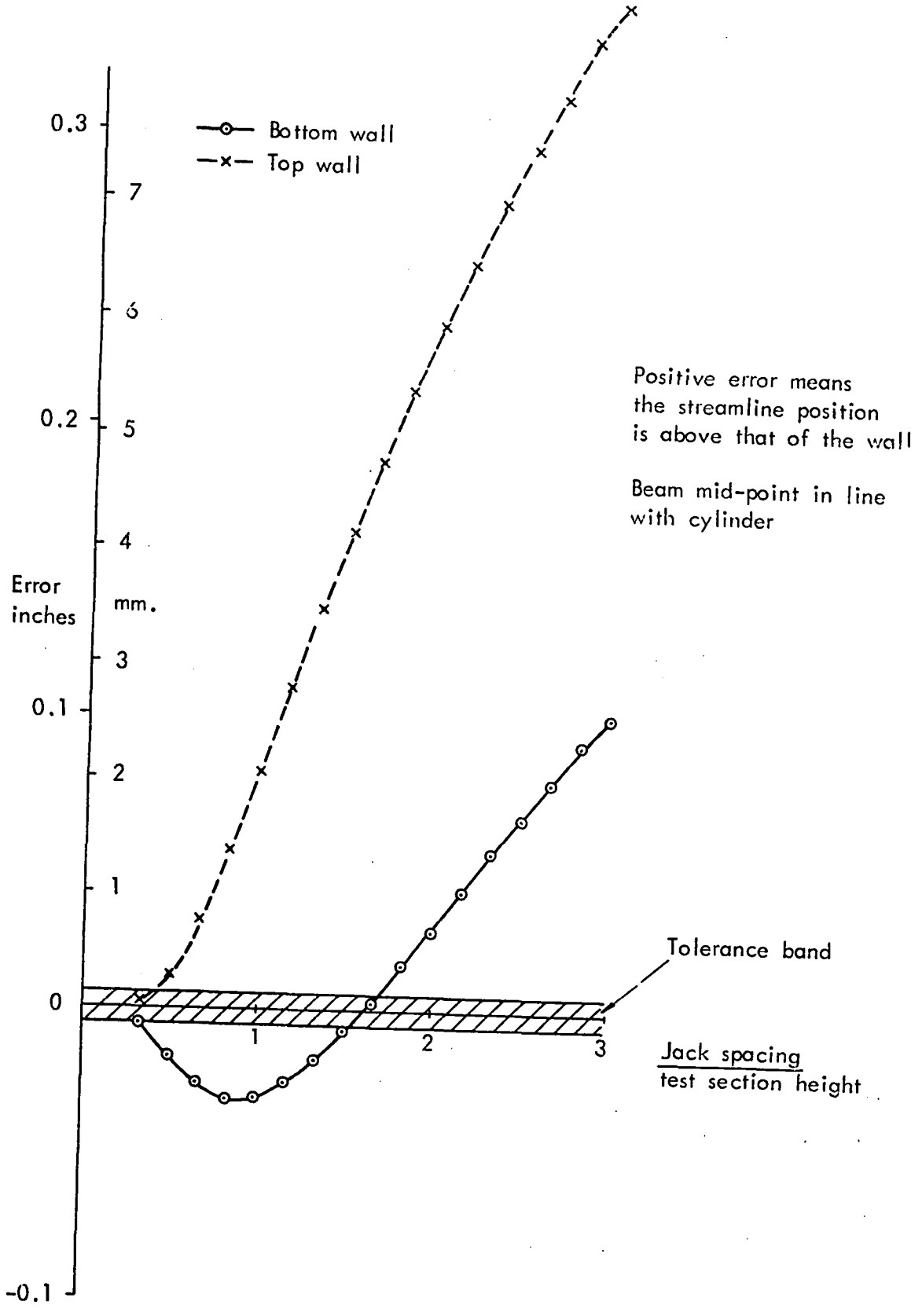

FIG. 4.1 BEAM AND STREAMLINE ANALYSIS

APPENDIX C

CONTROL SOFTWARE FOR TWO DIMENSIONAL AIRFOIL TESTS USING A SELF-STREAMLINING FLEXIBLE WALLED TRANSONIC TEST SECTION

NASA CR-165941 AUGUST 1982

APPENDIX D
CAST 7 WIND TUNNEL TESTING

A comprehensive test programme in various European wind tunnels has been carried out using the CAST 7 aerofoil under the leadership of the GARTEur Action Group to compare different tunnel flows. The CAST 7 was chosen for this programme because it features moderate rear loading and moderate adverse pressure gradient so that the aerofoil is relatively insensitive to Reynolds number effects. Also the aerofoil exhibits high sensitivity to changes in mach number and angle of attack near its design condition i.e. $M_\infty = 0.76$; $\alpha = 0.579$.

One of the tunnels involved in this programme was the flexible walled wind tunnel at Tech Un. Berlin which operates at similar test stagnation conditions as TSWT. Therefore it was fortunate that a CAST 7 aerofoil could be tested in TSWT to allow direct comparison for the first time between two similar flexible walled test sections operating at the same test Reynolds number.

The TSWT tests were not performed by the author but the hardware and software developed in previous tests was used. Wall streamlining was routinely performed for all the TSWT tests over a Mach number range from 0.3 to 0.82.

Plots of the various sets of lift coefficient versus Mach number data are shown on Figure A. The comparison between TSWT and Tech Un. Berlin lift data is excellent, particularly in the reproduction of the shock stall. There is also reasonable agreement between TSWT data and other conventional transonic wind tunnels despite differences in the Reynolds number between these tests.

These findings add further evidence to the validity of the Flexible Wall Testing Technique and in particular the claim that top and bottom wall interference is eliminated.

UNIVERSITY OF SOUTHAMPTON

CAST-7 DATA COMPARISONS

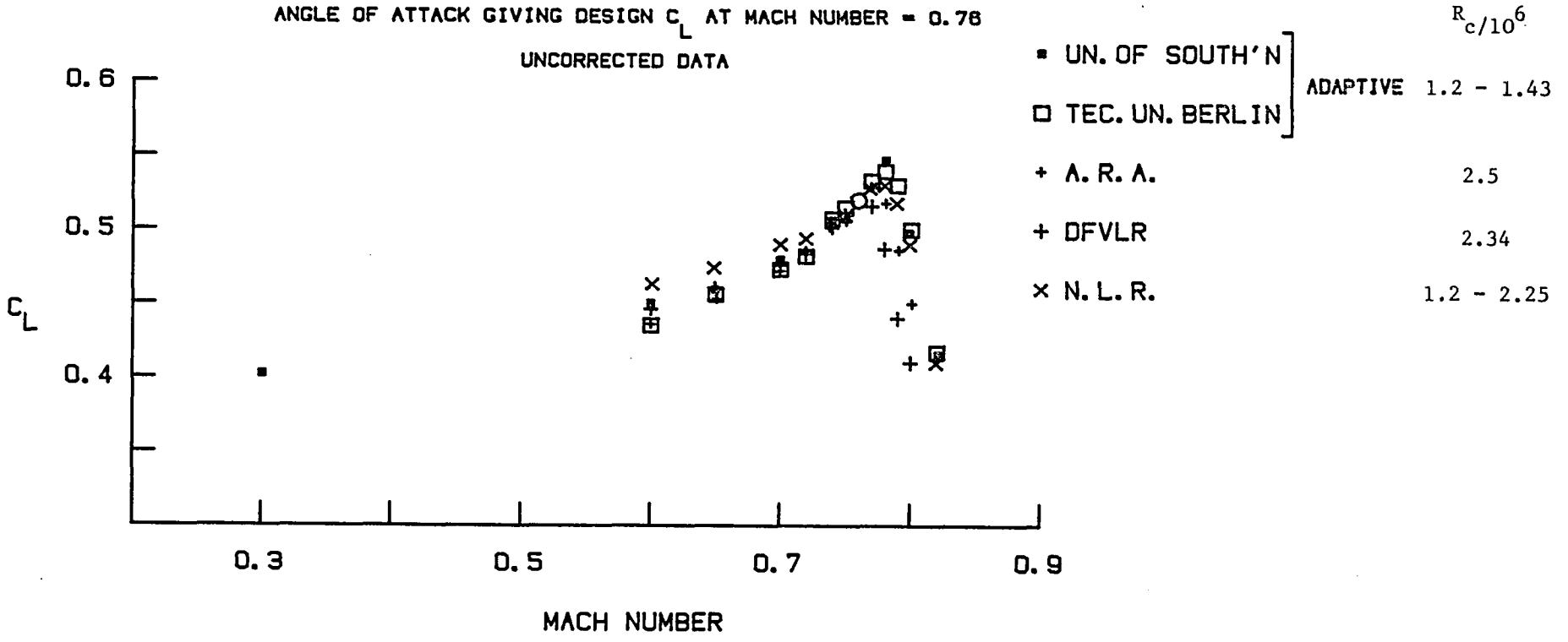

FIG. A COMPARISON OF CAST 7 LIFT DATA OBTAINED FROM VARIOUS EUROPEAN TRANSONIC WIND TUNNELS.

1. Report No.	2. Government Accession No.	3. Recipient's Catalog No.
NASA CR-172328		

4. Title and Subtitle	5. Report Date
The Design and Operational Development of Self-Streamlining Two-Dimensional Flexible Walled Test Sections	March 1984
	6. Performing Organization Code
7. Author(s)	8. Performing Organization Report No.
Stephen W. D. Wolf	
9. Performing Organization Name and Address	10. Work Unit No.
University of Southampton Department of Aeronautics and Astronautics SO9 5NH - Hampshire England	11. Contract or Grant No. NSG-7172
12. Sponsoring Agency Name and Address	13. Type of Report and Period Covered
National Aeronautics and Space Administration Washington, D.C. 20546	Contractor Report
	14. Sponsoring Agency Code 505-31-53-10

15. Supplementary Notes

Langley Technical Monitor: Charles L. Ladson

Ph.D. Thesis - University of Southampton

16. Abstract

Self-streamlining two-dimensional flexible walled test sections eliminate the uncertanties found in data from conventional test sections particularly at transonic speeds. The test section sidewalls are rigid, while the floor and ceiling are flexible and are positioned to streamline shapes by a system of jacks, without reference to the model. The walls are therefore self-streamlining. Data is taken from the model when the walls are good streamlines such that the inevitable residual wall induced interference are acceptably small and correctable. Successful two-dimensional validation testing at low speeds has led to the development of a new transonic flexible walled test section. Tunnel setting times have been minimised by the development of a rapid wall setting strategy coupled with on-line computer control of wall shapes using motorised jacks. Two-dimensional validation testing using symmetric and cambered aerofoils in the Mach number range up to about 0.85 where the walls are just supercritical, shows good agreement with reference data using small height-chord ratios between 1.5 and unity. The concept of a practical flexible walled test section has been shown by operational experience to be dependent on the use of a computer for data manipulation and wall control. Design analyses have confirmed the near optimum layout of the transonic test section and provide a basis for new test section design. This work has demonstrated the feasibility of almost eliminating wall induced interference in two-dimensional transonic testing allowing advantage to be taken of the improved flow quality and reduced power requirements or increase Reynolds number inherent with a shallow unventialted test section.

17. Key Words (Suggested by Author(s))	18. Distribution Statement
Adaptive Wall Wind Tunnel Transonic Wind Tunnel Airfoils Aerodynamics	Unclassified - Unlimited Star Category - 02

19. Security Classif. (of this report)	20. Security Classif. (of this page)	21. No. of Pages	22. Price
Unclassified	Unclassified	282	A13